

NI

cult
7

NASA CR-165404



(NASA-CR-165404) FUEL/OXIDIZER-RICH
HIGH-PRESSURE PREBURNERS Final Report
(Aerojet Liquid Rocket Co.) 254 p
HC A12/MF A01

N82-10245

CSCC 211

Unclass

G3/28 37445

FUEL/OXIDIZER-RICH
HIGH-PRESSURE PREBURNERS

by

L. Schoenman



AEROJET LIQUID ROCKET COMPANY

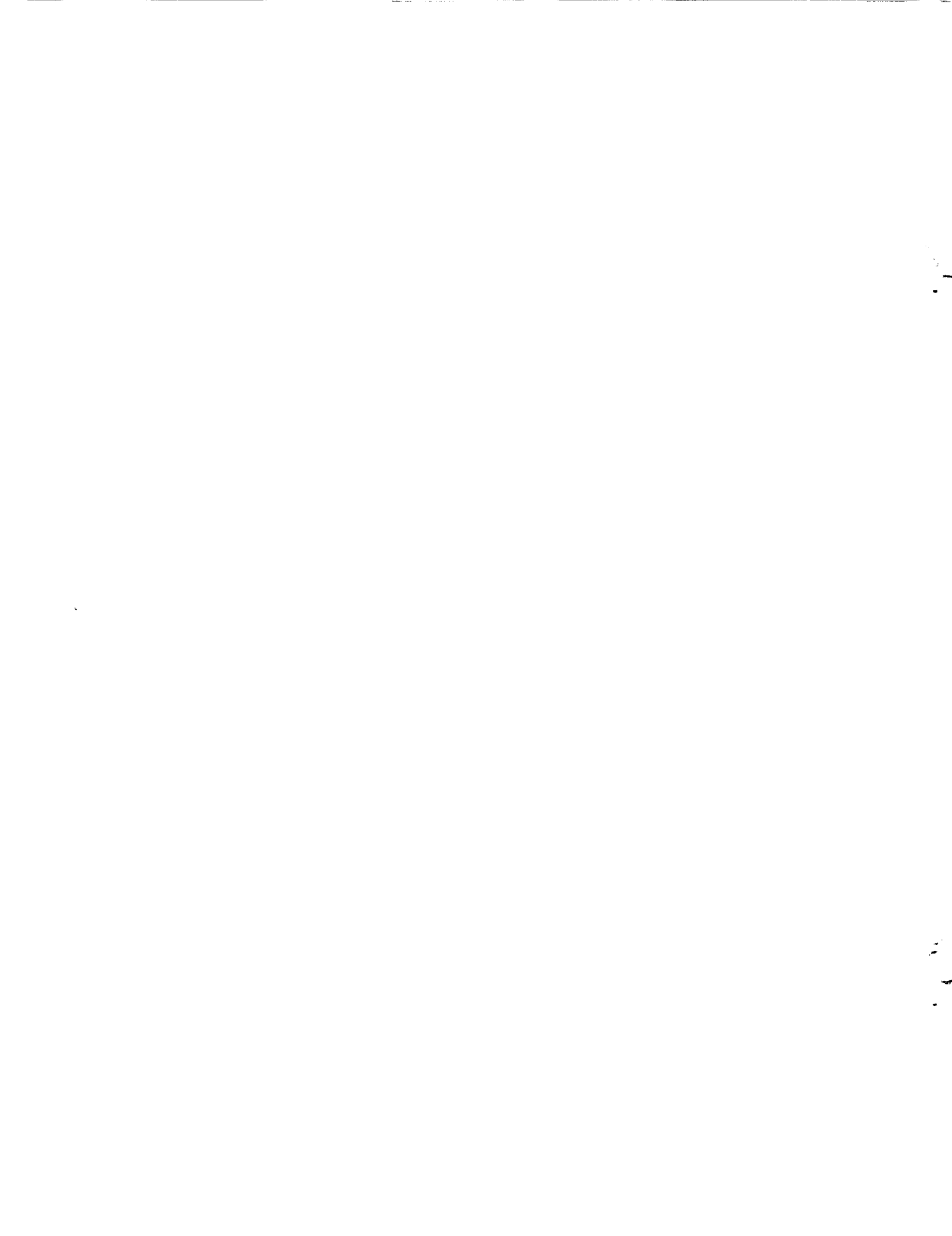
Prepared for

NATIONAL AERONAUTICS AND SPACE ADMINISTRATION

NASA/Lewis Research Center

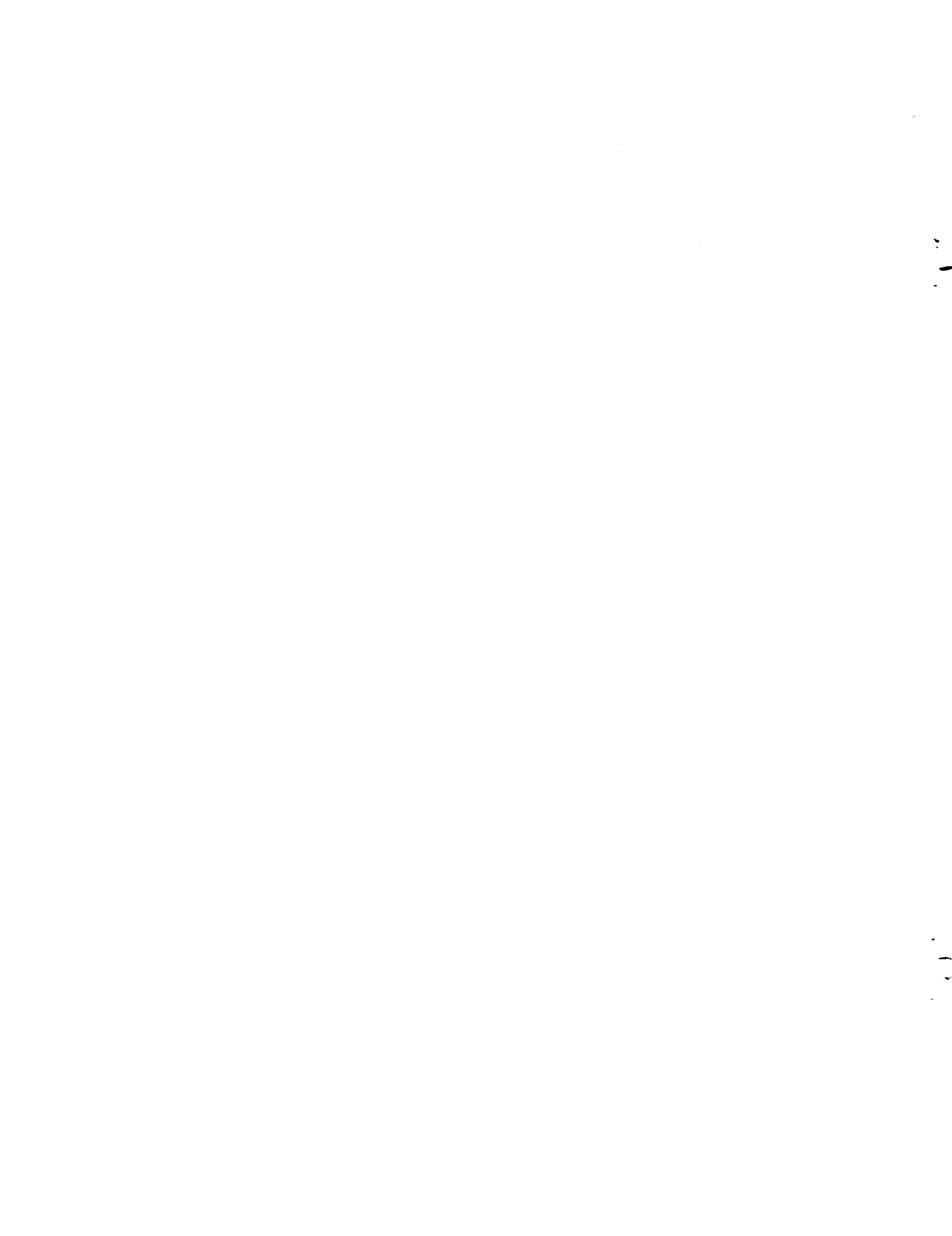
Contract NAS 3-21753

H. Price, Project Manager



1. Report No. CR 165404		2. Government Accession No.		3. Recipient's Catalog No.	
4. Title and Subtitle Fuel/Oxidizer-Rich High-Pressure Preburners				5. Report Date October 1981	
				6. Performing Organization Code	
7. Author(s) L. Schoenman				8. Performing Organization Report No.	
9. Performing Organization Name and Address Aerojet Liquid Rocket Company Post Office Box 13222 Sacramento, California 95813				10. Work Unit No.	
				11. Contract or Grant No. NAS 3-21753	
12. Sponsoring Agency Name and Address National Aeronautics and Space Administration NASA/Lewis Research Center 21000 Brookpark Rd. Cleveland, Ohio 44135				13. Type of Report and Period Covered Contractor Report, Final	
				14. Sponsoring Agency Code	
15. Supplementary Notes Project Manager - Harold G. Price NASA/Lewis Research Center 21000 Brookpark Rd. Cleveland, Ohio 44135					
16. Abstract <p>This report documents the analyses, designs, fabrication, and cold-flow acceptance testing of LOX/RP-1 preburner components required for a high-pressure staged-combustion rocket engine. Separate designs of injectors, combustion chambers, turbine simulators, and hot-gas mixing devices are provided for fuel-rich and oxidizer-rich operation.</p> <p>The fuel-rich design addresses the problem of non-equilibrium LOX/RP-1 combustion. The development and use of a pseudo-kinetic combustion model for predicting operating efficiency, physical properties of the combustion products, and the potential for generating solid carbon is presented.</p> <p>The oxygen-rich design addresses the design criteria for the prevention of metal ignition. This is accomplished by the selection of materials and the generation of well-mixed gases. The combining of unique propellant injector element designs with secondary mixing devices is predicted to be the best approach.</p> <p>The rocket engine preburner components fabricated to address the technical issues were delivered to NASA for testing under follow-on Contract NAS 3-22647.</p>					
17. Key Words (Suggested by Author(s)) Staged-Combustion Rocket Fuel for LOX/RP-1 Propellants Fuel- and Oxidizer-Rich Combustion High-Pressure Combustion Performance and Stability Non-equilibrium Fuel-Rich Combustion Like-on-Like (LOL) Doublets; Fuel-Oxidizer-Fuel (FOF)-Triplets Fuel Main Injector Simulator (FMIS); Turbine Simulator (TS)				18. Distribution Statement Unclassified - Unlimited	
19. Security Classif. (of this report) Unclassified		20. Security Classif. (of this page) Unclassified		21. No. of Pages 244	22. Price*

* For sale by the National Technical Information Service, Springfield, Virginia 22161



FOREWORD

This final report, submitted per the requirements of Contract NAS 3-21753, documents the design and fabrication of the test hardware for the Fuel/Oxidizer-Rich, High-Pressure Preburner Program. The work for this program was performed by the Aerojet Liquid Rocket Company for the NASA-Lewis Research Center. The contractual activities, initiated on 2 January 1979 and completed on 22 May 1981, provided for the design, fabrication, and delivery of fuel- and oxidizer-rich preburner injectors, chambers, and turbine and main injector simulators.

The NASA-Lewis project manager was Mr. H. Price. The ALRC program manager was Mr. J. W. Salmon, the project engineer was Mr. L. Schoenman, and the Operations project manager was Dr. R. J. LaBotz.

PRECEDING PAGE BLANK NOT FILMED

TABLE OF CONTENTS

	<u>Page</u>
I. Introduction	1
A. Gas Generator/Preburner History	1
B. Program Objective	2
II. Summary	5
III. Description of Designs and Delivered Experimental Test Hardware	7
A. Assembly	7
B. Injector Assembly	7
1. Major Propellant Manifold	14
2. Faceplates	14
C. Chambers	39
D. Turbine Simulator	43
E. Igniters	43
F. Acoustic Resonators	52
G. Main Injector Simulator	52
H. Throat Sections	58
I. Instrumentation Rake	58
IV. Concept Selection and Supporting Analyses	63
A. Fuel-Rich Preburner	63
1. Problem Definition and Past History	63
2. Concept Selection	69
3. Technical Approach to Model Development	69
4. Materials Selection Design Criteria	91
5. Structural Analysis	93
6. Igniter Design and Ignition Analyses	100
7. Stability Analyses	103
8. Thermal Analyses	108
9. Injector Pattern	114
B. Oxidizer-Rich Preburner	133
1. Problem Definition and Past History	133
2. Concept Selection	134

TABLE OF CONTENTS (cont.)

	<u>Page</u>
3. Materials Selection	134
4. Ignition Analyses	137
5. Stability Analyses	137
6. Thermal Analyses	141
7. Injector Pattern Selection	149
V. Hardware Fabrication	163
A. Procedures	163
B. Problems	163
C. Product Assurance	170
VI. Cold-Flow Testing	179
A. Single-Element Cold-Flow Testing	179
B. Loose Platelet Stack Cold-Flow Testing	181
C. Final Injector Assembly Cold-Flow Testing	201
D. Turbine Simulator Cold-Flow Testing	217
E. Igniter Cold-Flow Testing	228
VII. Conclusions and Recommendations	235
References	237
Appendix A - Fuel-Rich Combustion Model Bibliography	239
Distribution List for Final Report - CR-165404	243

LIST OF TABLES

<u>Table No.</u>		<u>Page</u>
I-I	Preburner Design and Operating Requirements	3
III-I	Fuel- and Oxidizer-Rich Preburner Injector	40
III-II	Turbine Simulator Bar Spacing to Produce Required Ratio	48
IV-I	Coaxial Vortex Characteristics	125
IV-II	Fuel-Rich Preburner LOL-Showerhead Injector Design Summary	130
IV-III	LOL Injector Element Parameters	157
IV-IV	LOL Propellant Stream Characteristics	158
IV-V	Propellant Vaporization Efficiencies Versus Fuel Temperature	159
V-I	Preburner Aerojet Parts List and Major Purchased Items	165
V-II	Cold-Flow Data of Platelet Injector After Repair	171
VI-I	Fuel-Rich Pattern Single-Element Loose Platelet Cold Flow	194
VI-II	Loose Stack Cold-Flow Data for Fuel-Rich Platelet Injector SN-2	197
VI-III	Fuel-Rich Injector Cold-Flow Data (PN 1191403-39)	209
VI-IV	Oxidizer Platelet Injector Cold-Flow Data (PN 1191403-39)	213
VI-V	LOL Oxidizer-Rich Injector Cold-Flow Data	216
VI-VI	Turbine Simulator Cold-Flow Test Configuration	220
VI-VII	Cold-Flow Test Data Summary	223
VI-VIII	Igniter Cold-Flow Data	229

LIST OF FIGURES

<u>Figure No.</u>		<u>Page</u>
III-1	Preburner Assembly and Instrumentation Schematic	8
III-2	Fuel/Oxidizer-Rich High-Pressure Preburner Assembly	9
III-3	Major Components of Test Assembly	11
III-4	Required Components for Completion of Assembly - Nuts, Bolts, and Seals	12
III-5	Preburner Assembled for Cold-Flow Testing	13
III-6	Injector Manifold Assembly, PN 1191404	15
III-7	Injector Major Propellant Manifold Assembly	17
III-8	Minor Propellant Manifold Assembly, PN 1191403	18
III-9	Fuel-Rich Concentric Vortex Platelet Injector, PN 1191403-39	21
III-10	Typical Bonded Platelet Stack and Machined Body	22
III-11	Fuel-Rich Platelet Assembly	23
III-12	Fuel-Rich Faceplate, Close-Up	25
III-13	Oxidizer-Rich Platelet Assembly	26
III-14	Oxidizer-Rich Concentric Vortex Injector Faceplate Assembly	29
III-15	Fuel-Rich EDM'd Injector Pattern	30
III-16	Fuel-Rich Like-On-Like/Showerhead Injector Components	32
III-17	Oxidizer-Rich EDM'd Injector Pattern	33
III-18	Oxidizer-Rich EDM'd Injector Components	35
III-19	Manifold and Outer Ring Flange Assemblies	36
III-20	Injector Manifold - Minor Propellant	38
III-21	Chamber Assembly (Rev. CDN File 6006)	41
III-22	15-In. Chamber and Liner, PN 1191401	42
III-23	Turbine Simulator Schematic	44
III-24	Turbine Simulator Assembly, PN 1191521	45
III-25	Turbine Simulator	47
III-26	Igniter Assembly	49
III-27	Hydrogen-Oxygen Igniter, PN 1191522	51

LIST OF FIGURES (cont.)

<u>Figure No.</u>		<u>Page</u>
III-28	Detail Drawings of Throats, Main Injector Simulators, Resonator Cavity, and Tuning Blocks	53
III-29	Acoustic Resonator Flange Assembly, PN 1191402, -3, and -4 + Tuning Blocks	56
III-30	Main Injector Simulators, PN 1191402-8, -10, and -11	57
III-31	Fuel- and Oxidizer-Rich Throats, PN 1191402-1 and -2, CDN File 6006	57
III-32	Instrumentation Rake Assembly	59
IV-1	LOX-RP-1 Gas Generator Design Criteria Summary	65
IV-2	State-of-the-Art GG Designs Use Mechanical Mixing to Obtain Uniform Temperature Distribution	66
IV-3	State-of-the-Art GG Designs Use Reverse Flow and Side Outlet Designs to Obtain Uniform Temperature Distributions	67
IV-4	Turbine Nozzle Area History - Titan I First Stage Gas Generator (XLR87-AJ-3)	68
IV-5	Mixture Ratio Influence on Turbine Nozzle Area Reduction - Titan I First Stage Gas Generator	70
IV-6	Fuel-Rich Combustion C* vs Mixture Ratio, Predictions and Test Data	71
IV-7	Fuel-Rich Combustion Model Input, Output, and Design Parameters	73
IV-8	Fuel-Rich Combustion Model Study - Model Development Logic	74
IV-9	Fuel-Rich LO ₂ /RP-1 Combustion Model Logic	75
IV-10	SEA Literature Search Strategy	76
IV-11	Chemical Reaction Sets for Fuel-Rich LO ₂ /RP-1 Combustion Model	77
IV-12	RP-1 Fuel Vapor Cracking Model, Two-Step Global Reaction	77
IV-13	Complete Fuel-Rich Reaction Mechanism	78
IV-14	Screened Fuel-Rich Reaction Mechanism	79
IV-15	Kinetic Mechanisms	80
IV-16	Soot Formation Mechanisms	80

LIST OF FIGURES (cont.)

<u>Figure No.</u>		<u>Page</u>
IV-17	Fuel Vaporization Model	82
IV-18	Fuel-Rich LOX/RP-1 Combustion Model Calibration Using Titan I Data	83
IV-19	Fuel-Rich Combustion Model Comparison with ODE	84
IV-20	Calculated Titan I GG Fuel Vaporization	85
IV-21	Fuel-Rich Combustion Model - Effect of Starting MR	86
IV-22	Predicted Effect of Starting MR on Solid Carbon Formation	88
IV-23	Evidence of Solid Carbon Formation Directly from Liquid-Phase Heating	89
IV-24	Ignition Characteristics of Candidate Materials in an Oxygen Atmosphere	92
IV-25	Low-Cost Test Hardware Fabricated from Standard Commercial Flanges	94
IV-26	Schematic of Detailed Flange Structural Model	95
IV-27	Heat Sink Chamber Stress, Strain, and Cycle Fatigue Limits	96
IV-28	Bolted Joint Analysis Summary Table	97
IV-29	Flange Separation and Seal Cold-Flow Data	99
IV-30	Typical O ₂ /H ₂ Igniter Design	101
IV-31	Results of Fuel-Rich Preburner Ignition Analyses	102
IV-32	Fuel-Rich Preburner Chug Stability Analysis	105
IV-33	Resonator Cavity Sizes for Fuel-Rich Preburner High-Frequency Instability Modes (Tangential, Radial, and Combined)	106
	Fuel-Rich Preburner Longitudinal Instability Modes	107
IV-35	Design Criteria for Non-Freezing Fuel Manifold	109
IV-36	Concentric Vortex Element Flow Schematic	111
IV-37	Fuel-Rich Preburner EDM'd Pattern Design	112
IV-38	Maximum Operating Mixture Ratios for Uncooled Chamber Designs	113

LIST OF FIGURES (cont.)

<u>Figure No.</u>		<u>Page</u>
IV-39	Streak-Resistant Capabilities of Candidate Materials for Fuel-Rich Preburner Design	115
IV-40	Allowable O/F Variance for Required Turbine Inlet Temperature Uniformity	117
IV-41	LOX/RP-1 Preburner Injection Element Rating Criteria	118
IV-42	Comparison of Vortex and LOL Doublet Element	120
IV-43	Typical Parameters Which Control Vortex Element Optimization	121
IV-44	Geometric Considerations Influencing Element Packaging	122
IV-45	Chamber Diameter Selection Based on Contraction Ratio and Standard Pipe Sizes	123
IV-46	Fuel-Rich Preburner Vaporization Profile Prediction Using Priem Vaporization Model	126
IV-47	Prediction Fuel-Rich Preburner Mixing Profile	127
IV-48	Fuel Preheating Influence on Vaporization Efficiency	128
IV-49	Ignition Characteristics of Candidate Materials	135
IV-50	Effect of Chromium on the Oxidation Resistance of Steel in a Normal Combustion Atmosphere	136
IV-51	Results of Oxidizer-Rich Preburner Ignition Analyses (Flowrate Versus Mixture Ratio)	138
IV-52	Oxidizer-Rich LOL Injector Chugging Analysis	139
IV-53	Oxidizer-Rich Concentric Vortex Injector Chugging Analysis	140
IV-54	Oxidizer-Rich LOX/RP-1 Preburner Predicted Longitudinal Instability Modes	142
IV-55	Oxidizer-Rich LOX/RP-1 Preburner Potential Tangential and Radial Instability Modes	143
IV-56	Stability-Related Instrumentation	144
IV-57	Chamber Wall Surface Heating Rate of 304 Stainless Steel Pipe	146
IV-58	Transient Heating Analyses for Nickel, Copper, and Aluminum Oxide	147

LIST OF FIGURES (cont.)

<u>Figure No.</u>		<u>Page</u>
IV-59	Wall Temperature Profiles for an Al ₂ O ₃ -Lined Steel Chamber	148
IV-60	Comparison of Required Mixing Efficiency of Fuel-Rich and Oxidizer-Rich Injectors	151
IV-61	Conceptual Drawing of Element Candidates	152
IV-62	Evolution of Oxidizer-Rich LOL Element Pattern for High-Pressure Preburner Application	154
IV-63	Effect of Gas Density on Drop Size	156
IV-64	Manifold and Element Pattern Layout of Selected EDM'd Design	160
IV-65	Coaxial Vortex Injector Element Configuration	161
V-1	Standard Flange Sizes	164
V-2	Fuel-Rich EDM'd Injector After Braze Repair with Reinforcing Ring	166
V-3	Fuel-Rich Vortex Injector After Brazing of Faceplate	168
V-4	Platelet Injectors Following Removal of Faceplates	169
V-5	Ultrasonic Inspection of Axial Welds on Unlined L* Sections (PN 1191401)	173
V-6	Ultrasonic Inspection of Oxidizer-Rich EDM'd Injector PN 1193105-19)	175
V-7	Oxidizer-Rich EDM'd Injector Before Final Weld Assembly	176
V-8	Oxidizer Injection Orifice Dimensions Defined	177
VI-1	Swirler Element Designs Selected for Testing	180
VI-2	Six-Vane Swirler Spray, $\Delta P = 2.02\text{M N/m}^2$ (293 psid), $\dot{w} = 0.64$ kg/sec (1.40 lb/sec) H ₂ O (Configuration 1)	182
VI-3	Six-Vane Swirler Spray, $\Delta P = 2.68\text{M N/m}^2$ (390 psid), $\dot{w} = 0.64$ kg/sec (1.40 lb/sec) H ₂ O (Configuration 3)	183
VI-4	Six-Vane Swirler Spray, $\Delta P = 2.19\text{M N/m}^2$ (318 psid), $\dot{w} = 0.64$ kg/sec (1.41 lb/sec) H ₂ O (Configuration 1)	184
VI-5	Six-Vane Swirler Pressure Drop Data	185
VI-6	Three-Vane Swirler Pressure Drop Data	186
VI-7	Major Circuit of Oxidizer-Rich Preburner, $\Delta P = 2.76\text{M N/m}^2$ (400 psid)	187

LIST OF FIGURES (cont.)

<u>Figure No.</u>		<u>Page</u>
VI-8	Major Circuit of Oxidizer-Rich Preburner, $\Delta P = 1.38\text{M N/m}^2$ (200 psid)	190
VI-9	Minor Circuit (Fuel) of Oxidizer-Rich Preburner, $\Delta P = 2.76\text{M N/m}^2$ (400 psid)	191
VI-10	Minor Circuit (Fuel) of Oxidizer-Rich Preburner, $\Delta P = 1.38\text{M N/m}^2$ (200 psid)	192
VI-11	Fuel-Rich Vortex Injector Cold-Flow, Oxidizer Circuit, $\Delta P = 2.07\text{M N/m}^2$ (300 psid), Design Mod. 3 Single-Element Flow	195
VI-12	Fuel-Rich Vortex Injector Cold-Flow, Fuel Circuit, $\Delta P = 2.07\text{M N/m}^2$ (300 psid), Design Mod. 3, Single-Element Flow	196
VI-13	Fuel-Rich Vortex Injector Cold-Flow, Oxidizer Circuit, $\Delta P = 2.07\text{M N/m}^2$ (300 psid), Design Mod. 4, Single-Element Flow	198
VI-14	Fuel-Rich Vortex Injector Cold-Flow, Fuel Circuit, $\Delta P = 2.07\text{M N/m}^2$ (300 psid), Design Mod. 4, Single-Element Flow	199
VI-15	Fuel-Rich Vortex Injector Cold-Flow, Both Circuits, $\Delta P = 2.07\text{M N/m}^2$ (300 psid), Design Mod. 4 Single Element Flow	200
VI-16	Cold-Flow Procedures For All Injector Assemblies	202
VI-17	LOL EDM'd Fuel-Rich Injector Cold-Flow (Oxidizer Circuit, Fuel Circuit, Both Circuits)	203
VI-18	Fuel-Rich Injector Cold-Flow - Fuel Circuit	206
VI-19	Fuel-Rich Injector Cold-Flow - Oxidizer Circuit	207
VI-20	Fuel-Rich Injector Cold-Flow - Both Circuits	208
VI-21	Oxidizer-Rich Vortex Injector - Oxidizer Circuit (Major); Fuel Circuit (Minor)	211
VI-22	Oxidizer-Rich Vortex Injector - Both Circuits	212
VI-23	LOL Oxidizer-Rich Injector, Oxidizer Circuit, $\Delta P = 0.15\text{M N/m}^2$ (22 psid)	214
VI-24	Oxidizer-Rich LOL Injector Cold-Flow (Fuel Circuits Only)	215
VI-25	Preburner Assembly Cold-Flow Test Setup	218
VI-26	Preburner Assembly GN ₂ Cold-Flow Setup Schematic	219

LIST OF FIGURES (cont.,)

<u>Figure No.</u>		<u>Page</u>
VI-27	Mach Number Corrections and Nomenclature for Cold-Flow Testing	225
VI-28	Pressure Ratio Versus Percent Open Area for Oxidizer- and Fuel-Rich Turbine Simulators	227
VI-29	Cold-Flow Supply Pressure Versus Flowrate for H ₂ and O ₂	232

I. INTRODUCTION

Previous NASA-sponsored studies have shown that advanced high-pressure, high-density fuel engines will be required for future earth-to-orbit vehicles. These engines will be in the 2668.8 kN (600,000 lbf) range, will use liquid oxygen and hydrocarbon fuels, and will operate at chamber pressures of about 27576 kPa (4000 psia). Most likely, they will require a staged-combustion turbopump drive cycle. With use of this cycle, the energy needed to pump the propellants to high pressures is derived by burning a portion of the propellants in high-pressure preburners and passing the hot gases from the preburners through the turbines of the fuel and oxidizer turbopumps.

Preliminary engine design studies (NASA CR-135141) have shown that in order to obtain sufficient turbine drive power without exceeding acceptable materials-limited turbine inlet temperatures, separate fuel-rich and oxidizer-rich preburners are required to drive the fuel turbopump and oxidizer turbopump, respectively. The use of separate fuel- and oxidizer-rich preburners also eases seal design problems in the turbopumps since there is fuel-rich turbine drive gas in the fuel turbopump turbine and oxygen-rich turbine drive gas in the liquid oxygen turbopump turbine.

These preburners must operate at pressures of 27576 to 48258 kPa (4000 to 7000 psia) and at extremely fuel-rich (O/F \approx 0.25:1) and oxidizer-rich (O/F \approx 40:1) mixture ratios in order to provide turbine drive gases having temperatures in the 889-944°K (1600-1700°R) range.

The necessity of advancing the existing LOX/hydrocarbon preburner technology becomes even more apparent in the light of previous development experience. Fuel-rich hydrocarbon preburners have experienced two specific problems: (1) reduced combustion efficiency due to non-equilibrium, forward-kinetic-rate-limited performance, and (2) hydrocarbon polymer formation and solid carbon deposition adversely affecting (fouling and reducing) gas turbine efficiency. The primary problem with oxidizer-rich preburners has been combustion chamber metal wall ignition in the oxidizing environment due to hot streaks.

A. GAS GENERATOR/PREBURNER HISTORY

Past gas generator (GG) and preburner programs provide an understanding of the problems associated with high-pressure preburner testing. For example, all previous LO₂/RP-1 gas generators have been operated fuel-rich and have experienced carbon deposition problems to some degree. With increased flight time, ALRC's Titan I Stage I and II GG's have consistently encountered progressive turbine throat area reduction due to carbon deposition and have had to be preprogrammed for this effect to ensure adequate turbine power throughout the flight. Total firing time for these booster engines is

I, A, Gas Generator/Preburner History (cont.)

typically 150 seconds. What was acceptable carbon deposition for the limited firing life of these engines is probably excessive for future long-life reusable LO₂/HC preburners.

Typical combustion efficiency for these gas generators has been as low as 80%, based on equilibrium combustion. Two factors which contribute to the apparent poor combustion efficiency are forward-rate kinetics, which limits the energy available at the preburner operating conditions, and incomplete vaporization of the fuel-rich propellant.

Combustion stability has been a major developmental concern, as exemplified by the F-1 booster engine GG stability problem. Due to the power balance requirement of this engine, a turbine inlet gas temperature in excess of 833°K (1500°F) was required. However, rough combustion was encountered at the required higher operating gas temperature. The transition to rough combustion generally occurred at gas temperatures between 833 and 889°K (1500 and 1600°F). Stability was also dependent upon injector pattern, test flowrates, and even upon as subtle a change as two different injectors of nominally the same design.

Historically, the achievement of uniform gas temperatures at the turbine inlet has also been a problem, and elaborate gas mixing devices have been required to prevent damage to the turbine.

All previous operational LO₂/RP-1 engines have used fuel-rich gas generators for the turbopump drive, and none have operated in the pressure range of interest. Staged-combustion preburner technology has been limited to LO₂/LH₂ propellants, and oxidizer-rich technology has been limited to LO₂/LH₂ and storable propellants.

B. PROGRAM OBJECTIVE

The objective of this program was to provide a technology base for the design of high-pressure preburners using LOX/RP-1 propellants, in accordance with the design and operating requirements outlined in Table I-I. This report documents the design and fabrication of the test hardware required to provide this technology base. Testing and test data analyses were accomplished during a follow-on activity. The required hardware was designed on the basis of analytical model predictions which established design criteria and test plan scope. Injector design was stressed as a means for controlling desired combustion energy release rates, gas temperature distribution, stability, and ignition response.

TABLE I-I. PREBURNER DESIGN AND OPERATING REQUIREMENTS

<u>Parameter</u>	<u>Design</u>	<u>Range of Interest</u>
Chamber Pressure	TBD*	13,788 to 48,258 kPa (2000 to 7000 psia)
Mixture Ratio		
Fuel-Rich	0.22	0.2 to 0.25**
Oxidizer-Rich	45	35 to 45
Performance	> 98% ERE	
Combustion Length	Minimum to meet performance requirement	
Effluent Gas Tempera- ture Uniformity	± 28°K (± 50°R)	
Combustion Pressure Stability	< ± 5% Pc variations	
Service Life	Minimum of 10 hrs 300-500 firings	
Total Propellant Flow	56.7 kg/sec (125 lb/sec)	
Propellant Flow, Oxidizer- Rich Preburner	39.9 kg/sec (88 lb/sec)	
Propellant Flow, Fuel- Rich Preburner	16.8 kg/sec (37 lb/sec)	

*13,788 to 17,235 kPa
(2000 to 2500 psia selected for this demonstration program)

**Increased from 2.5 to 3.5 following Task I analyses

I, B, Program Objective (cont.)

The Fuel/Oxidizer-Rich, High-Pressure Preburners Program was accomplished and reported upon in accordance with the following eight tasks:

- Task I - Preburner Analysis and Conceptual Design
- Task II - Preburner Design Details
- Task III - Detailed Design of Turbine and Main Injector Simulators
- Task IV - Fabrication of Test Hardware
- Task V - Test Plan
- Task VI - Hardware Delivery
- Task VII - Reporting
- Task VIII - Product Assurance

II. SUMMARY

This contract provided for the analysis, design, fabrication, and cold-flow acceptance testing of components required for the hot-fire testing of high-pressure fuel-rich and oxidizer-rich preburners suitable for a staged-combustion engine operating with LOX and RP-1 propellants. These components included bipropellant preburner injectors, combustion chambers, turbine and main injector simulators, mixing rings, and throats.

Conceptual combustor designs utilizing staged-propellant injection (stoichiometric combustion with downstream dilution), hot core with off-MR barrier for cooling, and uniform mixture ratio propellant injection schemes were considered in Task I.

Detailed analyses of the kinetics of carbon formation, propellant mixing rates, and chamber wall heat loads indicated that the uniform mixture ratio concept, augmented by a simple secondary mechanical mixing ring, is the best approach for providing safe, stable combustion with a minimum quantity of solid carbon generation.

Two fuel-rich and two oxidizer-rich injectors of the uniform mixture ratio type were designed, fabricated, and cold-flow acceptance-tested. One fuel- and one oxidizer-rich injector design employed a combination of hydraulically atomized Like-on-Like (LOL) and shower elements. The other fuel-rich and other oxidizer-rich injector design utilized mechanical atomization obtained from concentric vortex elements. All approaches relied upon the self-atomization of the individual propellants and avoided contact of RP-1 and LOX streams prior to atomization to preclude freezing of the fuel prior to combustion.

A secondary hot-gas mixer, consisting of a simple, sharp-edged orifice plate located in the flow stream approximately 1.3 chamber diameters downstream of the injector face, was predicted to be necessary to obtain the $\pm 28^\circ\text{K}$ ($\pm 50^\circ\text{F}$) gas temperature uniformity goals of the program. The gas temperature nonuniformity was predicted to vary as much as ± 56 to $\pm 111^\circ\text{K}$ (± 100 to $\pm 200^\circ\text{F}$) without the use of this mixer.

A simple-to-build heat sink combustion chamber was designed to allow testing with and without the secondary mixing orifice. The chamber contained an easily replaceable pipe liner which allowed the mixer to be located in different positions along the chamber axis. A gas sampling and temperature measurement rake was designed to evaluate the gas composition and temperature uniformity across the stream. The use of a flanged rake section allowed these measurements to be made at different mixing length distances from either the injector or the secondary mixing orifice. The flanged rake section contained provision for two probes located 90° apart to provide a total of ten gas temperature and four gas composition samples.

II, Summary (cont.)

A turbine simulator containing removable and adjustable simulated turbine blades was designed, fabricated and adjusted in cold flow to provide an upstream-to-downstream pressure ratio of ≈ 1.5 . Different blade designs were provided for fuel- and oxidizer-rich operation.

A main injector simulator plate containing numerous orifices was designed to simulate the pressure drop and potential carbon particle plugging of the main injector of a staged-combustion engine cycle.

The preburner assembly was subjected to proof and leak testing at 24,129 kPa (3500 psia) and to cold-flow calibration testing with both water (to simulate liquid propellants) and with GN_2 (to simulate gaseous combustion products in the turbine and main injector simulator).

This report contains the design details, documentation of the fabrication processes, and the results of the cold-flow testing. The test results are documented in Contract NAS 3-22647, which was a follow-on test program.

III. DESCRIPTION OF DESIGNS AND DELIVERED EXPERIMENTAL TEST HARDWARE

This section of the report documents the hardware that was designed, fabricated, and delivered for the hot-fire test program. The detailed analyses which support the design selection are provided in Section IV of this report.

The documentation of the test hardware is accomplished by the fabrication drawings, photographs of the components, and a brief description of the design and its functions.

A. ASSEMBLY

The preburner assembly, shown schematically in Figure III-1 and in detail in Figure III-2, contains the following major components: injector, acoustic resonator ring, lined and unlined chamber sections of different lengths, throat, turbine simulator, main injector simulator, and igniter. The igniter, chambers, and portions of the injector, turbine simulator, main injector simulator, and resonator are common to both the fuel-rich and oxidizer-rich preburner assemblies. Different injector faceplates, turbine simulator blades, main injector simulators, and throats are provided to accommodate the specific flowrates of the fuel- and oxidizer-rich design conditions. Figure III-3 identifies the major components of the test assembly by part number and function and indicates which items are common to both fuel- and oxidizer-rich operation.

An instrumentation rake assembly (PN 1191411) was designed to measure gas temperature profiles and remove gas samples from the stream. This item was not fabricated under this contract.

The assembly drawing (1191408), shown in Figure III-2, requires the use of the major propellant injector manifold, one of four faceplates, and the resonator cavity flange, stacked in the sequence shown. The relative positions of all components downstream of the resonator flange are mechanically interchangeable. They can be assembled in any sequence, and any item can be omitted or replaced by another flanged assembly. Figure III-4 identifies the nuts, bolts, seals, and inlet connections required to complete the assembly. Figure III-5 shows a photograph of a typical assembly taken during one of the cold-flow tests. The assembly shown is for the fuel-rich testing.

B. INJECTOR ASSEMBLY

The injector is comprised of two subassemblies: a major propellant manifold, and a faceplate which contains the minor propellant manifold and the propellant injection pattern. The major propellant manifold can be utilized for either fuel- or oxidizer-rich testing. Any one of four faceplates fabricated can be bolted to the major propellant manifold to provide an injector assembly.

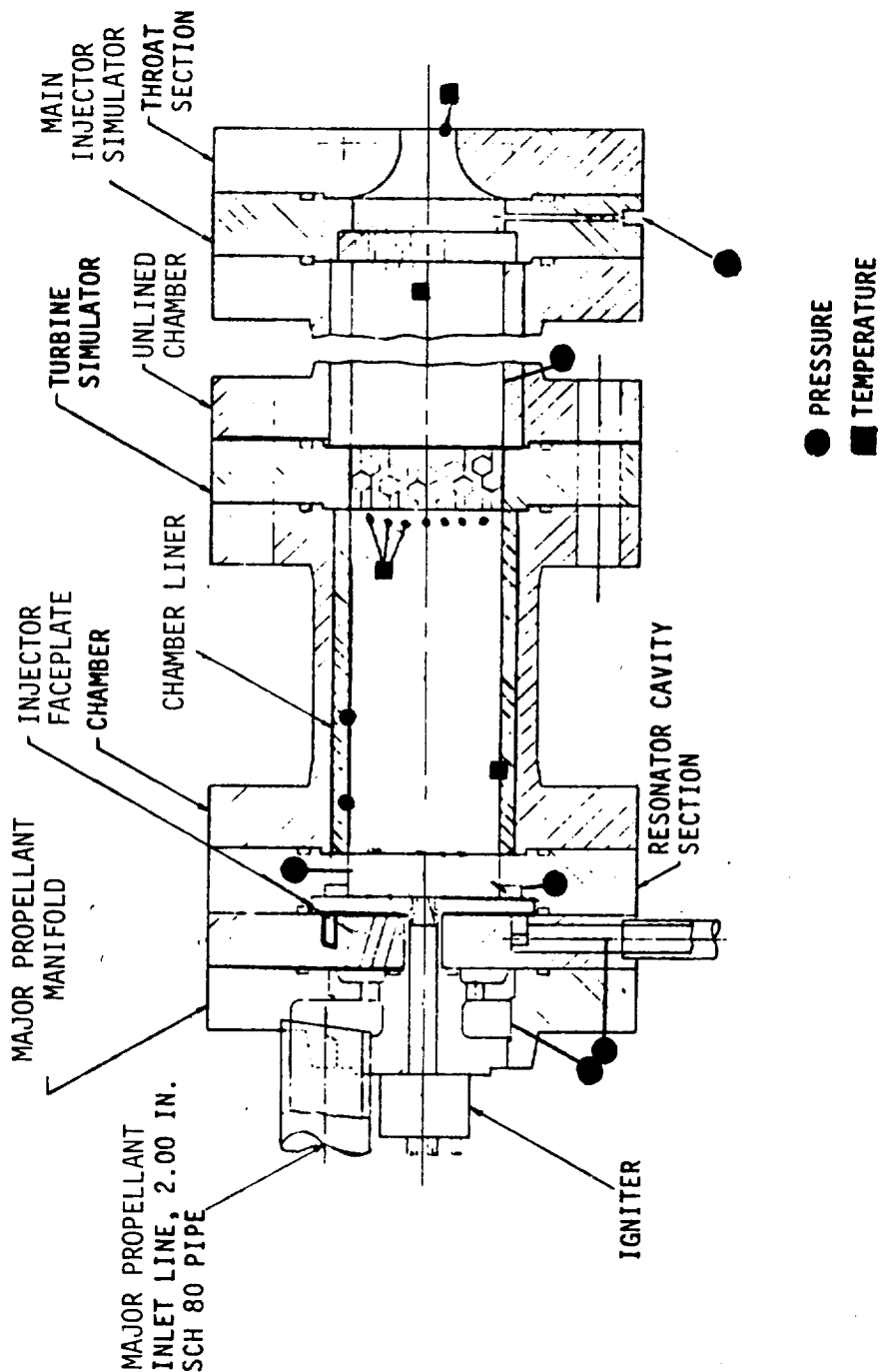
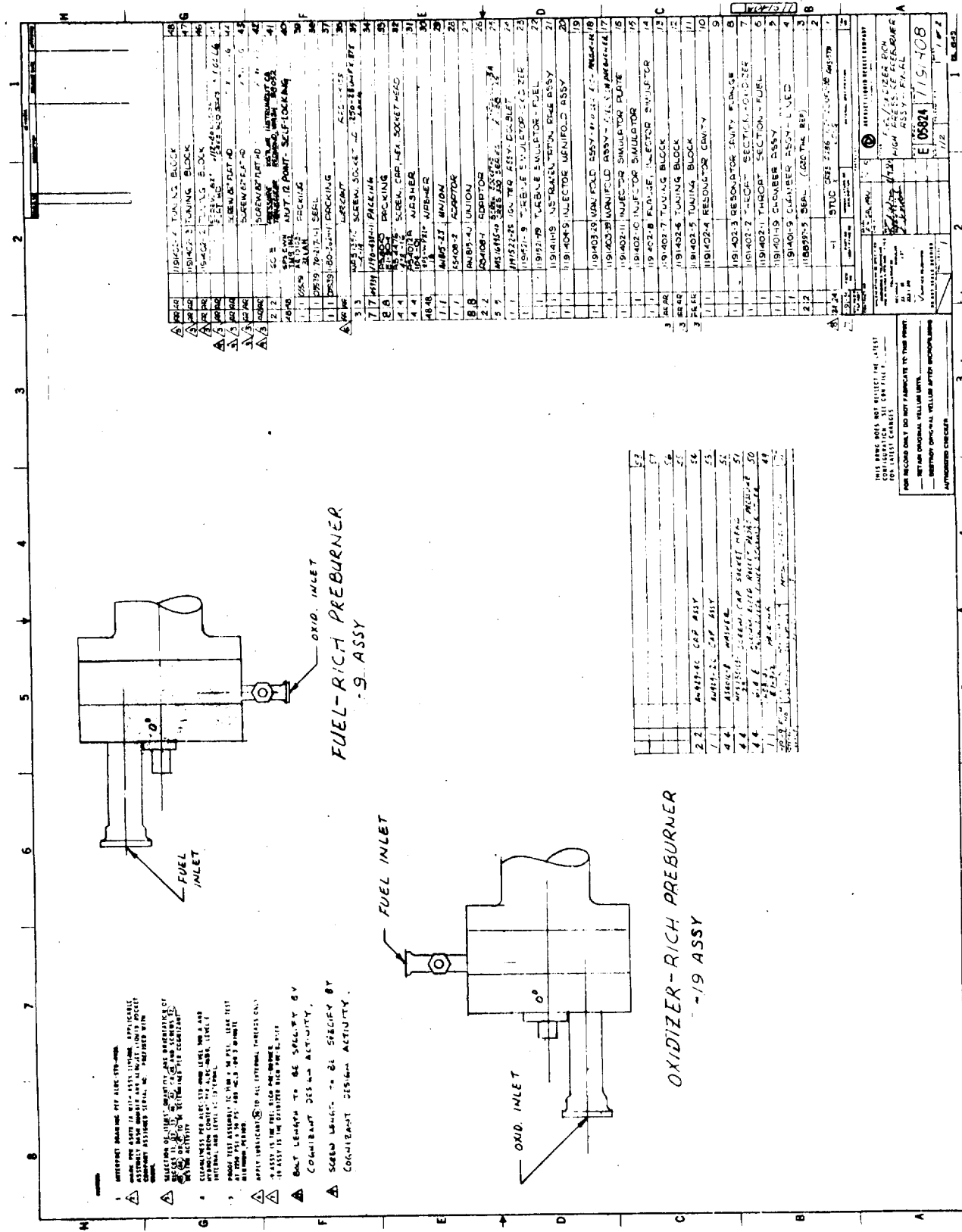


Figure III-1. Preburner Assembly and Instrumentation Schematic



- 1. INTERPRET DRAWING REF. AEGIS 179-1000.
- 2. MAKE ONE COPY OF THIS DRAWING. SPECIFICALLY, MAKE ONE COPY FOR THE AIR FORCE AND ONE FOR THE AIR FORCE. THE AIR FORCE COPY SHOULD BE KEPT IN THE AIR FORCE FILE.
- 3. CHECK FOR CORRECTIONS AND REVISIONS. IF ANY CORRECTIONS ARE MADE, THEY SHOULD BE MADE IN THE ORIGINAL DRAWING AND IN ALL COPIES.
- 4. EXAMINE THIS DRAWING FOR ANY ERRORS. IF ANY ERRORS ARE FOUND, THEY SHOULD BE REPORTED TO THE DESIGNER IMMEDIATELY.
- 5. THIS DRAWING IS THE PROPERTY OF THE AIR FORCE. IT IS TO BE KEPT IN THE AIR FORCE FILE AND NOT TO BE REPRODUCED OR COPIED WITHOUT THE AUTHORITY OF THE AIR FORCE.
- 6. APPLY INDICATED TO ALL EXTERNAL SURFACES ONLY.
- 7. THIS ASSY IS THE FUEL-RICH ONE-WHOLE.
- 8. THIS ASSY IS THE OXIDIZER-RICH ONE-WHOLE.
- 9. ONLY REMARKS TO BE SPECIFIED BY CONTRACTOR DESIGN ACTIVITY.
- 10. SCALE LENGTHS TO BE SPECIFIED BY CONTRACTOR DESIGN ACTIVITY.

FUEL-RICH PREBURNER -9 ASSY

OXIDIZER-RICH PREBURNER -19 ASSY

22	ANALOG CAP ASSY	1
23	ANALOG CAP ASSY	1
24	ANALOG CAP ASSY	1
25	ANALOG CAP ASSY	1
26	ANALOG CAP ASSY	1
27	ANALOG CAP ASSY	1
28	ANALOG CAP ASSY	1
29	ANALOG CAP ASSY	1
30	ANALOG CAP ASSY	1
31	ANALOG CAP ASSY	1
32	ANALOG CAP ASSY	1
33	ANALOG CAP ASSY	1
34	ANALOG CAP ASSY	1
35	ANALOG CAP ASSY	1
36	ANALOG CAP ASSY	1
37	ANALOG CAP ASSY	1
38	ANALOG CAP ASSY	1
39	ANALOG CAP ASSY	1
40	ANALOG CAP ASSY	1
41	ANALOG CAP ASSY	1
42	ANALOG CAP ASSY	1
43	ANALOG CAP ASSY	1
44	ANALOG CAP ASSY	1
45	ANALOG CAP ASSY	1
46	ANALOG CAP ASSY	1
47	ANALOG CAP ASSY	1
48	ANALOG CAP ASSY	1
49	ANALOG CAP ASSY	1
50	ANALOG CAP ASSY	1
51	ANALOG CAP ASSY	1
52	ANALOG CAP ASSY	1
53	ANALOG CAP ASSY	1
54	ANALOG CAP ASSY	1
55	ANALOG CAP ASSY	1
56	ANALOG CAP ASSY	1
57	ANALOG CAP ASSY	1
58	ANALOG CAP ASSY	1
59	ANALOG CAP ASSY	1
60	ANALOG CAP ASSY	1
61	ANALOG CAP ASSY	1
62	ANALOG CAP ASSY	1
63	ANALOG CAP ASSY	1
64	ANALOG CAP ASSY	1
65	ANALOG CAP ASSY	1
66	ANALOG CAP ASSY	1
67	ANALOG CAP ASSY	1
68	ANALOG CAP ASSY	1
69	ANALOG CAP ASSY	1
70	ANALOG CAP ASSY	1
71	ANALOG CAP ASSY	1
72	ANALOG CAP ASSY	1
73	ANALOG CAP ASSY	1
74	ANALOG CAP ASSY	1
75	ANALOG CAP ASSY	1
76	ANALOG CAP ASSY	1
77	ANALOG CAP ASSY	1
78	ANALOG CAP ASSY	1
79	ANALOG CAP ASSY	1
80	ANALOG CAP ASSY	1
81	ANALOG CAP ASSY	1
82	ANALOG CAP ASSY	1
83	ANALOG CAP ASSY	1
84	ANALOG CAP ASSY	1
85	ANALOG CAP ASSY	1
86	ANALOG CAP ASSY	1
87	ANALOG CAP ASSY	1
88	ANALOG CAP ASSY	1
89	ANALOG CAP ASSY	1
90	ANALOG CAP ASSY	1
91	ANALOG CAP ASSY	1
92	ANALOG CAP ASSY	1
93	ANALOG CAP ASSY	1
94	ANALOG CAP ASSY	1
95	ANALOG CAP ASSY	1
96	ANALOG CAP ASSY	1
97	ANALOG CAP ASSY	1
98	ANALOG CAP ASSY	1
99	ANALOG CAP ASSY	1
100	ANALOG CAP ASSY	1

THIS DRAWING IS NOT TO BE USED FOR CONSTRUCTION OF THE PREBURNER. IT IS TO BE USED FOR IDENTIFICATION OF PARTS ONLY. FOR RECORD ONLY. DO NOT FABRICATE TO THIS DRAWING. RETURN ORIGINAL YELLOW UNITS. RETURN ORIGINAL YELLOW PARTS ENCLOSURES. APPROVED CHECKER

Figure III-2. Fuel/Oxidizer-Rich High-Pressure Preburner Assembly (Sheet 1 of 2)

ORIGINAL PAGE IS OF POOR QUALITY

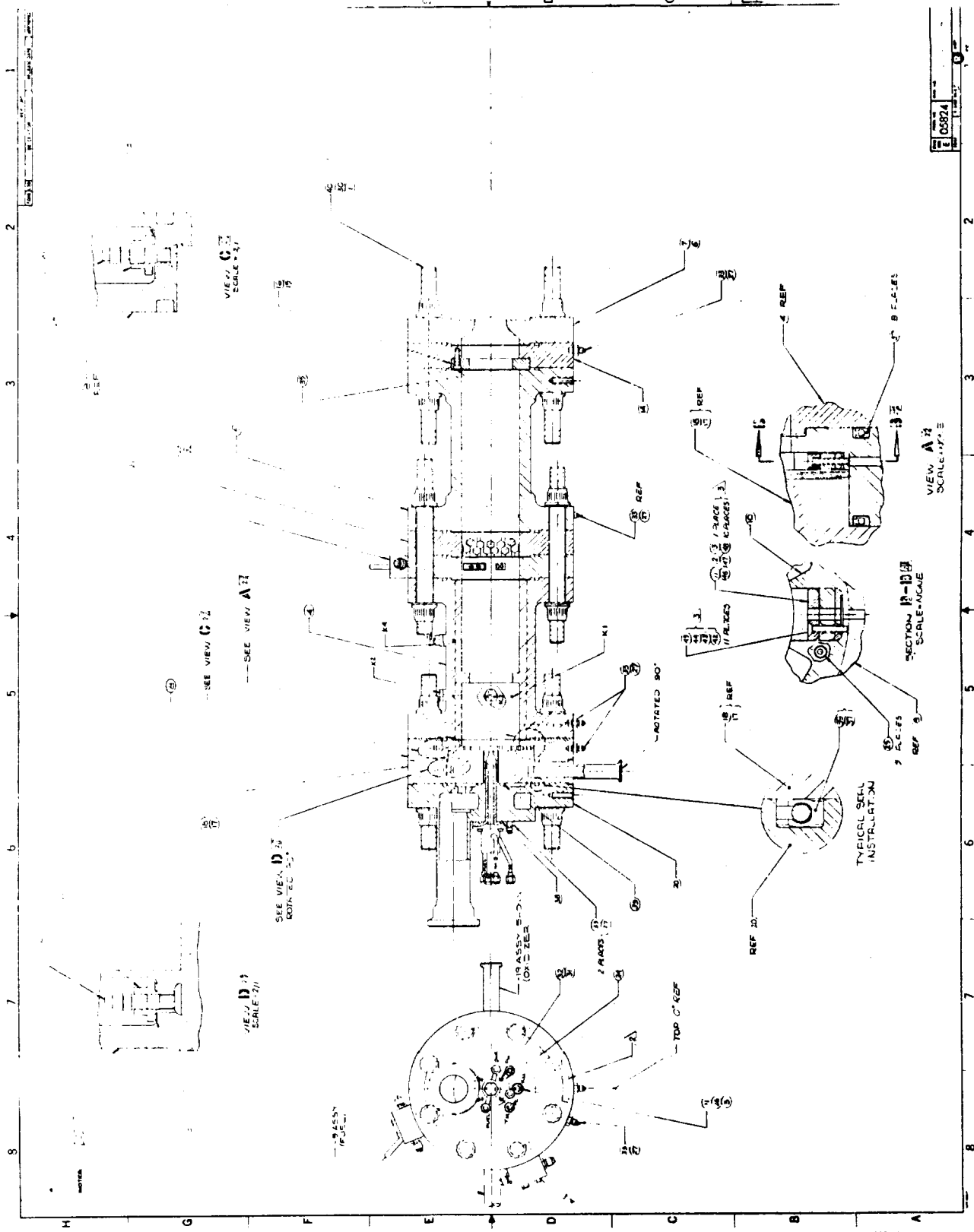


Figure III-2. Fuel/Oxidizer-Rich High-Pressure Preburner Assembly (Sheet 2 of 2)

	<u>Common Hardware</u>	<u>Specialized Hardware</u>	
	Fuel- and Oxidizer-Rich Operation	Fuel-Rich	Oxidizer-Rich
Injectors	Major Propellant Manifold 1191404	Faceplate 1191403-19 (Platelet) 119305-19 (EDM)	Faceplate 1191403-9 (Platelet) 1193105-9 (EDM)
Resonator	Flanged Assembly 1191402	Variable Cavity Dim.	Variable Cavity Dim.
Chambers	Lined Long 1191401-29 Lined Short 1191401-9 Unlined Long 1191401-39 Unlined Short 1191401-19		
Throat		Flanged Assembly 1191402-1	Flanged Assembly 1191402-2
Turbine Simulator	Flanged Retainer 1191521	Assembly Containing Blades 1191521-19	Assembly Containing Blades 1191521-9
Main Injector Simulator	Flanged Assembly with "O" ΔP Ring 1191402-15	Fuel ΔP Plate 1191402-10	Oxidizer ΔP Plate 1191402-11
Igniter	1191522		

Figure III-3. Major Components of Test Assembly

Function	Size	Type	Part No.	Item No.	Material	Quantity		Torque	Lube
						Assy	Total Prog.		
Chamber Nuts	1.125-12 UNJF 38	12 Pt 90°	1WN 1M 9 1812	40	Alloy Steel	48	112	475 ±25 ft-lb	S-122 or Equivalent
Washers, Chamber	1.125	Flat High Strength	WP-27-18	10	A286	48	120		
Studs Chamber Length Short Med. Long	1.125-12 UNJF 1.125-12 UNJF 1.125-12 UNJF		1191408-1 1191408-1 1191408-1	1	A286	24	68		
Injector Internal	.500-20 UNF 1.75 in. long	Socket Int.	NAS 1351C8-28	51	Cres	4	16	Hand Tight	
Resonator Tune Block Screw	.112-40 UNC3A 1.10 in. long	82° Flat Head		45	Cres	11	2100	Hand Tight	
Resonator Ring	.112-40 UNC3A 0.38 in. long	Socket Int.		25	Cres	5	100	Hand Tight	
Igniter Flange	.250-38 UNF 1.00 in. long	Socket Int.	NAS 1351C-4-16	32	Cres 80KSI Min Ty	4	16	110 ±10 in.-lb	S-122
Rake Flange Rake Probe	.250-28UNF 2.001 .112-40 x .38	Socket			Cres	Same as Resonator		75 ±10 in.-lb	S-122
Inj. Sim. Plate	.250-28 UNJF 0.750 in. long	Socket Int.	NAS 1351C-4-12	35		3	24	Hand Tight	
Jack Out	.625-18 UNF2A 3.00 in. long	Socket or Hex Head	Std.		Any Steel Alloy	4	6	As Req'd	
Washer Injector Int.	.500	Plain Flat	AS 4012-B	52	Cres	4	16	-	
Screw Proof Press	.750-16 UNF 2.00 in. long	Hex or Socket Head	Std.		Any Steel Alloy	8	16	500 ±25 in.-lb	S-122
Igniter Washer	.250	Plain Flat	AS 4012A 104-01	31	Cres	4	16	-	
Rake Probe Nuts	.112-40	Hex			Cres	8	50	Hand Tight	

NUTS & BOLTS

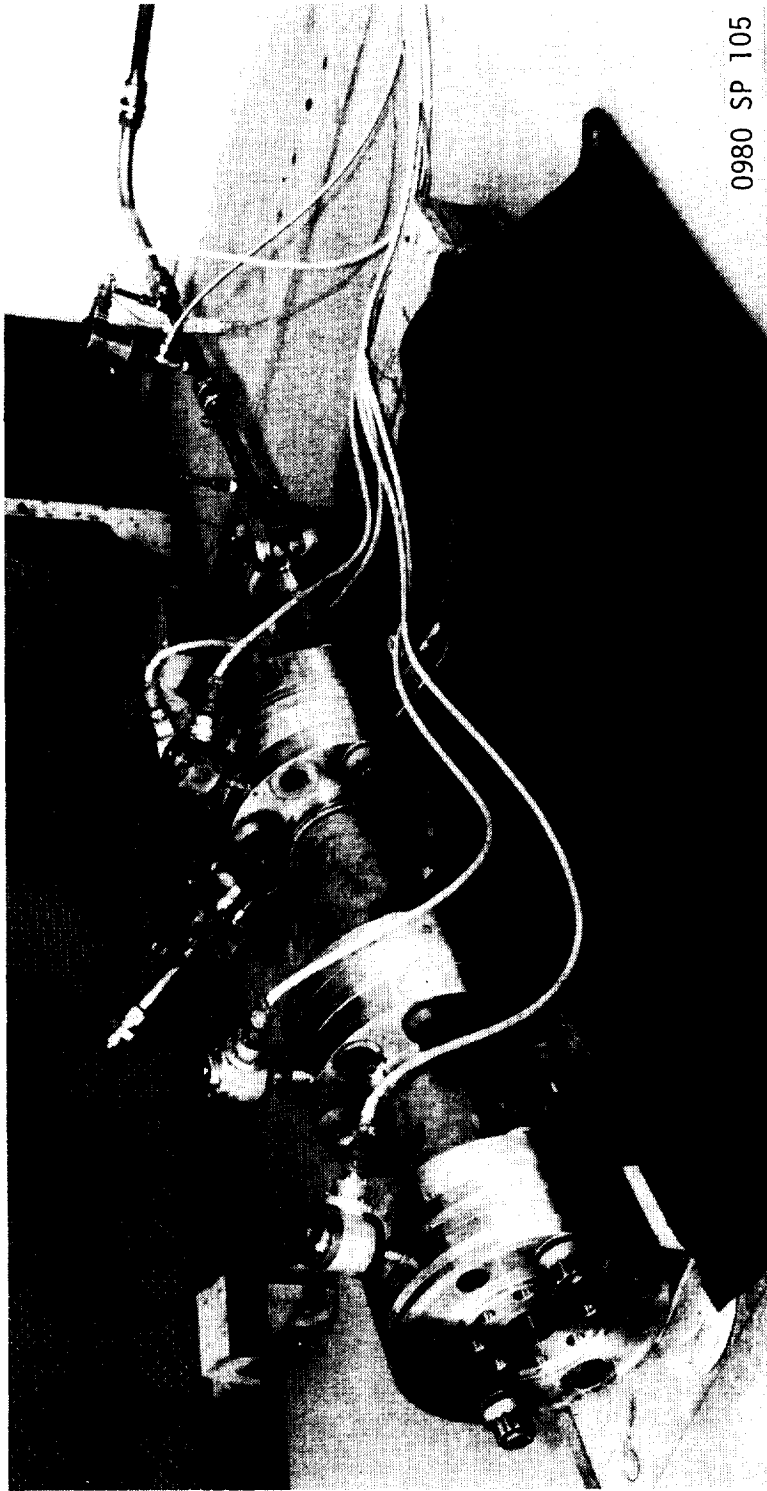
Seals Function	Type	Size	Material	Source	Part No.	Item No.	Assy	Total Program
Chamber Flange	RACO Face	1/4	Tef/SS	Fluorocarbon	1190438-1-1	53	7	30
Chamber Flange	RACO Face	3/16	Tef/SS	Fluorocarbon	1180362-1-1	37	1	25
Igniter Flange	RACO Face	1/8	Tef/SS	Fluorocarbon	1170217-1-1	38	1	25
Injector Internal	Omni Shaft	3/16	Tef/SS	Fluorocarbon	AR10103321AH	39	1	25
Spark Plug External							1	12
Aft Closure	O-Ring	1.50	Neoprene or Butyl	Parker	2-118		1	12
Kistler Boss	Crush	.03	Cu	ALRC	1188597-5	3	2	8
Rake	RACO	3/16	Tef/SS	Fluorocarbon	1160121-1-1		2	25
Press Taps All	O-Ring		Teflon	ALRC J	ASR040EL904	33	7	
Drain Major Prop.	O-Ring		Teflon	ALRC J	ASR040EL902	49	1	
Drain Hot Gas								
Inlet Line Major	Crush	2" Sch 80	SS	Greyloc			1	6
Inlet Line Minor	Crush	1" Sch 80	SS	Greyloc			1	6

SEALS

Press Taps	Union	1/4	SS	ALRC J	AN 8154J	27	7	
Inlet Lines	Greyloc	2" Sch 80 1" Sch 80	304 or 316	Greyloc	2GR-2042822		1	2
			304 or 316		1GR-1159524		1	4
Drain Plug Liq.	Union	1/8	SS	ALRC J	AN 8152J	29	1	2
Drain Plug Gas	AN Large Head	1/4						

INLETS & CONNECTIONS

Figure III-4. Required Components for Completion of Assembly, Nuts, Bolts and Seals



0980 SP 105

Figure III-5. Preburner Assembled for Cold-Flow Testing

ORIGINAL PAGE IS
OF POOR QUALITY

III, B, Injector Assembly (cont.)

1. Major Propellant Manifold

The major propellant manifold, shown in the drawing of Figure III-6 and the photograph of Figure III-7, is fabricated of 304 stainless steel. This component receives the major propellant through a 5-cm (2-in.) Schedule 80 pipe which contains a Greyloc 2GR20 hub welded on one end. The propellant flows from the inlet pipe into an annular distribution plenum and discharges through twelve 1.4-cm (0.553-in.) diameter holes, as shown in Figure III-7. The attachment of the faceplate forms a second plenum between the two subassemblies. The major propellant injection elements are fed from this second flow-distribution plenum.

The major manifold also contains a centrally located port which receives the igniter. Additional appropriately positioned pressure measurement and drain ports are provided. Four 0.75-10-UNC bolt holes are provided on the back face for mounting to the test stand.

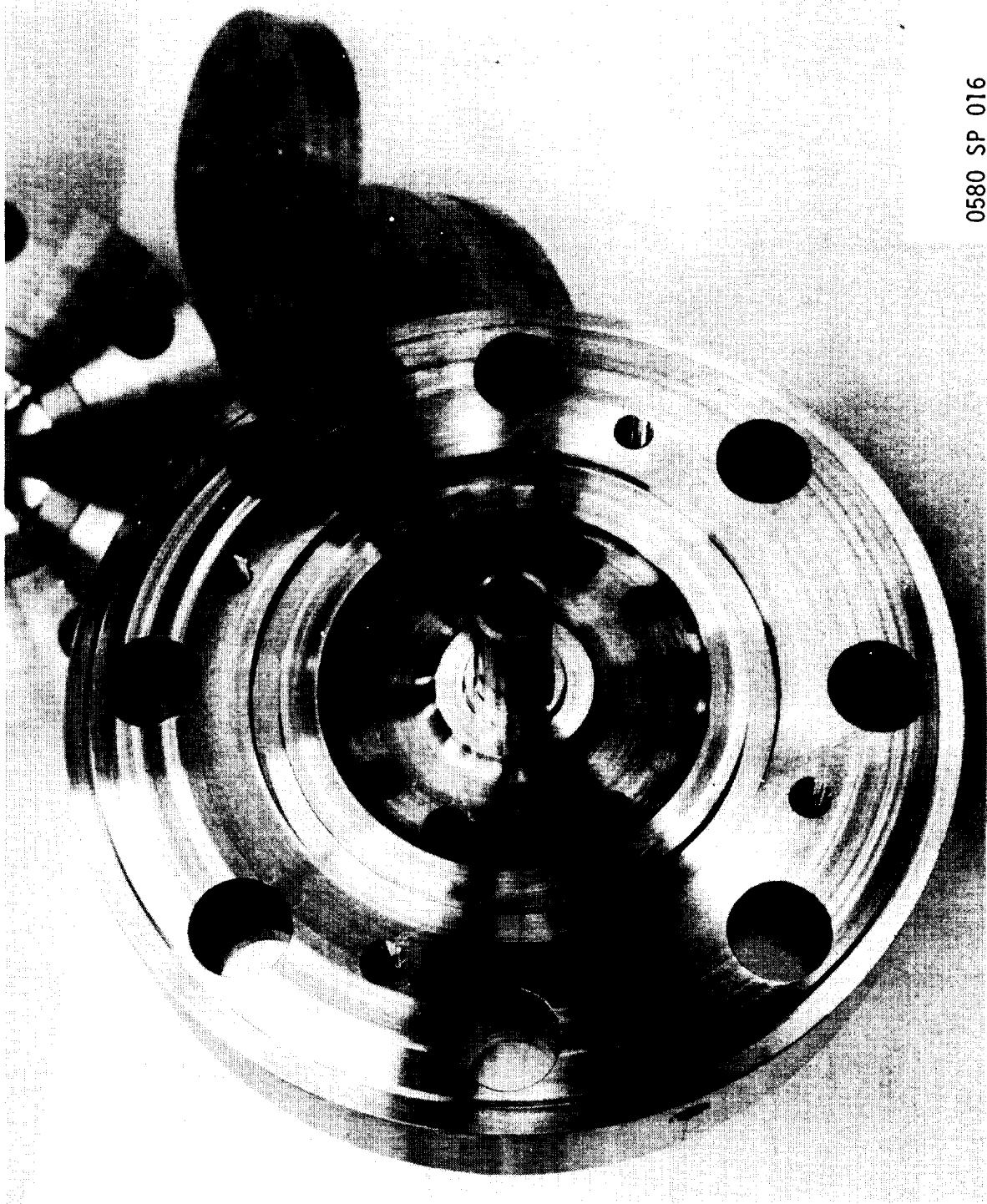
2. Faceplates

The injector assembly is completed by bolting one of four faceplates to the major propellant manifold assembly. Faceplates are shown in Figures III-8 through III-20. A shaft seal which slides onto the igniter guide tube and face seal located slightly outboard of the second distribution plenum provides a leak-proof assembly. The seal design, manufacturer, and part number are identified in Figure III-4. Four 0.50-20-UNF bolts hold the major manifold and faceplate injector together. When the injector is assembled to the preburner, eight additional 2.86-cm (1.125-in.) bolts provide the clamping force required to retain the high operating pressures.

The four oversize holes in the faceplate which receives the 0.50-20 holding bolts contain 0.625-28-UNF threads. These threaded holes can be used as jack mounts for separating the injector subassemblies.

The faceplate is supplied with propellant via a 1.91-cm (3/4-in.) Schedule 80 line which has a Greyloc hub welded on one end. The minor propellant flows through this inlet pipe into an annular manifold which is located between the core and flange subassemblies. The propellant then flows radially inward through holes which are drilled parallel to the face. These radial holes intersect numerous axial holes which deliver the propellant to the EDM'd or platelet orifice pattern. The major propellant flows axially through the faceplate.

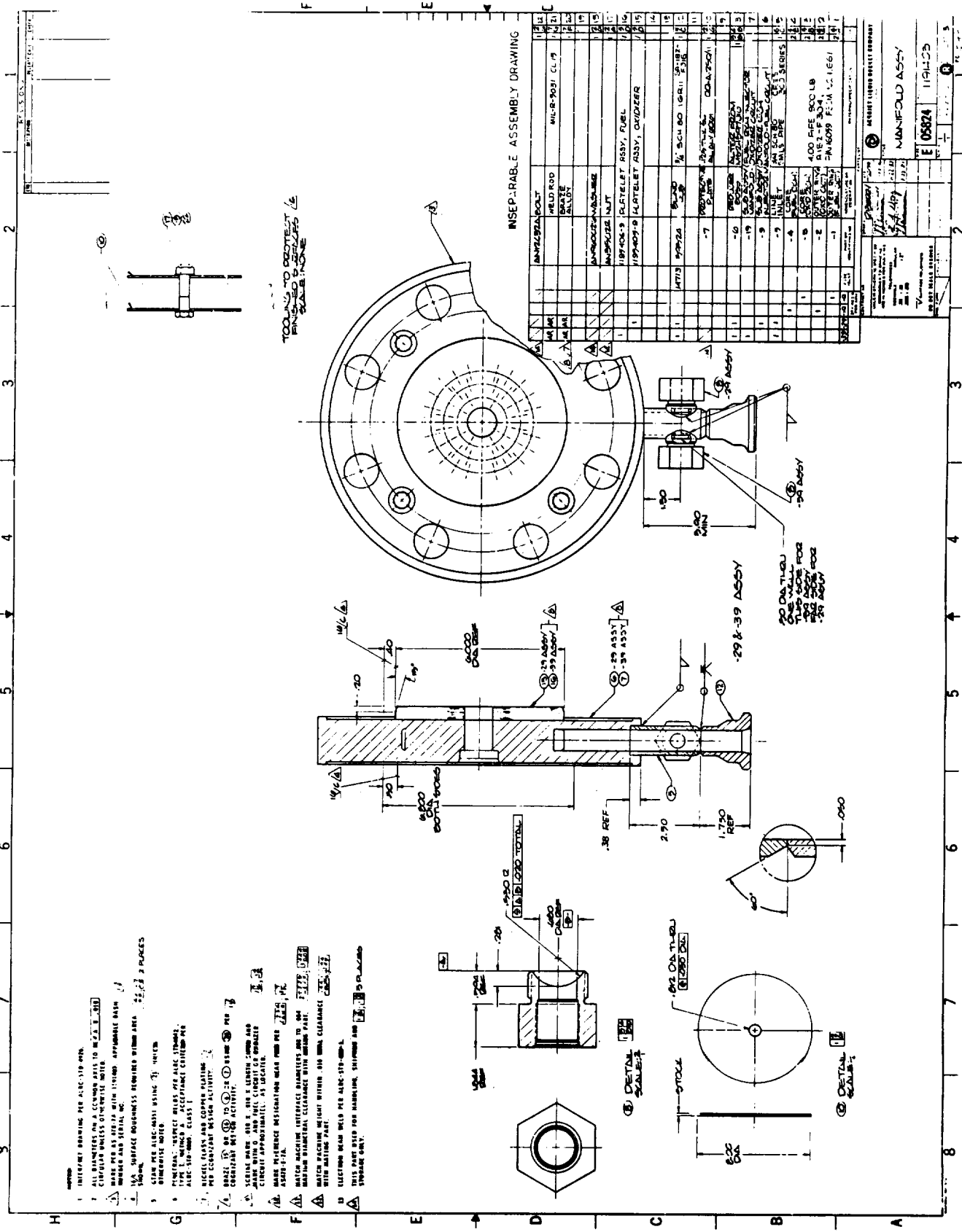
The inlet line contains a weld-on reducer boss which is to be used as a purge port. A second smaller boss for injecting a degrease solvent

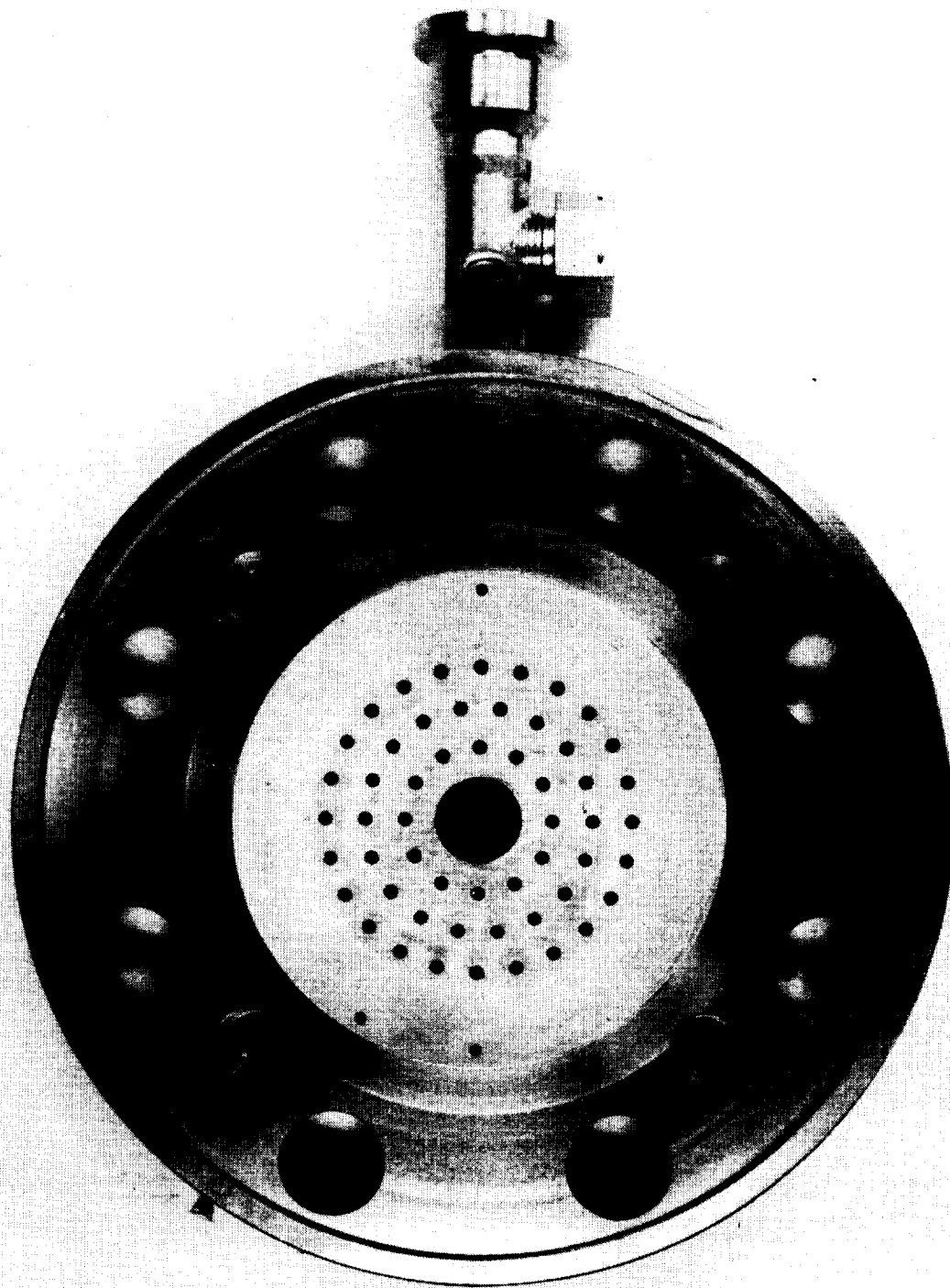


0580 SP 016

Figure III-7. Injector Major Propellant Manifold Assembly

ORIGINAL PAGE IS
OF POOR QUALITY





0880 SP 028

Figure III-9. Fuel-Rich Concentric Vortex Platelet Injector,
PN 1191403-39

ORIGINAL PAGE IS
OF POOR QUALITY

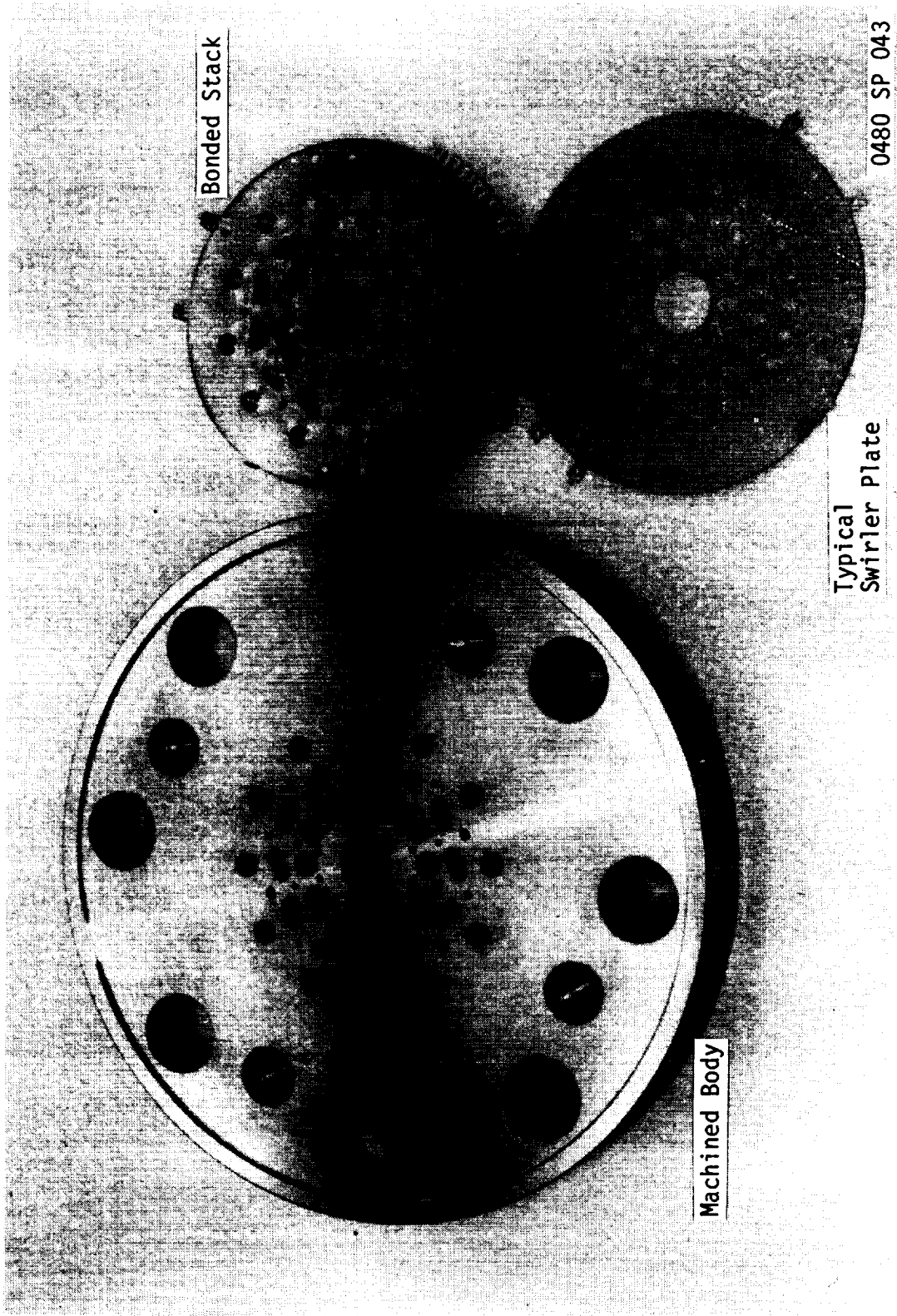


Figure III-10. Typical Bonded Platelet Stack and Machined Body

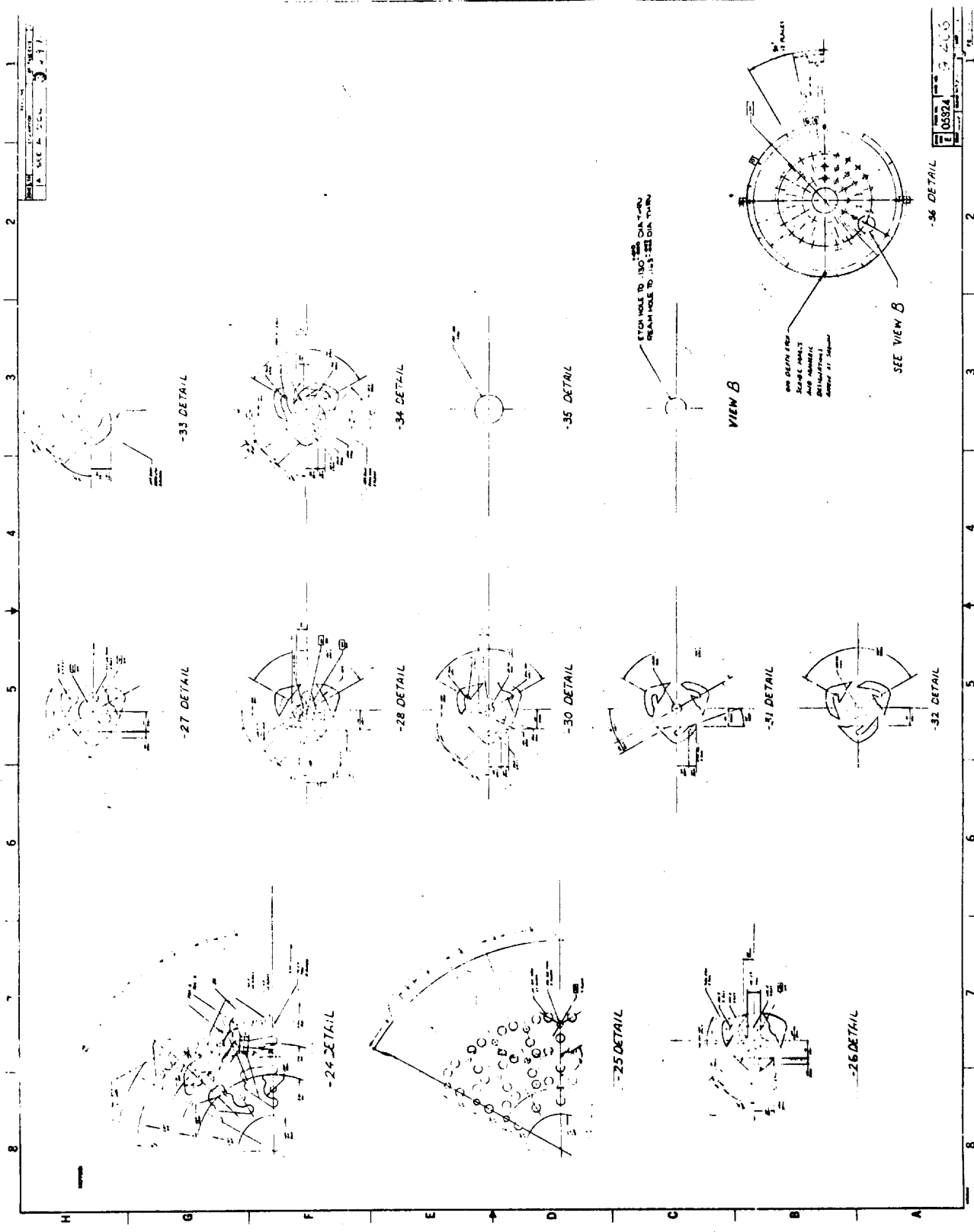
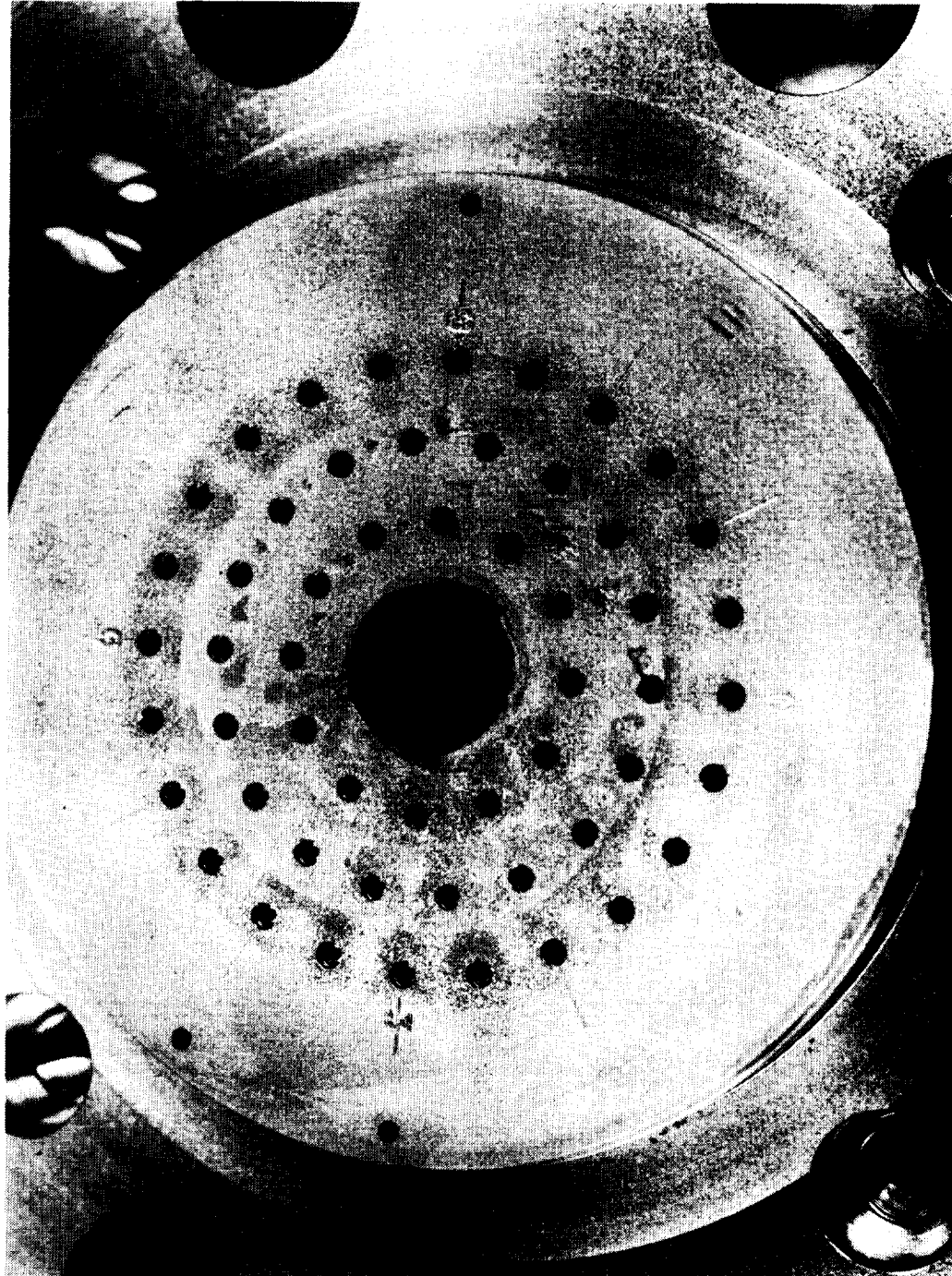


Figure III-11. Fuel-Rich Platelet Assembly (Sheet 2 of 2)



C0780-021-B

Figure III-12. Fuel-Rich Faceplate, Close-Up

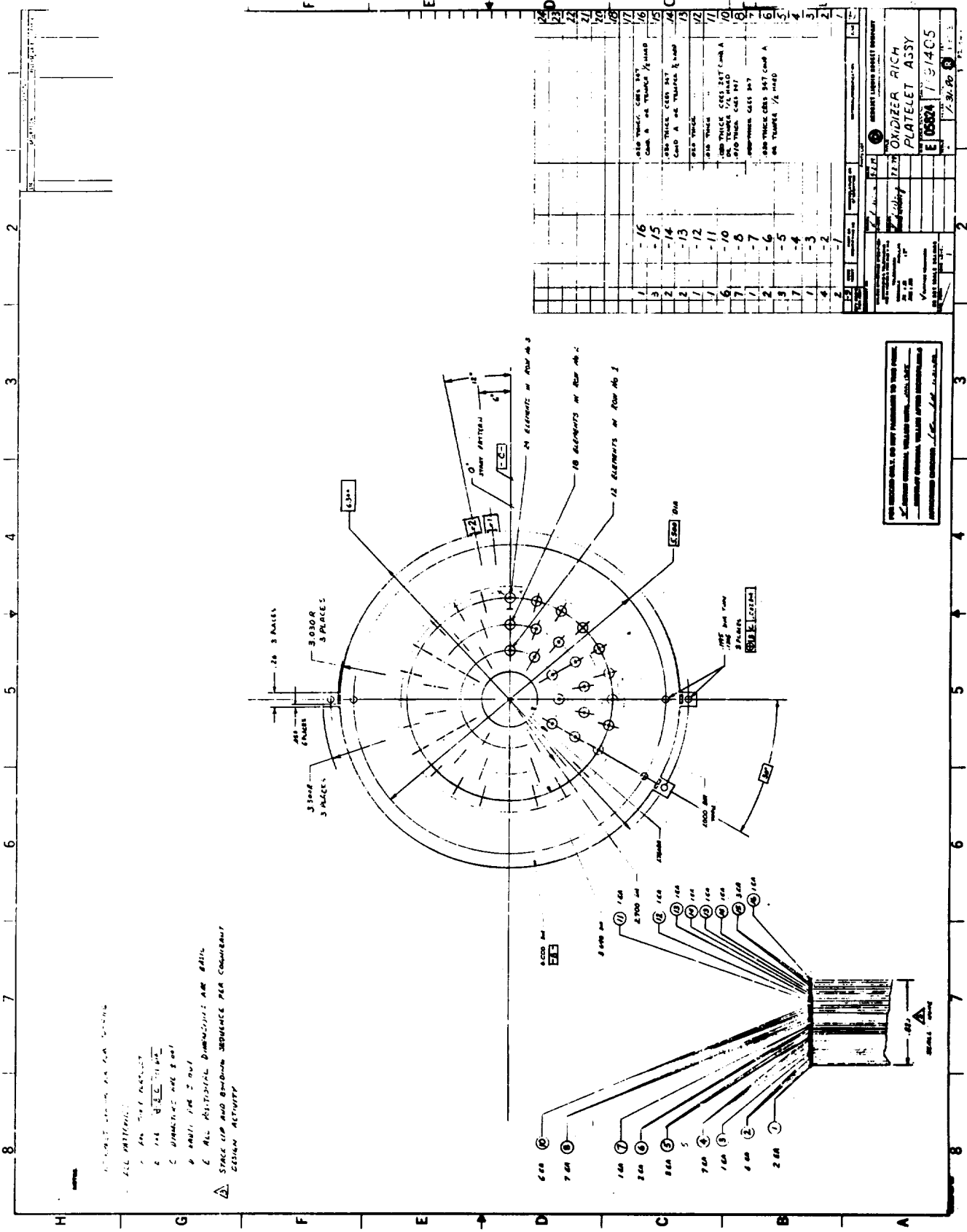


Figure III-13. Oxidizer-Rich Platelet Assembly (Sheet 1 of 3)

ORIGINAL PAGE IS OF POOR QUALITY

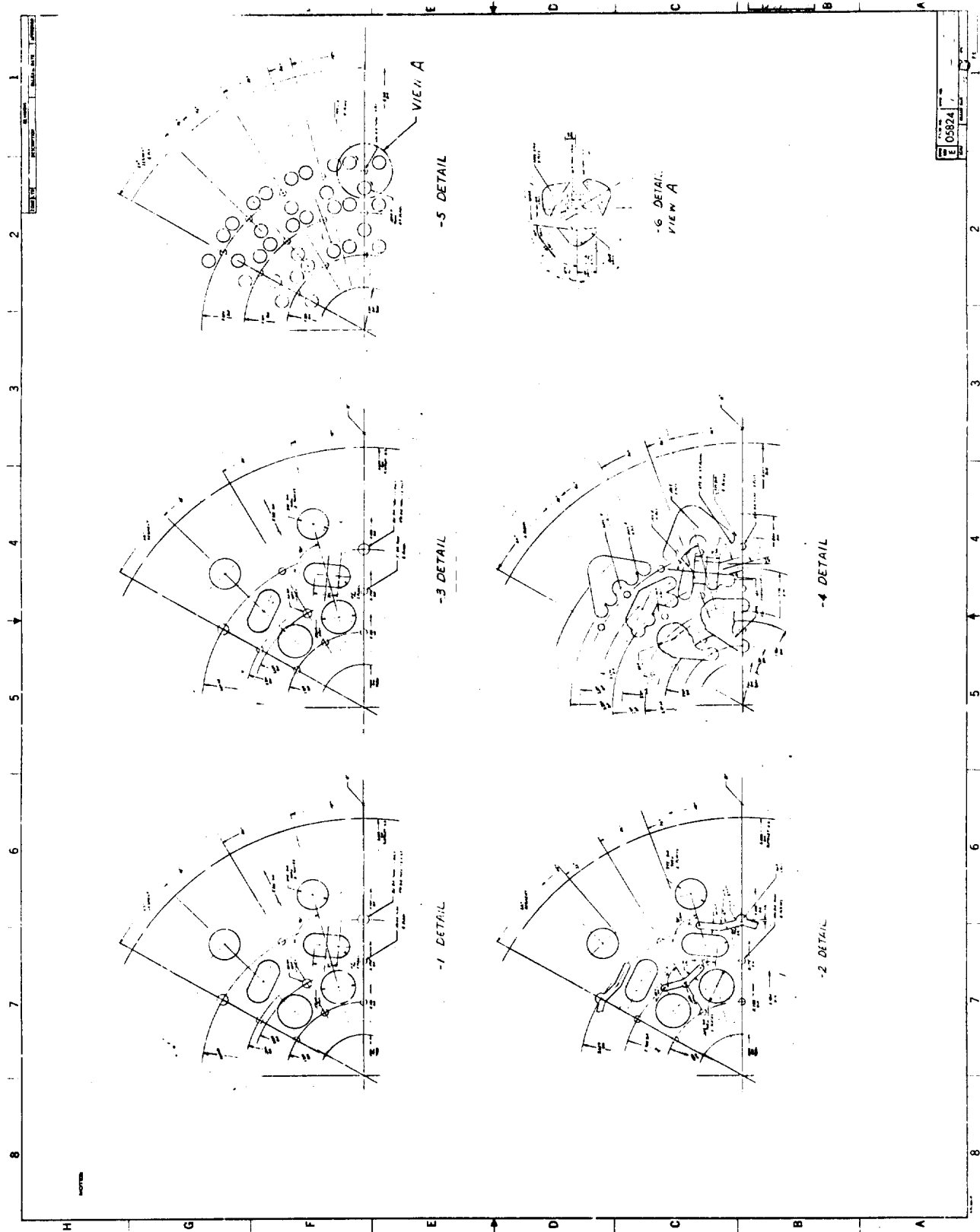


Figure III-13. Oxidizer-Rich Platelet Assembly (Sheet 2 of 3)

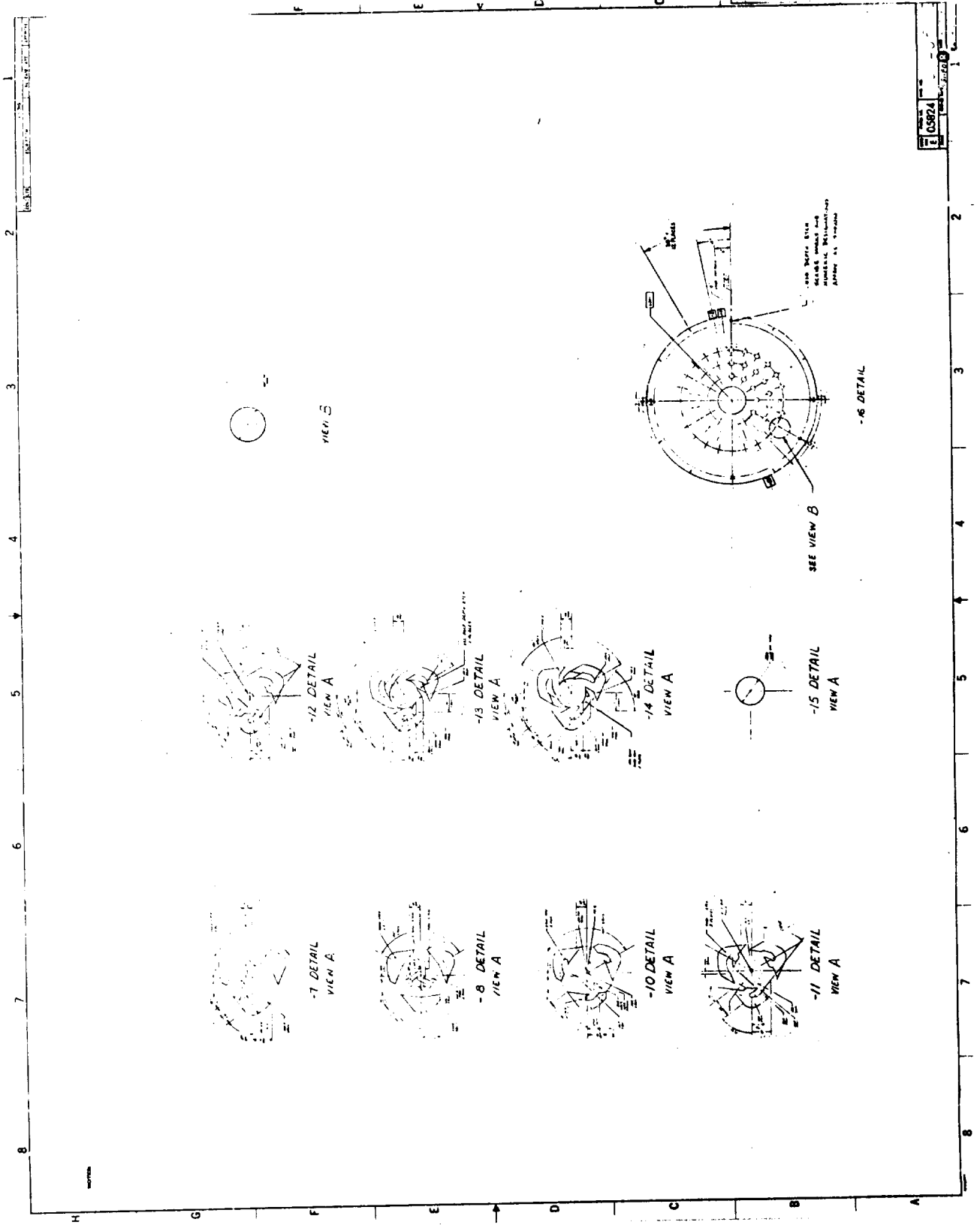


Figure III-13. Oxidizer-Rich Platelet Assembly (Sheet 3 of 3)

0480 SP 045

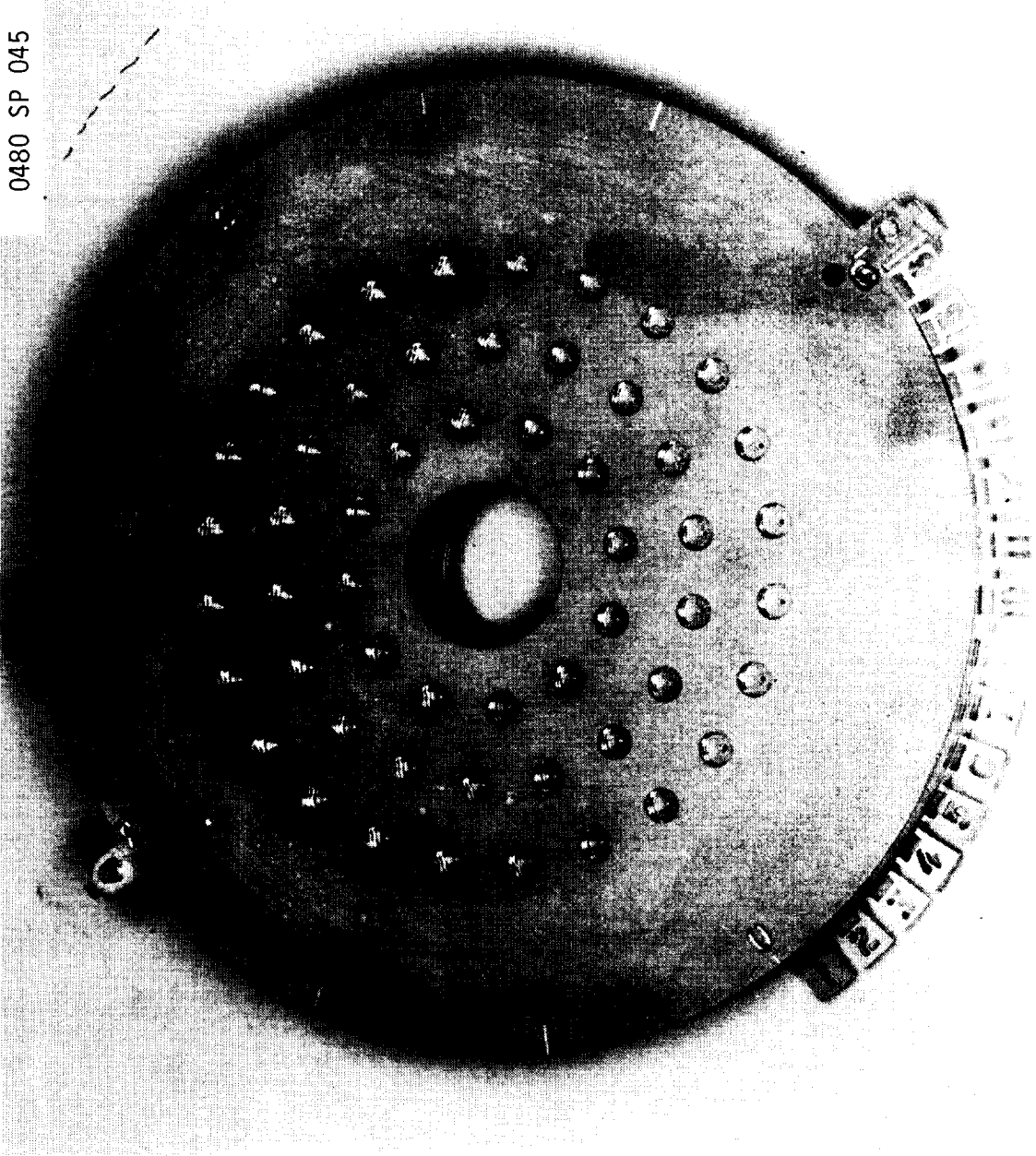


Figure III-14. Oxidizer-Rich Concentric Vortex Injector Faceplate Assembly

ORIGINAL PAGE IS
OF POOR QUALITY

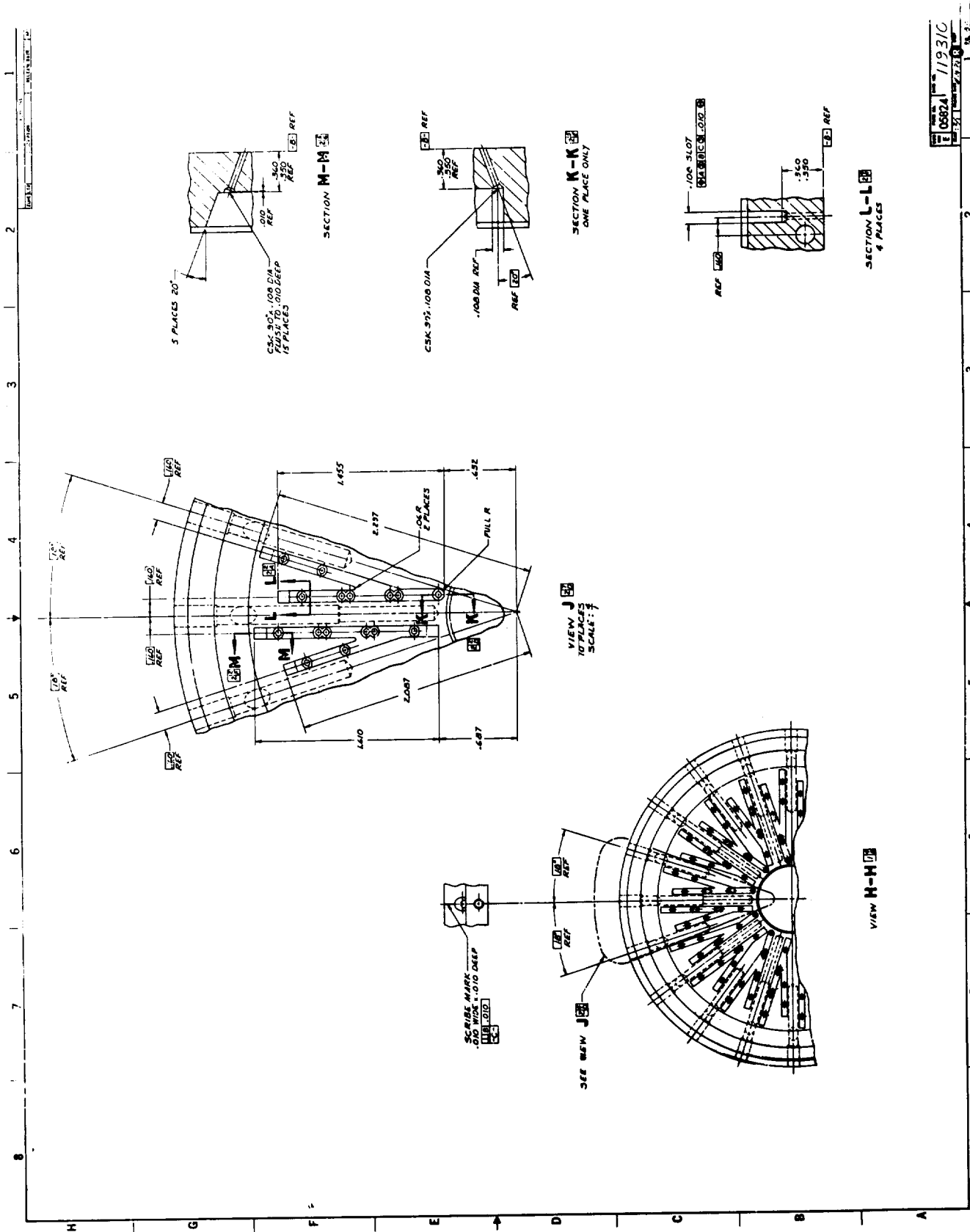
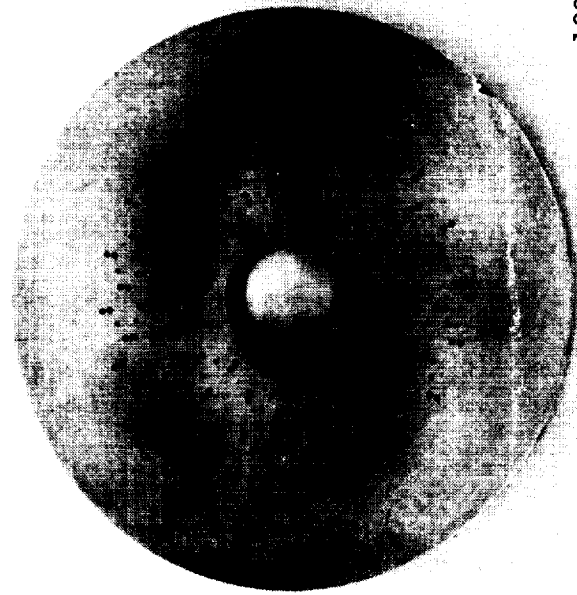
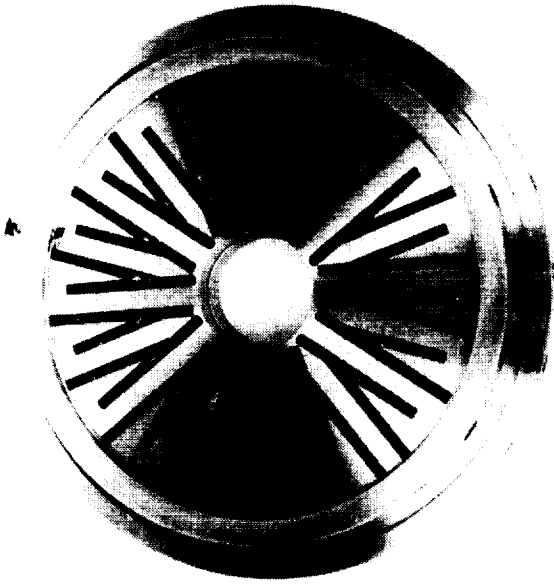


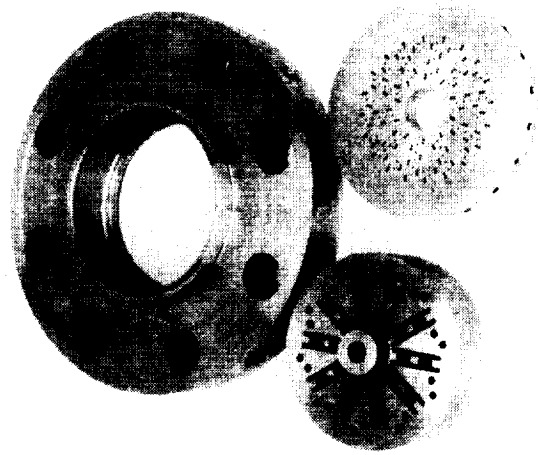
Figure III-15. Fuel-Rich Injector Pattern (2 of 2)



1080 SP 043

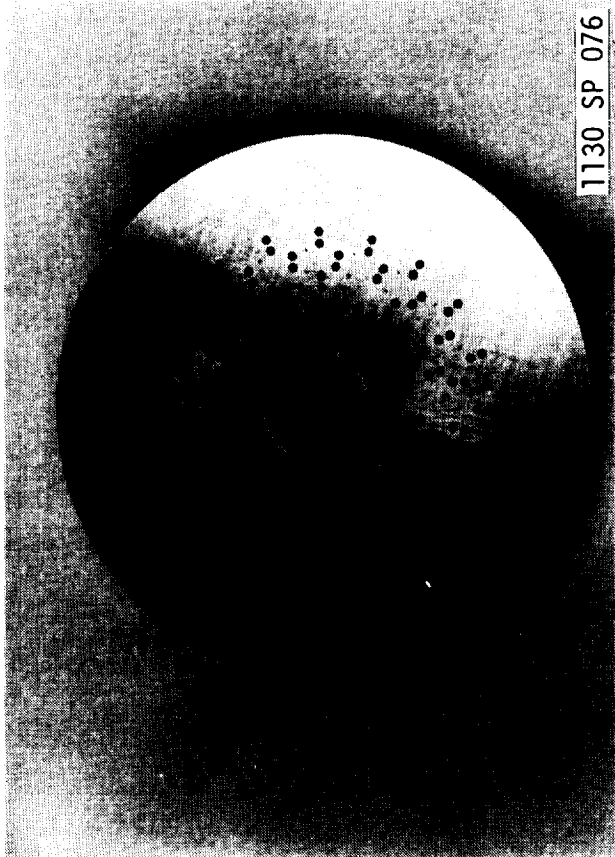


1080 SP 044



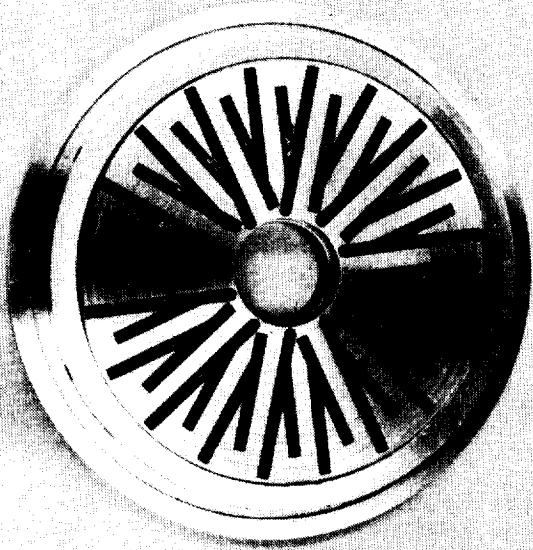
1080 SP 045

Figure III-16. Fuel-Rich Like-On-Like/Showerhead Injector Components

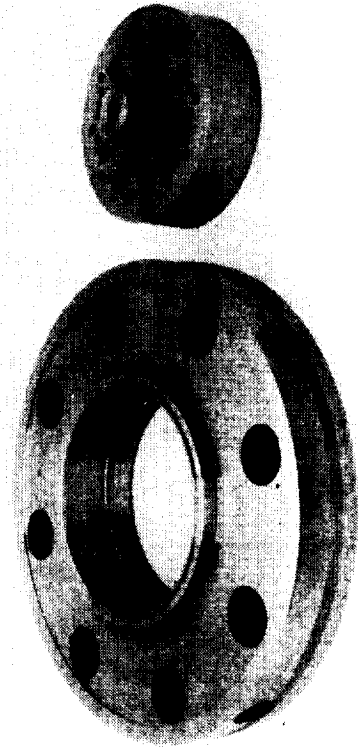


1130 SP 076

NICKEL FACEPLATE



1180 SP 075



1180 SP 077

304 STAINLESS STEEL

Figure III-18. Oxidizer-Rich EDM'd Injector Components

ORIGINAL PAGE IS
OF POOR QUALITY

III, B, Injector Assembly (cont.)

between tests was added, as shown in Figure III-9. This allows for cleaning of the assembly without removal from the test stand.

The location of the inlet line and purge boss was selected to mate with an existing ALRC test stand and valves. The fuel- and oxidizer-rich configurations are to be assembled with the inlet lines rotated 180°, as shown in Figure III-2.

A total of four faceplates were designed: two fuel-rich and two oxidizer-rich. These designs consist of a fuel-rich and an oxidizer-rich concentric vortex pattern having 54 elements, and a LOL/shower-type EDM element pattern for the fuel-rich and oxidizer-rich operation. Each concentric vortex element injects the minor propellant as a hollow cone spray which is completely surrounded by the major propellant (also injected as a hollow cone spray). Details of the EDM pattern injectors are provided in Table III-I.

All faceplate components are fabricated from 304 stainless steel, except for the platelets, which are 347 stainless steel, and the pattern plate of the LOX-rich EDM pattern, which is Nickel 200.

C. CHAMBERS

The chamber sections, shown in Figure III-21 and III-22, are a heat sink design and are fabricated from 304 stainless steel double extra-strong 12.7- and 15.2-cm (5- and 6-in.) diameter pipe and commercial 10.2-cm (4-in.) pipe size forged, weld-on flanges. These flanges meet ANSI B 16.5 and ASME standards. The pipe ends and flanges are modified to allow for electron-beam (EB) welding. The use of commercial 10.2-cm (4-in.) flanges on 12.7-cm (5-in.) and 15.2-cm (6-in.) pipe provides a low-cost fabrication approach and allows the 6205 kPa (900 psia) rated flange to be used at much higher pressures.

The front and back end of each chamber section contains a pilot to provide diametrical alignment when the sections are bolted together. This pilot and interface geometry is employed on all components, starting with the downstream face of the resonator flange. This allows for full interchangeability, thus permitting the sequence of hardware assembly to be varied in order to meet the needs of the individual tests.

Two types of chambers were designed and fabricated. Those utilizing the 15.2-cm (6-in.) diameter pipe can accommodate an easily replaceable drop-in liner with a 10.2-cm (4-in.) inside diameter and 1.27-cm (0.5-in.) thick wall. The replaceable liner approach was selected for use near the injector where local hot streaks could cause erosion of the chamber wall. The ability to replace liners in the test area was considered essential in order to minimize down-time between tests should local streaking develop. The

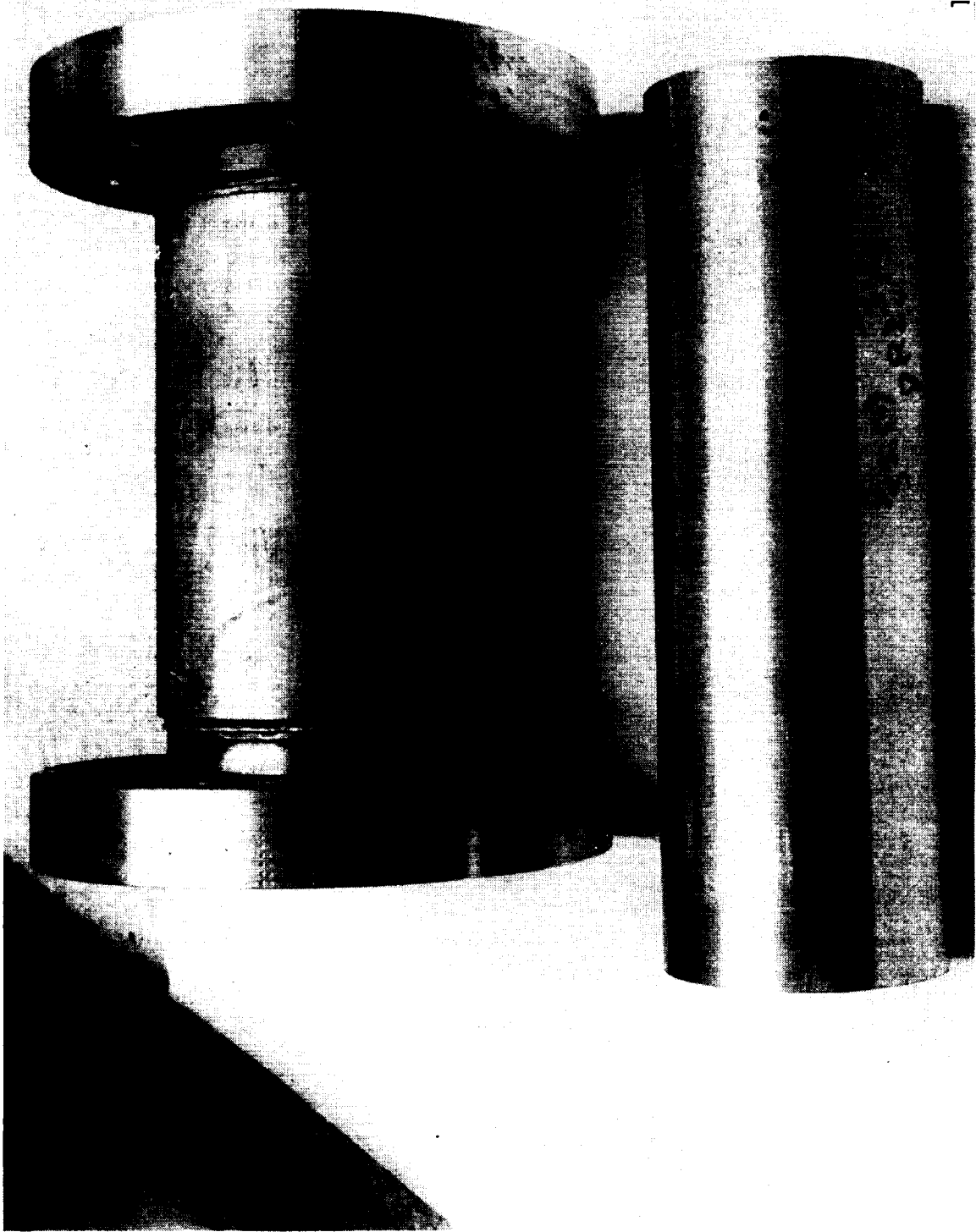
TABLE III-I. FUEL- AND OXIDIZER-RICH PREBURNER INJECTOR
PATTERN SUMMARY

<u>Fuel Circuit</u>	<u>Fuel-Rich</u>	<u>Oxidizer-Rich</u>
Orifice Diameter, cm (in.)	0.142 (0.056)	0.0559 (0.022)
Orifice L/D	6.6	4.2/8.4
Orifice Chamfer	45°	None
Orifice Cd	0.85*	0.85*
Orifice Type	LOL	Showerhead
Orifice Number	160	60/10***
Pressure Drop, kPa (psi)	2758 (400)	2758 (400)
Flowrate @ $\eta = 1.0$ kg/sec (lb/sec)	13.49 (29.75)	0.943 (2.08)
Injection Velocity, m/sec (ft/sec)	88.4 (290)	88.4 (290)
Tilt Angle	Tangential Fans	2°**
<u>Oxidizer Circuit</u>		
Orifice Diameter, cm (in.)	0.1016 (0.040)/0.051 (0.020)	0.2286 (0.090)
Orifice L/D	2.5/5.0	5.5
Orifice Chamfer	None	45°
Orifice Cd	0.68/0.85	0.85*
Orifice Type	Showerhead	LOL
Orifice Number	70/10	140
Pressure Drop, kPa (psi)	2758 (400)	2758 (400)
Flowrate @ $\eta = 1.0$ kg/sec (lb/sec)	3.43 (7.56)	38.6 (85.0)
Injection Velocity, m/sec (ft/sec)	72.2 (237)	72.2 (237)
Tilt Angle	2°**	Tangential Fans

*Orifice Cd for attached flow (Cd = 0.85 for long L/D and 0.68 for short L/D)

**The lean showerhead outer row barrier streams are tilted 2° inboard and 2° sideways towards the mating rich LOL fan in order to enhance mixing and to shield the wall from the hot lean flame. The lean inner row streams are tilted 2° sideways only. (See Figure III-17, p. 33)

***The 10 showerhead elements in the innermost row are smaller than the core elements.



1180 SP 078

Figure III-22. 15 In. Chamber and Liner, PN 1191401

III, C, Chambers (cont.)

design can accommodate liners fabricated from metal or ceramic pipe sections and can be segmented, as shown in Figure III-21, to install turbulators or boundary layer trips to improve mixing of the hot-gas flow. The liners fabricated for the first test were a composite comprised of 0.635-cm (0.25-in.) of Nickel 200 and 0.635-cm (0.25-in.) of flame-sprayed copper.

The lined chamber section contains four bosses which can be employed to install helium-bleed Kistler pressure transducers or thermocouple probes. The lined and unlined sections provide a pressure port in the forward flange.

D. TURBINE SIMULATOR

The turbine simulator, shown in Figures III-23 through III-25, is designed to provide a high pressure drop across the gas stream. The design pressure ratio P_{up}/P_{down} for both the fuel- and oxidizer-rich assemblies is 1.5.

The simulator is fabricated from a blank 304 stainless steel forged flange and slotted to receive standard size hexagonal bar stock, as shown in Figure III-23. The higher strength of 17-4 ph alloy was required for the bars because of the high stresses at the ends of the bars. The bars are locked into position by set screws.

The large difference in mass flowrates between the fuel- and oxidizer-rich operating conditions resulted in a requirement of different bar dimensions for each condition, as noted in Figure III-23.

Since accurate prediction of the pressure drop was not practical, the design allows for the axial space between the bars to be adjusted in order to obtain the required pressure ratio. Shims of varying thickness were fabricated for this purpose.

The proper spacing was obtained experimentally in a series of cold-flow tests that are summarized in Section VI. The bar spacing which provided the proper pressure ratio when flowing GN_2 is defined in Table III-II. These data supersede the preliminary values shown in the drawings. The gap dimensions are minimum values, as determined by dropping 3.8-cm (1.5-in.) long go/no-go gage pins between the bars.

E. IGNITERS

The igniter, shown in Figures III-26 and III-27, operates with GH_2 and GOX and is a modification of an existing ALRC design. The igniter tube is fabricated from OFHC copper which provides heat sink cooling

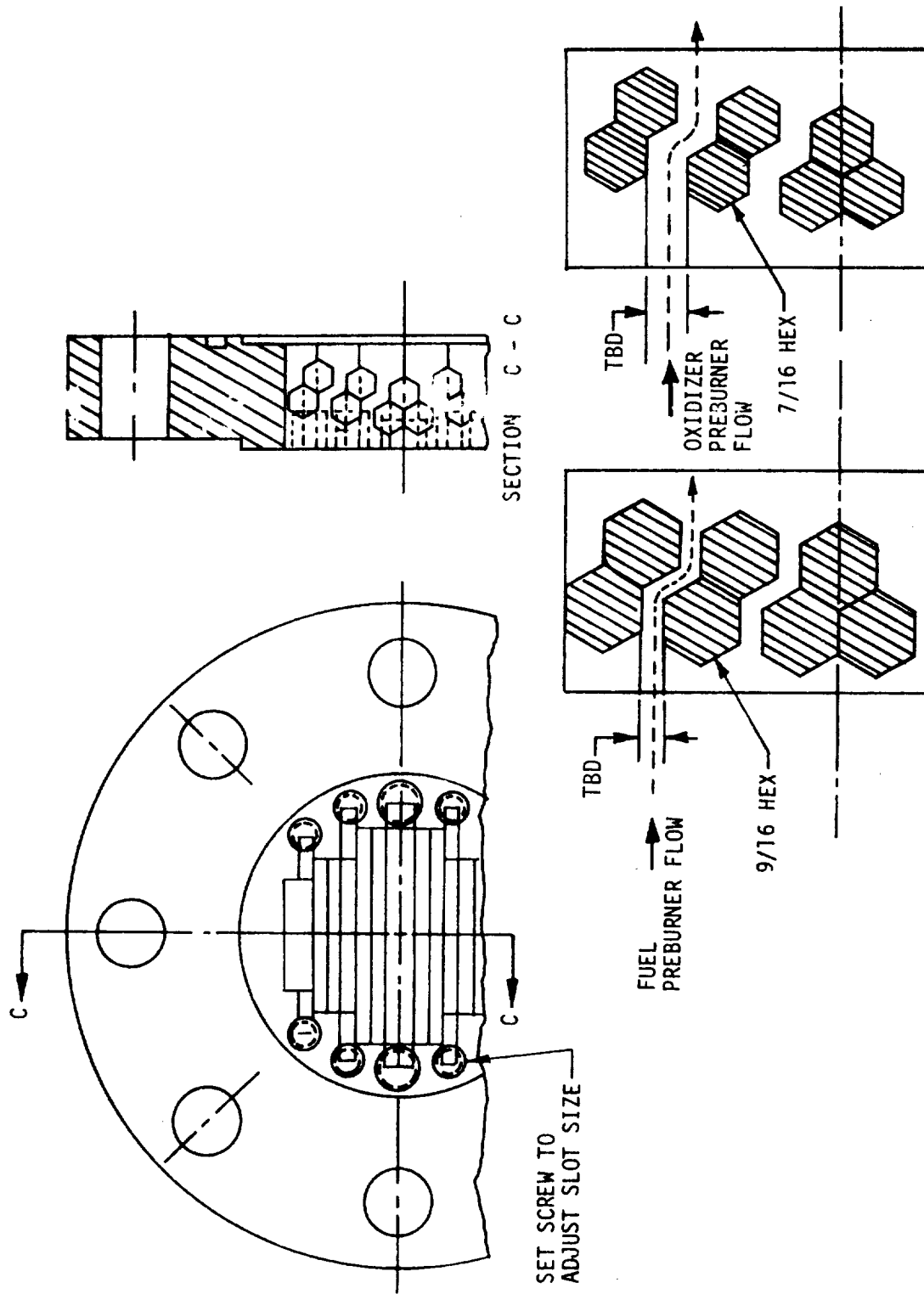


Figure III-23. Turbine Simulator Schematic

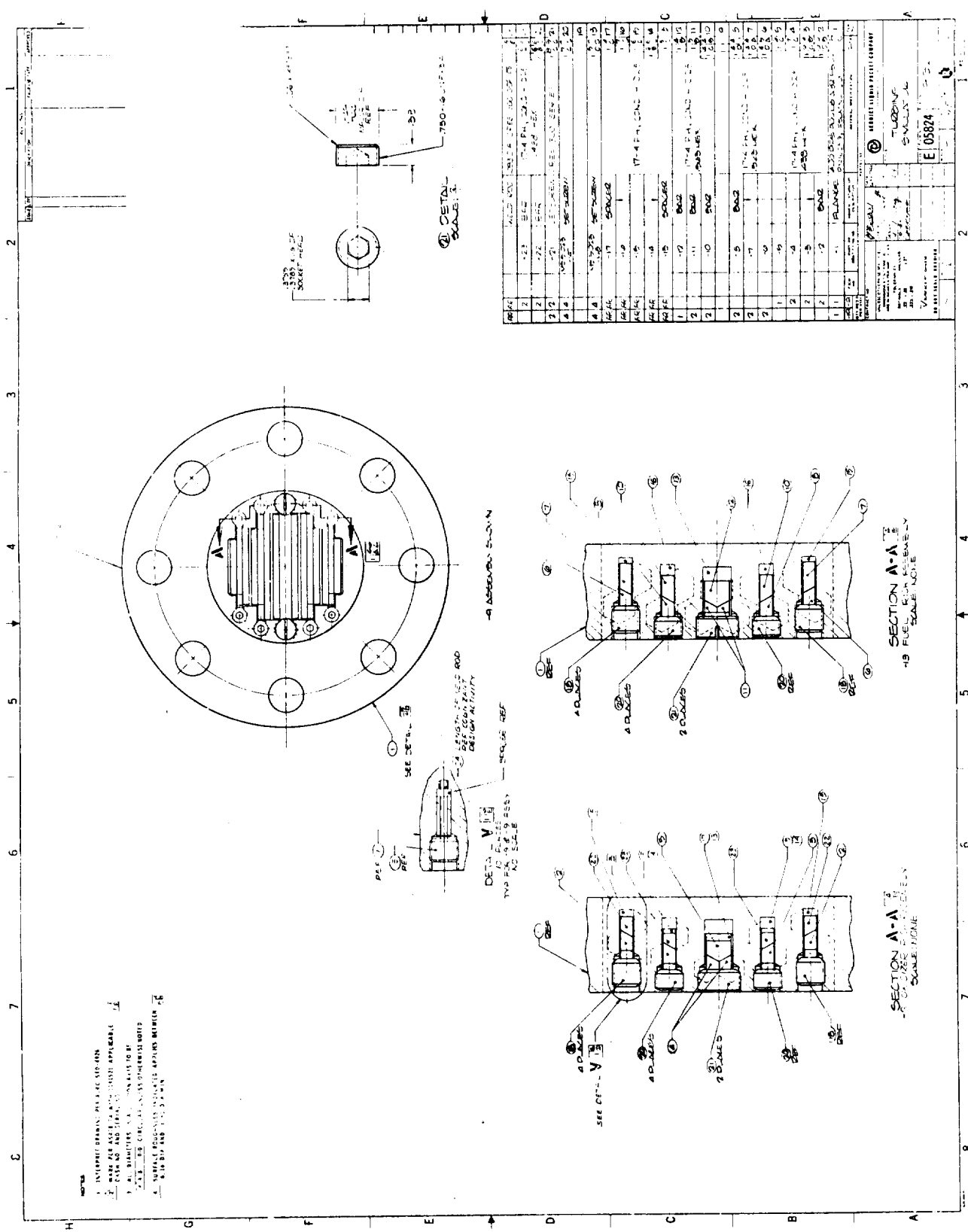
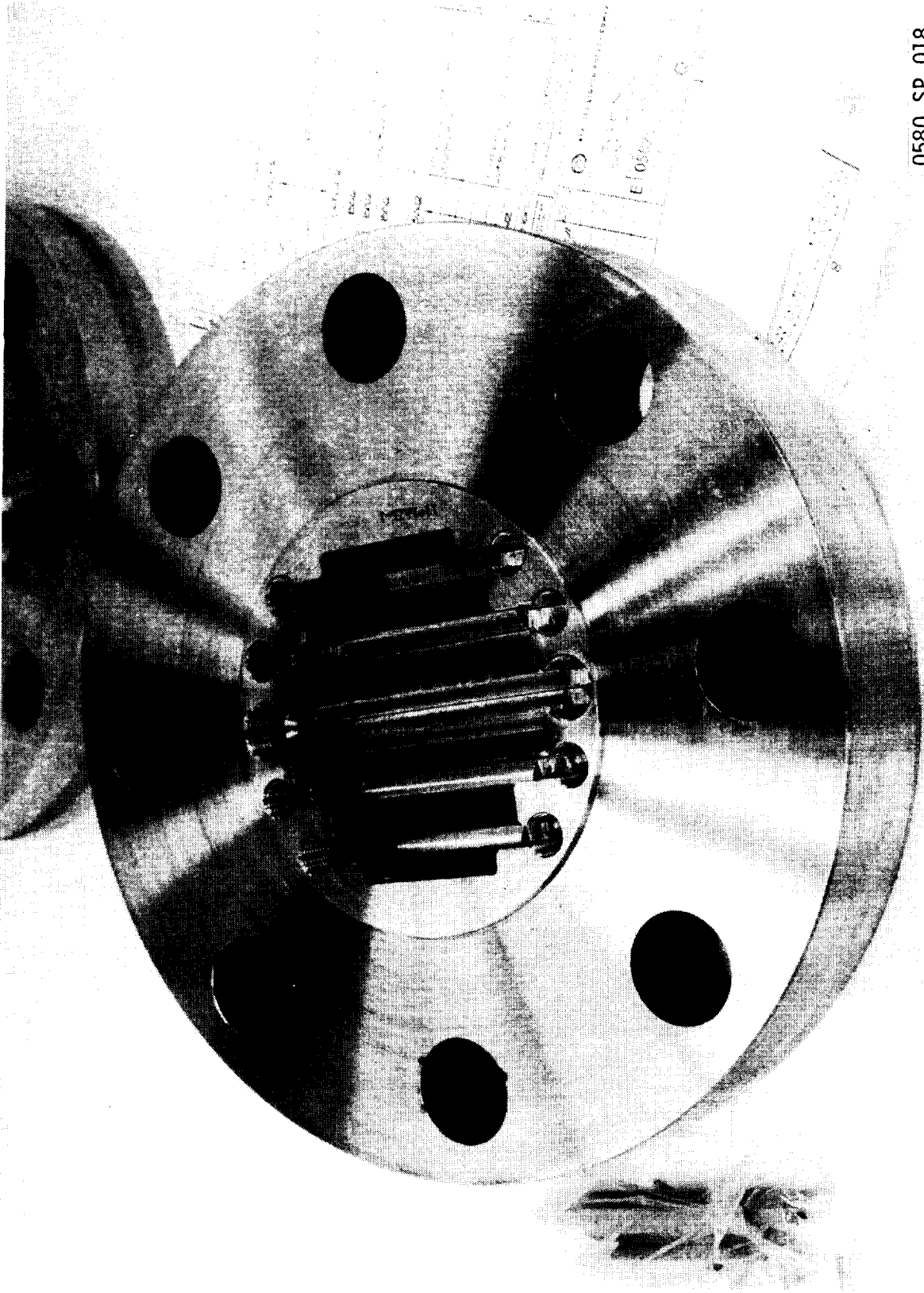


Figure III-24. Turbine Simulator Assembly, PN 1191521 (Sheet 1 of 2)

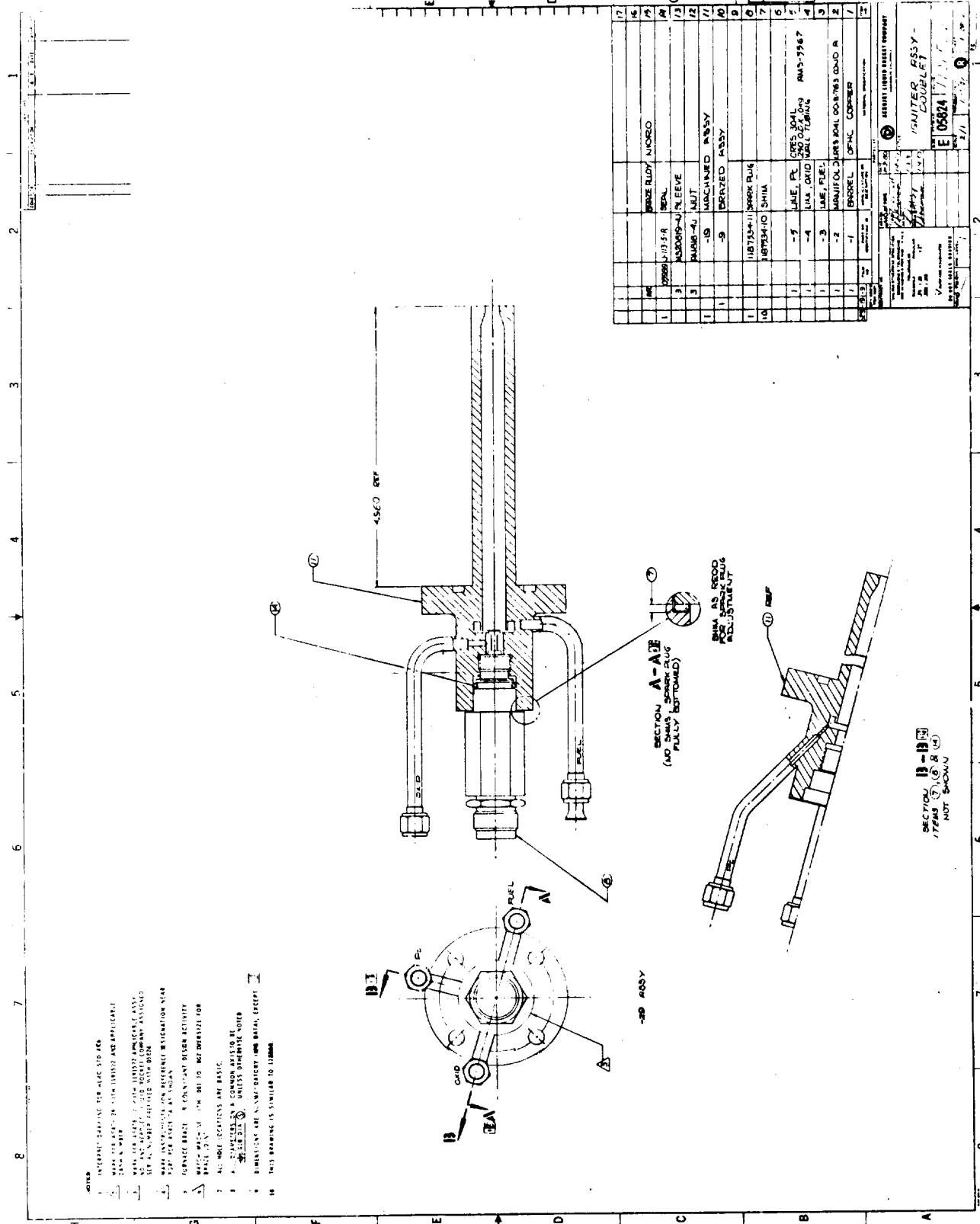


0580 SP 018

Figure III-25. Turbine Simulator

TABLE III-II. TURBINE SIMULATOR BAR SPACING TO PRODUCE
REQUIRED PRESSURE RATIO

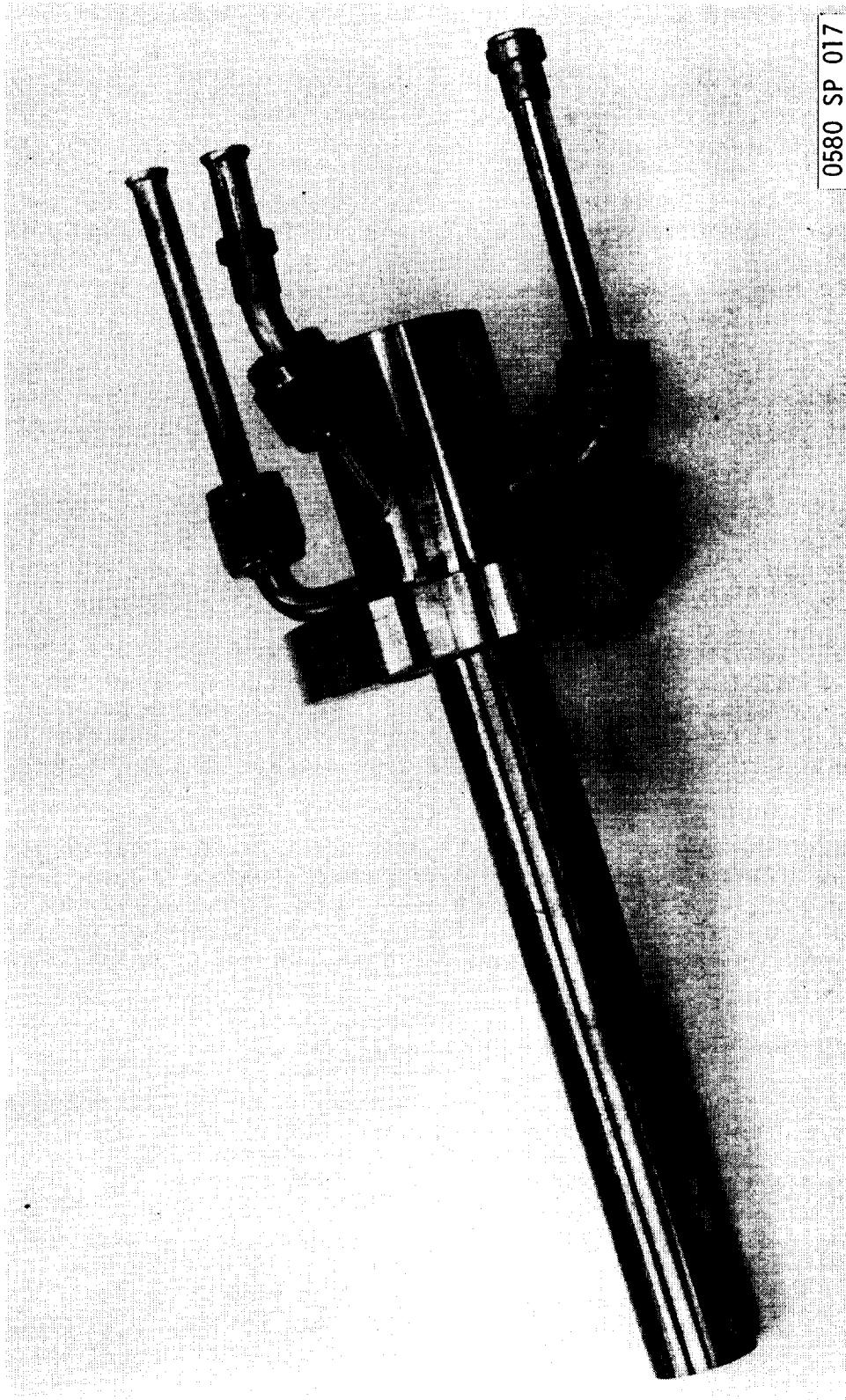
	Fuel-Rich		Oxidizer-Rich	
	Min. Gap, <u>in.</u>	Shim Thickness, <u>in.</u>	Min. Gap, <u>in.</u>	Shim Thickness, <u>in.</u>
Edge Gap	.003	.227	.065	.076
Slot 1	.080	.072	.230	Zero
Slot 2	.064	Zero	.198	Zero
Slot 3	.069	.072	.192	Zero
Slot 4	.087	.227	.230	.076
Edge Gap	.023		.083	
	<u>cm</u>	<u>cm</u>	<u>cm</u>	<u>cm</u>
Edge Gap	.0076	.577	.165	.193
Slot 1	.203	.183	.584	Zero
Slot 2	.163	Zero	.503	Zero
Slot 3	.175	.183	.488	Zero
Slot 4	.221	.577	.584	.193
Edge Gap	.058		.211	



- NOTES
1. INTERMITTENT TESTING PER MIL-STD-456.
 2. WHEN THE ASSEMBLY IS SHOWN IN THIS DRAWING, THE APPLICABLE DRAWING NUMBER IS TO BE USED.
 3. THIS DRAWING IS THE PROPERTY OF THE GOVERNMENT AND IS LOANED TO YOU; IT AND ITS CONTENTS ARE NOT TO BE DISTRIBUTED OUTSIDE YOUR ORGANIZATION.
 4. THIS DRAWING IS THE PROPERTY OF THE GOVERNMENT AND IS LOANED TO YOU; IT AND ITS CONTENTS ARE NOT TO BE DISTRIBUTED OUTSIDE YOUR ORGANIZATION.
 5. THIS DRAWING IS THE PROPERTY OF THE GOVERNMENT AND IS LOANED TO YOU; IT AND ITS CONTENTS ARE NOT TO BE DISTRIBUTED OUTSIDE YOUR ORGANIZATION.
 6. THIS DRAWING IS THE PROPERTY OF THE GOVERNMENT AND IS LOANED TO YOU; IT AND ITS CONTENTS ARE NOT TO BE DISTRIBUTED OUTSIDE YOUR ORGANIZATION.
 7. ALL DIMENSIONS ARE IN INCHES UNLESS OTHERWISE SPECIFIED.
 8. ALL DIMENSIONS ARE IN INCHES UNLESS OTHERWISE SPECIFIED.
 9. ALL DIMENSIONS ARE IN INCHES UNLESS OTHERWISE SPECIFIED.
 10. THIS DRAWING IS THE PROPERTY OF THE GOVERNMENT AND IS LOANED TO YOU; IT AND ITS CONTENTS ARE NOT TO BE DISTRIBUTED OUTSIDE YOUR ORGANIZATION.

QTY	DESCRIPTION	REF
1	NOZZLE	1
1	NOZZLE	2
1	NOZZLE	3
1	NOZZLE	4
1	NOZZLE	5
1	NOZZLE	6
1	NOZZLE	7
1	NOZZLE	8
1	NOZZLE	9
1	NOZZLE	10
1	NOZZLE	11
1	NOZZLE	12
1	NOZZLE	13
1	NOZZLE	14
1	NOZZLE	15
1	NOZZLE	16
1	NOZZLE	17
1	NOZZLE	18
1	NOZZLE	19
1	NOZZLE	20
1	NOZZLE	21
1	NOZZLE	22
1	NOZZLE	23
1	NOZZLE	24
1	NOZZLE	25
1	NOZZLE	26
1	NOZZLE	27
1	NOZZLE	28
1	NOZZLE	29
1	NOZZLE	30
1	NOZZLE	31
1	NOZZLE	32
1	NOZZLE	33
1	NOZZLE	34
1	NOZZLE	35
1	NOZZLE	36
1	NOZZLE	37
1	NOZZLE	38
1	NOZZLE	39
1	NOZZLE	40
1	NOZZLE	41
1	NOZZLE	42
1	NOZZLE	43
1	NOZZLE	44
1	NOZZLE	45
1	NOZZLE	46
1	NOZZLE	47
1	NOZZLE	48
1	NOZZLE	49
1	NOZZLE	50
1	NOZZLE	51
1	NOZZLE	52
1	NOZZLE	53
1	NOZZLE	54
1	NOZZLE	55
1	NOZZLE	56
1	NOZZLE	57
1	NOZZLE	58
1	NOZZLE	59
1	NOZZLE	60
1	NOZZLE	61
1	NOZZLE	62
1	NOZZLE	63
1	NOZZLE	64
1	NOZZLE	65
1	NOZZLE	66
1	NOZZLE	67
1	NOZZLE	68
1	NOZZLE	69
1	NOZZLE	70
1	NOZZLE	71
1	NOZZLE	72
1	NOZZLE	73
1	NOZZLE	74
1	NOZZLE	75
1	NOZZLE	76
1	NOZZLE	77
1	NOZZLE	78
1	NOZZLE	79
1	NOZZLE	80
1	NOZZLE	81
1	NOZZLE	82
1	NOZZLE	83
1	NOZZLE	84
1	NOZZLE	85
1	NOZZLE	86
1	NOZZLE	87
1	NOZZLE	88
1	NOZZLE	89
1	NOZZLE	90
1	NOZZLE	91
1	NOZZLE	92
1	NOZZLE	93
1	NOZZLE	94
1	NOZZLE	95
1	NOZZLE	96
1	NOZZLE	97
1	NOZZLE	98
1	NOZZLE	99
1	NOZZLE	100

Figure III-26. Igniter Assembly (Sheet 1 of 2)



0580 SP 017

Figure III-27. Hydrogen-Oxygen Igniter, PN 1191522

ORIGINAL PAGE IS
OF POOR QUALITY

III, E, Igniters (cont.)

capability for about 0.4 sec of operation at a mixture ratio up to 5.0. The nominal operating mixture ratio is 3.5 at a flowrate of 0.041 kg/sec (0.09 lb/sec) of total flow per second.

The copper tube is brazed to a 304 stainless flange which contains the following parts and attachments: a 0.635-cm (0.25-in.) fuel supply tube, a 0.635-cm (0.25-in.) oxidizer supply tube, a 0.635-cm (0.25-in.) chamber pressure measurement tube, and a 7-mm threaded hole to receive a spark plug assembly (ALRC PN 1187534).

The igniter attaches to the major propellant manifold via four NAS 1351C-4-16 (0.25-28) socket head cap screws torqued to 161 cm-kg (140 in.-lb). The seals to be employed in this assembly are identified in Figure III-4.

F. ACOUSTIC RESONATORS

The acoustic resonator, shown in Figures III-28 and III-29, mates with any of the four injector faceplates on the upstream face and any of the chamber sections or flanges on the downstream face.

The resonator assembly is comprised of three major components: a forged flange, a resonator cavity partition insert, and a series of tuning blocks inserts. The energy absorption spectral frequency can be tuned to damp any of the most likely modes of high-frequency instability by adjusting these blocks. All components of this assembly are fabricated from 304 stainless steel.

One of the twelve cavities has been left open (i.e., has no block insert) to allow access for a Kistler high-frequency pressure transducer, and a second cavity contains a normal pressure measurement port. These must be aligned with the respective holes in the flange during assembly of the resonator. A drain port is provided to remove residual fuel and cleaning solvent after each test.

G. MAIN INJECTOR SIMULATOR

The main injector simulator provides the pressure drop expected to exist in the main injector of a staged-combustion engine cycle. Since different flow areas are required for the fuel- and oxidizer-rich preburners, two different designs needed to be fabricated. Figure III-30 shows the main injector simulators which are fabricated from 304 stainless steel. These consist of a flange section and a replaceable bolt-in disk section that allows the flow area to be adjusted for either the fuel or oxidizer flowrates. The disk is held in place by three screws. An additional ring which has a 10.31-cm (4.06-in.) diameter bore can be inserted into the flange to provide a spacer section if required. The 7.62-cm (3.00-in.) diameter bore of the

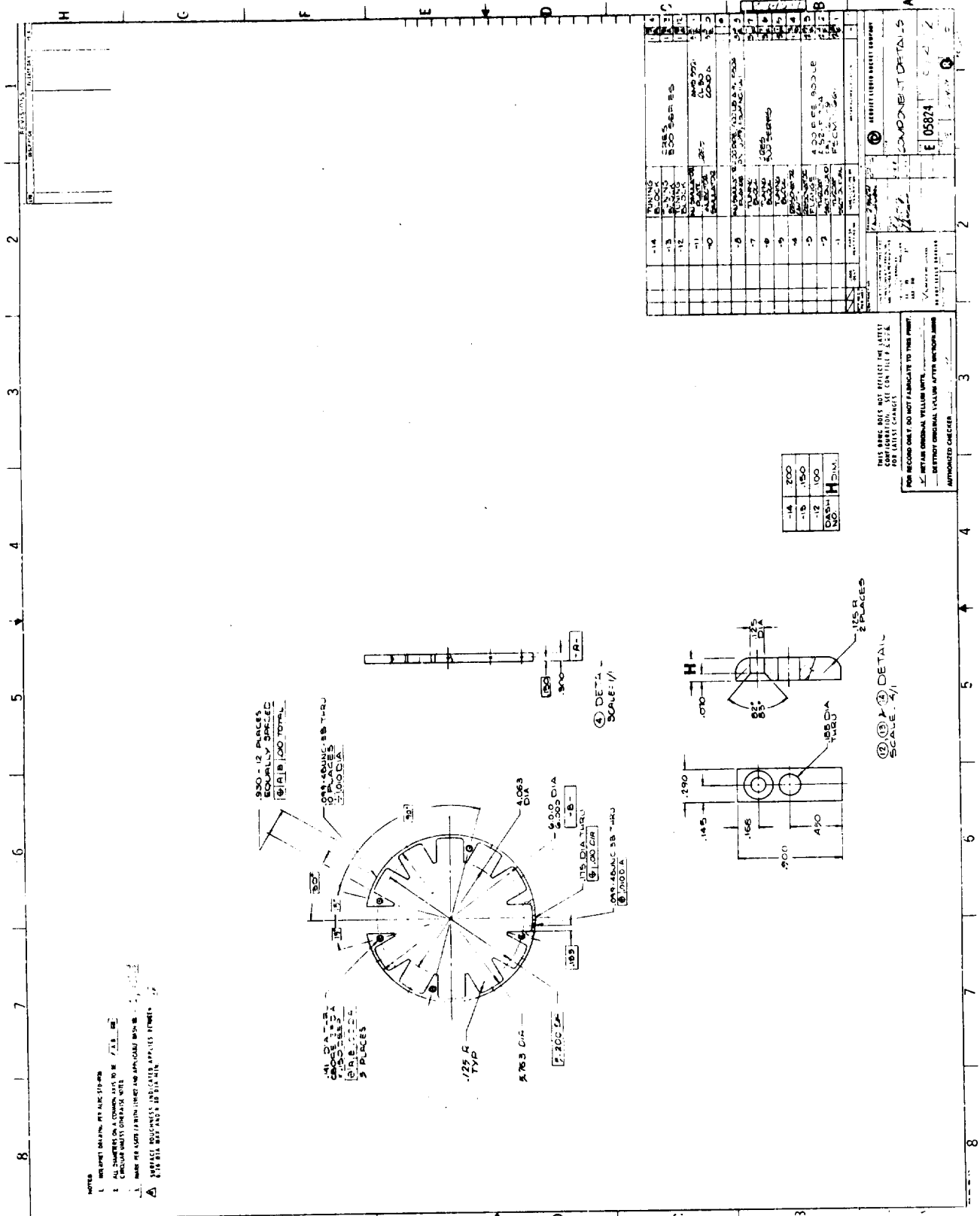


Figure III-28. Detail Drawings of Throats, Main Injector Simulators, Resonator Cavity and Tuning Blocks (Sheet 1 of 3)

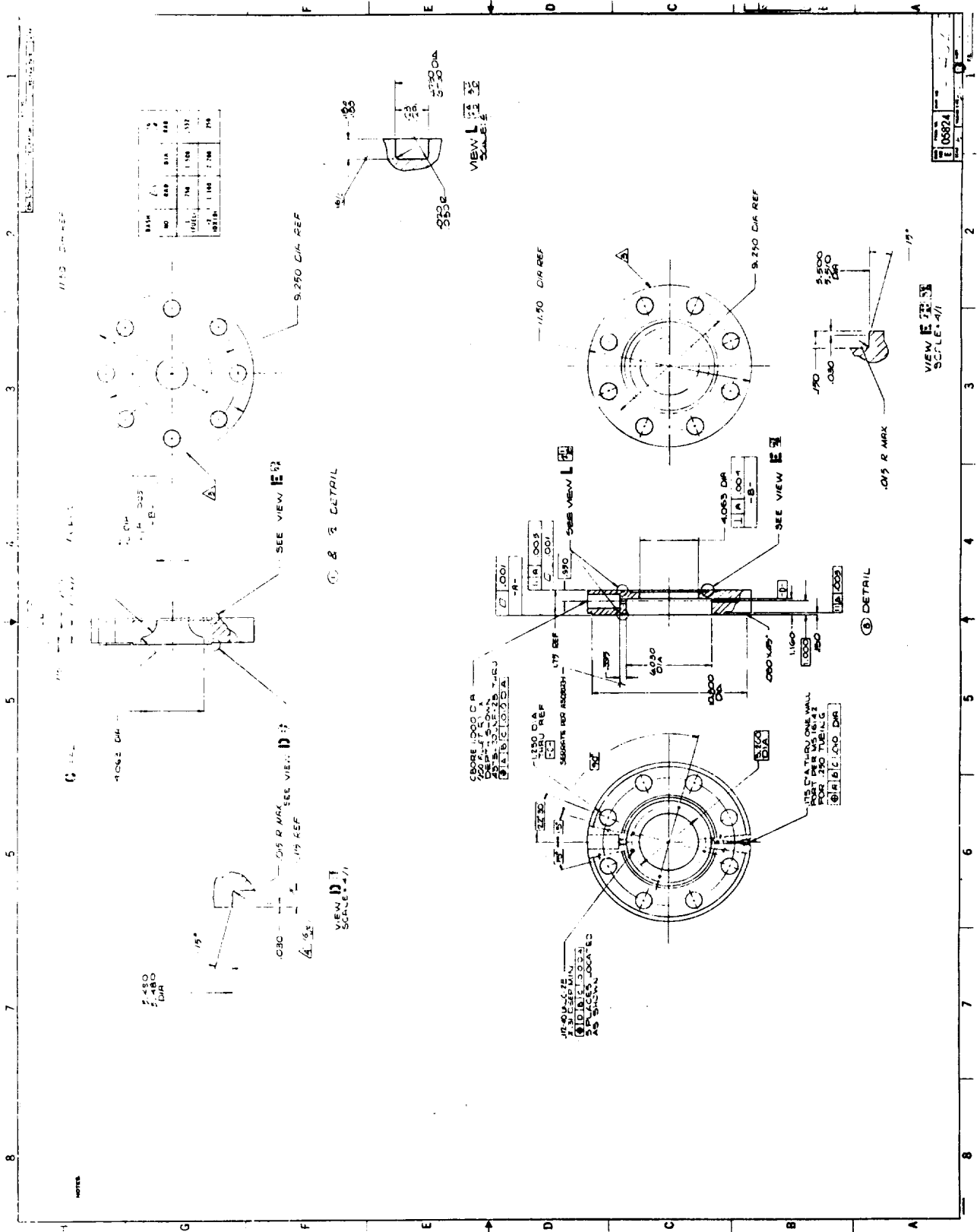


Figure III-28. Detail Drawings of Throats, Main Injector Simulators, Resonator Cavity and Tuning Blocks (Sheet 2 of 3)



Figure III-29. Acoustic Resonator Flange Assembly, PN 1191402, -3, and -4
Plus Tuning Blocks

0580 SP 019

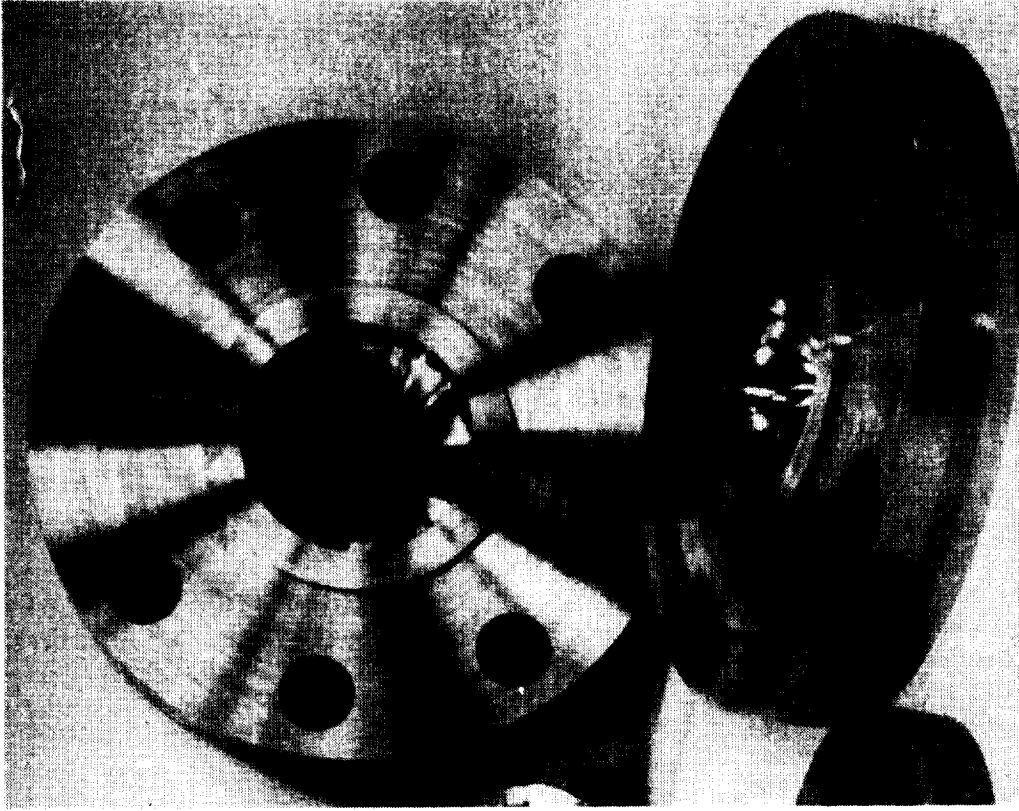


Figure III-31. Fuel- and Oxidizer-Rich Throats, PN 1191402-1 and -2

0580 SP 019

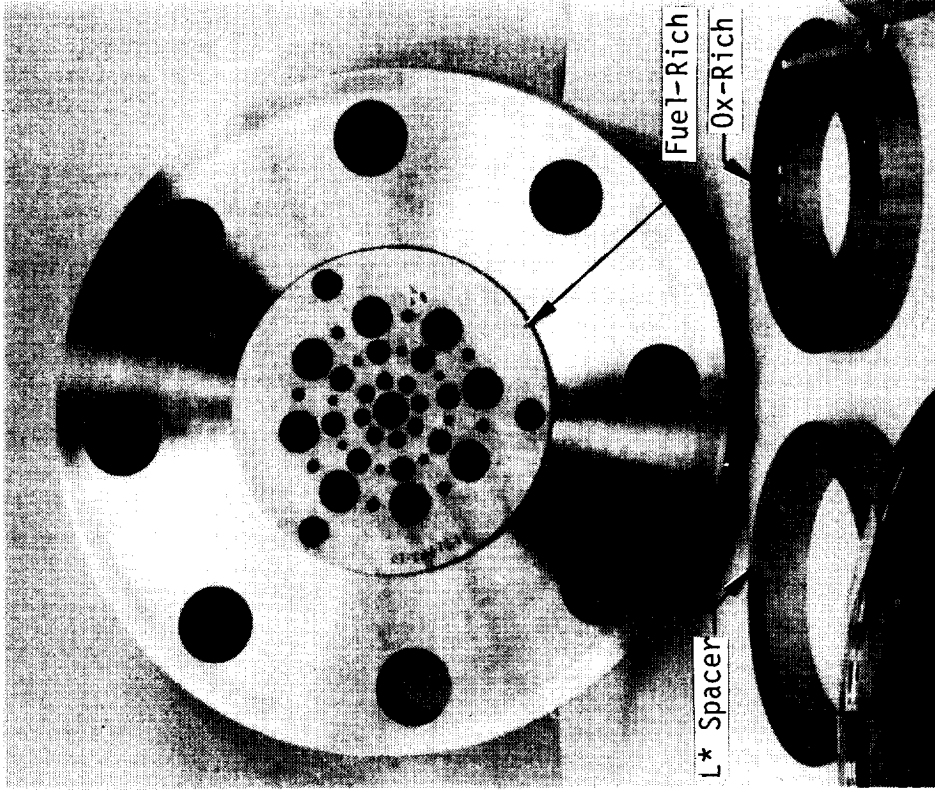


Figure III-30. Main Injector Simulators, PN 1191402-8, -10, and -11

III, G, Main Injector Simulator (cont.)

oxidizer main injector was required because it was not practical to generate sufficient flow area by drilling a large number of smaller holes. The residual material between the required number of smaller holes was insufficient to carry the pressure load.

The fuel-rich simulator contains holes of varying diameters. The sizes were varied to allow orifice plugging data for a range of hole sizes to be obtained.

H. THROAT SECTIONS

Design details for the throat sections of the fuel- and oxidizer-rich preburners are shown in Figure III-28 (p. 54). Photographs of these parts are provided in Figure III-31. The throats are fabricated from commercially available 304 stainless steel forged blank flanges. The downstream side of the throat is configured to interface with the forward side of the chambers and also to receive a proof and leak check plate. The latter plate is attached via eight 0.75-16 bolts which thread into the back face of the throat plate. (Note: The oxidizer-rich throat diameter, B diameter on Figure III-28, was modified prior to testing to read 2.510 in place of 2.200.)

I. INSTRUMENTATION RAKE

The instrumentation rake, shown in Figure III-32, was designed to measure the radial gas temperature profiles at two angular positions and to remove samples of hot-gas combustion products in the center of the chamber and near the wall.

The rake assembly is comprised of a flange and two removable probes. Each probe contains five 0.159-cm (0.063-in.) diameter grounded junction chromel-alumel (type K) thermocouples and two gas sample tubes 0.159-cm (0.063-in.) in diameter. The probes are joined to the flange via four 0.25-20 x 2-in.-long bolts. The seal requirements are defined in Figure III-4. Rakes and probes were not fabricated as part of this program.

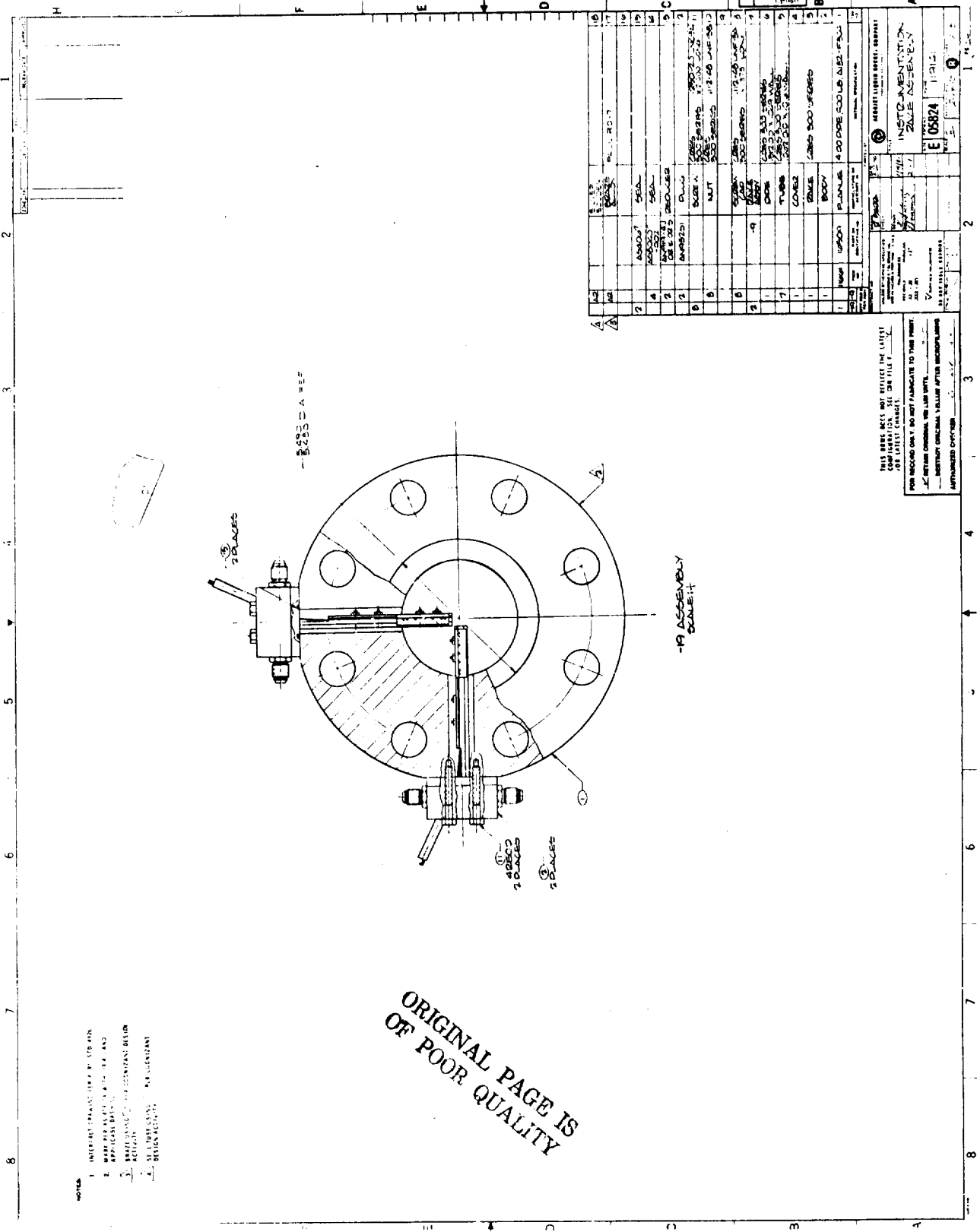


Figure III-32. Instrumentation Rake Assembly (1 of 3)

IV. CONCEPT SELECTION AND SUPPORTING ANALYSES

A. FUEL-RICH PREBURNER

1. Problem Definition and Past History

The fuel-rich preburner of a staged-combustion engine is intended to provide a uniform-temperature, high-pressure source of hot gas which will not foul the turbine and main propellant injector. The design and operational parameters and problems which must be considered are discussed below.

a. Gas Temperature Uniformity

Production of uniform temperature gas is, of course, the primary goal of all the preburners. Thermal streaking must be avoided to ensure high performance and long-life turbine operation. It is necessary to achieve virtually complete propellant vaporization, especially of the rich propellant (diluent), and to achieve uniform mixing between the vaporized diluent and bipropellant reaction products to provide a homogeneous gas mixture that will ensure a uniform turbine inlet temperature.

b. Carbon Deposition

Past history has demonstrated that fuel-rich operation with hydrocarbon fuels produces solid carbon products in the turbine drive gas mixture which deposit upon the turbine nozzle surfaces and degrade turbine performance with time. The carbon which passes through the turbine may also adversely affect the operation of the secondary injector on a staged-cycle engine. Both are inconsistent with the long cycle-life, minimum maintenance, and engine reusability goals for STS applications.

c. Stability

Combustion stability is an important factor in all the combustors. The significant differences in propellant properties are expected to make propellant vaporization a more important consideration with fuel-rich than oxygen-rich operation. Fuel freezing, which is often accompanied by "pops" and rough combustion, can occur with certain element designs, particularly with the oxidizer-rich concepts.

d. Performance

Fuel-rich preburner gas temperatures and reaction rates are sufficiently low that forward-rate reaction kinetics control performance. This may result in gas temperatures and properties differing from the predicted equilibrium values. Therefore, gas residence times and kinetic reaction times must be controlled to assure high performance and stable operation.

IV, A, Fuel-Rich Preburner (cont.)

e. Ignition

Ignition and flammability are important considerations affecting preburner operation. The ignition process impacts the way a combustor must be started if damage due to excessive overpressure or undesirable mixture ratios is to be avoided. The flammability limits of a propellant combination define the safe limits of operation during the ignition process and steady-state combustion.

The state of the art of gas generator design at the start of this technology program is summarized in Figure IV-1. This is based on experience with LOX/RP-1 gas generators for engines such as the F-1, Titan I, etc., as detailed in Reference 1. Figures IV-2 and IV-3 provide conceptual drawings of gas generator designs which have been employed in past programs.

Some elements of design practice stated in the monograph (Ref. 1) are as follows:

- ° Film Cooling has been used extensively to maintain safe wall temperatures. This, however, results in a nonuniform MR distribution and required turbulence rings and side outlets to remix the coolant. It is presently believed that much of this could be circumvented by proper injector design.

- ° Manifold Volume was dictated by engine start and shutdown transients with the volume of the minor propellant minimized. A 50% (major propellant) excess dilution above that required to react with drainable minor propellant at rated MR is suggested, along with liberally sized purge and drain ports.

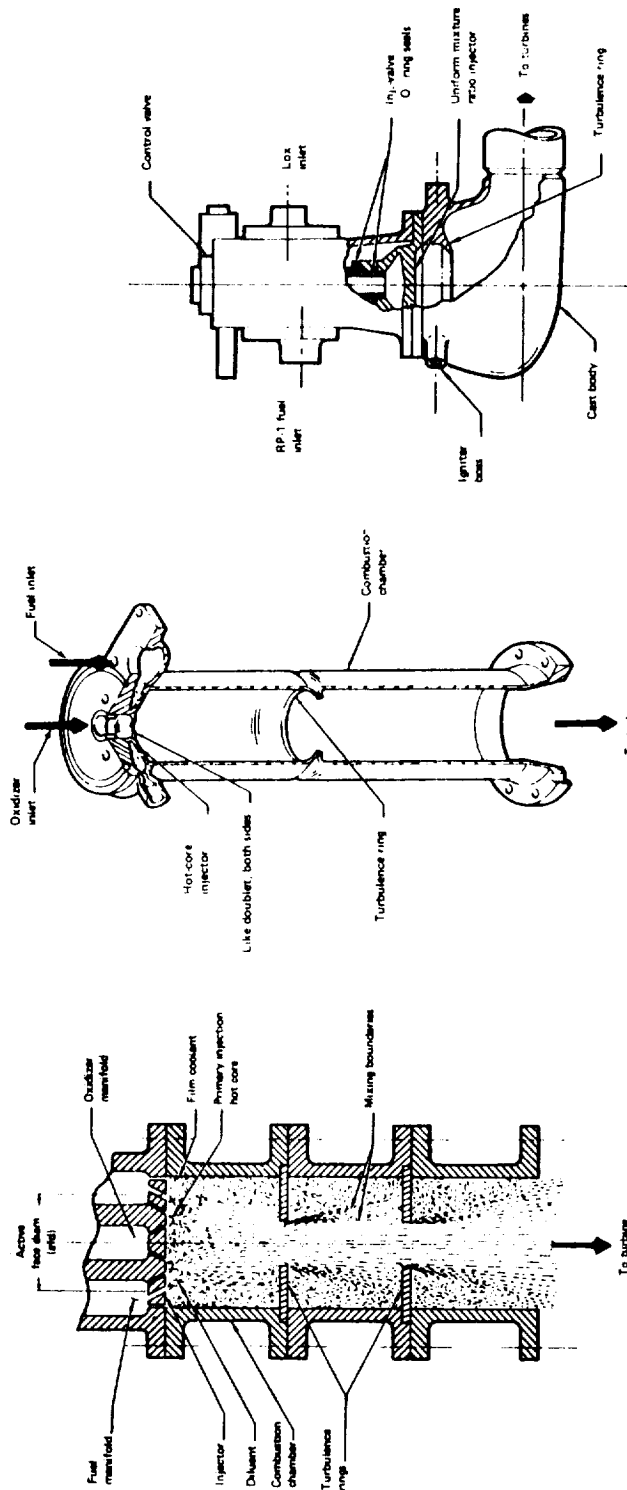
- ° Injection Elements prescribed are like-on-like (LOL) doublets and fuel-oxidizer-fuel (FOF) triplets for fuel-rich combustors. It appears that little work has been done on element optimization for gas generators where one propellant flow is considerably higher than the other.

One of the objectives of this program has been to apply 1980 injector design technology to determine if the required clean burning and mixing of combustion gases can be achieved without the need for mechanical mixing devices.

An example of a 1950 vintage LOX/RP-1 gas generator injector design and the resulting turbine nozzle area reduction in nine successive long-duration firings is shown in Figure IV-4. Each successive test, represented by the solid line, resulted in a loss of flow area during the test and incomplete recovery between tests. The effect of operating mixture ratio

PARAMETER	FUEL-RICH	OX-RICH
MAX P _c N/m ² /PSIA TEMP. °K/°F	1000/1500 (F-1)	NO DATA BASE
ELEMENT TYPE	F-1 H-1, E-1 ATLAS MA-2	NO DATA BASE
FACE MATERIAL	LOL DOUBLET FOF TRIPLET	NO DATA BASE
CHAMBER MATERIEL	COPPER	NO DATA BASE
MIXING DEVICES	CRES OR HASTELLOY C	NO DATA BASE
INTERPROPELLANT SEALS	SPLASH RING, TURBINE RING, OR SIDE OUTLETS	NO DATA BASE
	NONE, OR DOUBLE WITH VENT	NO DATA BASE

Figure IV-1. LOX-RP-1 Gas Generator Design Criteria Summary

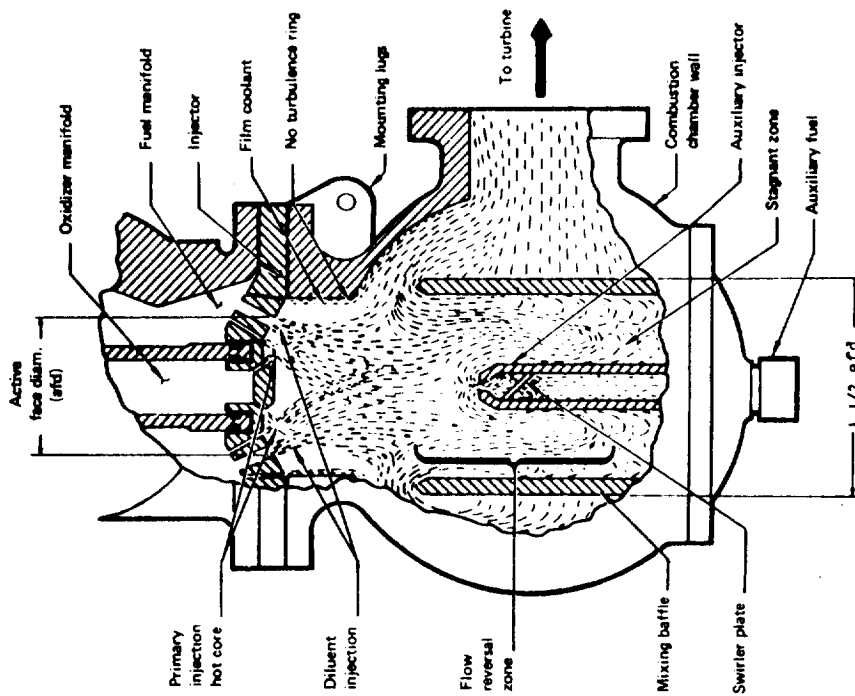


As of outer axial flow GG engine mid-chamber turbulence ring

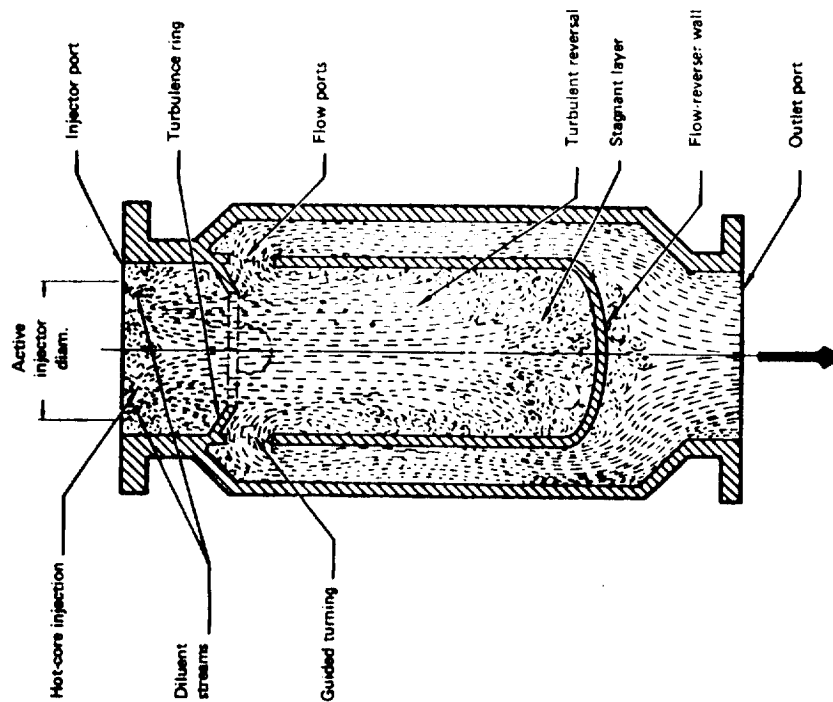
As of outer axial flow GG engine mid-chamber turbulence ring

As of outer axial flow GG engine mid-chamber turbulence ring

Figure IV-2. State-of-the-Art GG Designs Use Mechanical Mixing to Obtain Uniform Temperature Distribution



Side-outlet, reverse-flow GG

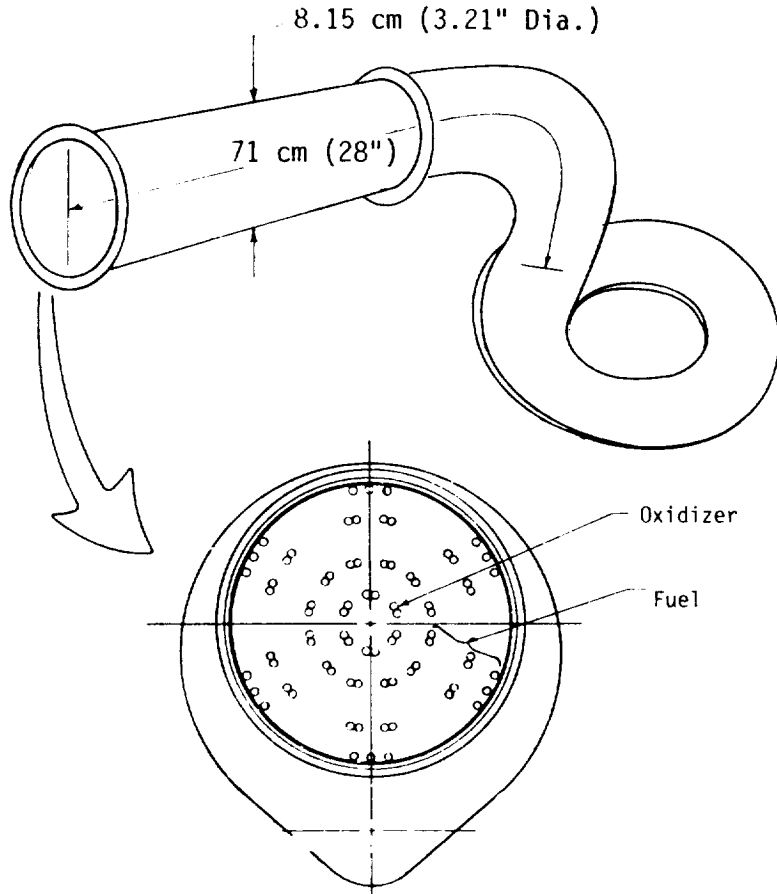


Axial-outlet, reverse-flow GG with turbulence ring near injector

Figure IV-3. State-of-the-Art GG Designs Use Reverse Flow and Side Outlet Designs to Obtain Uniform Temperature Distributions

ORIGINAL PAGE IS
OF POOR QUALITY

TITAN I GG



TURBINE NOZZLE AREA HISTORY
TITAN I FIRST-STAGE GAS GENERATOR (XLR87-AJ-3)

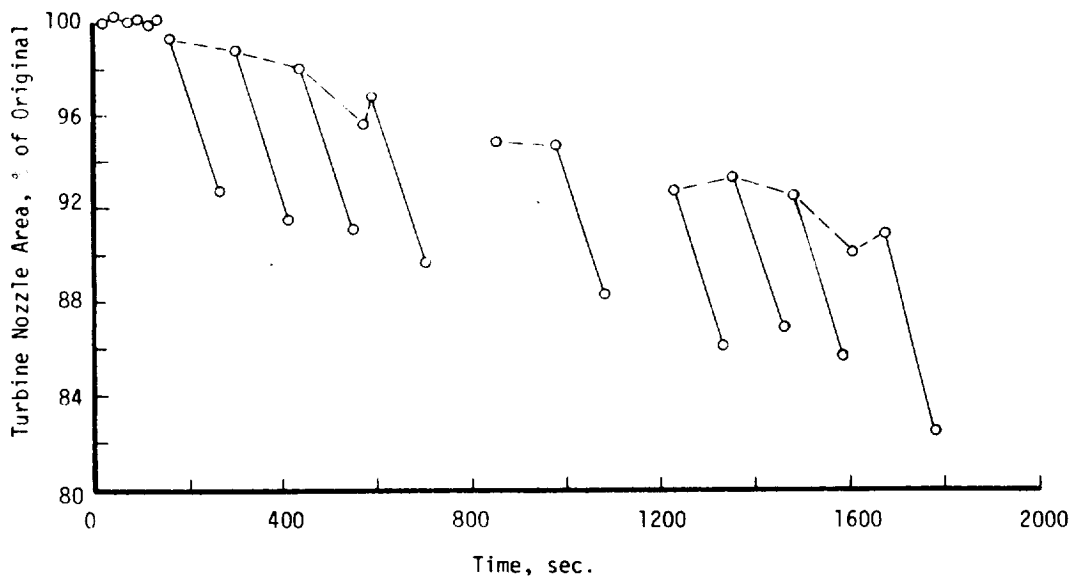


Figure IV-4. Turbine Nozzle Area History - Titan I First Stage Gas Generator (XLR87-AJ-3)

IV, A, Fuel-Rich Preburner (cont.)

on the area reduction is defined by the experimental data shown in Figure IV-5. These types of results were typical of most engines employing the LOX/RP-1 fuel-rich propellant combination.

2. Concept Selection

Three combustion concepts were considered applicable to the preburner design: 1) the hot core approach, 2) the stoichiometric burner with downstream dilution approach, and 3) the uniform mixture ratio combustor approach.

The hot core approach was employed in the Titan I injector, shown in Figure IV-4. The inner row of elements contained LOL oxidizer doublets and the outer 3 rows LOL fuel doublets. The hot core was surrounded by large amounts of fuel to provide cooling of the 71.1-cm (28-in.) long combustor. The turns provided the required mixing. The carbon buildup problems encountered were acceptable for a single-burn, non-reusable vehicle.

The stoichiometric combustor concept would burn at a high mixture ratio of 2 to 3. The resulting 3033°K (5000°F) combustion gases would be subsequently quenched by the spray injection of the remaining fuel. This approach provides the most difficult cooling requirements of all concepts considered.

The uniform mixture ratio approach is typical of a conventional injector design where the fuel and oxidizer sprays are fully mixed by the overlapping pattern of the individual injection elements. A fine uniform pattern is desired to obtain the maximum mixing in the shortest length.

The analytical approach to a singular concept selection is outlined in the following sections. The primary objectives of the analytical approach were to first develop a combustion model that will accurately predict combustion performance and gas properties for fuel-rich LO₂/RP-1 gas generators and to use the model to select the best combustor concept. A secondary objective was to evaluate the model's ability to accurately predict carbon formation in fuel-rich GG's.

3. Technical Approach to Model Development

As illustrated by the data of Figure IV-6, existing equilibrium prediction models do not accurately forecast fuel-rich combustion performance parameters. In this program, a "pseudo-kinetic" model approach was taken since existing gas-phase kinetic computer programs cannot handle heterogeneous combustion. The pseudo-kinetic model assumes instantaneous partial equilibrium combustion, followed by diluent heating and reaction and

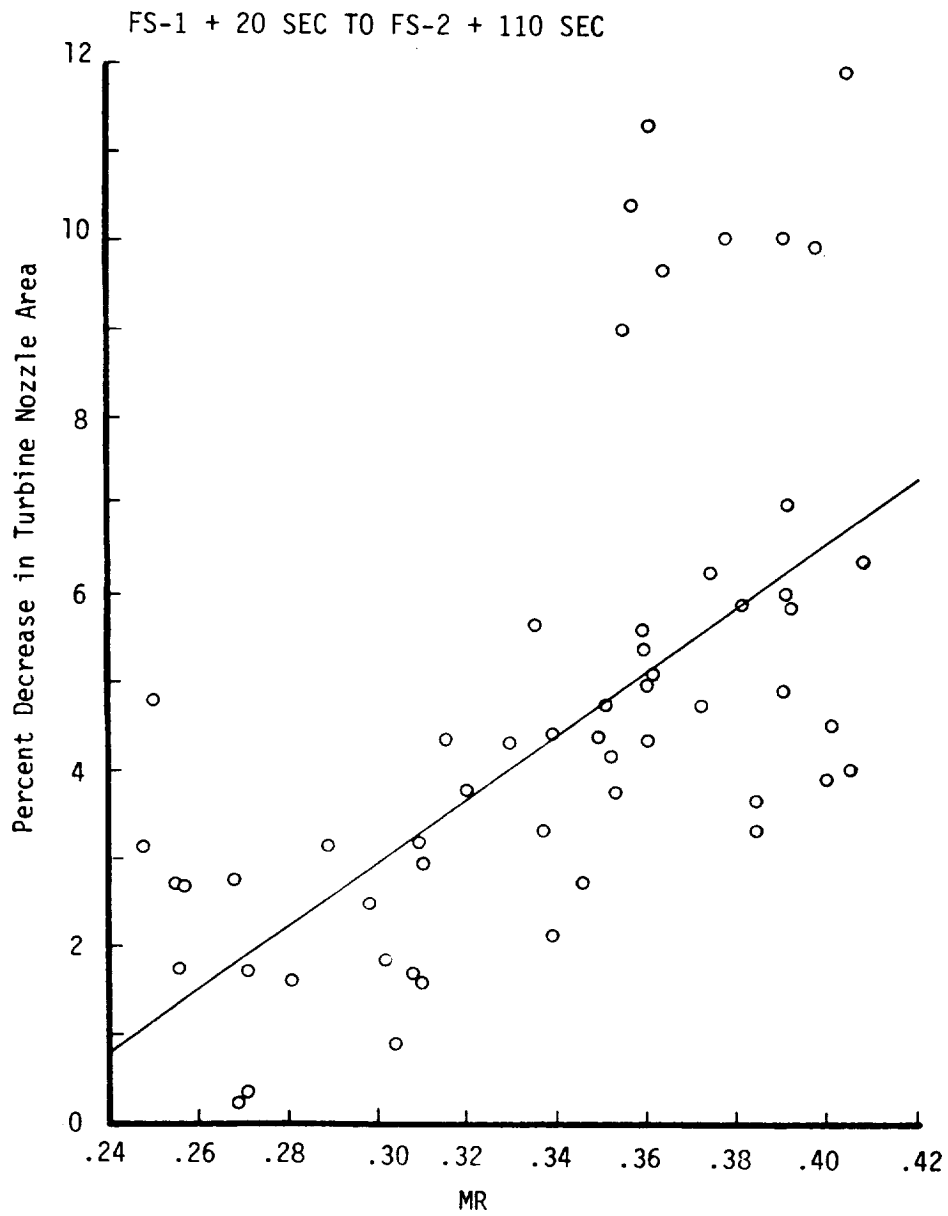


Figure IV-5. Mixture Ratio Influence on Turbine Nozzle Area Reduction - Titan I First Stage Gas Generator

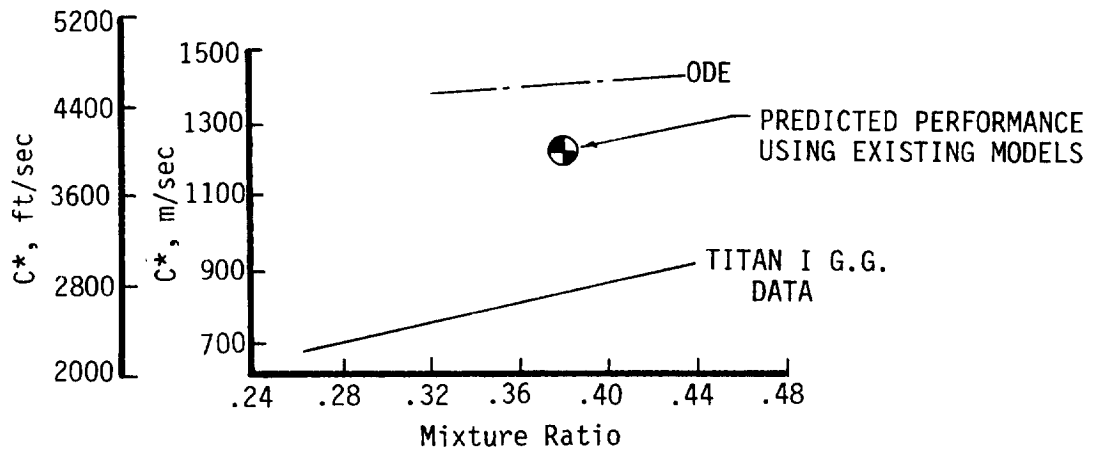


Figure IV-6. Fuel-Rich Combustion C^* vs Mixture Ratio, Predictions and Test Data

IV, A, Fuel-Rich Preburner (cont.)

kinetically limited thermal decomposition. This approach was taken to permit the development of a "user-oriented" combustion model. The model is intended for design concept evaluation and hence must be engineer-oriented. The model specifications were for GG design parameter input only. The input and parameters are shown in Figure IV-7.

a. Model Development

Development of the model was done by Software and Engineering Associates (SEA) under subcontract to ALRC. The development consisted of the tasks shown in Figure IV-8. A computerized literature search was conducted by SEA to obtain data for fuel cracking, reaction, and soot formation mechanisms.

A computer model formulation task was conducted in parallel with the literature search. The selected model concept is shown in Figure IV-9. It is assumed that all of the oxidizer reacts with a portion of the fuel to produce equilibrium combustion products. The JANNAF One-Dimensional Equilibrium (ODE) computer program was selected for this calculation. The remainder of the fuel is presumed to vaporize and react kinetically with the ODE combustion products. The JANNAF One-Dimensional Kinetics (ODK) computer program was selected for this purpose.

The fuel vaporization is modeled using a temperature-dependent rate expression to permit its insertion into the ODK program. The vaporized fuel undergoes kinetically limited combustion to form final products.

The computerized literature search was conducted as outlined in Figure IV-10. Appendix A identifies applicable references.

The combustion reactions, listed in Figure IV-11, were compiled for reaction screening. A two-step global fuel-cracking model was selected, as shown in Figure IV-12. These reactions, along with the complete reaction set, are listed in Figure IV-13. These reactions were screened by eliminating those reactions whose species generation rates were insignificant. The final reaction set is listed in Figure IV-14, and the final kinetic scheme is illustrated in Figure IV-15. The liquid RP-1 vaporized in the ODE combustion products and cracks to the products, as shown in Figure IV-16. The cracking products undergo further reaction to H₂ and CH₄ and C₂ hydrocarbons. The oxygen-related reactions were found to be effectively frozen and did not contribute to product formation.

For reasons of simplicity in the modeling process, it was assumed that the fuel could be modeled as paraffinic although it is in

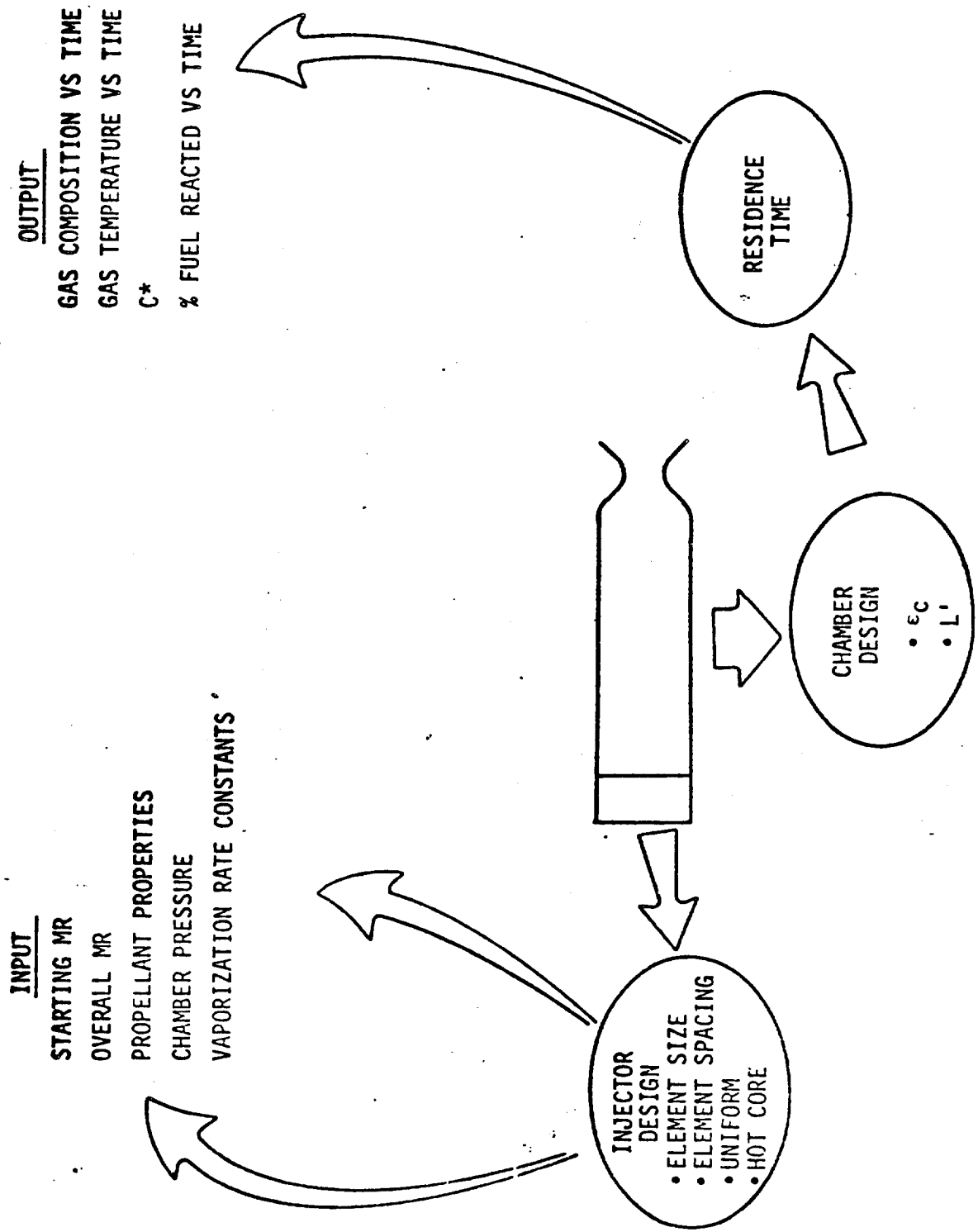


Figure IV-7. Fuel-Rich Combustion Model Input, Output, and Design Parameters

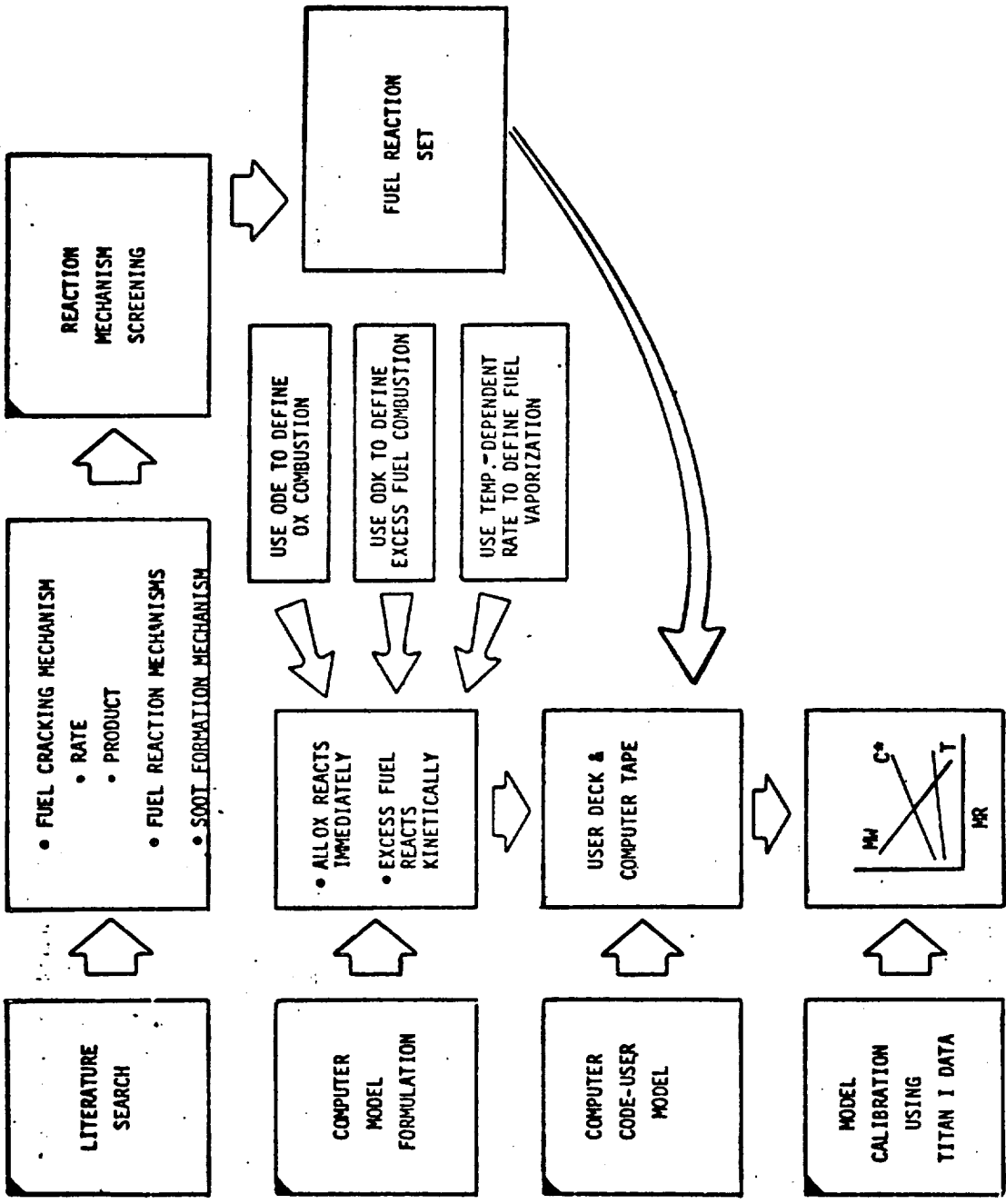


Figure IV-8. Fuel-Rich Combustion Model Study - Model Development Logic

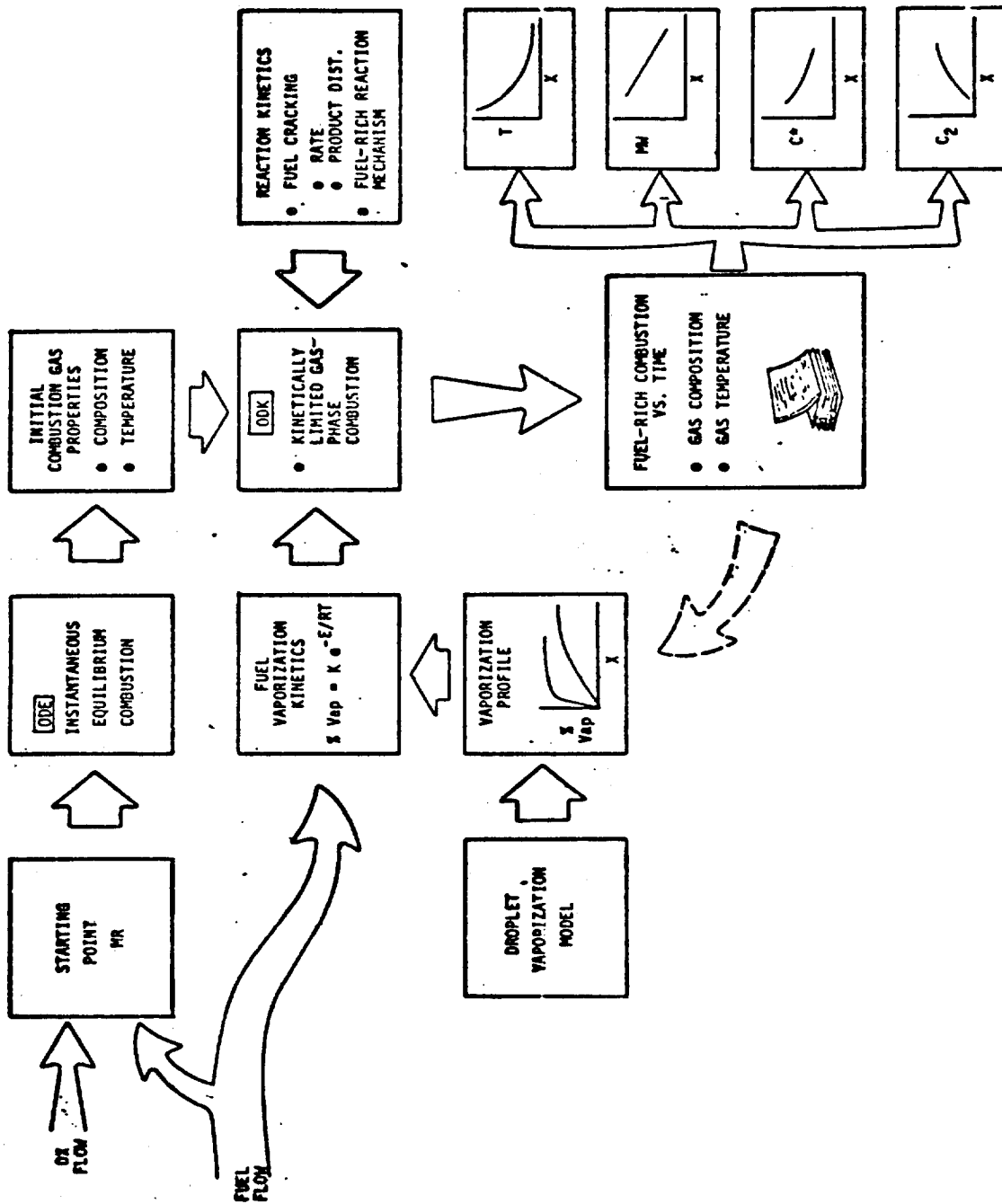


Figure IV-9. Fuel-Rich L02/RP-1 Combustion Model Logic

- DATA BASES SEARCHED BY COMPUTER

NTIS
COMPENDEX
SCISEARCH
CHEMICAL ABSTRACTS
CONFERENCE PAPER INDEX
POLLUTION ABSTRACTS

- KEY CONCEPTS USED FOR SEARCH

SOOT	KINETIC	PYROLYSIS
COKE	RATES	CRACKING

- SCAN RECENT PUBLICATIONS

COMBUSTION AND FLAME
COMBUSTION SCIENCE AND TECHNOLOGY

- REFERENCE FOLLOW-UP

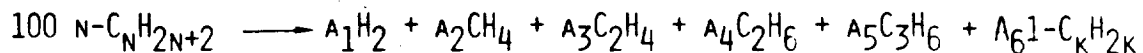
- PERSONAL COMMUNICATION WITH AUTHORS

Figure IV-10. SEA Literature Search Strategy

- I. HYDROCARBON DECOMPOSITION AND PARTIAL OXIDATION
- II. LOW-TEMPERATURE PYROLYSIS OF METHANE
- III. METHANE DECOMPOSITION AND PARTIAL OXIDATION
- IV. C2-SPECIES GENERATION AND PROPAGATION
- V. METHYLENE RADICAL REACTIONS
- VI. CARBON MONOXIDE OXIDATION
- VII. O-H BIMOLECULAR PROPAGATION
- VIII. O-H TERMOLECULAR TERMINATION
- IX. SOOT NUCLEATION AND COAGULATION (CARBON FORMATION)

Figure IV-11. Chemical Reaction Sets for Fuel-Rich LO₂/RP-1 Combustion Model

1. DECOMPOSITION OF PRIMARY PARAFFIN TO MAJOR FRAGMENTS AND OLEFINS (COLLECTIVELY IN LUMPED GROUP)



2. DECOMPOSITION OF OLEFINS TO MAJOR FRAGMENTS AND ACETYLENE

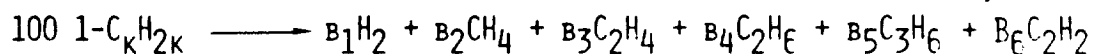


TABLE OF COEFFICIENTS

i	1	2	3	4	5	6
A _i	5	51	107	44	49	100
B _i	9	11	90	7	147	27

TABLE OF FIRST ORDER RATES:

$$k = 10^A \text{ EXP } (-E/RT) \text{ SEC}^{-1}$$

REACTION	A	E(KCAL)
1	14.146	60
2	13.150	55

Figure IV-12. RP-1 Fuel Vapor Cracking Model, Two-Step Global Reaction

C12H26(L)	=	C12H26	,A=3.2E4	,N=0.	,B=11.8,DCOCEANE VAPORIZATION *		
C12H26	H2+	CH4+	C2H6+	C2H6+	C3H6+	C7H14,A=1.4E14,N=0.,B=60.	
C7H14	H2+	CH4+	C2H6+	C2H6+	C3H6+	C2H2,A=1.413E13,N=0.,P=55.	
CM4	=	CM3 + H	,A=1.E17	,N=0	,B=85.8,	TABAYASH/BUR(1979) 9	
CM30	=	CM3 + H	,A=3.981E40,N=7.5	,B=22.0,	ENGLEMAN (1976)	12	
CO + H	=	CM0	,A=1.585E20,N=1.5	,B=0,	ENGLEMAN (1976)	22	
C2H5	=	C2H4 + H	,A=6.0E17	,N=0	,B=31.8,	TABAYASH/BUR(1979) 35	
C2H3	=	C2H2 + H	,A=7.94E14	,N=0	,B=31.5,	TABAYASH/BUR(1979) 39	
HO + O	=	HO2	,A=1.0E17	,N=0	,B=0,	ENGLEMAN (1976) 55	
H + HO	=	H2O	,A=1.995E22,N=2.0	,B=0,	ENGLEMAN (1976)	57	
H + O	=	HO	,A=7.943E15,N=0	,B=0,	ENGLEMAN (1976)	58	
H + O2	=	HO2	,A=1.995E15,N=0	,B=1.,	ENGLEMAN (1976)	59	
END TBR REAX							
CM2 + CM20	=	CM0 + CH3	,A=3.162E10,N=-.5	,B=6.,	ENGLEMAN (1976)	3	
CM20+ CM3	=	CM0 + CH4	,A=1.E10	,N=-.5	,B=6.,	ENGLEMAN (1976)	4
CM2 + H2	=	CM3 + H	,A=3.162E12,N=0	,B=7.,	ENGLEMAN (1976)	5	
CM3 + HO	=	CM2 + H2O	,A=6.309E10,N=-.7	,B=2.,	ENGLEMAN (1976)	6	
CM2 + O2	=	CM20 + O	,A=5.011E11,N=-.5	,B=7.,	ENGLEMAN (1976)	7	
CM3 + O2	=	CM20 + HO	,A=3.162E13,N=0	,B=20.,	ENGLEMAN (1976)	8	
CM3 + HO2	=	CM4 + O2	,A=1.E11	,N=-.5	,B=6.,	ENGLEMAN (1976)	10
CM3 + O2	=	CM30 + O	,A=3.162E12,N=0	,B=30.,	ENGLEMAN (1976)	11	
CM4 + O	=	CM3 + HO	,A=1.995E13,N=0	,B=9.,	ENGLEMAN (1976)	14	
CM4 + H	=	CM3 + H2	,A=6.310E13,N=0	,B=11.9,	ENGLEMAN (1976)	15	
CM4 + HO	=	CM3 + H2O	,A=3.162E13,N=0	,B=5.,	ENGLEMAN (1976)	16	
CM3 + O	=	CM20 + H	,A=5.012E13,N=0	,B=0,	ENGLEMAN (1976)	17	
CM3 + HO	=	CM20 + H2	,A=7.5E12	,N=0	,B=0,	TABAYASH/BUR(1979) 18	
CM20+ O	=	CM0 + HO	,A=1.0E11	,N=-1.	,B=3.5,	ENGLEMAN (1976)	19
CM20+ H	=	CM0 + H2	,A=1.259E10,N=-1.	,B=3.2,	ENGLEMAN (1976)	20	
CM20+ HO	=	CM0 + H2O	,A=3.162E10,N=-1.	,B=0,	ENGLEMAN (1976)	21	
CM0 + H	=	CO + H2	,A=1.585E12,N=-.5	,B=0,	ENGLEMAN (1976)	23	
CM0 + HO	=	CO + H2O	,A=3.162E10,N=-1.	,B=0,	ENGLEMAN (1976)	24	
CM0 + O	=	CO + HO	,A=3.162E11,N=-1.	,B=0.5,	ENGLEMAN (1976)	25	
CM0 + O2	=	CO + HO2	,A=1.585E12,N=0	,B=7.,	ENGLEMAN (1976)	26	
C2H6	=	CM3 + CM3	,A=1.0E13	,N=0	,B=66.8,	TABAYASH/BUR(1979) 27	
C2H5+ H	=	CM3 + CM3	,A=1.0E13	,N=0	,B=0,	TABAYASH/BUR(1979) 28	
CM3 + CM3	=	C2H4 + H2	,A=6.026E16,N=0	,B=43.,	GARDNER (1974) 29		
CM3 + C2H6	=	C2H5 + CM4	,A=5.0E14	,N=0	,B=21.5,	TABAYASH/BUR(1979) 30	
CM3 + CH4	=	C2H6 + H	,A=8.0E13	,N=0	,B=40.,	TABAYASH/BUR(1979) 31	
CM3 + CH4	=	C2H5 + H2	,A=1.0E13	,N=0	,B=23.,	TABAYASH/BUR(1979) 32	
CM3 + C2H4	=	C2H3 + CM4	,A=5.0E12	,N=0	,B=13.,	TABAYASH/BUR(1979) 33	
C2H5	=	C2H4 + H	,A=2.818E13,N=0	,B=40.8,	JENSEN (1974) 36		
C2H4	=	C2H2 + H2	,A=2.09E17	,N=0	,B=70.1,	TABAYASH/BUR(1979) 37	
C2H4+H	=	C2H3 + H2	,A=7.E14	,N=0	,B=14.5,	TABAYASH/BUR(1979) 38	
C2H3+ H	=	C2H2 + H2	,A=4.571E12,N=0	,B=2.5,	EBERIUS (1973) 40		
C2H2+ H	=	C2H + H2	,A=1.807E14,N=0	,B=19.,	JENSEN (1974) 41		
C2H + H	=	C2 + H2	,A=6.023E13,N=0	,B=36.,	JENSEN (1974) 42		
CM2 + CH4	=	CM3 + CM3	,A=2.49E13	,N=0	,B=25.6,	TABAYASH/BUR(1979) 43	
CM2 + C2H6	=	C2H5 + CM3	,A=1.22E13	,N=0	,B=15.7,	TABAYASH/BUR(1979) 44	
CM2 + C2H4	=	C2H3 + CM3	,A=1.09E13	,N=0	,B=12.0,	TABAYASH/BUR(1979) 45	
CM2 + CM4	=	C2H4 + H	,A=6.E13	,N=0	,B=0.,	TABAYASH/BUR(1979) 46	
C2H6+ H	=	C2H5 + H2	,A=1.072E14,N=0	,B=9.23,	TABAYASH/BUR(1979) 47		
CO + HO	=	CO2 + H	,A=1.514E07,N=-1.3	,B=0.75,	ENGLEMAN (1976)	48	
H + HO	=	H2 + O	,A=7.943E09,N=-1.	,B=7.,	ENGLEMAN (1976)	49	
H + HO2	=	HO + HO	,A=2.512E14,N=0	,B=1.4,	ENGLEMAN (1976)	50	
HO + H2	=	H + H2O	,A=2.512E13,N=0	,B=5.2,	ENGLEMAN (1976)	51	
HO + O	=	H + O2	,A=2.512E13,N=0	,B=0,	ENGLEMAN (1976)	52	
H + HO2	=	H2 + O2	,A=2.512E13,N=0	,B=.7,	ENGLEMAN (1976)	53	
HO + HO	=	H2O + O	,A=6.310E12,N=0	,B=1.,	ENGLEMAN (1976)	54	
HO	=	H + H	,A=1.995E14,N=0	,B=96.,	ENGLEMAN (1976)	56	
M2			,A=2.5E11	,N=-0.7	,B=6.,	ENGLEMAN(1976)	65
CM + CM4	=	CM2 + CM3	,A=1.E10	,N=-0.5	,B=6.,	ENGLEMAN (1976)	66
CM + CO2	=	CM0 + CO	,A=5.E11	,N=-0.5	,B=10.,	ENGLEMAN (1976)	67
C1 + HO	=	CM0 + H	,A=1.E10	,N=-0.5	,B=15.,	ENGLEMAN (1976)	68
CM + HO2	=	CM2 + O2	,A=3.16E11	,N=-0.7	,B=5.,	ENGLEMAN (1976)	69
C12 + H	=	CM + H2	,A=5.E11	,N=-0.5	,B=5.,	ENGLEMAN (1976)	70
CM2 + HO	=	CM + H2O	,A=7.9E17	,N=0.	,B=95.,	SUNDARAM-FROMCNT	71
C2H4	=	CM3 + CM3	,A=3.E12	,N=0.	,B=19.,	SUNDARAM-FROMCNT	72
C2H5 + H	=	CM3 + C3H6	,A=4.E13	,N=0.	,B=0.,	SUNDARAM-FROMCNT	73
C2H4 + C2H4	=	CM3 + C2H5	,A=8.9E16	,N=0.	,B=65.,	SUNDARAM-FROMCNT	74
C2H4 + C2H4	=	CM2 + H	,A=2.E9	,N=0.	,B=31.5,	SUNDARAM-FROMCNT	75
C2H2 + H	=	C2H3	,A=6.E13	,N=0.	,B=1.3,	SUNDARAM-FROMCNT	76
C2H3 + H	=	C2H4	,A=1.E13	,N=0.	,B=0.,	SUNDARAM-FROMCNT	77

Figure IV-13. Complete Fuel-Rich Reaction Mechanism

C12H26(L) = C12H26	,A=1.0E4,	N=0.,	B=10.,	DODECANE VAPORIZATION *	
C12H26 = H2 + CH4 + C2H4 + C2H6 + C3H6 + C3H6 +			C7H14,A=1.4E14,N=0.,B=60., *		
C7H14 = H2 + CH4 + C2H4 + C2H6 + C3H6 + C2H2,			A=1.413E13,N=0.,B=55., *		
CH4 = CH3 + H	,A=1.E17	,N=0	,B=85.8,	TABAYASH/HUR(1979)	9
C2H5 = C2H4 + H	,A=6.8E17	,N=0	,B=31.8,	TABAYASH/HUR(1979)	35
C2H4 = C2H2 + H2	,A=2.09E17	,N=0	,B=79.1,	TABAYASH/HUR(1979)	37
C2H3 = C2H2 + H	,A=7.94E14	,N=0	,B=31.5,	TABAYASH/HUR(1979)	39
END TBR REAX					
CH4 + H = CH3 + H2	,A=6.310E13	,N=0	,B=11.9,	ENGLEMAN (1976)	15
CH3 + C2H6 = C2H5 + CH4	,A=5.0E14	,N=0	,B=21.5,	TABAYASH/HUR(1979)	30
CH3 + CH4 = C2H6 + H	,A=8.0E13	,N=0	,B=40.,	TABAYASH/HUR(1979)	31
CH3 + CH4 = C2H5 + H2	,A=1.0E13	,N=0	,B=23.,	TABAYASH/HUR(1979)	32
CH3 + C2H4 = C2H3 + CH4	,A=5.0E12	,N=0	,B=13.,	TABAYASH/HUR(1979)	33
C2H4+H = C2H3 + H2	,A=7.E14	,N=0	,B=14.5,	TABAYASHI (1979)	38
C2H3+H = C2H2 + H2	,A=4.571E12	,N=0	,B=2.5,	EBERIUS (1973)	40
C2H6+H = C2H5 + H2	,A=1.072E14	,N=0	,B=9.23,	TABAYASH/HUR(1979)	47
C2H4 + C2H6 = C2H3 + CH3	,A=7.9E17	,N=0.	,B=95.,	SUNDARAM-FROMONT	71
C2H2 + H = C2H3 + C2H5	,A=8.9E16	,N=0.	,B=65.,	SUNDARAM-FROMONT	74
C2H3 + H = C2H3	,A=4.E13	,N=0.	,B=1.3,	SUNDARAM-FROMONT	76
C2H3 + H = C2H4	,A=1.E13	,N=0.	,B=0.,	SUNDARAM-FROMONT	77

Figure IV-14. Screened Fuel-Rich Reaction Mechanism

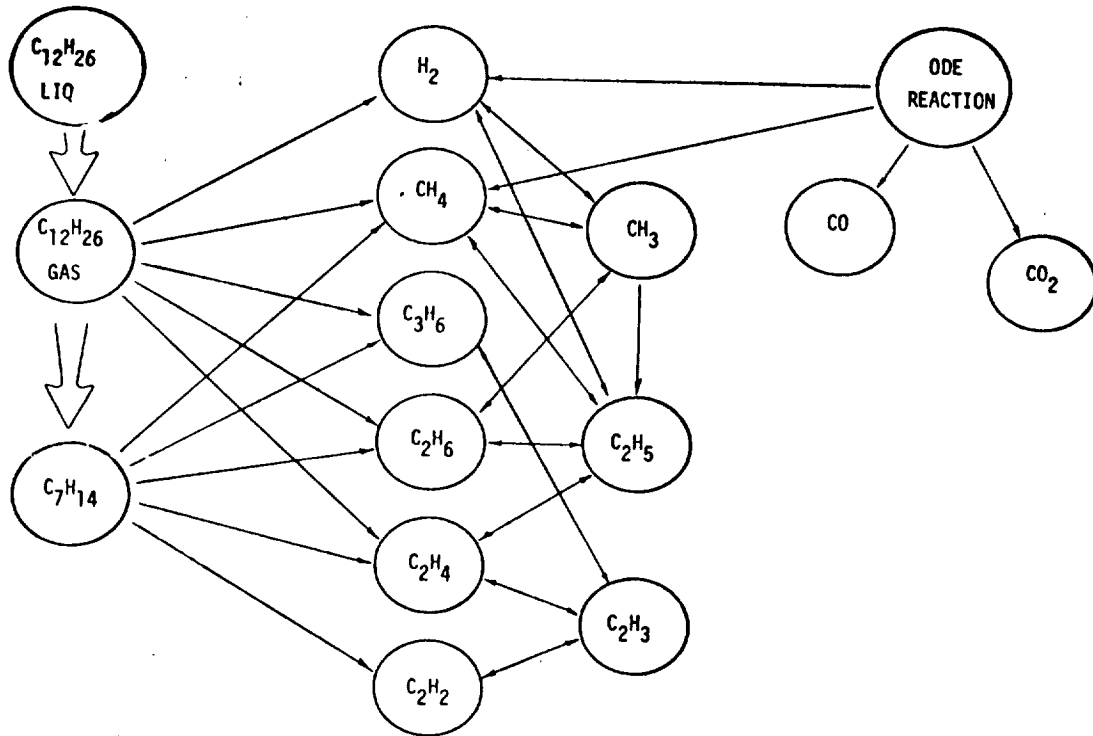


Figure IV-15. Kinetic Mechanisms

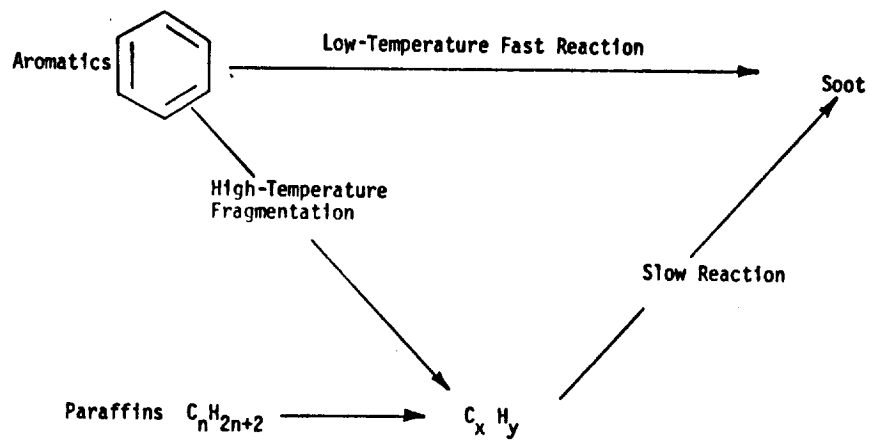
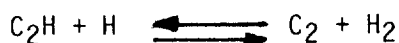
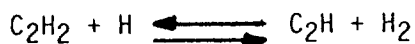


Figure IV-16. Soot Formation Mechanisms

IV, A, Fuel-Rich Preburner (cont.)

reality a complex mixture of hydrocarbons. RP-1 contains up to 5% aromatics. Only the high-temperature soot formation mechanism was pursued. The following high-temperature carbon formation scheme proposed by Jensen was selected for evaluation:



The screening task revealed that this reaction does not yield measurable (10^{-8} mole fraction) carbon and was therefore eliminated from the screened reaction set. Closer examination of the reaction shows that the reverse reaction is favored at normal combustion temperatures. It was concluded that other reactions were responsible for soot. It is known that C_2 hydrocarbons such as C_2H_2 are precursors to soot and that large quantities of C_2 hydrocarbons are indicative of high soot formation.

The fuel vaporization model output for a set of assumed conditions is illustrated in Figure IV-17. The ΔH term is used to indicate the injector atomization. Low values of ΔH are characteristic of fine sprays and high values are characteristic of coarse sprays. The proper values for ΔH and A are determined by comparing these vaporization curves to those predicted using the ALRC vaporization model. A complete listing of the resulting computer model of the fuel-rich combustion cannot be provided in this document because of the extensive volume of data and complexity of the model.

b. Model Calibration

The model was initially calibrated with the Titan I LOX/RP-1 GG data. The twenty calibration computer runs made are summarized in Figure IV-18. As can be seen in Figure IV-19, the model does an excellent job of predicting the Titan I GG performance and gas temperature but does not predict the carbon formation. The input conditions for this model calibration are shown in Figure IV-20. A starting mixture ratio of 2.0 was found to give better results than the MR = 1.2 condition, as shown in Figure IV-21. This is reasonable in light of the hot core design used on the Titan I GG.

η_{vap}	=	$1 - C_f/C_i$	A	=	Constant, 1×10^4
C_f/C_i	=	$e^{-X/V (Ae^{-\Delta H/RT})}$	ΔH	=	Activation Energy K Cal
X	=	Length, in.	R	=	Gas Constant, 1.987
V	=	Chamber Velocity, in./sec	T	=	Temperature, 1111°K (2000°R)

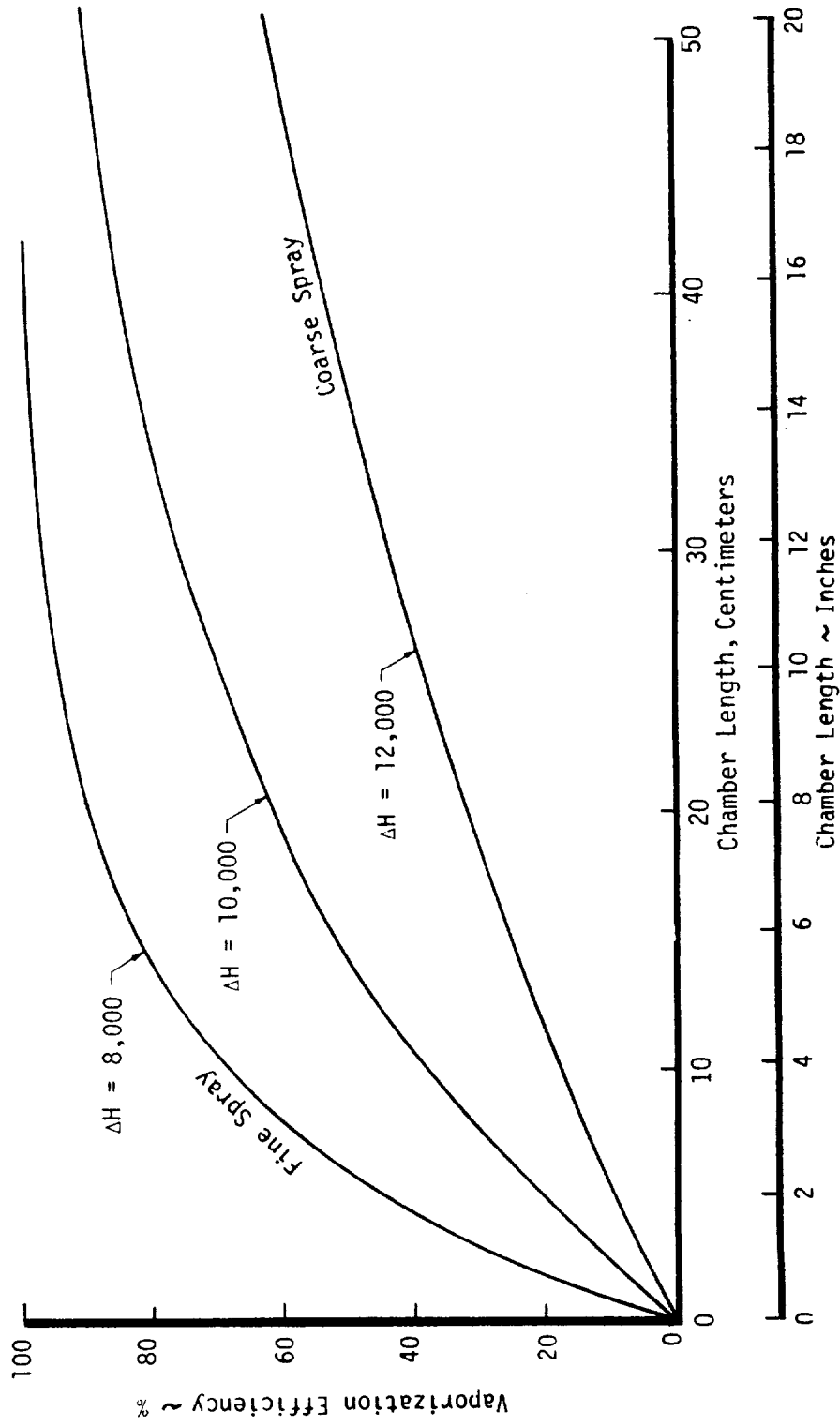


Figure IV-17. Fuel Vaporization Model

RUN NO.	OBJECTIVE	INPUT	RESULTS
1	Checkout run of the complete set version delivered by SEA.	Beginning MR = 1.2 Overall MR = 0.3R A = 3.2×10^5 for 1st reaction (Vaporization) A = 1.413×10^{14} for 3rd reaction HM/N = HI = 0.005 Pr = 3033 kPa (440 psia)	Molecular weight low Negative mole fraction for some species obtained.
2	Checkout run of the screened version delivered by SEA.	Same as Run #1	Run terminated due to unnormalized argument in square root.
3	Create a new temporary file identical to the screened version delivered to ALRC.		A new file name LOXRP created.
4	Beginning MR influence.	LOXRP file Same as Run #1 except beginning MR = 2.0	No negative mole fraction MW & T higher than MR = 1.2 (Run #1) at beginning but lower as kinetic reactions proceed. MW & T decrease as τ (residual time) increases. Main products: CO, H ₂ O, H ₂ , GH ₂ , CO ₂ , CH ₄ (RP-1 vapor not included)
5	Correction on some rate constants on the original screened model.	Screened version A = 3.2×10^4 Reaction #1 A = 1.413×10^{13} Reaction #3 HM/N = HI = 0.01 Beginning MR = 1.2 Run by SEA	Slower vaporization rate compared to Run #1 & 4 Higher T & MW than Run #1 with same beginning (ODE condition). MW & T lower than Run #4, but T higher and MW lower than Run #4 as kinetic reactions proceed.
6	Correction on some rate constants on complete reaction set file.	Complete reaction set Same correction as Run #5 HM/N = HI = 0.01 Beginning MR = 1.2	Slower vaporization rate compared to Run #1 & 4 Higher T & MW than Run #1 (Same initial ODE results) No appreciable C ₂ Run stopped at $\tau = 4.606 \times 10^{-3}$ ms by max. time
7	Rerun the case of Run #6	Same as Run #6 except printout format	Negative mole fractions obtained at $\tau = 4.646 \times 10^{-3}$ ms
8	Rerun the case of Run #7 except the MR change.	Same as Run #7 except beginning MR = 2.0	Negative mole fractions still obtained.
9	To obtain non-negative mole fraction result.	Same as Run #8 except HM/N = HI = 0.005	Non-negative mole fraction result obtained. C ₂ almost non-existent and decreasing with τ . Small amount of C ₂ H Mix MW close to Titan data. T higher than Titan
10,11,12	To screen out some lesser important reactions from the complete set version in order to reduce run time while retaining carbon formation reactions.	Same as Run #9 except some reactions deleted.	Similar results obtained while run time is reduced.
13	To simulate coagulation by C ₄ formation.	Same as Run #10 Reaction C ₂ + C ₂ → C ₄ added	Small amount of C ₄ obtained, C ₄ not growing
14,15	To force the C ₂ formation reaction to be irreversible by forming photon	Same as Run #10 except reaction #4? C ₂ H + H → C ₂ + H ₂ + Photon HM/N = HI = 0.002 for Run #15	Negative mole fraction obtained.
16	Gas properties prediction	LOXRP File Beginning MR = 2.0 HM/N = HI = 0.01	At $\tau = 6.97$ ms, X = 27 in. MW = 29.38 (mix), 27.44 (gas) T = 926°K (1666°R), C* (gas) = 826 m/sec (2744 ft/sec) Y = 1.125
17	Overall MR Influence	Run by SEA Beginning MR = 1.2 HM/N = HI = 0.005 Screened version A = 3×10^4 , B = 9.3 Reaction #1 Overall MR = 0.32	At $\tau = 6.97$ ms, X = 68.6 cm (27 in.) MW = 29.25 (mix), 26.46 (gas) T = 847°K (1525°R), C* (gas) = 814 m/sec (2669 ft/sec), Y = 1.131
18	Same as Run #17	Same as Run #17 except Overall MR = 0.3R HM/N = HI = 0.01	At $\tau = 6.97$ ms, X = 68.6 cm (27 in.) MW = 26.09 (mix), 24.09 (gas) T = 912°K (1642°R), C* (gas) 880 m/sec (2887 ft/sec), Y = 1.148
19	Same as Run #17, 18	Same as Run #18 except Overall MR = 0.44	At $\tau = 6.97$ ms, X = 27 in. MW = 23.35 (mix), 21.92 (gas) T = 1011°K (1823°R), C* (gas) = 966 m/sec (3170 ft/sec), Y = 1.166
20	High Pc Case	Run by SEA Non-Titan Case Pc = 34470 kPa (5000 psia) Beginning MR = 1.2 Overall MR = 0.3 HM/N = HI = 0.005	At $\tau = 7.12$ ms, X = 6.7 in. MW = 28.85 (mix), 25.31 (gas) T = 1079°K (1943°R), C* (gas) = 938 m/sec (3076 ft/sec), Y = 1.132

Figure IV-18. Fuel-Rich LOX/RP-1 Combustion Model Calibration Using Titan I Data

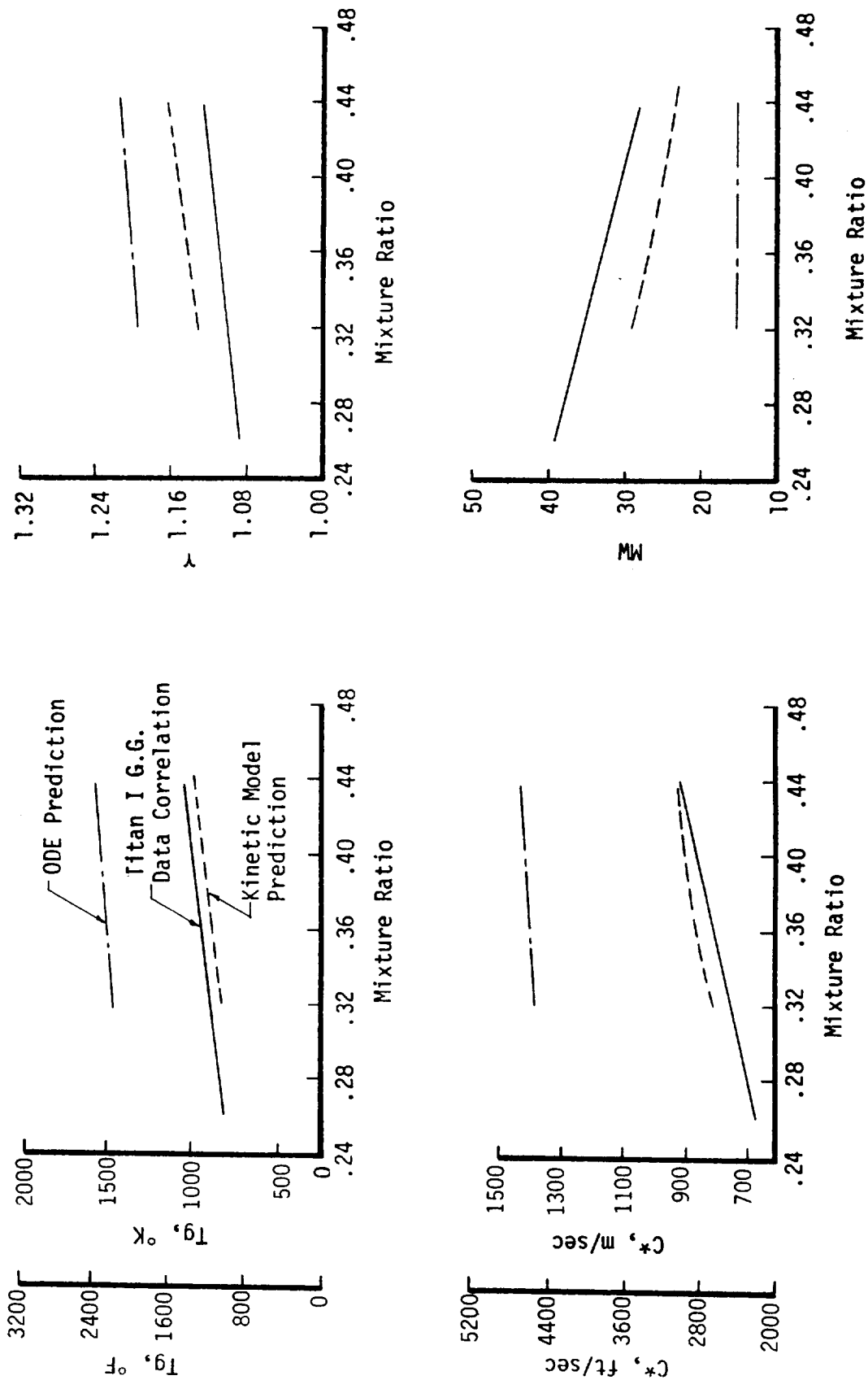


Figure IV-19. Fuel-Rich Combustion Model Comparison with ODE

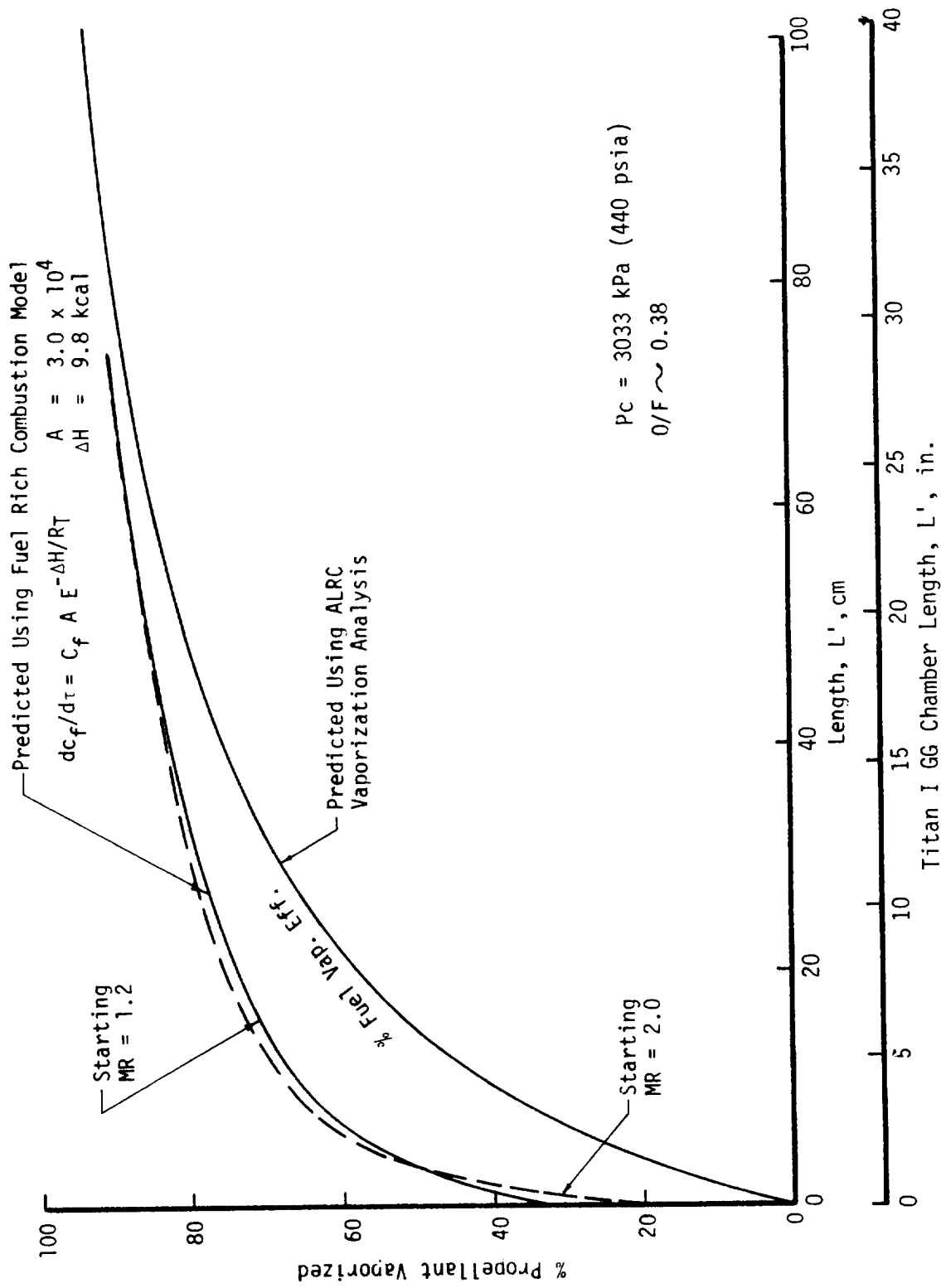


Figure IV-20. Calculated Titan I GG Fuel Vaporization Profile

	<u>m/sec</u>	<u>C*</u> (ft/sec)	<u>°K</u>	<u>T_g</u> (°F)	<u>MW</u>	<u>γ</u>	<u>C₂ Molecules</u>
Starting MR = 1.2	800	(2887)	912	(1182)	26	1.15	0.042
Titan I GG	840	(2755)	983	(1310)	32	1.11	-
Starting MR = 2.0	835	(2738)	923	(1202)	28	1.12	0.164

Figure IV-21. Fuel-Rich Combustion - Effect of Starting MR

C-2

IV, A, Fuel-Rich Preburner (cont.)

c. Model Application to Preburner Design

The model was subsequently used to evaluate preburner design concepts, as illustrated in Figure IV-22. The degree of uniformity is simulated by the starting mixture ratio. A higher initial MR corresponds to a less uniform combustion condition. The results show that the uniform mixture ratio design provides the best combustion.

The bulk of the carbon formation in the Titan I GG is believed to be due to coking and low-temperature, fast-forming carbon from aromatic components. This postulation is supported by heated tube coking experiments and recent LO₂/RP-1 combustion movies, as illustrated in Figure IV-23. Coking is known to occur rapidly above temperatures of 561°K (550°F). Fuel droplet vaporization involves heating the droplet rapidly to the saturation temperature which can easily exceed 561°K (556°F). Rapidly formed carbon is, in fact, observed in RP-1 sprays immediately at the injector face. This means that the carbon is formed in a matter of microseconds, such that reaction kinetics are not controlling. It is concluded that carbon formation in fuel-rich gas generators cannot be avoided with RP-1 fuel and that the designer must accommodate carbon formation.

d. Conclusions and Recommendations

The conclusions and recommendations are summarized as follows:

- ° The model predicts correct Titan GG mixture-ratio trends for MW, γ , Tg, and C*.
- ° The model does not predict soot formation (C₂) by gas-phase reactions at the Titan I 1st stage gas generator conditions.
- ° Most of the carbon formation in the Titan I 1st stage gas generator is due to coking rather than sooting.
- ° Carbon formation occurs within the combustion spray. It is not kinetically limited due to the high temperatures.
- ° It is not recommended that further carbon formation analytical modeling be conducted at this time.
- ° It is recommended that fuel-rich GG's be designed to accommodate coking.
- ° It is recommended that the model be used in its present form for design evaluation.

<u>PREBURNER CONCEPT</u>	<u>MODEL SIMULATION</u>
Uniform MR	Low Starting MR (1.2)
Hot Core	High Starting MR (2.0)
Stoichiometric	Stoichiometric Starting MR (3.4)

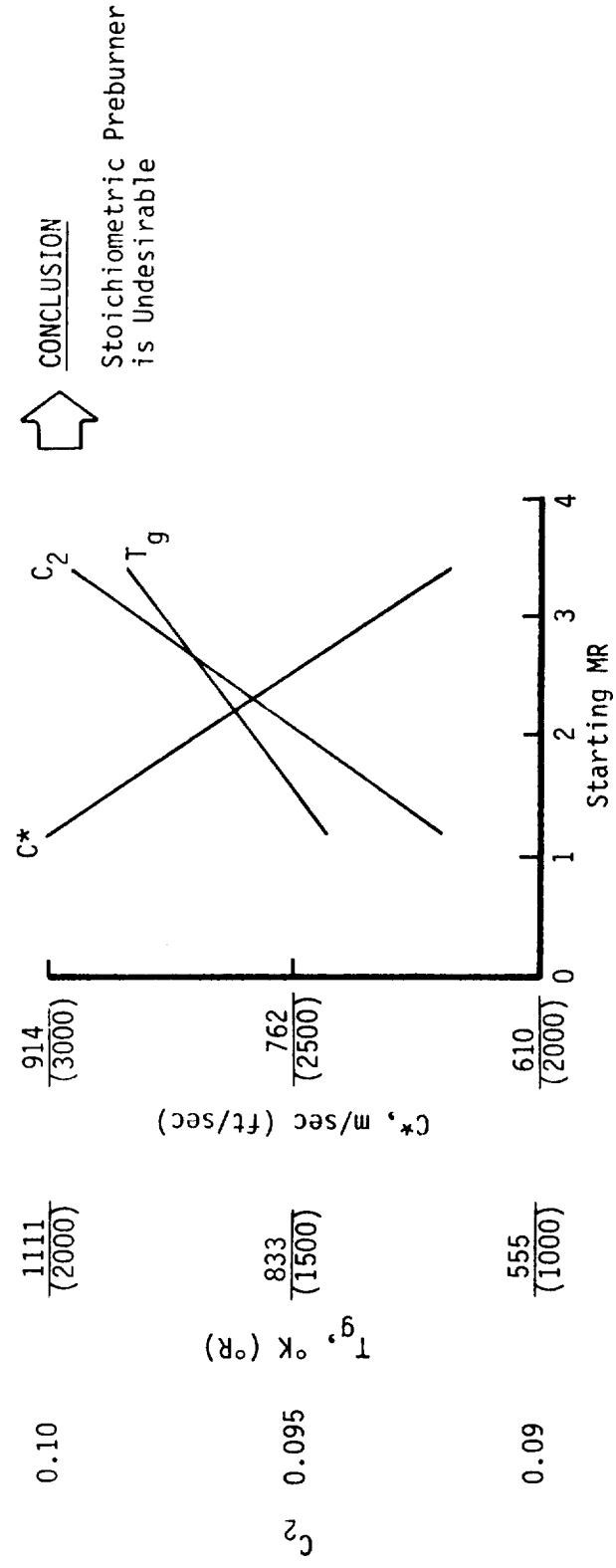


Figure IV-22. Predicted Effect of Starting MR on Solid Carbon Formation

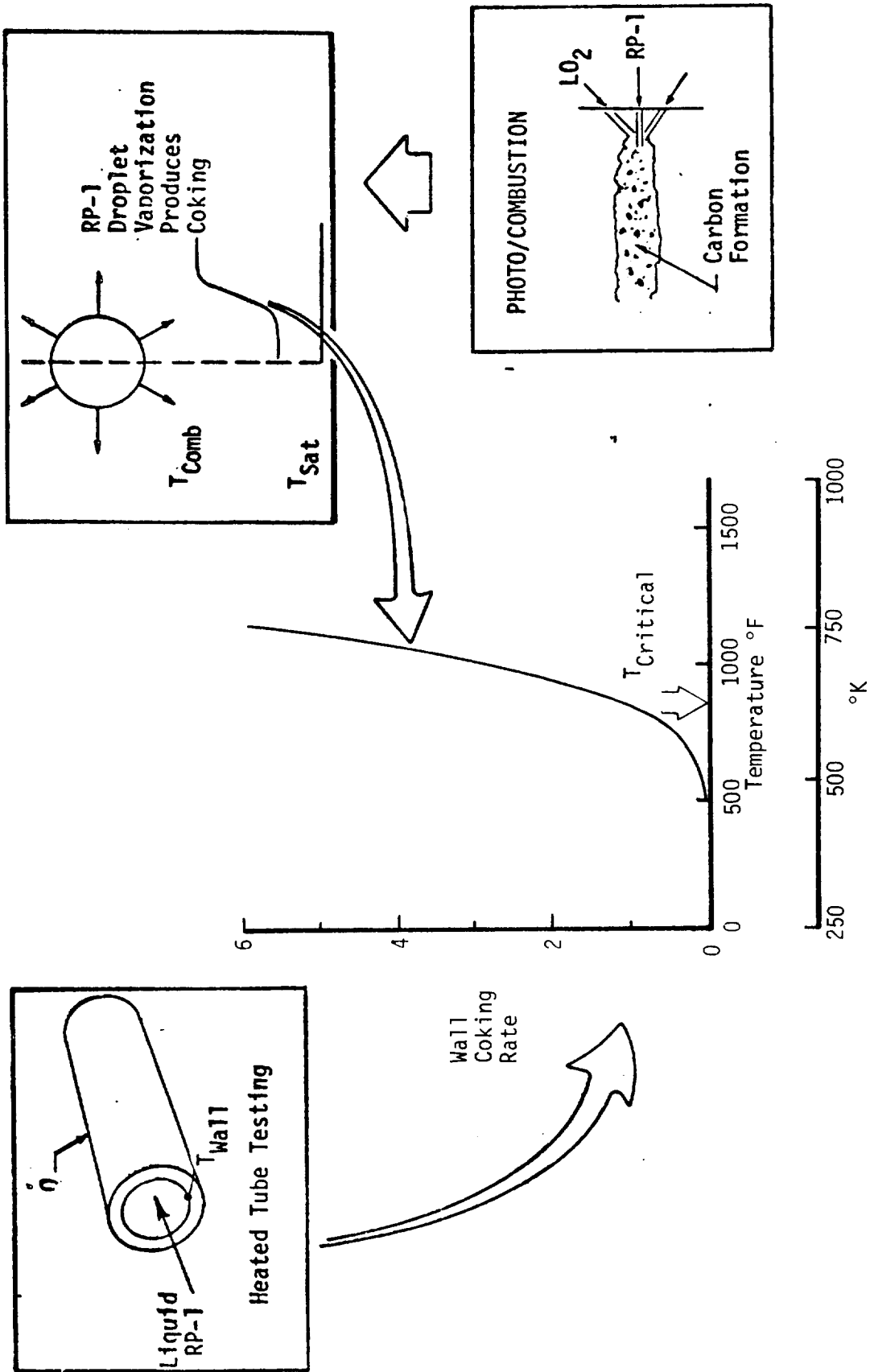


Figure IV-23. Evidence of Solid Carbon Formation Directly from Liquid-Phase Heating

IV, A, Fuel-Rich Preburner (cont.)

Basically it is now believed that, with the exception of carbon formation rates, the model is very adequate to predict LOX/RP-1 fuel-rich combustion trends in terms of the essential properties required for design. Further, the model has been developed to accept key combustor design variables such as fuel vaporization rates and starting mixture ratio so that it can be used to evaluate preliminary design concepts as well as provide a tool for test data correlation. At this point, our recommendation is to utilize the model as currently developed to evaluate the various fuel-rich preburner design options while recognizing its limitations in predicting carbon formation. Additional improvements may be warranted once the test data from this current technology program are obtained and evaluated.

After completion of this study, the uniform MR design was recommended on the basis of the following considerations:

- Titan I GG data base and test history F-1 GG data base and test history.
- NASA GG design monograph recommendations.
- Detailed analysis which indicates hot core zones will be difficult to mix or dilute and offer no advantage in reduced residence time.
- Easier task of component cooling and lower ultimate cost and higher reliability.
- Reduced potential for carbon deposition.

IV, A, Fuel-Rich Preburner (cont.)

4. Materials Selection Design Criteria

The materials to be employed for this program should be

- compatible with LOX, RP-1, and the resulting combustion products;
- low-cost and readily available;
- easily weldable by electron-beam and TIG procedures;
- brazeable by demonstrated processes.

Since weight was not a consideration, there was no advantage to utilizing high-strength alloys as these require special heat treatments or, in the case of specialty alloys, have long delivery schedules.

Much of the test hardware is to be utilized for both fuel- and oxidizer-rich operation. As a result, chemical compatibility with hot fuel and liquid oxygen and the ignition temperature of candidate metals in hot oxygen at high pressure were major factors. RP-1 and the fuel-rich combustion products were compatible with most materials at elevated temperature for the short test durations of interest.

Figure IV-24 identifies the ignition characteristics of candidate materials in oxygen at high temperature and pressure. This chart shows stainless steels with a high chromium content and "A" nickel as being superior.

CRES 304 (18% Ch - 8% Ni) was selected for all structural components because it best met the selection criteria.

Nickel was selected for the face of the EDM'd oxidizer-rich injector and for the chamber liners because its thermal conductivity is approximately 2 to 3 times higher than that of 304 stainless steel. The higher thermal conductivity of nickel provides for better thermal diffusion of local hot spots and thus additional design margin.

CRES 347 was selected for the platelet injectors because of its superior bonding characteristics. The alloy, 17-4 PH (heat-treated to condition 1025) was selected for the turbine simulator blades to provide the strength required at the end supports.

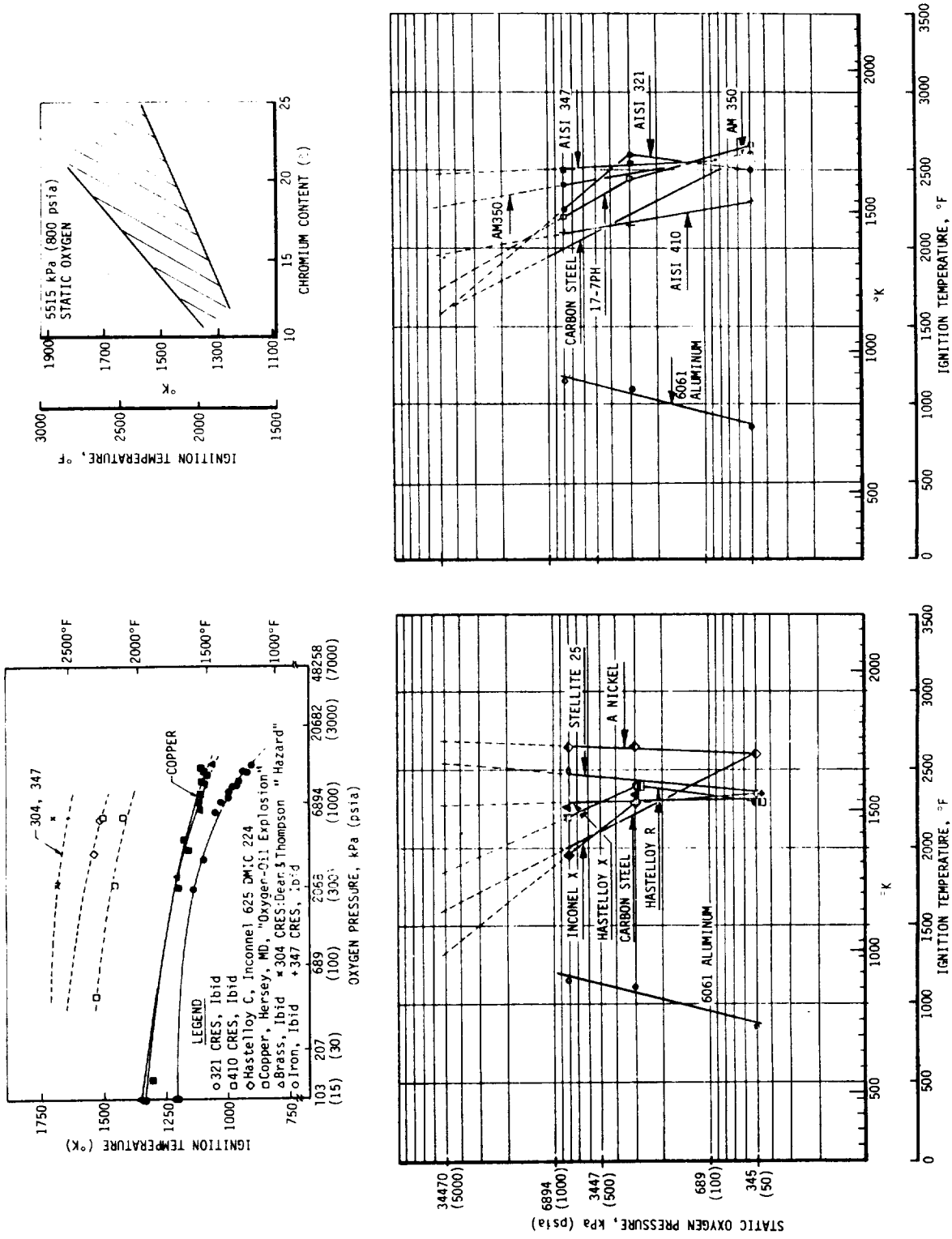


Figure IV-24. Ignition Characteristics of Candidate Materials in an Oxygen Atmosphere

IV, A, Fuel-Rich Preburner (cont.)

5. Structural Analyses

a. Objectives

Structural analyses were conducted to verify that ASME-rated, commercially available 6205 kPa (900 psia) 304 stainless steel slip-on flanges (shown in Figure IV-25) could be employed as low-cost building blocks for all components and that the resulting flange deflections and stresses were acceptable at high pressures. Additional analyses to verify the structural adequacy of the injector faceplates, manifolding, and inlet lines were also conducted.

b. Approach

The typical flange design, shown in Figure IV-26, was considered for detailed structural analysis. The design approach required the electron-beam welding of a modified 10.2-cm (4-in.) diameter flange to a 12.7-cm (5-in.) diameter Schedule double-extra strong pipe. Finite element structural analyses of the selected geometry were conducted at the following conditions:

- 1) 31712 kPa (4600 psia) internal pressure at 294°K (70°F)
- 2) 17235 kPa (2500 psia) with a superimposed thermal profile corresponding to 20 sec of burn time in a heat-sink mode.

The bolt preload was varied to determine the influence of this parameter on the flange separation.

This computer model was employed to analyze the assembly and components shown in Figures III-2 through III-32. The initial target for maximum flange deflection was 0.005 cm (0.002 in.). This small value was arbitrarily selected to preclude extrusion of the Teflon jacket of the spring-energized RACO seal.

The injector faceplate structural analyses employed both simple approximations and more detailed analyses.

The details of this analytical effort are documented in Reference 2.

c. Structural Analysis Summary

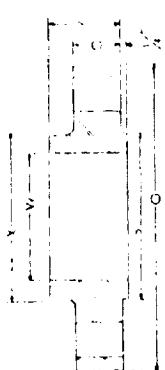
The structural analyses, summarized in Figures IV-27 and IV-28, show an allowable 100 to 200 thermal cycle fatigue limit capability

900 lb. BLIND FLANGES*



NOMINAL PIPE SIZE	OUTSIDE DIA. OF FLANGE	THICK. OF FLANGE	DIAM. OF RAISED FACE	DIA. OF GROOVE	DIMENSIONS				APPROX. WEIGHT IN POUNDS	LIST PRICE	
					NO. OF BOLTS	DIA. OF BOLT CIRCLE	LENGTH OF STUD BOLTS	WELD BEAD TONGUE & GROOVE			
3	9 1/2	1 1/4	5	7 1/2	8	7 1/2	5 3/4	5 1/2	6	32	
4	11 1/2	1 3/4	6 3/16	9 1/4	8	9 1/4	6 3/4	6 1/2	7	54	DN
5	13 3/4	2	7 3/16	11	8	11	7 1/2	7 1/4	7 3/4	87	
6	15	2 1/2	8 1/2	12 1/2	10	12 1/2	8 1/2	8 1/4	8 3/4	125	APPLI.

900 lb. SLIP-ON FLANGES



NOMINAL PIPE SIZE	OUTSIDE DIA. OF FLANGE	THICK. OF FLANGE	DIA. OF RAISED FACE	DIA. OF GROOVE	NO. OF BOLTS	DIA. OF BOLT CIRCLE	LENGTH OF STUD BOLTS	WELD BEAD TONGUE & GROOVE	APPROX. WEIGHT IN POUNDS	LIST PRICE	
											3
4	11 1/2	1 3/4	6 3/16	9 1/4	8	9 1/4	6 3/4	6 1/2	7	53	DN
5	13 3/4	2	7 3/16	11	8	11	7 1/2	7 1/4	7 3/4	83	

Figure IV-25. Low-Cost Test Hardware Fabricated From Standard Commercial Flanges

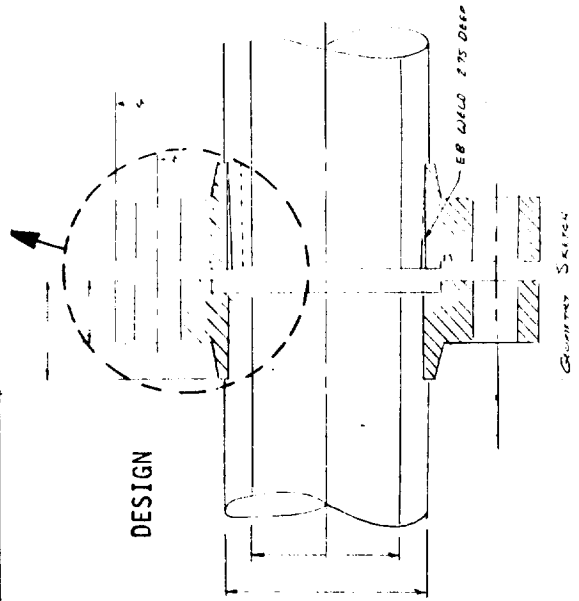


Figure IV-26. Schematic of Detailed Flange Structural Model

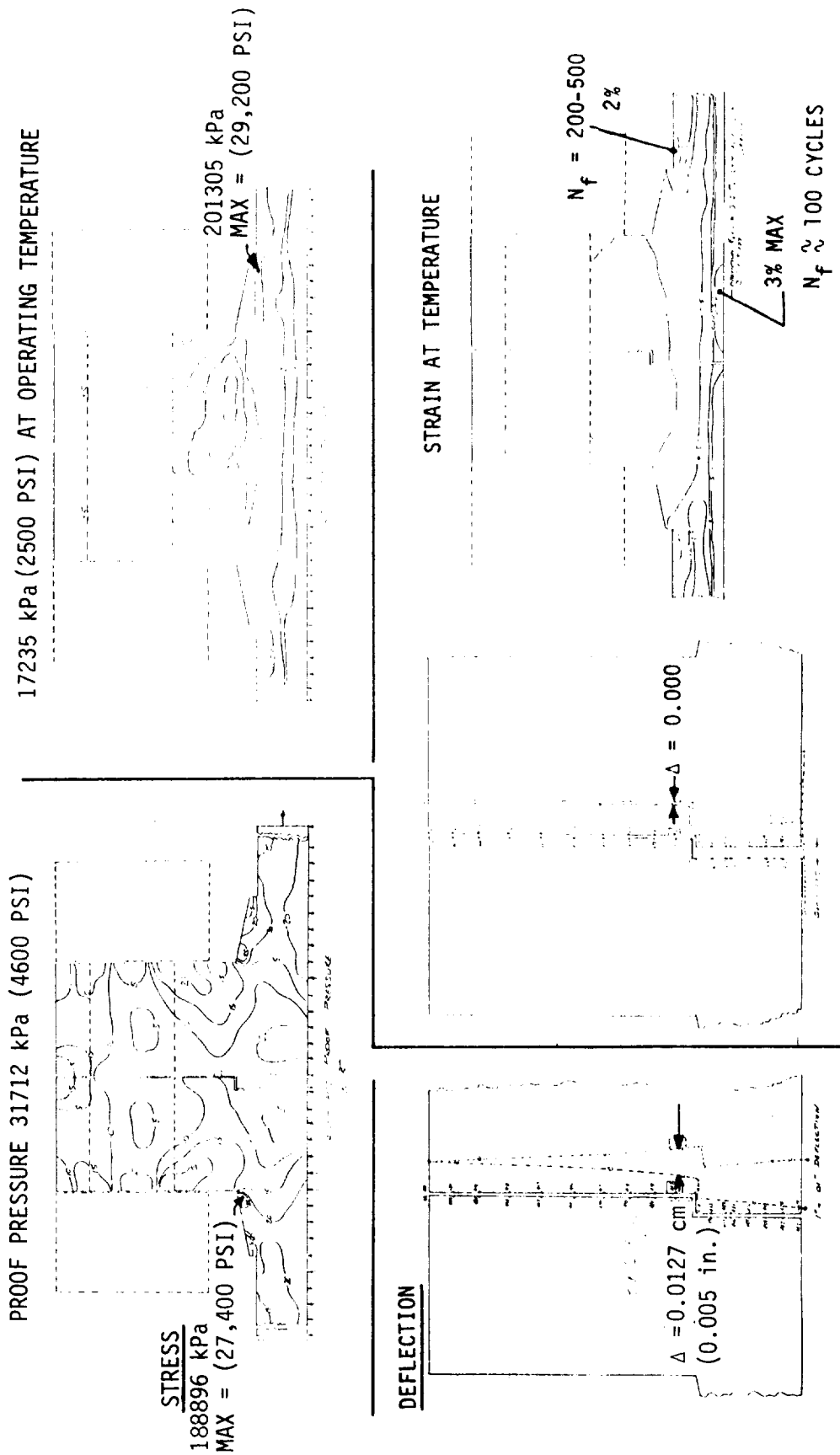


Figure IV-27. Heat Sink Chamber Stress, Strain, and Cycle Fatigue Limits

CASE	MAX STRESS (EL. NO.)	ALLOWABLE STRESS (TEMP.)	MARGIN OF SAFETY**	BOLT STRESS	MAX STRAIN (EL. NO.)	DISPL. @ SEAL
PRELOAD* + ΔP = 31712 kPa (4600 PSI)	188,795 kPa (27,386 PSI) (334)	F _{ty} = 193,032 kPa (28,000 PSI) 311°K (100°F)	+0.02 (YIELD)	598,399 kPa (86,800 PSI)	-	0.1166 cm. (0.00459 in.)
PRELOAD* + ΔP = 17235 kPa (2500 PSI) + ΔT	201,208 kPa (29,186 PSI) (150)	F _{ty} = 406,746 kPa (59,000 PSI) 439°K (330°F)	+0.44 UIT	590,816 kPa (85,700 PSI)	3.0% (177)	0.000 cm (0.000 in.)

Figure IV-28. Bolted Joint Analysis Summary Table

IV, A, Fuel-Rich Preburner (cont.)

and a flange separation of 0.0117 cm (0.0046 in.) at the 31712 kPa (4600 psia) proof-pressure condition. A bolt preload torque of 134 m-kg (970 ft-lb) was required in order to limit the separation to 0.0117 cm (0.0046 in.). This preload resulted in acceptable stresses in the A286 bolt, under the bolt head, and in the flange. It was further recommended that the pipe-to-flange electron-beam-weld penetration be 6.99 cm (2.75 in.) deep in order to obtain the rigidity required to prevent additional flange rotation and excess flange separation at the seal interface.

d. Details of the Stress Analyses

(1) Flanges

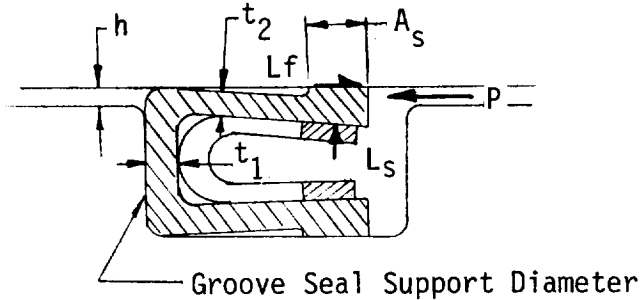
The 4.45-cm (1-3/4-in.) thick bolted flange design was analyzed to determine an acceptable combination of proof-pressure and bolt preload that would minimize deflection at the seal and limit the stresses to acceptable levels. In addition, the flange was analyzed at an operating pressure of 17235 kPa (2500 psia), with the temperature distribution predicted to exist at the end of a 20-sec firing. The analysis showed that a deflection of $\delta = 0.0117$ cm (0.0046 in.) at the seal required a maximum obtainable bolt preload of approximately 134 m-kg (970 ft-lb) torque and that the proof-pressure condition must be limited to 31712 kPa (4600 psia). The predicted flange displacement at operating temperature and pressure is zero. Under these operating conditions, the thermal expansion closes the gap while the pressure is 17235 kPa (2500 psia). It is expected that the seals will still hold the proof pressure with a 0.0117-cm (0.0046-in.) displacement, even though the targeted displacement was 0.005 cm (0.002 in.). The proof-pressure test will be used to verify the deflection values.*

Additional data which relate flange separation to allowable working pressure were obtained from Reference 3 subsequent to the analyses. Typical data taken from this report (shown in Figure IV-29) indicate that the RACO seal was able to withstand 48,258 kPa (7000 psia) for 5 minutes with a flange separation of 0.0356 cm (0.014 in.). These data indicated that the 0.0117-cm (0.0046-in.) flange deflection would not be a problem and that there was considerable design margin.

*Actual flange deflections were measured during the initial proof and leak tests to verify the above analyses. The measured flange deflections ranged between 0.0152 and 0.0229 cm (0.006 and 0.009 in.) at a bolt torque of 41.5 to 48.4 m-kg (300 to 350 ft-lb) at a proof-pressure of 24129 kPa (3500 psia). These data indicated that flange separation would not be a problem and that the bolt torque could be reduced from 134 to 69.1 m-kg (970 to 500 ft-lb). No leakage was noted during the proof and leak tests (see Section IV). Subsequent hot-fire testing up to 17235 kPa (2500 psia) showed the flange and seal design to be completely acceptable.

$$t_1 = 0.046/0.051 \text{ cm} \\ (0.018/0.020 \text{ in.})$$

$$t_2 = 0.046/0.051 \text{ cm} \\ (0.018/0.020 \text{ in.})$$



TEST CONDITIONS:

RACO-Type Face Seal

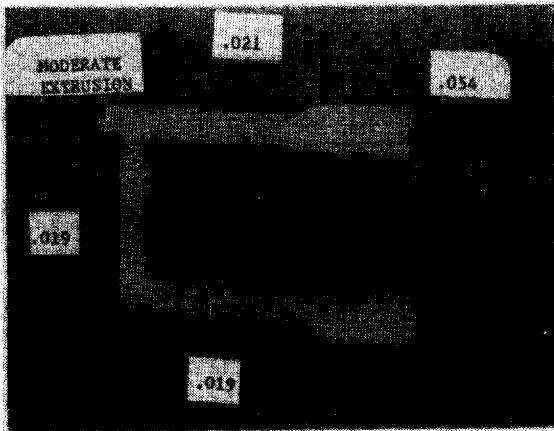
$$h = 0.041 \text{ to } 0.051 \text{ cm} \\ (0.061 \text{ to } 0.020 \text{ in.})$$

$$P = 0.48258 \text{ kPa} \\ (7000 \text{ psig})$$

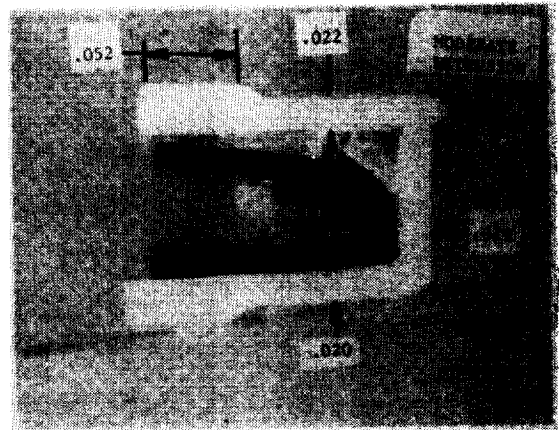
- A. Flange Separation (h)
Less Than Leg Thickness (t_2)

Test Results:

Moderate Extrusion at 0.0356-cm (0.041-in.) Shim Test
at 48258 kPa (7000 psig) (Run SP-59-112)
Resulted in "0" Leakage after 5 Minutes of
Hold Time



- A. INNER SEAL PN 701722-1
(0.0513-cm/0.020-in. TOTAL
FLANGE SEPARATION AT SEAL
SUPPORT DIA.)



- B. OUTER SEAL PN 701770-1
(0.0417-cm/0.0168-in. TOTAL
FLANGE SEPARATION AT SEAL
SUPPORT DIA.)

Figure IV-29. Flange Separation and Seal Cold-Flow Data

IV, A, Fuel-Rich Preburner (cont.)

With a safety factor of 1.0 on yield strength and 1.4 on ultimate strength, the minimum margin of safety on yield strength is +0.02 for the 31712 kPa (4600 psia) proof-pressure case and +0.44 on ultimate strength for the operating case. Even with the large preload of 134 m-kg (970 ft-lb) torque, the bearing surface area under the bolt heads is adequate to keep the bearing stress below yield. Also, a fatigue analysis shows the flange to be good for approximately 41 cycles with a safety factor of 4 on cycle life.

(2) Injector Manifold Analysis

The injector manifold analyses are documented in Reference 4. This report indicated that the designs shown in Figures III-15 and III-17 were structurally acceptable for the following loading conditions:

Transient ΔP 13788 kPa (2000 psia).

Steady-state pressure 20682 kPa (3000 psia) with 6894 kPa (1000 psia) drop across the faceplate when the faceplate is at 811°K (1000°F).

6. Igniter Design and Ignition Analyses

a. Objectives

The program was based on utilizing a modification of an existing $\text{GH}_2\text{-GO}_2$ igniter design. The objectives of this activity were as follows:

1. Define preburner ignition limits for a centrally mounted torch igniter (igniter MR vs flowrate)
2. Select an igniter operating point (mixture ratio; total flowrate)
3. Define the allowable fire duration of the heat sink ignition tube

The igniter employed is shown schematically in Figure IV-30 and in detail in Figure III-26.

b. Results

The results of the fuel-rich preburner ignition analyses are displayed in Figure IV-31. This figure indicates that an igniter flowrate

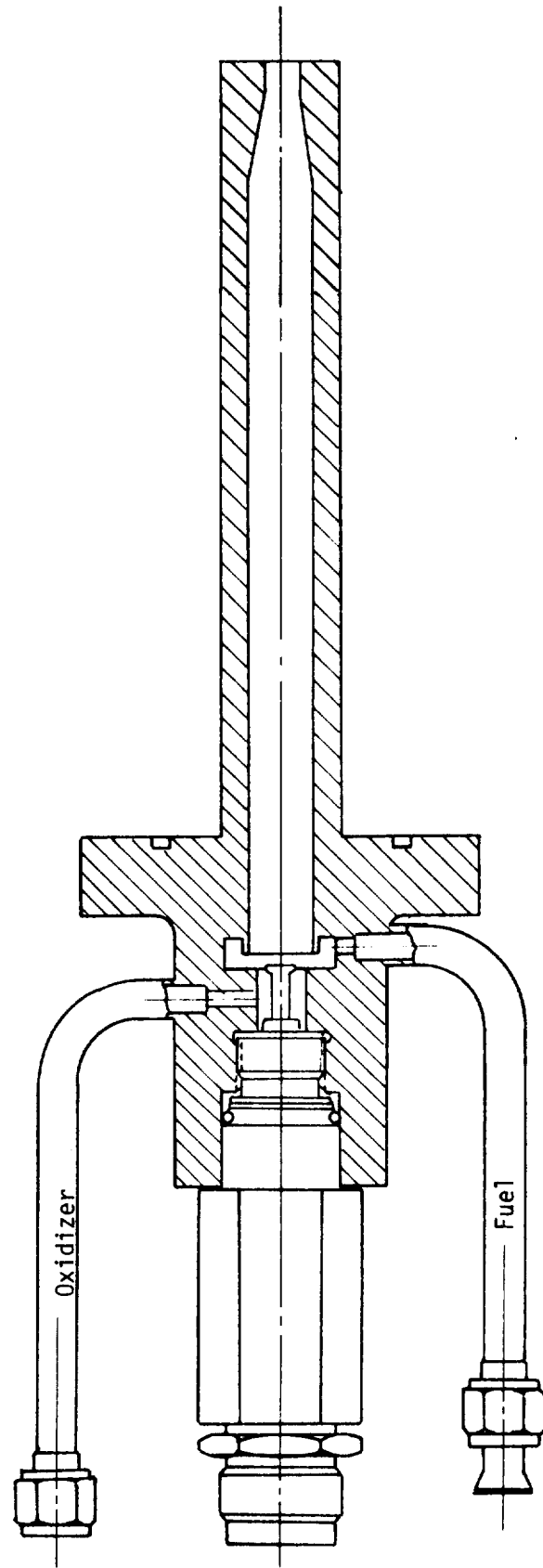


Figure IV-30. Typical O₂/H₂ Igniter Design

TORCH IGNITER PREDICTED IGNITION LIMITS

OX-RICH PREBURNER

MR = 40

COLD-FLOW PRESSURES $P_c = 172$ & 345 kPa (25 & 50 psia)

AVERAGE PROPELLANT VELOCITY (V_0) = 93.6 m/sec (307 ft/sec)

CENTRALLY MOUNTED (COAXIAL) O_2/H_2 IGNITER

THROAT DIAMETER (DJ) = 0.64 cm (0.25 in.)

SPARK GAP = 0.076 cm (0.030 in.)

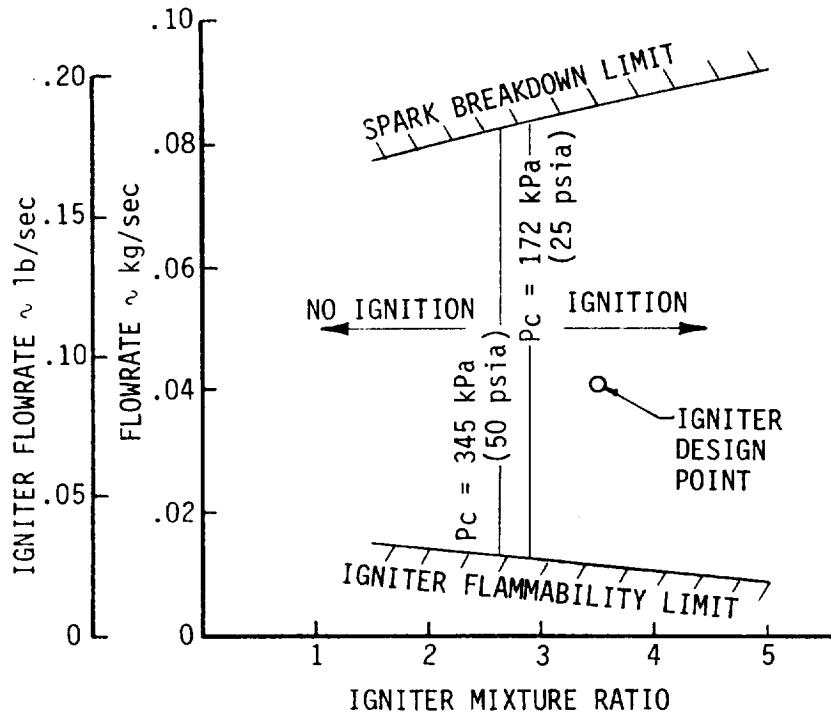


Figure IV-31. Results of Fuel-Rich Preburner Ignition Analyses

IV, A, Fuel-Rich Preburner (cont.)

of 0.041 kg/sec (0.09 lb/sec) at a O/F (MR) ratio of 3.5 would provide reliable ignition. The igniter throat was sized to yield a chamber pressure of 3102 kPa (450 psia) at the design flowrate.

c. Thermal Analyses

Thermal transient analyses of the cylindrical chamber and throat region were conducted for the nominal MR of 3.5 and for an assumed worst-case thermal condition of a 3311°K (5500°F) streak. The wall material was assumed to be OFHC copper.

The worst-case thermal condition indicated that throat and chamber temperatures could reach 1144°K (1600°F) and 867°K (1100°F), respectively, in a 0.4-sec igniter burn. The nominal maximum temperature in a 0.4-sec burn would be $\approx 1033^{\circ}\text{K}$ ($\approx 1400^{\circ}\text{F}$) at the throat.

The data on the ignition of copper in oxygen (Figure IV-24) suggest a 1144°K (1600°F) limit at 6894 kPa (1000 psia). The igniter was therefore rated for a duration that is not to exceed 0.4 sec of operation.

7. Stability Analyses

a. Objective

The objective of this activity was to make design recommendations for oxidizer- and fuel-rich preburner injector concepts and specify the chamber lengths, acoustic resonator sizes, and injector pressure drops required to prevent unstable operation.

b. Approach

The stability analyses were made for two fuel-rich injector pattern designs using the following ALRC analytical models:

Chugging	=	LFCS1
1L	=	MCTL
High Frequency	=	IFAR6

Total combustion time lags were determined as follows:

$$\tau_{\text{lean}} = \tau_{\text{atom}} + \tau_{\text{vap}}, 20\%$$

$$\tau_{\text{rich}} = \tau_{\text{atom}} + \tau_{\text{vap}}, \text{stoichiometric}$$

IV, A, Fuel-Rich Preburner (cont.)

c. Results

(1) Chug Stability

A conservative prediction of the chug stability margin for the RP-1-rich preburner injectors is shown in Figure IV-32. The analyses indicated that both the LOL and concentric vortex patterns would be stable over a wide operating range. The nominal operating point is based on a 2758 and 2068 kPa (400 to 300 psia) pressure drop and a chamber length of 30.5 cm (12 in.) or longer for the two designs respectively. The concentric vortex design is predicted to have a greater stability margin than the LOL pattern at an L' of 30.5 cm (12 in.) in spite of the lower pressure drop.

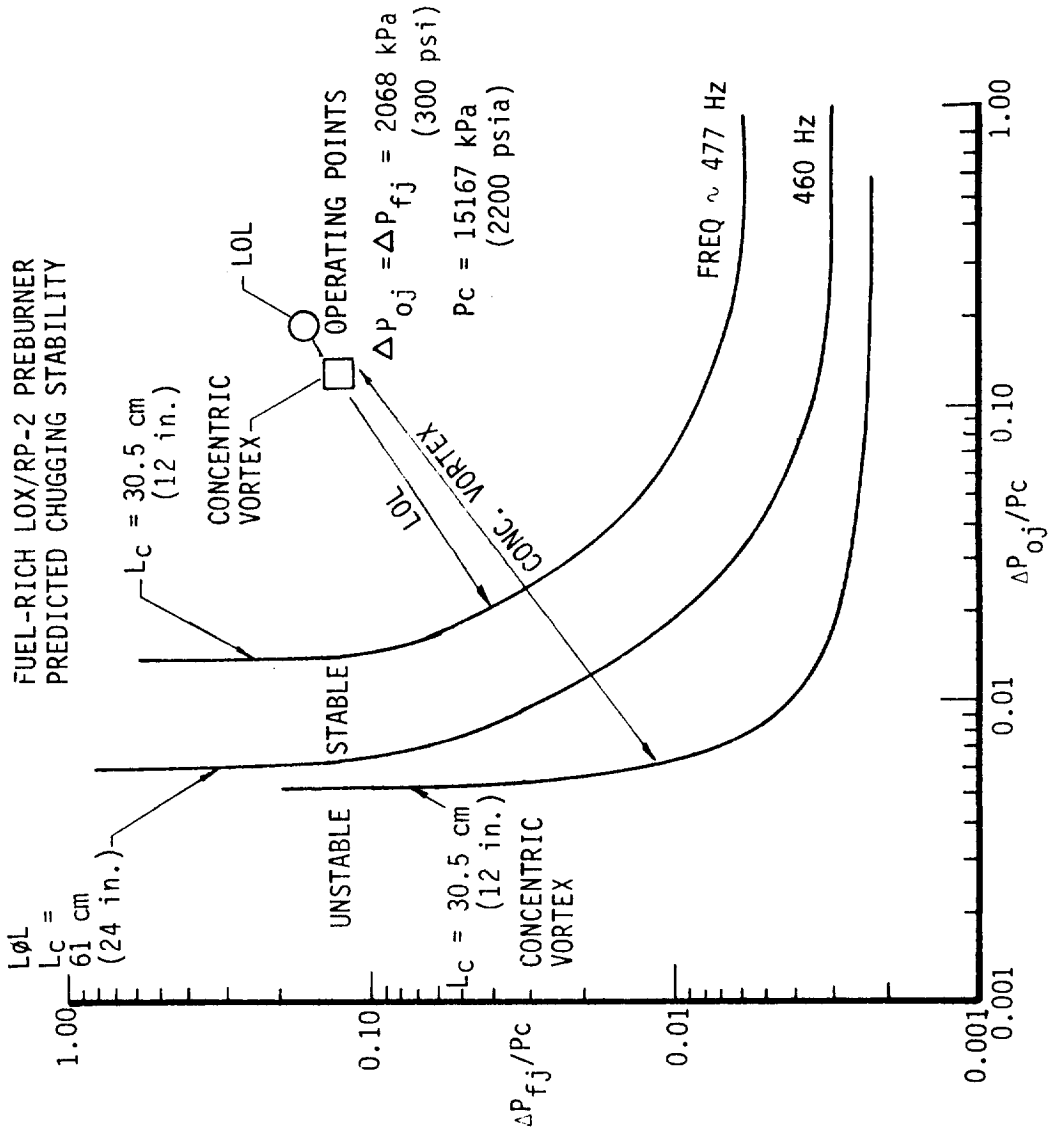
(2) Transverse and Combined Instability Modes

The potential modes of high-frequency instability for the two injector patterns are the same since the chamber geometry and gas properties are common to both. These are shown in Figure IV-33. Both designs are predicted to be stable when the twelve 1/4-wave tube cavities are 0.762 cm (0.3 in.) wide and 1.65 cm (0.65 in.) deep.

The injector sensitive frequency should be lower for LOL injectors (i.e., larger sensitive time lags, τ_s). Also, the LOL injectors are expected to distribute the sensitive combustion over a greater axial length and will have lower interaction indices (additional stabilizing factors). The acoustic mode stability is already known to be acceptable for a similar preburner injector design tested at the MSFC (Ref. 5) and a Titan I fuel-rich preburner tested at ALRC. The stability modes of these designs are quite similar to the LOL element design selected.

(3) Longitudinal Stability

The operating points of the two fuel-rich injectors relative to the various modes of longitudinal instability are shown in Figure IV-34. The LOL preburner injectors will be more stable than the concentric vortex patterns for any given length due to increased total lags, τ_s , and highly distributed combustion. The data shown in Figure IV-34 infer that the concentric vortex injector could be unstable in longitudinal modes with an L' of 31.8 cm (12.5 in.) but would be acceptable with an L' of 40.6 cm (16 in.). This assessment is based on a conservative concentrated combustion assumption. If a mild longitudinal instability occurs, it may be stopped by judicious placement of the mixing rings. This proper placement aids in damping the longitudinal modes and also enhances combustion at velocity antinodes. The MSFC fuel-rich preburner results (Ref. 5) have not shown any 1L mode in a 30.5-cm (12-in.) long chamber; therefore, on the basis of similarity, it is considered unlikely that the LOL designs will not produce any 1L instability.



SUMMARY OF PREDICTED STABILITY

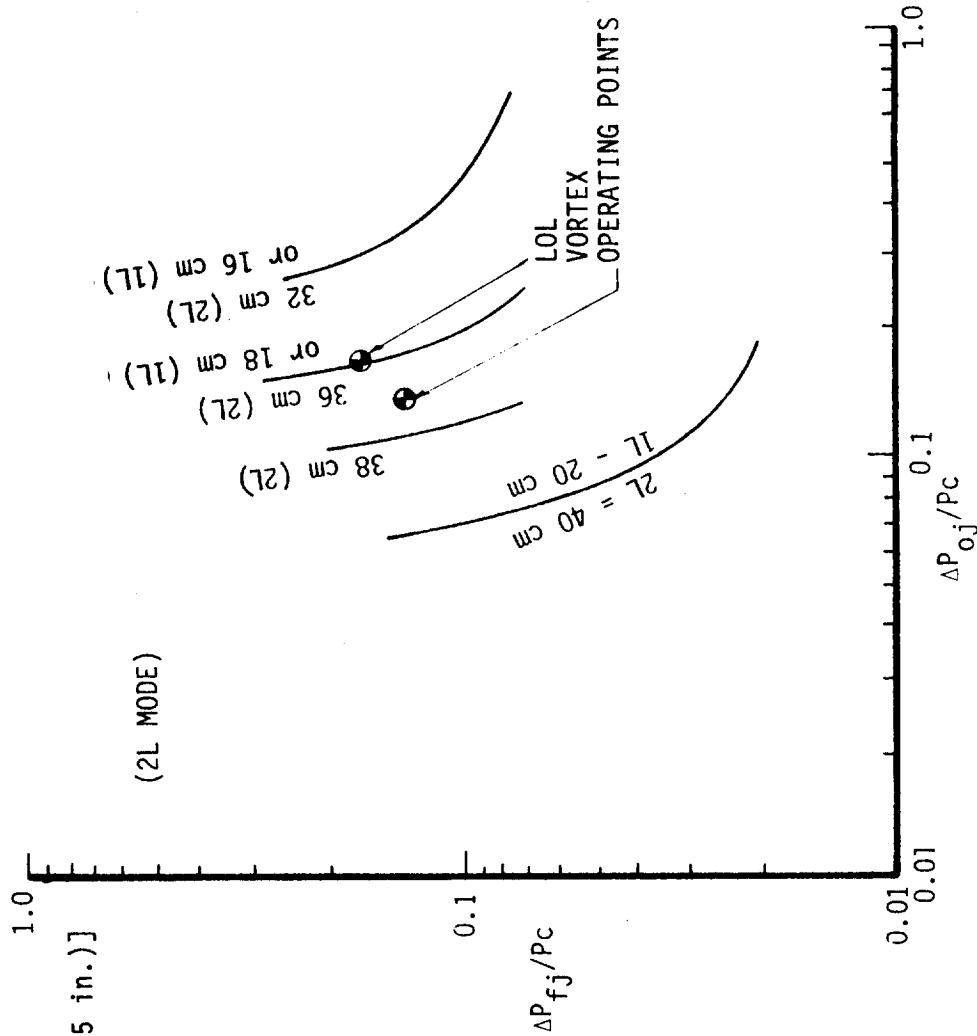
NEARLY EQUALLY SENSITIVE
TO OXIDIZER AND FUEL

NO CHUGGING PROBLEM WITH
L_c NEAR 30.5 cm (12 in.) OR
LONGER

τ_{ox} = 0.52 ms
SHOWERHEAD

τ_{fu} = 0.54 ms
LOL 294°K (70°F)

Figure IV-32. Fuel-Rich Preburner Chug Stability Analysis



- PREDICTED STABILITY [$L_c = 31.7$ cm (12.5 in.)]
 - No 1L Instability
 - 2L Instability Possible
- RECOMMENDED DESIGN CHANGE
 - Increasing L_c to 40.6 cm (16 in.) for stability in 1L and 2L

Figure IV-34. Fuel-Rich Preburner Longitudinal Instability Modes

IV, A, Fuel-Rich Preburner (cont.)

8. Thermal Analyses

The thermal design considerations included the following:

- ° Prevention of propellant freezing in the injector manifolding
- ° Face cooling
- ° Duration capability (design margin) on heat sink chambers (nickel, stainless steel, copper)
- ° Requirements for refractory-lined or other lined chambers and cooled chamber segments
- a. Criteria for Prevention of Propellant Freezing in the Injector Manifolding

The potential for freezing the RP-1 in the manifolding due to the presence of LOX at +89°K (-300°F) in an adjacent passage was evaluated as a function of the following variables:

- ° Propellant velocity
- ° Separation wall thickness (304 Stainless Steel)

It was assumed that RP-1 is a solid below +228°K (-50°F) and that an insulating film of fuel continues to build until a stable RP-1 passage of reduced flow size is formed.

Figure IV-35 defines the thickness of the solid RP-1 film which could develop as a function of the above variables. Both greater wall thickness between the channels and greater RP-1 velocity are conducive to preventing the development of thick films. This figure indicates that a solid film of up to 0.0152 cm (0.006 in.) could develop for very thin walls, but that the more likely maximum is under 0.00254 cm (0.001 in.) for the velocity and wall thickness of interest to the injector designs.

These passage reductions are small and are not considered a problem in restricting the flow. The passage sizes were increased slightly in the design to allow for a small buildup of solid (frozen) RP-1.

b. Injector Face Cooling

The primary method for cooling the injector face at high chamber pressures is to shield the face from the high-temperature combustion gases. The shielding is accomplished by surrounding each minor propellant

RP-1 FREEZING THICKNESS
(FLAT PLATE ANALYSIS)

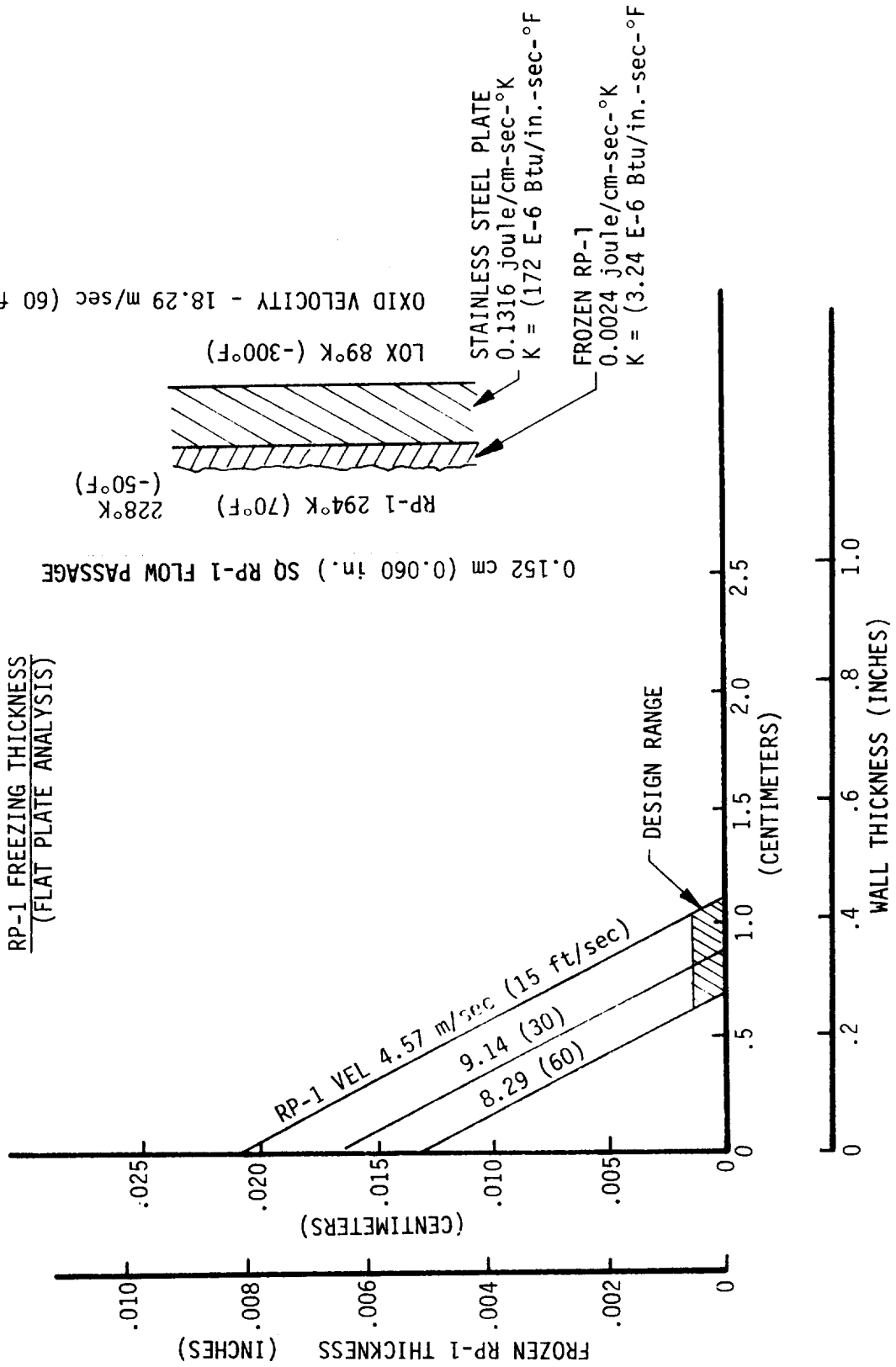


Figure IV-35. Design Criteria for Non-Freezing Fuel Manifold

IV, A, Fuel-Rich Preburner (cont.)

spray or jet with the spray of the rich propellant. The high flowrate of the rich propellant dilutes the hot combustion gas.

Secondary convective face cooling is provided by the injection orifices and by propellant flow passages within the injector. These cooling schemes are shown schematically in Figures IV-36 and IV-37.

c. Heat Sink Chamber Designs

If the mixed mean temperature of the preburner combustion products were to fall into the range from 922 to 1089°K (1200 to 1500°F), material melting should not be a problem. However, since the mixing of the high-temperature combustion products with the excess fuel- and oxidizer-rich propellant requires some distance, a certain degree of flow nonuniformity can be expected in the forward and mid-chamber regions.

Figure IV-38 identifies the relation between local mixture ratio and the flame temperature for both fuel- and oxidizer-rich operating regions. It shows, as a function of mixture ratio, the operating region where heat sink chamber designs are acceptable and active cooling is required. The figures showing temperature versus axial distance indicate a potential for chamber damage if the lean propellant fan hits the chamber wall. The expected problem zone is limited to the first 13 cm (5 in.) of chamber length.

Since the injectors were designed to preclude the lean propellant from hitting the wall, a value judgement was made not to employ a water-cooled section in the head end. (Water cooled chambers are significantly more costly to design and fabricate and also complicate the testing.)

In order to provide some added protection to the 304 stainless steel chamber pressure vessel structure at the head end, provision was made to install low-cost expendable flame liners. The minimum length of the lined section is 29.2 cm (11.5 in.).

Thermal transient analyses of the chamber wall heating profiles in a 15-sec firing were conducted for the baseline stainless steel wall and for various candidate liner materials. Fuel-rich streaks having local mixture ratios of 0.2 to 2.0 were considered. Liners of copper, nickel, aluminum oxide, and aluminum oxide flame-sprayed over stainless steel were considered.

The following three parameters were calculated for design purposes: 1) the surface temperatures at the end of the 15-sec test; 2) a through-the-wall thermal profile; and 3) the wall temperature of the backside or seal locations.

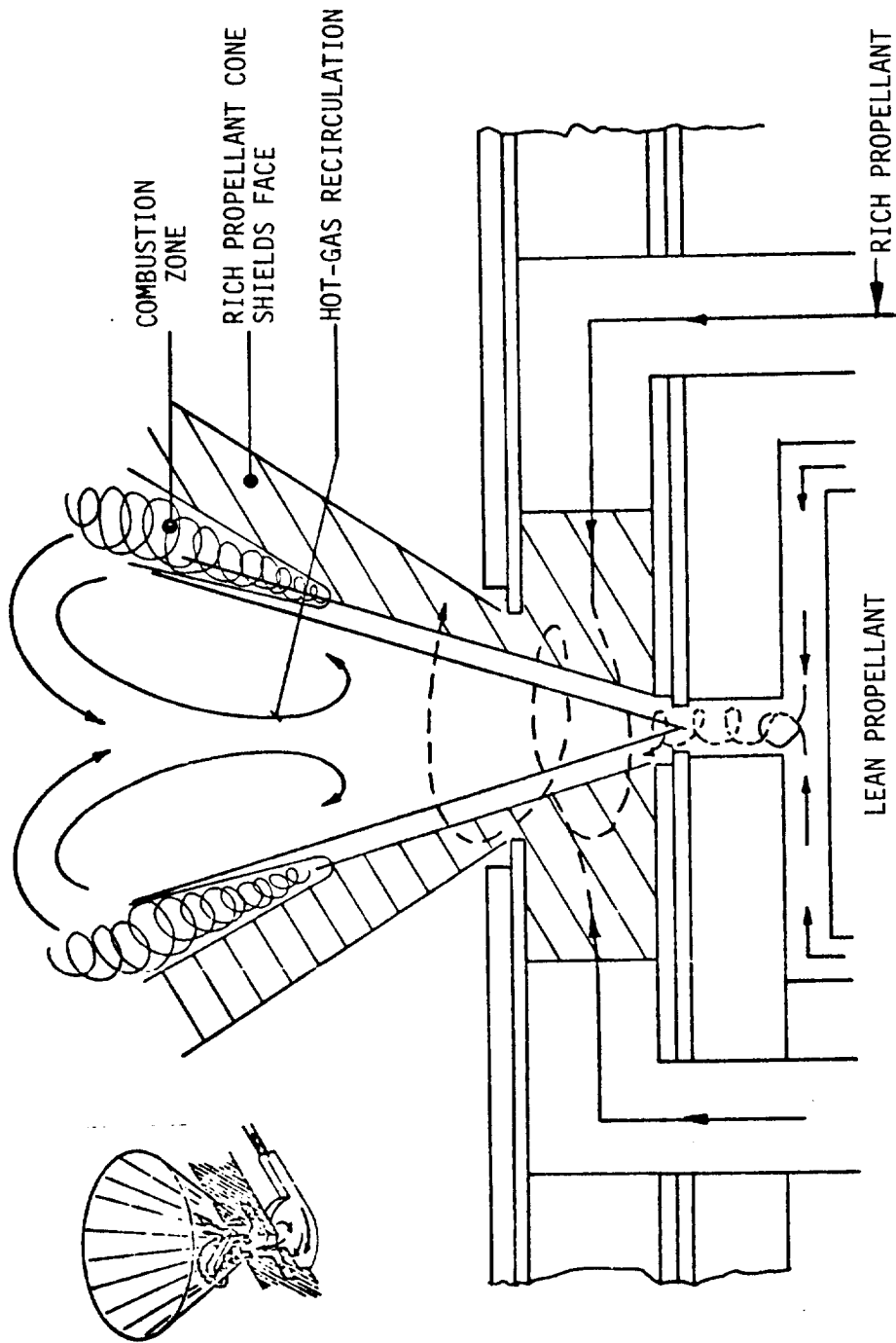


Figure IV-36. Concentric Vortex Element Flow Schematic

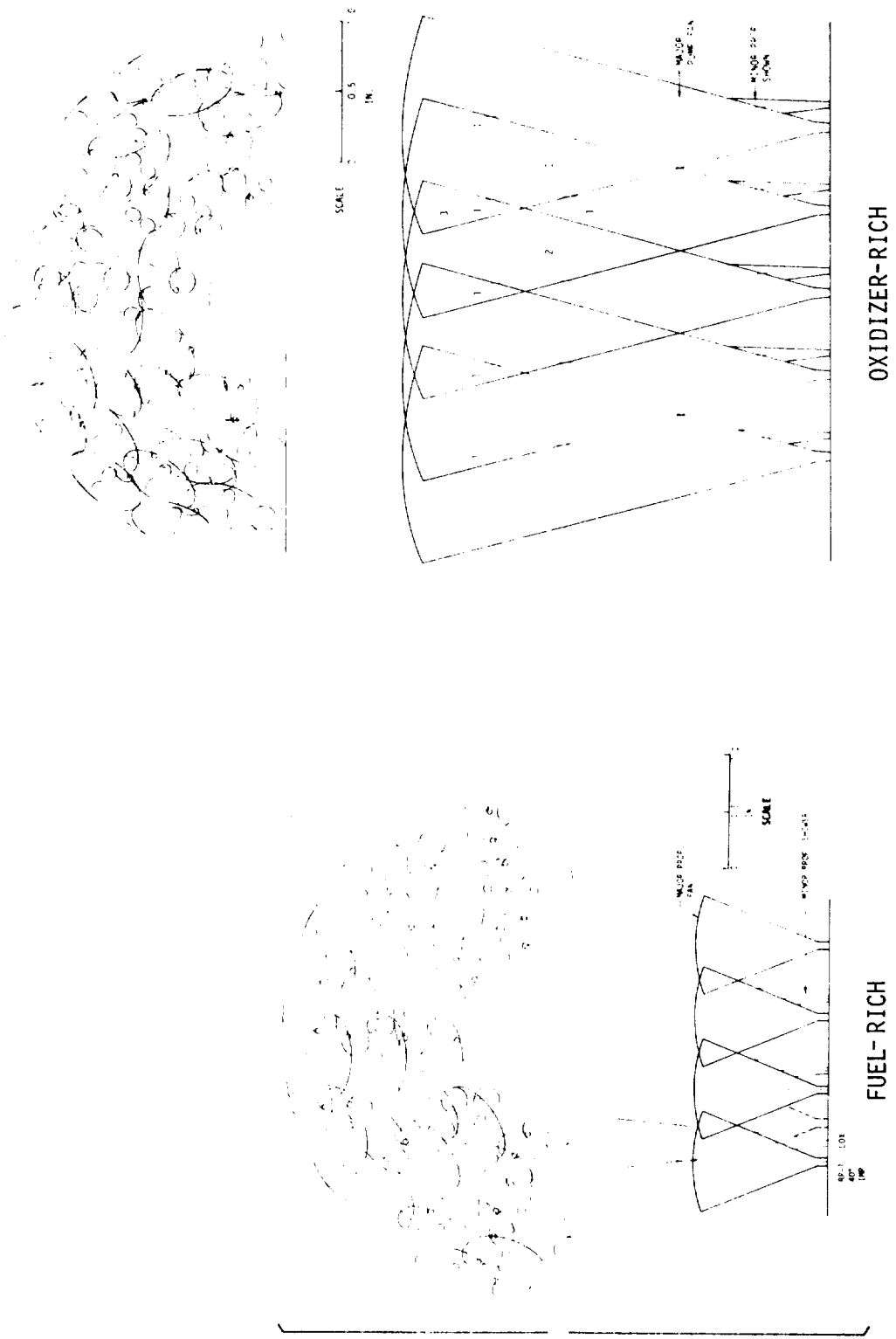
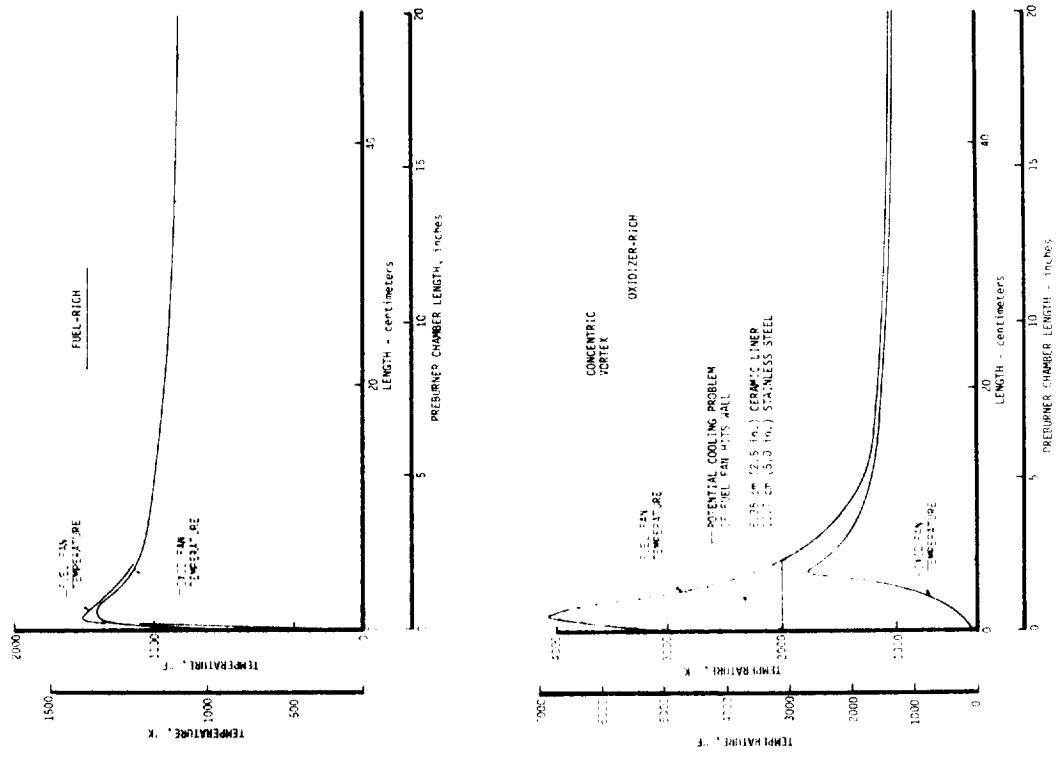


Figure IV-37. Fuel-Rich Preburner EDM'd Pattern Design

ORIGINAL PAGE IS
OF POOR QUALITY



GAS TEMPERATURE VERSUS MIXTURE RATIO

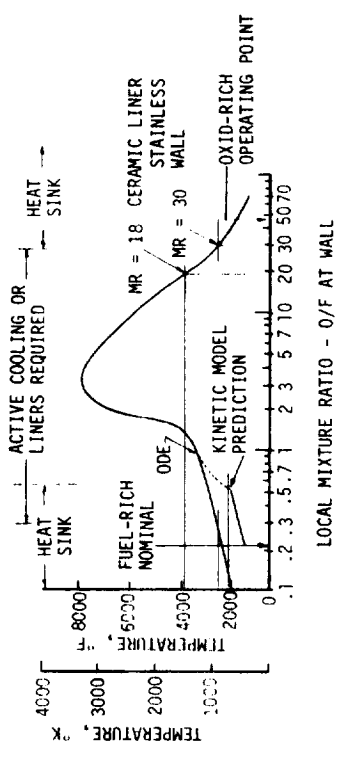


Figure IV-38. Maximum Operating Mixture Ratios for Uncooled Chamber Designs

IV, A, Fuel-Rich Preburner (cont.)

The wall thermal profile was employed in the structural analyses to compute cycle life, flange rotation, and the ability of the wall to withstand an internal pressure of 17235 kPa (2500 psia) when hot.

The seal surface temperatures were employed to select seal materials. The backside temperature of the unlined chamber was predicted to be 450°K (350°F) at the end of the test. The seal temperature would be less than this due to the added mass of the flange.

Figure IV-39 shows that a 1.91-cm (0.75-in.) thick stainless steel wall would reach approximately 1089°K (1500°F) in 15 sec at the nominal mixture ratio (0.3) and approximately 1422°K (2100°F) if the local MR were as high as 1.0. These conditions were considered acceptable.

The upper curves in Figure IV-39 indicate that a small deposit of zirconia inside the stainless steel liner would extend the allowable maximum MR to almost 2.0. This extra coating was not considered necessary for the fuel-rich testing.

The thermal conclusions and recommendations resulting from these analyses are as follows:

- RP-1 freezing can be eliminated by proper design
- Injector face heat flux is expected to be low due to blockage by the rich propellant fan
- The wall temperature of a heat sink stainless steel fuel-rich preburner is not expected to exceed 1256°K (1800°F)

9. Injector Pattern

a. Objectives

The objectives of this activity were to evaluate candidate injection element types and element packaging and to select the element type and quantity required to achieve the technical goals. These goals included a uniform gas temperature of $\pm 28^{\circ}\text{K}$ ($\pm 50^{\circ}\text{F}$) at the turbine inlet to minimize solid coke and carbon generation and assure stable combustion.

b. Requirements

The requirements which influence the element type selection are as follows:

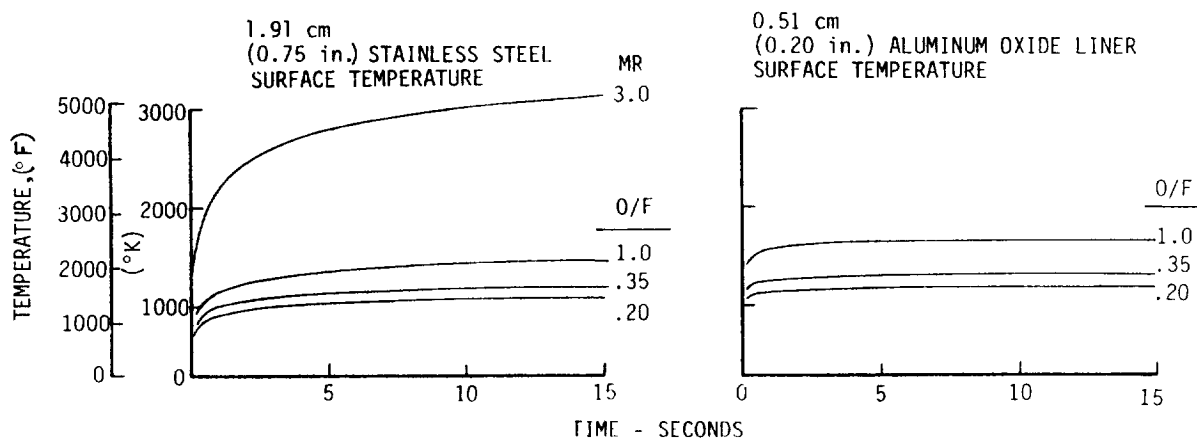
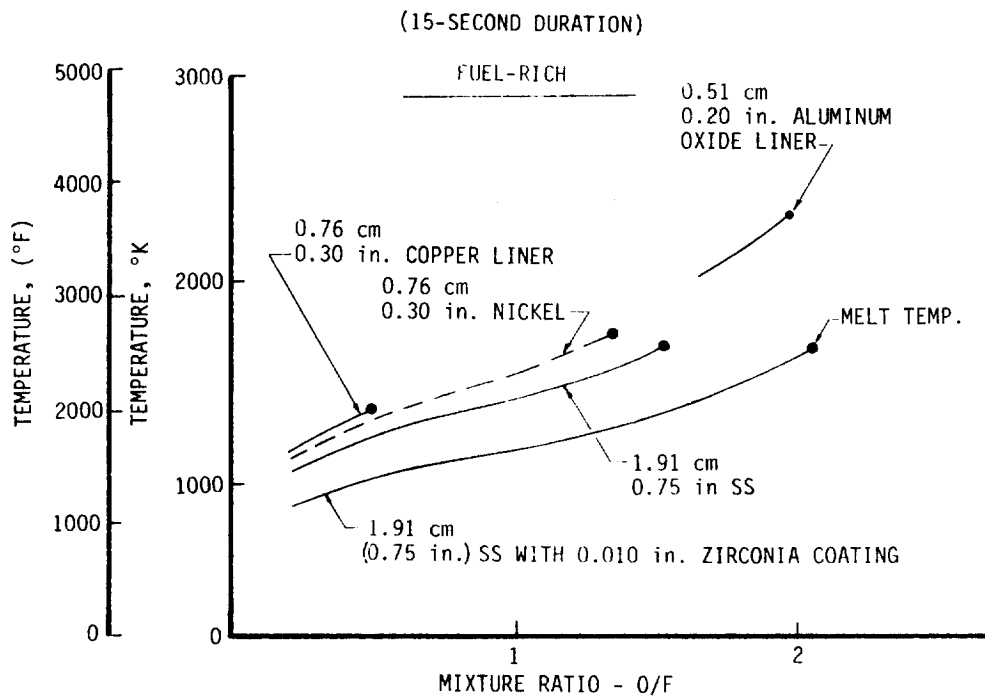


Figure IV-39. Streak-Resistant Capabilities of Candidate Materials for Fuel-Rich Preburner Design

IV, A, Fuel-Rich Preburner (cont.)

<u>Requirement</u>	<u>Functional Purpose</u>
Fine atomization of rich propellant	Rapid quenching of flame with excess fuel
Uniform mixing	Minimize chamber length and hot streaks
Encapsulate lean propellant ligament perimeter at atomization plane	Maximize liquid/liquid contact and gas/gas mixing rate. Protect the chamber wall and injector face from combustion source
Minimize atomization time lag	Enhance chug stability margin
Avoid lean propellant droplet concentrations	Minimize hot streaks/coking
Maximize RP-1 injection orifice size Avoid RP-1 freezing	Minimize plugged holes Potential detonation/unpredictable combustion characteristics
Minimize hot coring with fuel-rich preburner	Minimize coke formation; maximize fuel vaporization

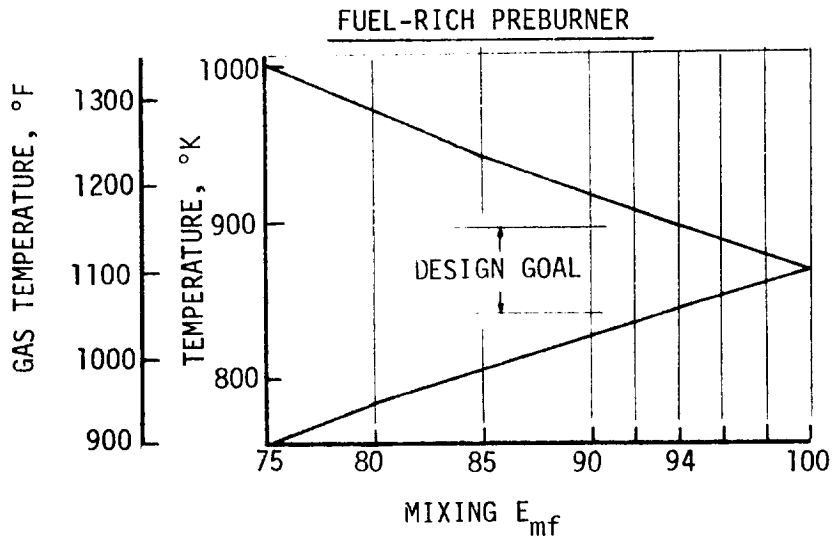
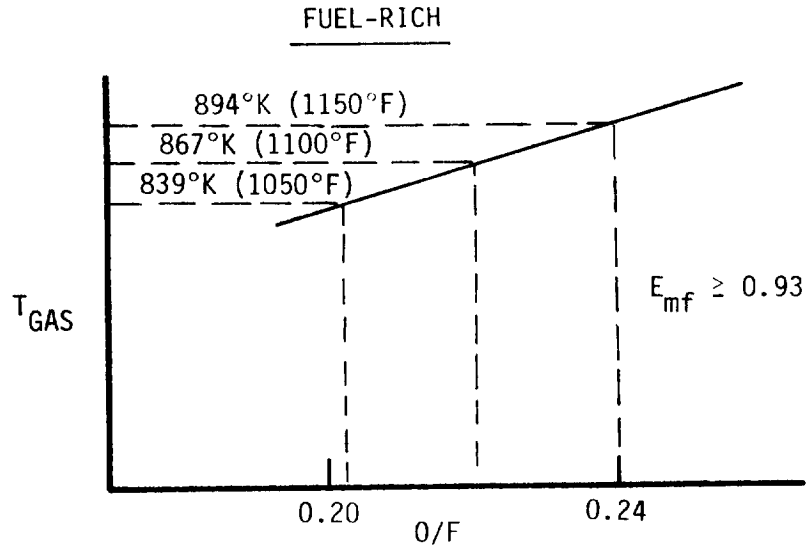
The criteria for maintaining the gas temperature uniformity are related to an allowable mixture ratio variation of 0.20 to 0.24 for a nominal gas temperature of 839 to 894°K (1050°F to 1150°F), as shown in Figure IV-40. This, in turn, requires a mixing efficiency (E_{mf}) of 93% or better. Mixing efficiencies of this magnitude are not developed with conventional injectors having a high flow per element.

The conclusions reached from these analyses were that a fine element pattern and secondary mixing devices within the combustion chamber would be required for all conventional element designs.

c. Element Selection

Candidate elements and their manifolding concepts are identified in Figure IV-41. The unlike impinging elements (such as doublets and triplets which normally provide superior mixing characteristics) were not selected for the LOX/RP-1 preburner for the following reasons:

- 1) Unlike elements have demonstrated poor stability characteristics with this propellant combination.



PREBURNER DESIGN AND OPERATING REQUIREMENT:

	O/F	$T_{NOMINAL}$ ($^{\circ}F$)
FUEL-RICH	0.22	867°K (1100*)
PERFORMANCE	> 98% ERE	
ΔT_{GAS}		$\pm 28^{\circ}K$ ($\pm 50^{\circ}F$)

*ADVANCED HIGH-PRESSURE ENGINE STUDY FOR MIXED-MODE VEHICLE APPLICATIONS, CONTRACT NAS 3-19727, NASA CR-135141.

Figure IV-40. Allowable O/F Variance for Required Turbine Inlet Temperature Uniformity

RATING		REMARKS/CAUSE FOR REJECTION												
E: EXCELLENT (5 Pts)		(One or More "Unacceptable" Rating is Sufficient Cause for Concept Rejection)												
G: GOOD (4)														
F: FAIR (3)														
P: POOR (2)														
U: UNACCEPTABLE (-oo)														
MANIFOLD CONCEPT	INJECTION ELEMENT CONCEPT	FUNCTIONAL INJECTOR REQUIREMENTS	ATOMIZATION (Small Drop Size)	MIXING (Uniform)	INJECTOR FACE COMPATIBILITY (Low Heat Flux)	CHAMBER WALL COMPATIBILITY (No Streaks)	CHUG STABILITY (Short Comb. Time Lags)	HIGH-FREQUENCY COMB. STABILITY (Uniform Atom. Distrib.)	INJ. MOMENTUM BALANCE (Axial Resultant)	RP-1 FREEZING (Oxid.-Rich P.B. Only)	NUMERICAL RATING (Perf. Inf. = 5.0)	REMARKS/CAUSE FOR REJECTION		
1	Post Type		E	G	E	G	E	F	E	E	4.43	Recommended Injector		
2	Post Type		L:E R:U	F	E	E	G	G	E	?	-	Poor Atomization of Rich Propellant		
3	Post Type		U	U	E	E	P	E	E	-	-	Low Performance For Liq/Liq		
4	Post Type		G	E	F	F	E	P	G	U	-	PP-1 Freezing Potential		
5	Concentric Ring	Conventional Triplet (Rich-Lean-Rich)	E	F-P	P	G-F	E	P	G	U	-	In Oxidizer-Rich Preburner		
6	Concentric Ring	Pentad (4R:1L)	E	F	P	G-F	E	P	E	U	-	2nd Choice; Can Utilize Post Manifold		
7	Concentric Ring	Pre-Atomized Triplet	G	G	P	G-F	G	F	G	-	3.50			
8	Concentric Ring	Like-On-Like Doublet	F	F	F-P	G-F	F	G	G	-	3.29	1960 G.G. Technology Baseline		
9	Concentric Ring	X-Doublet	G	U	F	E	U	F	G	-	-	Excessive T ₁ Variation & Resurge Prone		
10	Concentric Ring	Splash Plate	G	P	P	G	F	P	U	?	-	Excessive Momentum Imbalance		
11	Concentric Ring	Unlike Doublet	L:E R:U	U	P	F-P	F	P	P	U	-			
12	Concentric Ring	V-Doublet	F	F	F	F	F	E	G	-	3.29	May be Best for 600K Preburner Stability		
13	Concentric Ring	Showerhead	U	U	U	E	P	E	E	-	-	Low Performance; Large T ₁ Variation		

Figure IV-41. LOX/RP-1 Preburner Injection Element Rating Criteria

IV, A, Fuel-Rich Preburner (cont.)

- 2) The large difference in propellant mass flowrates results in a large mismatch in the diameters of the impinging streams, thus reducing the mixing efficiency.
- 3) The heat load to the injector face at high chamber pressures could cause thermal failures.

Two element types were selected for further optimization:

- 1) A self-atomizing coaxial vortex element was selected because it provided the best atomization characteristics for a given orifice diameter and created the most favorable thermal environment for protecting the injector face.
- 2) The second element that was selected employs a Like-on-Like (LOL) impinging doublet element for the major propellant and an axial showerhead injection element for the minor propellant. The quantity of axial holes was established on the basis of minimum orifice diameter and economics. The ratio of the impinging to the non-impinging orifice quantity was 2.

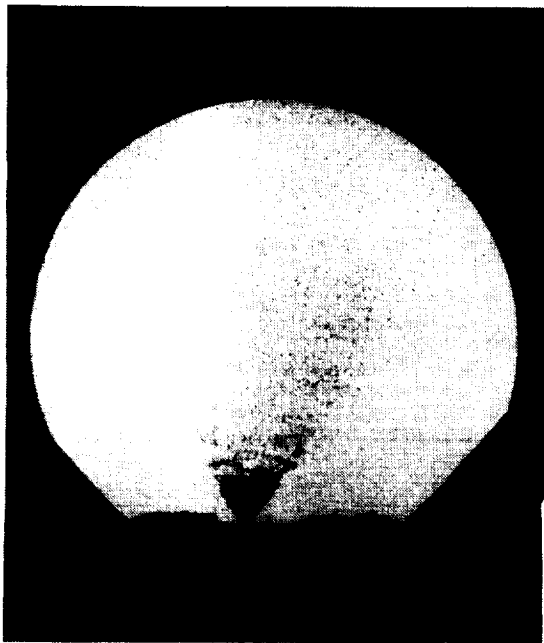
Figure IV-42 provides a photograph of a typical vortex spray cone and an LOL doublet element. The atomization characteristics of the vortex element are noted to be more uniform and result in smaller drop sizes than those of the LOL element.

d. Coaxial Vortex Element Detailed Design

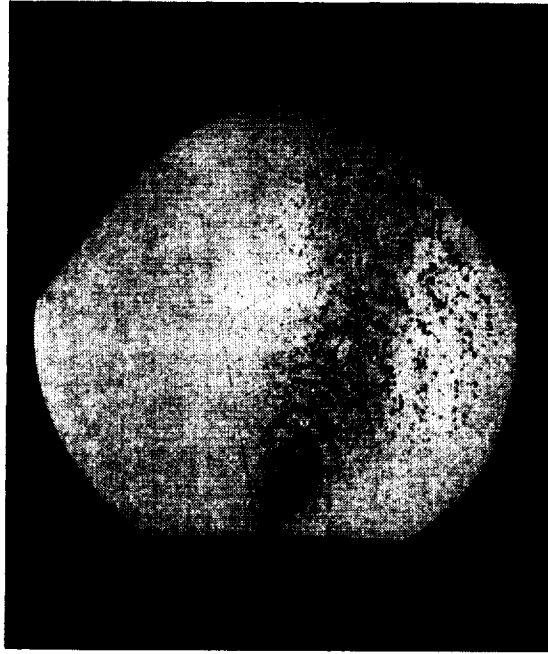
The principle of operation of the coaxial vortex element is illustrated in Figure IV-43. The parameters which control the drop size, vaporization rate, and subsequent mixing are 1) the element quantity (NE), 2) the spray cone angles (α), and 3) the element positions relative to each other. Figure IV-43 also provides typical parametric data which quantify the relationship between these parameters.

These analyses, combined with the packaging requirements and chamber diameter selection, are shown in Figures IV-44 and IV-45.

The oxidizer-rich preburner controls the fuel-rich design envelope due to the need for chamber hardware interchangeability. Thus the fuel-rich chamber diameter was sized to accommodate the higher flowrate of



VORTEX ELEMENT



LOL DOUBLET ELEMENT

Figure IV-42. Comparison of Vortex and LOL Doublet Element

ORIGINAL PAGE IS
OF POOR QUALITY

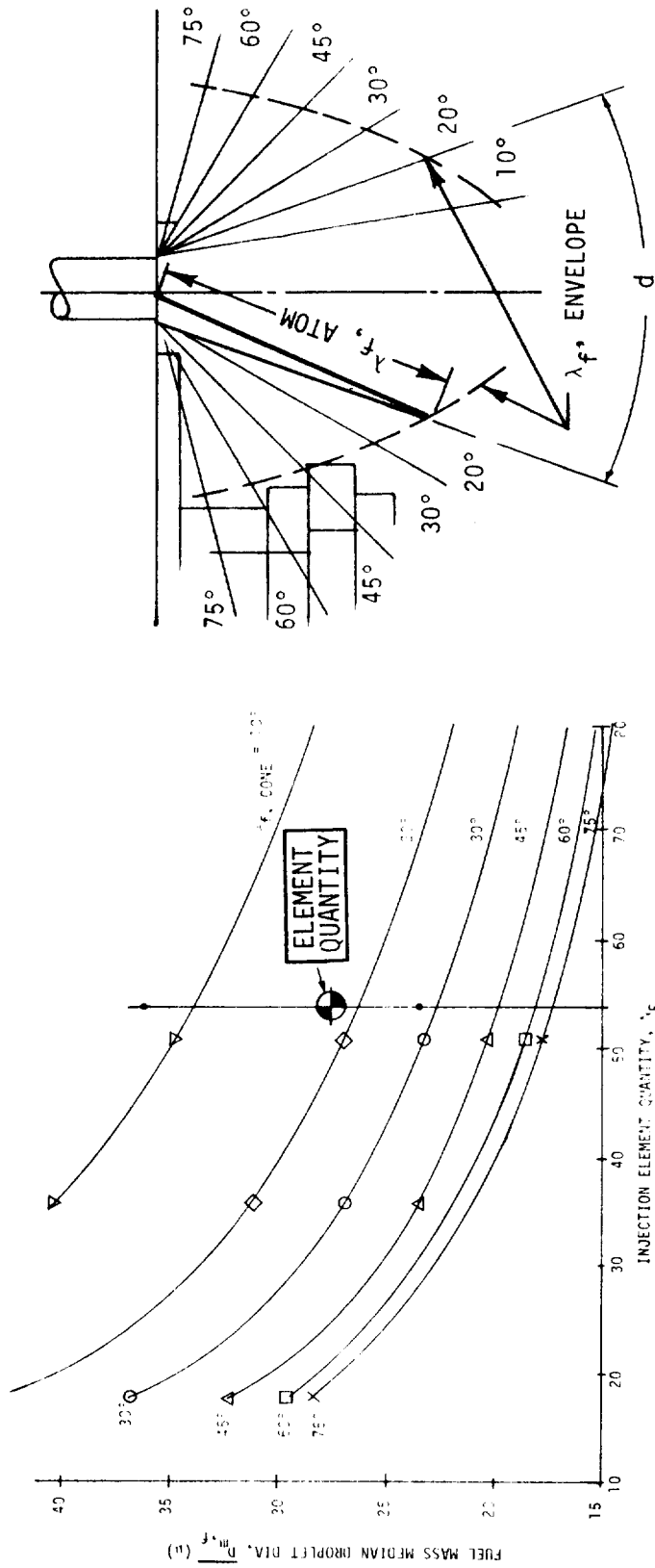


Figure IV-43. Typical Parameters Which Control Vortex Element Optimization

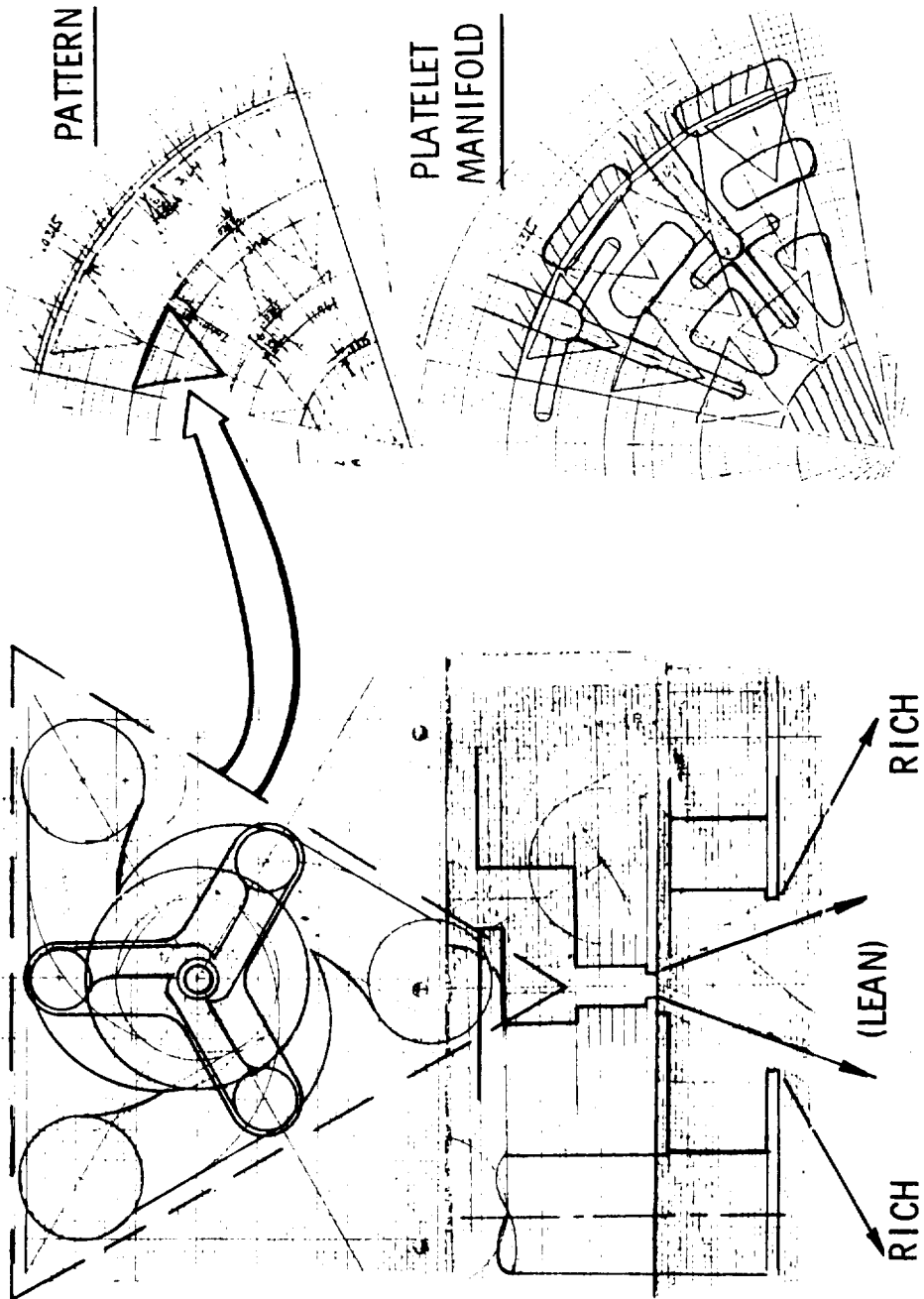


Figure IV-44. Geometric Considerations Influencing Element Packaging

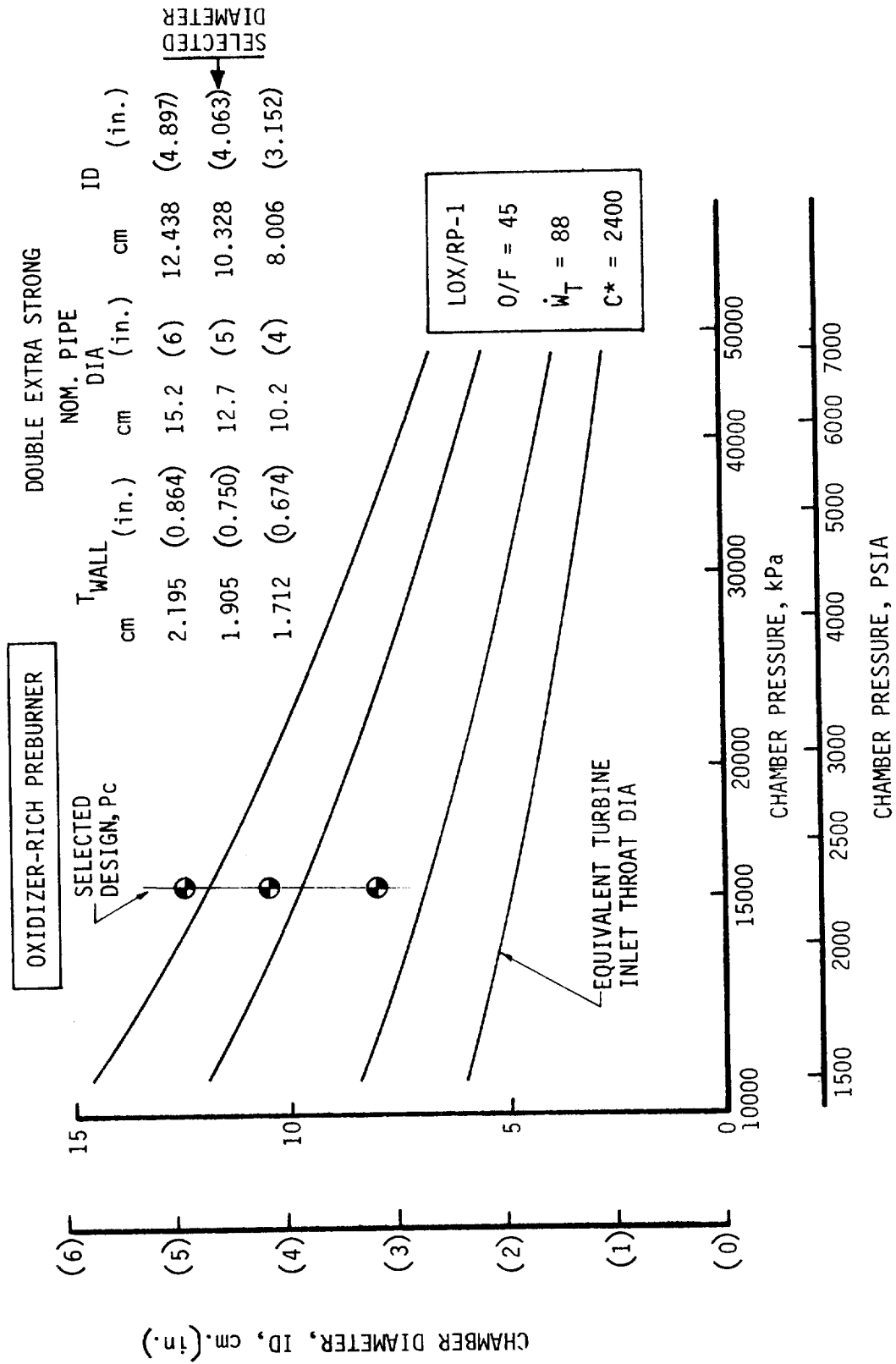


Figure IV-45. Chamber Diameter Selection Based on Contraction Ratio and Standard Pipe Sizes

IV, A, Fuel-Rich Preburner (cont.)

the oxidizer-rich preburner. Separate throat sections were provided to obtain the required flow/chamber pressure relationship.

The element quantity/chamber diameter selection process examined nominal pipe sizes of 10, 13, and 15 cm (4, 5, and 6 in.) diameter of double-extra strength wall thickness. Figure IV-45 shows that the selected 13-cm (5-in.) pipe size results in a 10.3-cm (4.063-in.) chamber diameter and a typical contraction ratio of 4.

The resulting envelope established by the chamber diameter, the drop size vs element quantity relation, and the element packaging shown in Figure IV-44 resulted in the selection of 54 elements for both the fuel- and oxidizer-rich design. Table IV-I defines the spray characteristics of the coaxial vortex element. Figure IV-46 shows that the predicted spray cone angles are 75° for the outer fuel cone and 40° for the inner oxidizer cone. The experimental preassembly flow data presented in Section IV showed the actual fuel and oxidizer cone angles to be 78 and 34°, respectively. The 34° oxidizer cone angle was found to result in impingement within the cup when both circuits are flowing and was subsequently reduced to a 20° angle. Figure IV-46 also shows the predicted percent of propellant vaporized as a function of distance from the injector. The oxidizer is completely vaporized in 5 cm (2 in.) whereas the fuel is only 50 to 90% vaporized in the same length. The concentric stream design provides for the containment of each hot oxidizer-enriched jet within the fuel-rich cone. This protects both the injector face and chamber wall from hot combustion products produced by the difference in vaporization rates. The uncertainty in the fuel vaporization rate prediction is caused by uncertainties in the gas temperature which surrounds the fuel droplets and by the hot-gas recirculation pattern within the spray cones.

One of the hypotheses on coke and soot formation is that these solids are formed by the pyrolysis of the RP-1 during the exposure of the excess liquid fuel to the hot fuel-rich gases. To minimize sooting, the preburner element and mixer are designed to mix and thus quench the pyrolysis (producing hot streaks) as quickly as possible. Figure IV-47 provides a prediction of the temperature of the gas-phase mixture along the chamber axis. The gas temperature decreases as the larger fuel drops absorb heat from the surrounding gas.

As Figure IV-48 shows, preheating the fuel is predicted to substantially reduce the exposure time of RP-1 to the conditions which form solids. This is predicted to increase the efficiency and reduce sooting.

TABLE IV-I. COAXIAL VORTEX CHARACTERISTICS

PREBURNER PROPELLANT	FUEL-RICH		OXIDIZER-RICH	
	LOX	RP-1	LOX	RP-1
Cone Angle, θ (degree)	40°	75°	60°	20°
Orifice Diameter, cm (in.)	0.132 (0.052)	0.335 (0.132)	0.472 (0.186)	0.056 (0.022)
Fan Length, cm (in.)	1.186 (0.467)	1.445 (0.569)	3.266 (1.286)	0.584 (0.230)
Distance to 20% Vap., cm (in.)	0.145 (0.057)	0.102 (0.040)	0.015 (0.006)	0.419 (0.165)
Drop Radius, cm (in.)	0.0025 (0.0010)	(0.0019)	(0.0022)	(0.0009)
Combustion Time Lag, ms	0.22	0.22	0.54	0.14
Pressure Drop, kPa (psid)	2068 (300)	2068 (300)	2068 (300)	2068 (300)
Velocity, m/sec (ft/sec)	61.0 (200)	71.6 (235)	61.0 (200)	71.6 (235)

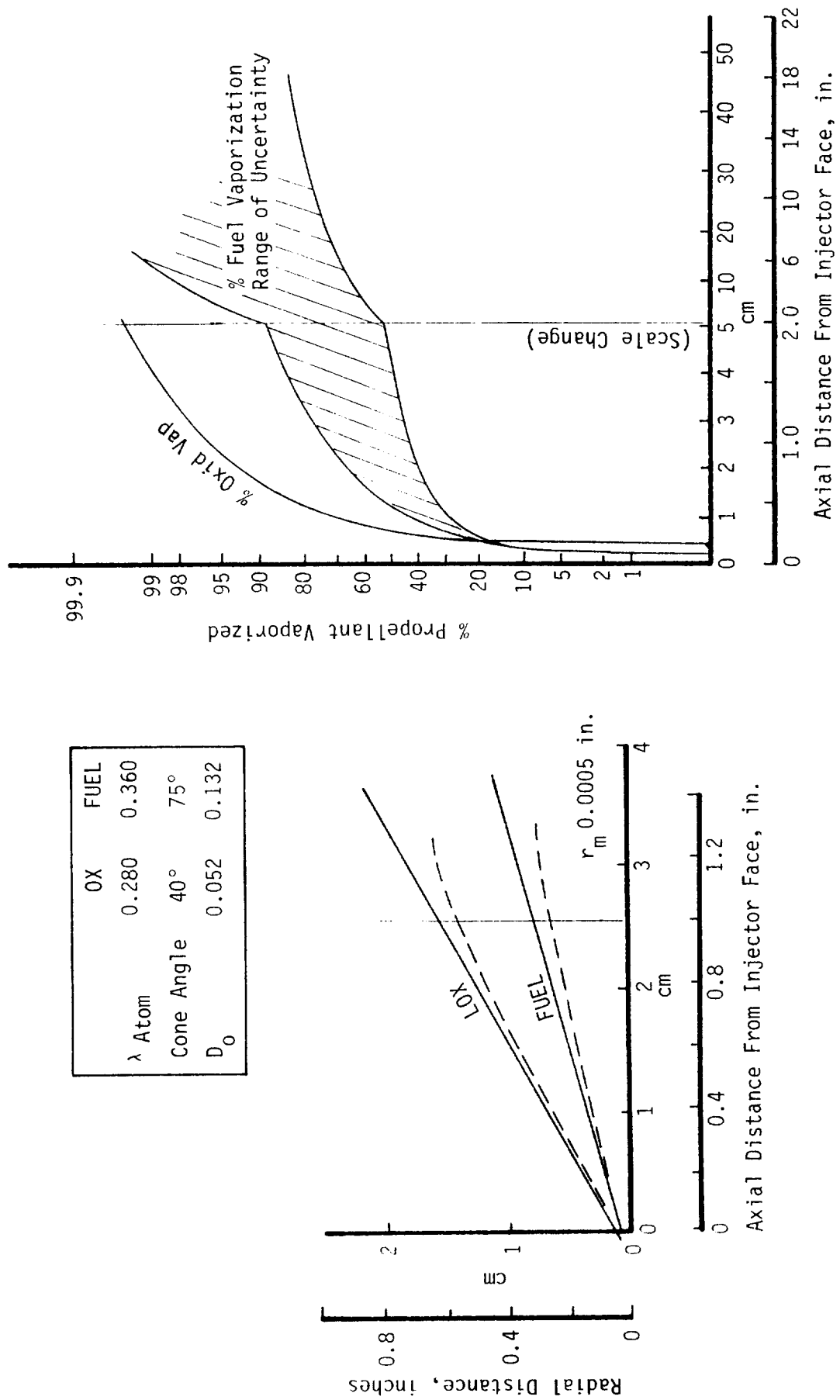


Figure IV-46. Fuel-Rich Preburner Vaporization Profile Prediction Using Priem Vaporization Model

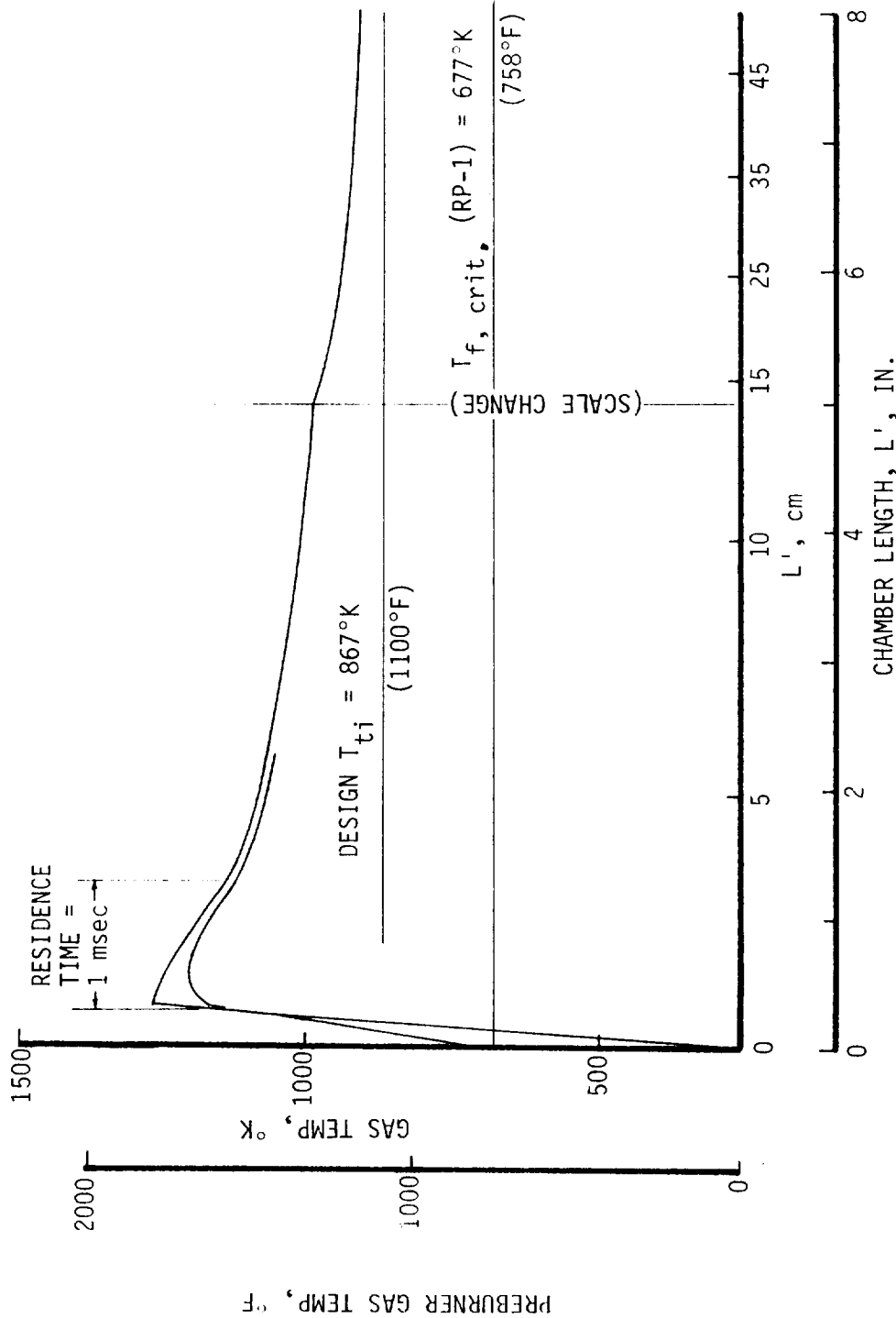


Figure IV-47. Predicted Fuel-Rich Preburner Mixing Profile

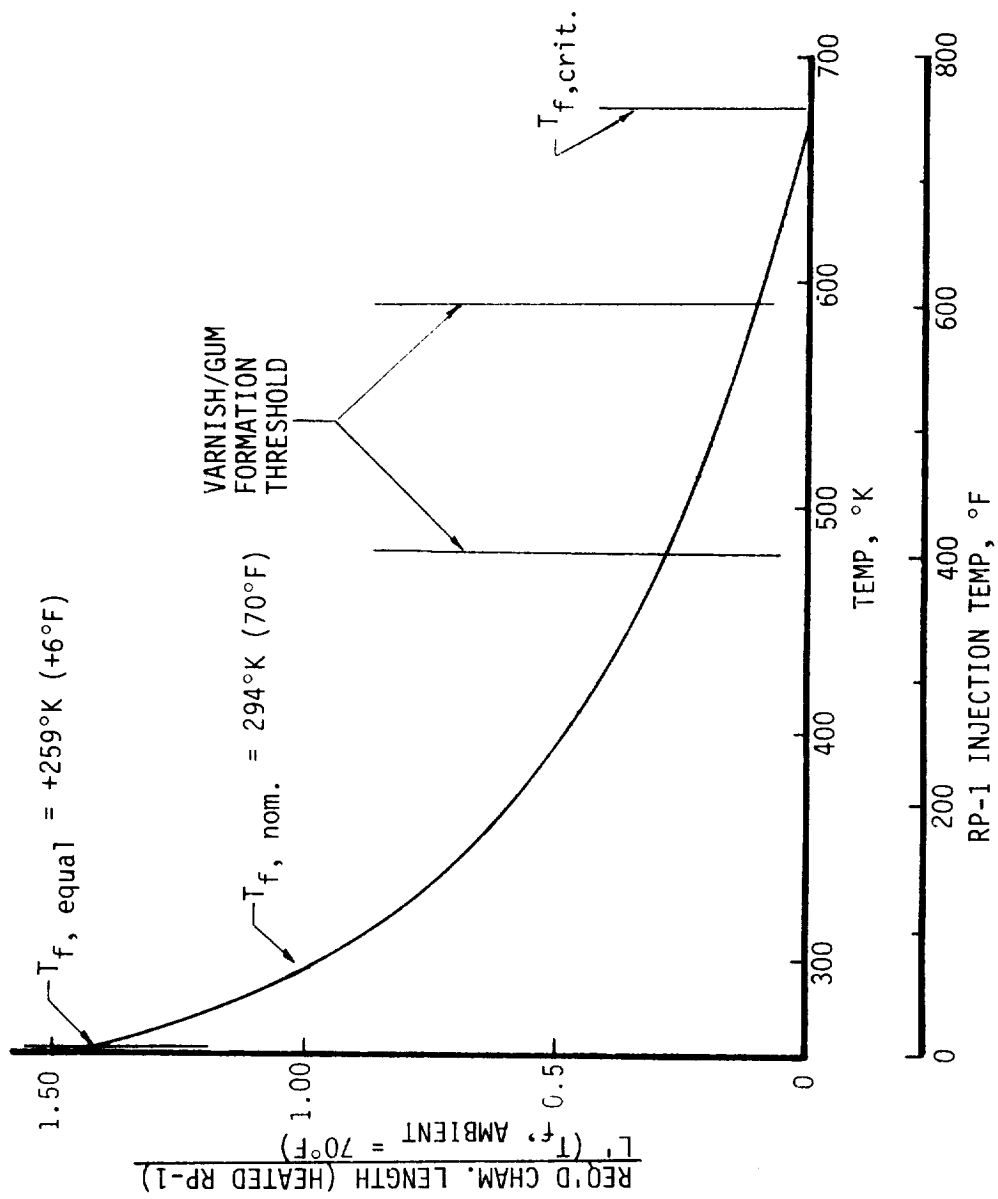


Figure IV-48. Fuel Preheating Influence on Vaporization Efficiency

IV, A, Fuel-Rich Preburner (cont.)

e. LOL EDM'd Doublet Injector

Design Philosophy

The LOL injector patterns analyzed herein are intended to provide a design alternative to the concentric vortex injector. These injector designs are based on existing technology, where possible, and are purposely designed to have different features than the original concentric vortex injector designs.

The LOL injectors will not produce the fine atomization or the degree of lean propellant encapsulation expected in the concentric vortex design. Rather, for satisfactory performance, a long chamber, warm fuel, and mixing rings are stipulated. A lean propellant showerhead flame instead of full "encapsulation" is proposed to minimize thermal exposure of the injector face and chamber walls.

The LOL/showerhead element pattern is expected to yield a more favorable axial mixture ratio distribution than the concentric vortex pattern by delaying the oxidizer (showerhead) vaporization and making it more compatible with the large fuel-rich LOL fan. The oxidizer showerhead streams of the outer element row are tilted 2° inboard and 2° sideways toward the adjacent fuel-rich LOL fan in order to enhance mixing and to shield the wall from the hot propellant flame. The lean inner row (core) streams are only tilted 2° sideways. The operating conditions and hardware geometry dimensions are shown in Table IV-II.

The predicted fuel- and oxidizer-rich preburner LOL propellant stream characteristics are summarized below:

TABLE IV-II. FUEL-RICH PREBURNER LOL - SHOWERHEAD
INJECTOR DESIGN SUMMARY

	<u>FUEL-RICH</u>
Chamber Diameter, cm (in.)	10.31 (4.06)
Throat Diameter, cm (in.)	3.12 (1.23) without turbine simulator; 4.06 (1.60) with turbine simulator.
Contraction Ratio	10.90 without turbine simulator; 6.4 with turbine simulator.
Chamber Length, cm (in.)	61.0 (24.0)
Chamber Pressure Upstream of Turbine, kPa (psia)	15,167 (2200.00)
Mixture Ratio	0.254
Mach No.	0.06
Oxidizer	LOX
Fuel	RP-1

	<u>FUEL CIRCUIT</u>	<u>OXIDIZER CIRCUIT</u>	
	LOL	Showerhead	Inner Row Only
Orifice Diameter, cm (in.)	0.142 (0.056)	0.102 (0.040)	0.051 (0.020)
Orifice L/D	6.6	2.5 (1.0*)	
Orifice Chamfer (Degree)	45°	None	
Orifice Cd	0.85	0.68	
Orifice Number	160	70	10
Pressure Drop, kPa (psid)	2758 (400)	2758 (400)	
Flowrate, kg/sec (lb/sec)	13.49 (29.75)	3.43 (7.56)	
Injection Velocity	290	237	
Tilt Angle	0°	2°	

*Machining error resulted in this value being smaller than the initial design.
No impact on the flow was expected since the flow was detached at both L/D
values.

IV, A, Fuel-Rich Preburner (cont.)

LOL PROPELLANT STREAM CHARACTERISTICS

PREBURNER	FUEL-RICH				OXIDIZER-RICH			
ELEMENT	Showerhead	LOL			LOL	Showerhead		
PROPELLANT	LOX	RP-1			LOX	RP-1		
Temperature, °K (°F)	100° -280°	294° 70°	367° 200°	422° 300°	100° -280°	294° 70°	367° 200°	422° 300°
Fan Length, cm (in.)	3.20 1.26	2.95 1.16	3.30 1.30	3.51 1.38	7.85 3.09	3.73 1.47	4.19 1.65	4.45 1.75
Injection Vel., m/sec (ft/sec)	72.2 237	78.3 257	83.5 274	88.1 289	73.2 240	78.3 257	83.5 274	88.4 290
Pressure Drop, kPa (psid)	2806 407	2447 355	2613 379	2758 400	2889 419	2447 355	2613 379	2758 400
ALRC Fan Model Drop Radius, cm (in.)	0.0051 0.0020	0.0084 0.0033	0.0074 0.0029	0.0069 0.0027	0.0107 0.0042	0.0099 0.0039	0.0089 0.0035	0.0084 0.0033
Combustion Time Lag (ms)	0.52	0.54	0.54	0.53	1.24	0.57	0.42	0.36

The injection of fuel into high-density (high-pressure) combustion gases was modeled on the data of Reference 5. These data indicate that the atomization of a single high-velocity showerhead element jet improves considerably when it is injected into a high-pressure gas. Thus the normally poor performance characteristics of a single showerhead element improve as the density of the downstream gas is increased.

In this application (at high pressure greater than 13,788 kPa (2000 psia) and low temperature of 922°K (1200°F)), the combustion gas density is about 0.025 kg/m³ (4 lb/ft³) versus about 0.00624 kg/m³ (0.1 lb/ft³) for typical low-pressure engines. This is expected to result in a substantial decrease in the size of droplets formed by the lean showerhead propellant streams. However, this is somewhat offset by the fact that the showerhead liquid stream will extend for several inches down the chamber while droplets are generated. Also, the biggest droplets are generated last.

Experimental evidence (Ref. 6 and 7) obtained from injecting liquids into a high-density gas cloud indicates that showerhead

IV, A, Fuel-Rich Preburner (cont.)

streams are stripped and diffused by the high drag so as to form a 7° (included angle) cone shape showerhead propellant stream. Assuming that each showerhead stream serves a 1.27-cm (0.5-in.) diameter circle of the chamber cross section, it would take a minimum of 10.27 cm (4 in.) of axial length for a 7° cone "apex" to generate a 1.27-cm (0.5-in.) diameter cone base that would supply some (albeit small) amount of lean propellant throughout the chamber cross section. Additional chamber length and mixing rings are expected to be required for further vaporization and mixing of the remaining lean propellant.

f. Manifolding Designs

The manifolds were designed so that the lean propellant would be supplied through an annulus feeding a cross-drilled radial array, while the rich propellant was fed axially from a flooded cross section. In order to assure uniform propellant flow distribution, all of the passages immediately preceding the injector face orifices were designed to have flow areas at least four times greater than the orifice areas being served. This results in manifold hydraulic dynamic heads of one-sixteenth of the injection orifice pressure drop.

g. Comparison of Selected Injector Designs

The fuel-rich LOX/RP-1 injector analysis has resulted in the following conclusions:

- (1) For a given chamber length and without the use of mixing devices, the LOL element will be lower-performing than the concentric vortex element.
- (2) The concentric vortex design will provide a more uniform gas temperature distribution, but both designs will require a secondary in-chamber mixing device to achieve the $\pm 28^{\circ}\text{K}$ ($\pm 50^{\circ}\text{F}$) gas temperature uniformity goal.
- (3) Unlike the concentric vortex design, the LOL pattern will not encapsulate the lean propellant streams. However, the showerhead will produce a thermally compatible environment for both the injector face and chamber wall.
- (4) While adequate, the chug stability margin of the LOL pattern will be smaller than that of the concentric vortex injector design.

IV, A, Fuel-Rich Preburner (cont.)

- (5) The first longitudinal mode stability margin of the LOL design will be greater than that of the concentric vortex injector design.

h. Recommendations for Injector Testing

The following recommendations are made for the LOX/RP-1 high-pressure preburner LOL injector design:

- (1) Make provision to test with the RP-1 temperature over a range from 283 to 422°K (50 to 300°F) and monitor performance, coking, streaking, and hydraulic admittances.
- (2) Make provision to fire with both 30.5- and 61-cm (12- and 24-in.) long chambers, and demonstrate the ability of in-chamber mixing rings to improve gas temperature uniformity. A temperature rake will be required to measure the mixing efficiency.
- (3) If the 61-cm (24-in.) long chamber performance with ambient fuel is low-performing, a mixing ring should be used.
- (4) A mixture ratio and chamber pressure "box" (operating envelope) with corners at +20% from "nominal" should be tested to monitor performance, coking, streaking, and hydraulic admittances.

B. OXIDIZER-RICH PREBURNER

1. Problem Definition and Past History

Operating a high-pressure combustor in an oxidizer-rich environment presents various problems which are very different from those associated with the fuel-rich preburner. Carbon formation, coking, and the attainment of ignition are no longer issues. The main issue in the design of the oxidizer-rich combustor is the prevention of hot spots and subsequent metal ignition. Secondary issues are the prevention of fuel freezing within the manifold prior to injection and fuel freezing following injection but prior to combustion.

A past history of high-pressure oxidizer-rich combustion with the LOX/RP-1 propellant combination was nonexistent at the time these designs were initiated. The small data base available for oxidizer-rich combustion at

IV, B, Oxidizer-Rich Preburner (cont.)

high pressure with other propellants generally presents a trail of catastrophic failures within the first second of operation. These failures are mainly the result of heating the injector face and/or chamber wall to a temperature where the metal ignites in the oxygen-rich environment.

2. Concept Selection

The same three concepts considered for the fuel-rich preburner were also applied to the oxidizer-rich design. These are as follows: 1) stoichiometric combustor with downstream diluent; 2) hot core plus film cooling and downstream mixer; 3) uniform mixture ratio, supplemented, if necessary, by a small turbulator.

Since the main problem source was considered to be hot spots caused by a local excess of fuel, it was easy to conclude that the uniform mixture ratio approach provided the greatest chance of successful operation.

The remainder of the design tasks concentrated on developing an injector combustion pattern which 1) avoids concentrations of fuel, 2) prevents the fuel from reaching the chamber wall or other metallic surfaces before being completely combusted, and 3) provides good mixing of the combusted gas with the excess of oxygen to reduce the gas temperature well below the ignition point of the materials selected for the injector and turbine.

3. Materials Selection

The major criteria for the selection of materials to be employed for this data-gathering program were as follows: 1) resistance to ignition at elevated temperature; 2) long-term resistance to oxidation; and 3) high thermal conductivity to diffuse the heat away from local hot spots. Figures IV-49 and IV-50 provide the data that were employed for the materials selection.

Most components were fabricated from 18-8 (18% chrome) grade 304 stainless steel. The 304 alloy was selected because of its availability and its superior electron-beam welding characteristics. Materials which could be subjected to local hot streaks, such as the turbulator, the chamber liner nearest to the injector, and the EDM'd injector face, were fabricated from Nickel 200. The thermal conductivity of Nickel 200 is greater than that of 18-8 stainless steel by about a factor of 3. As noted in Figure IV-49, nickel has proven to be resistant to ignition in oxygen up to 1700°K (2600°F).

As an additional protective measure, all components exposed directly to the high-velocity oxidizer-rich combustion stream were recommended to be flame-sprayed with a ceramic oxide coating. A zirconium oxide product,

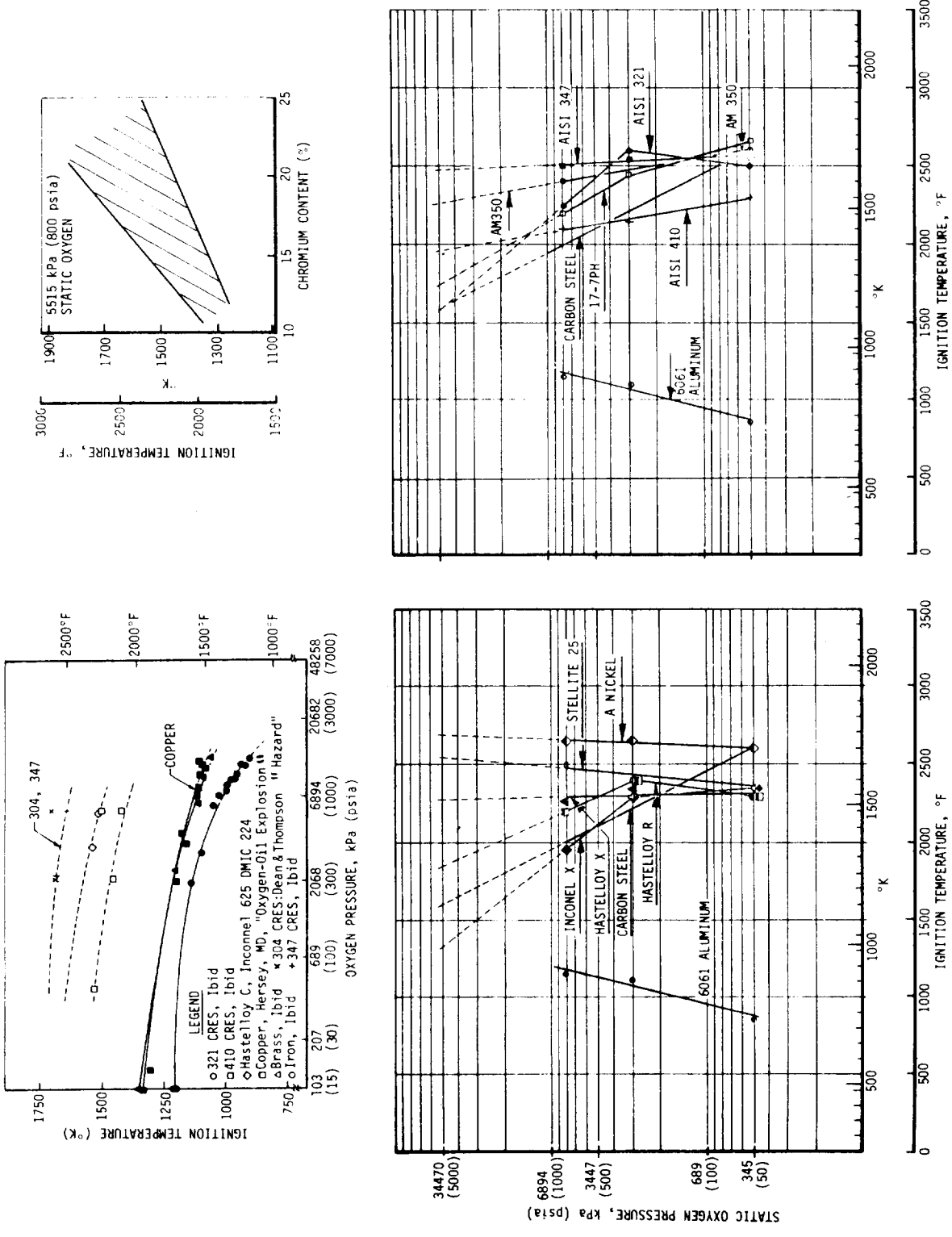


Figure IV-49. Ignition Characteristics of Candidate Materials

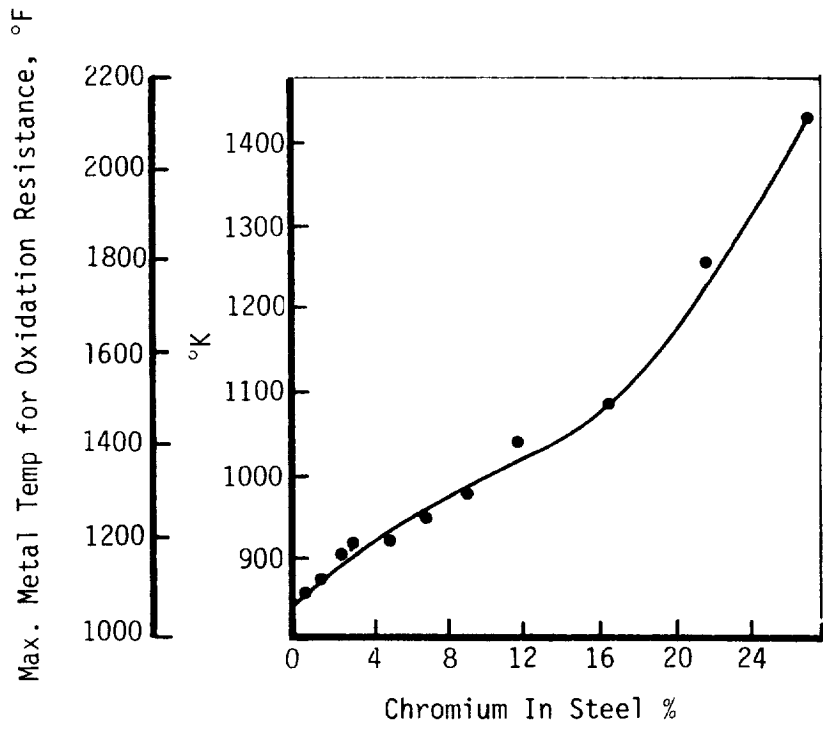


Figure IV-50. Effect of Chromium on the Oxidation Resistance of Steel in a Normal Combustion Atmosphere

IV, B, Oxidizer-Rich Preburner (cont.)

manufactured by Metco, Inc., was selected for this purpose on the basis of its good performance at NASA-LeRC. The Metco 202 NS was applied 0.025 cm (0.010 in.) thick over a 0.0076-cm (0.003-in.) thick 443 NS base coat.

4. Ignition Analyses

The energy requirements for igniting the LOX/RP-1 (MR = 40) liquid injection streams were calculated and converted to flowrates and supply pressures of GO_2/GH_2 . The igniter design was the same as that employed for the fuel-rich testing.

Figure IV-51 shows the results of the GO_2/GH_2 ignition analyses expressed as functions of flowrate and mixture ratio.

The selected design point parameters for ignition of the oxidizer-rich preburner are as follows:

MR	3.5
Total Flow	0.041 kg/sec (0.09 lb/sec)
Throat Diameter	0.64 cm (0.25 in.)
Spark Gap	0.064 to 0.076 cm (0.025 to 0.030 in.)
Power	50 mj at 300 sparks/sec

The spark energy shown is sufficient to ignite the O/H propellants which, in turn, ignite the oxidizer-rich preburner.

The igniter tube is fabricated from copper and can operate as a heat sink for 400 ms at full power. The torch temperature is $\approx 2778^\circ\text{K}$ ($\approx 5000^\circ\text{R}$).

5. Stability Analyses

High-frequency combustion and low-frequency chugging stability analyses were conducted for the concentric vortex platelet injector design and for the LOL doublet EDM'd pattern. The high-frequency stability analyses included longitudinal, tangential, and combined modes.

The results of the sensitive time lag chugging analyses, shown in Figures IV-52 and IV-53, indicate that both designs will be stable with a chamber length of 30.5 cm (12 in.) or longer. The required pressure drops for the two injectors at the design point pressure of 15167 kPa (2200 psia) are as follows:

Concentric vortex	$\Delta P_f = \Delta P_{ox} = 2068 \text{ kPa (300 psid)}$
LOL doublet/shower-head	$\Delta P_f = \Delta P_{ox} = 2758 \text{ kPa (400 psid)}$

TORCH IGNITER PREDICTED IGNITION LIMITS

OX-RICH PREBURNER

MR = 40

COLD-FLOW PRESSURES ($P_c = 172$ & 345 kPa (25 & 50 psia))

AVERAGE PROPELLANT VELOCITY = 93.6 m/sec (307 ft/sec)

CENTRALLY MOUNTED (COAXIAL) O_2/H_2 IGNITER

THROAT DIAMETER $D_T = 0.64$ cm (0.25 in.)

SPARK GAP = 0.076 cm (0.030 in.)

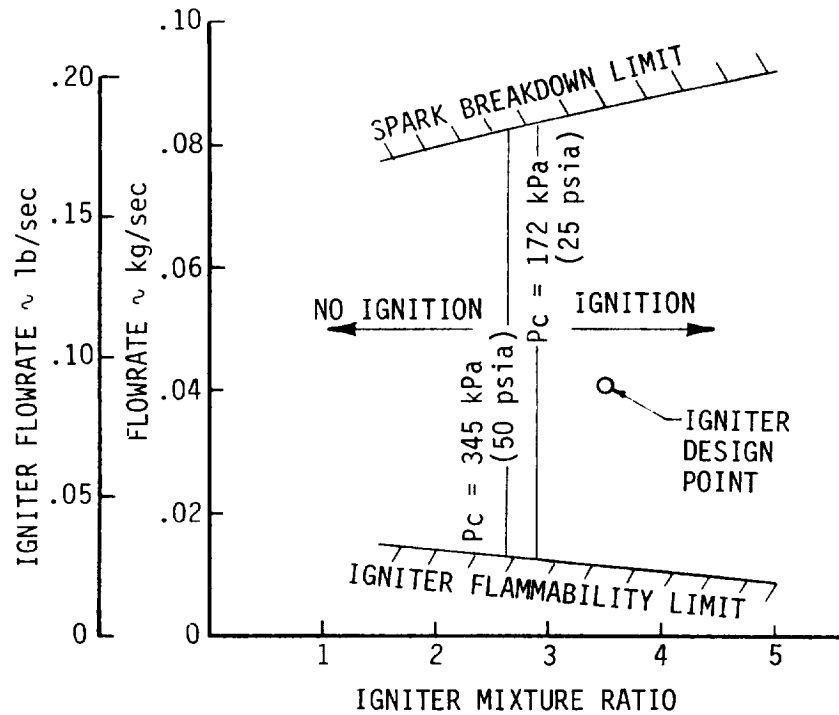


Figure IV-51. Results of Oxidizer-Rich Preburner Ignition Analyses (Flowrate Versus Mixture Ratio)

- No Chugging Problem with L_c near 30.5 cm (12 in.) or Longer

τ_{ox} = 1.24 ms
LOL

τ_{fuel} = 0.57 ms

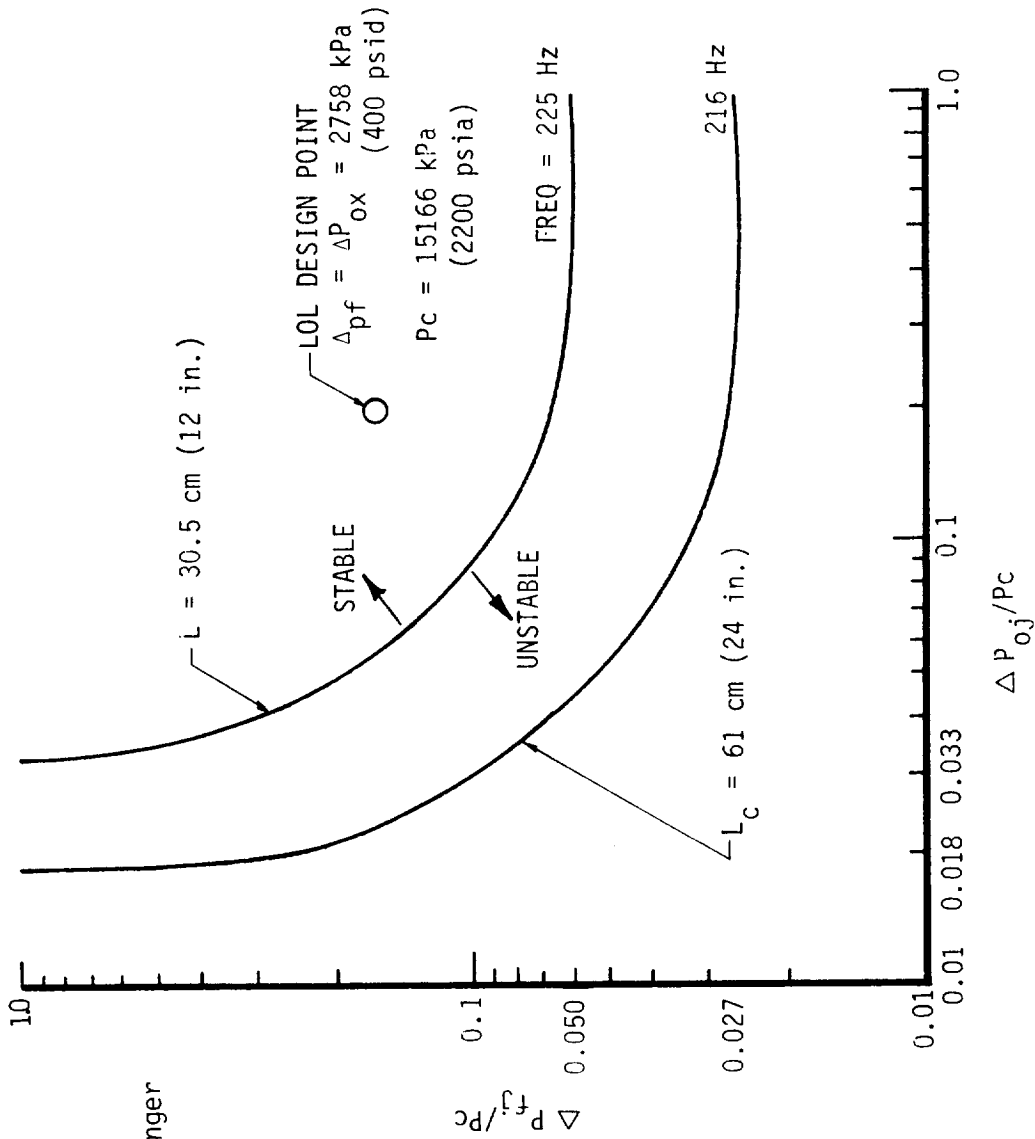


Figure IV-52. Oxidizer-Rich LOL Injector Chugging Analysis

SUMMARY OF PREDICTED STABILITY

- NO CHUGGING PROBLEM WITH L_c NEAR 30.5 cm (12 in.) OR LONGER

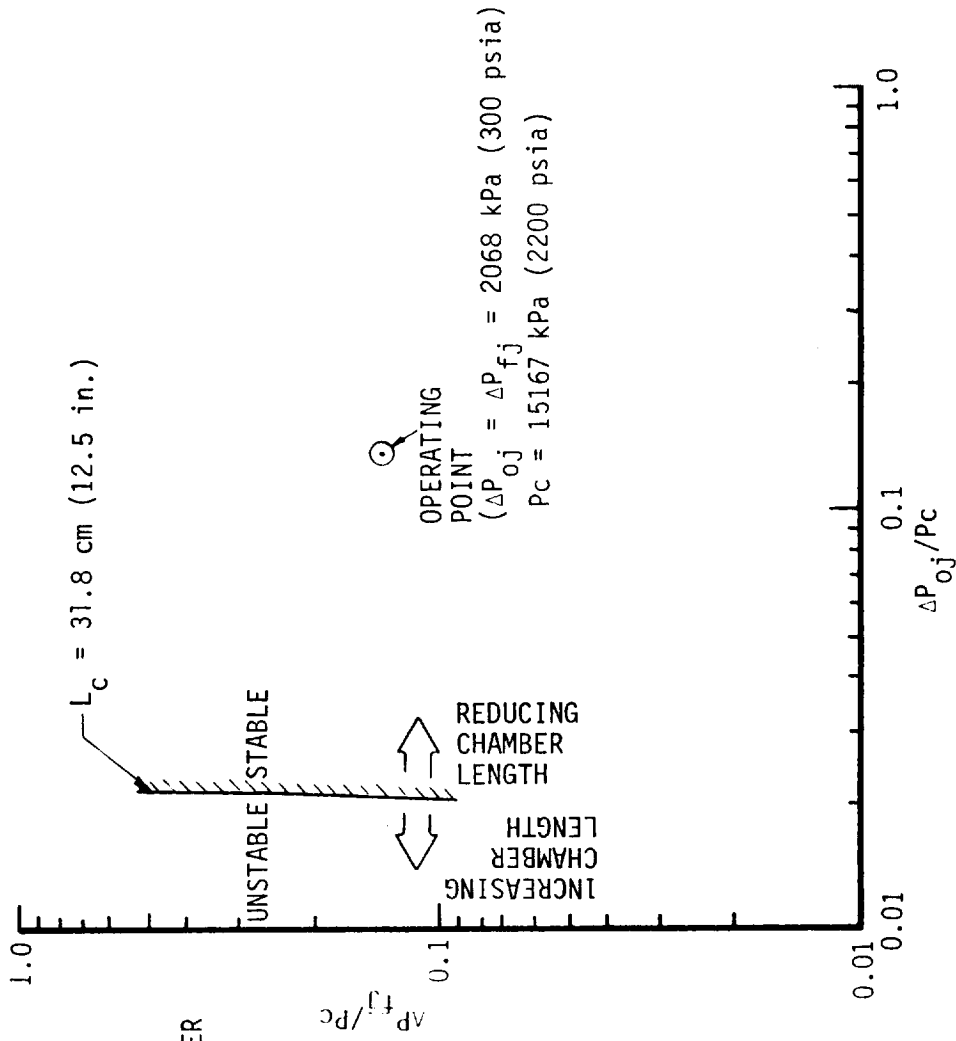


Figure IV-53. Oxidizer-Rich Concentric Vortex Injector Chugging Analysis

IV, B, Oxidizer-Rich Preburner (cont.)

The doublet injector requires the higher pressure drop in order to provide reasonable chug stability design margin at a 30.5-cm (12-in.) chamber length. The test hardware was designed to allow testing at 30.5-, 38-, and 68-cm (12-, 15-, and 27-in.) lengths.

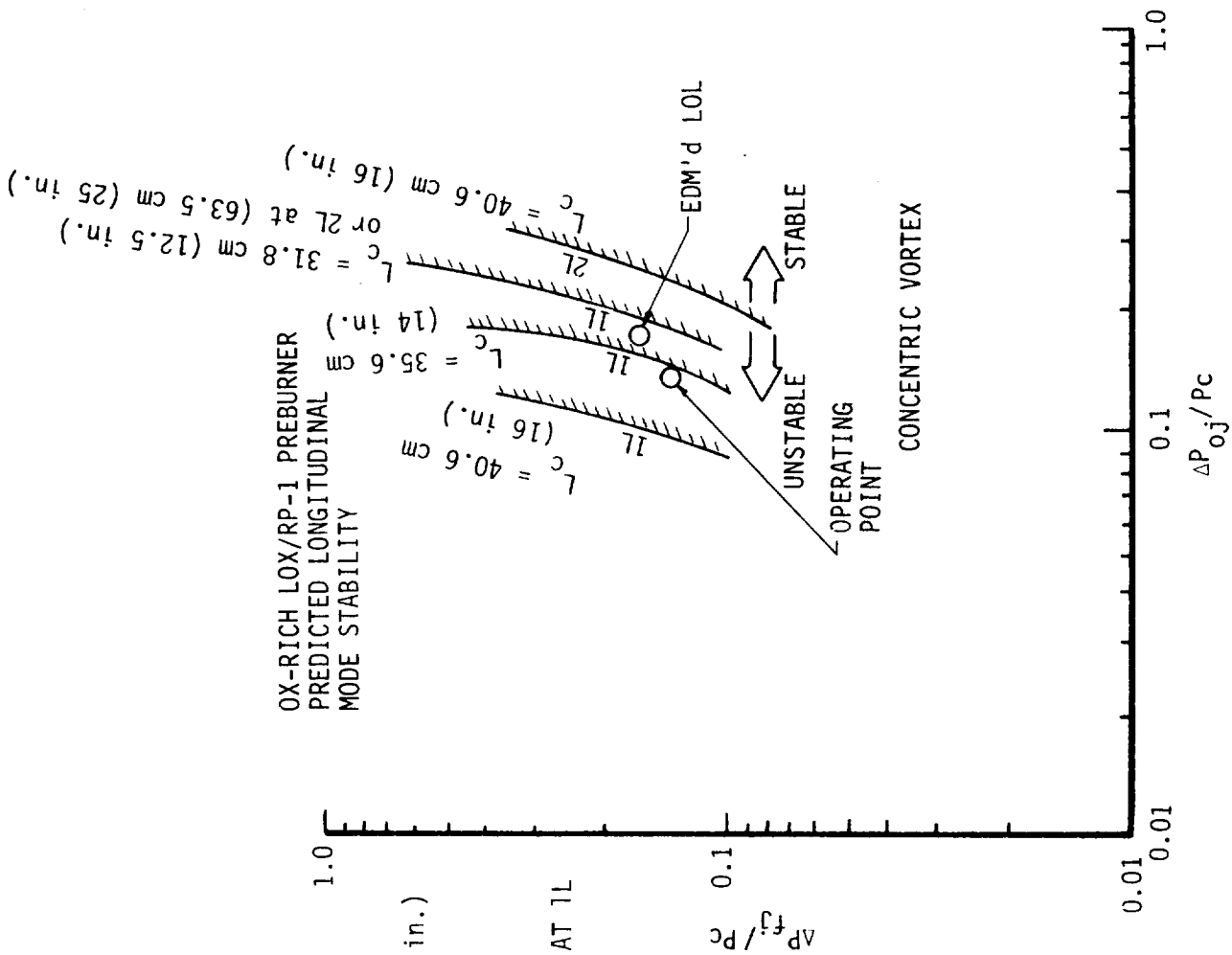
The results of the analyses defining the potential longitudinal instability modes for both injector designs are shown in Figure IV-54. The analyses indicated that a 36.8-cm (14.5-in.) L' chamber length is required to preclude a 1L mode with the concentric vortex injector. The minimum chamber length for the EDM'd LOL pattern was approximately 33 cm (13 in.). A 40.6-cm (16-in.) minimum chamber length was recommended for the initial testing of both injectors.

The analyses also indicated that a potential for 2L instability modes exists at lengths up to 63.5 cm (25 in.) However, without specific test data, it was not possible to predict an optimum test length which avoids both the 1L and 2L modes. Changes in chamber length, along with placement of turbulators acting as longitudinal baffles, are seen to provide the most practical method of establishing a stable configuration.

The potential tangential and radial instability modes, defined in Figure IV-55, would be attenuated by the use of tuned cavities located around the injector periphery. Analyses were conducted to determine the range of cavity sizes required to eliminate 1T, 2T, and 3T and 1R and 2R modes of instability. Cavities up to 2.54 cm (1 in.) deep and 0.76 cm (0.3 in.) wide were found to be effective. A 1.14 cm (0.45 in.) deep by 0.76 cm (0.3 in.) wide cavity was predicted to be optimum. The recommended 12-compartment cavity was 2.54 cm (1 in.) deep by 0.76 cm (0.3 in.) wide. The fabrication of screw-in type cavity tuning blocks of 0.51-, 0.38-, and 0.254-cm (0.20-, 0.15-, and 0.10-in.) height were recommended to allow the cavity size to be adjusted to the optimum value on the basis of experimental results. The 1.14-cm (0.45-in.) depth was recommended for the first test. Figure IV-56 defines the type and location of instrumentation required to properly identify and correct all potential modes of unstable operation.

6. Thermal Analyses

The thermal analyses required include 1) injector face cooling, 2) propellant freezing in the manifolds, and 3) chamber wall cooling. The generalized approach applicable to the first two cooling issues is covered in the fuel-rich design discussion in Section IV.A.8. Other issues, such as protecting the chamber wall with sufficient design margin to accommodate the effect of off-design MR operation, local hot streaks, or unexpected start- or shutdown transients, are covered in this section.



● PREDICTED STABILITY ($L_c = 31.8$ cm (12.5 in.))

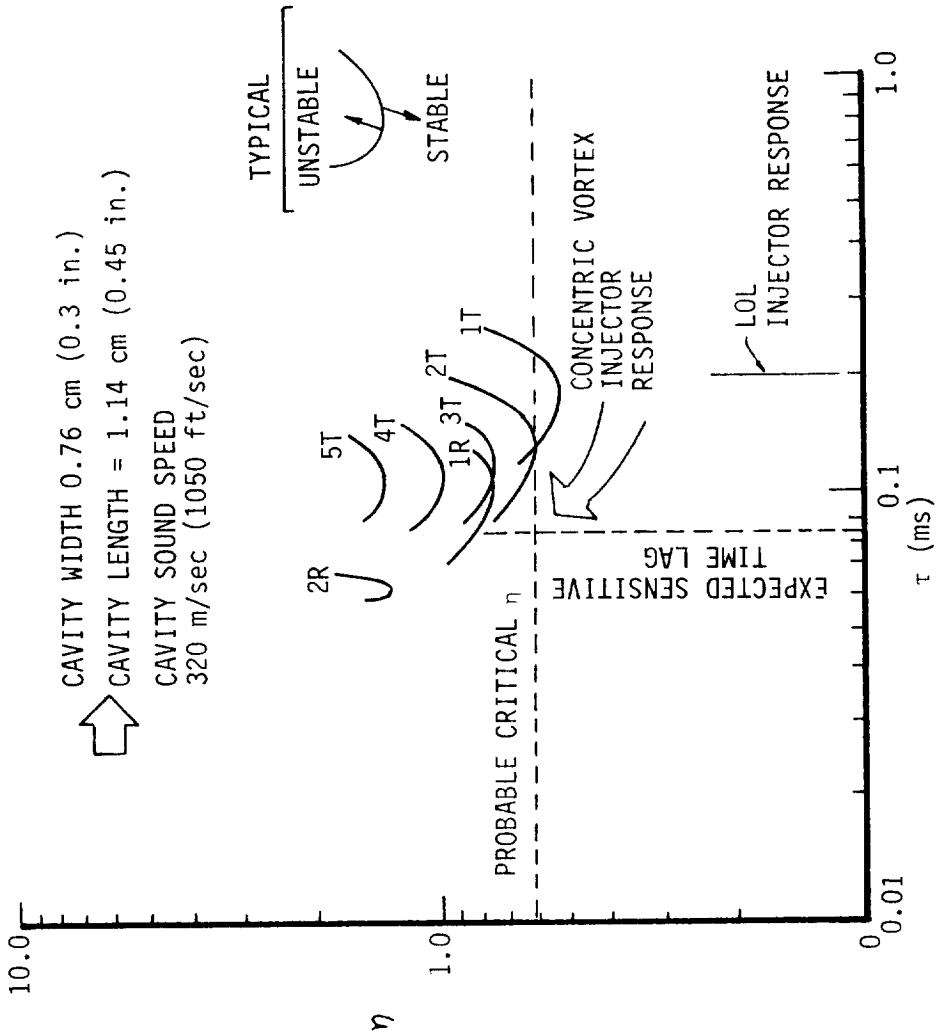
1L UNSTABLE

● RECOMMENDED DESIGN

L_c TO 40.6 cm (16 in.) FOR STABILITY AT 1L

POSSIBLE 2L INSTABILITY FOR ALL L_c 's

Figure IV-54. Oxidizer-Rich LOX/RP-1 Preburner Predicted Longitudinal Instability Modes



- PREDICTED INJECTOR RESPONSE
 - $\tau < 0.6$
 - $t_f = 0.084$ ms Concentric Vortex
 - $t_f = 0.19$ ms LoL
- CAVITY CONFIGURATION FOR FIRST TEST
 - 12 CAVITIES AT 1.14 cm (0.45 in.)
 - 0.76 cm (0.3 in.) wide
- TUNING BLOCKS RECOMMENDED
 - 24 AT 0.51 cm (0.20 in.)
 - 12 AT 0.38 cm (0.15 in.)
 - 12 AT 0.25 cm (0.10 in.)

Figure IV-55. Oxidizer-Rich LOX/RP-1 Preburner Potential Tangential and Radial Instability Modes

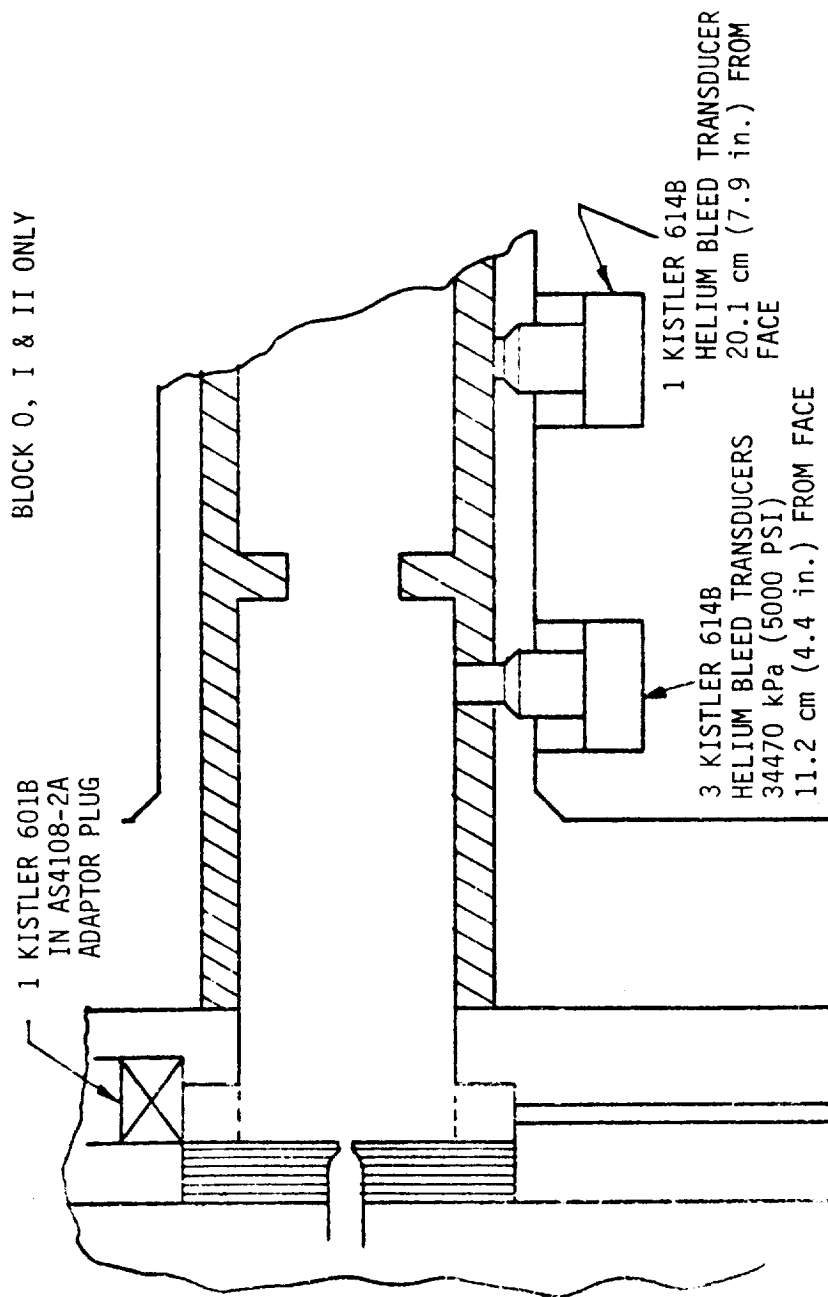


Figure IV-56. Stability-Related Instrumentation

IV, B, Oxidizer-Rich Preburner (cont.)

Various heat sink composite wall designs were analyzed in terms of their ability to withstand local mixture ratios lower (hotter) than the nominal overall value of 40. The selection criterion was to identify the design most capable of withstanding the maximum local mixture ratio for multiple 15-sec firings. The following chamber designs and liners were evaluated.:

- 1.91-cm (0.75-in.) CRES 304 SS wall (no liner)
- 0.76-cm (0.3-in.) thick nickel liner
- 0.76-cm (0.3-in.) thick copper liner
- 0.51-cm (0.2-in.) aluminum oxide ceramic liner
- 0.025-cm (0.010-in.) zirconia sprayed over 304 stainless steel

Figure IV-57 shows the chamber wall surface heating rate of an unlined 304 stainless steel pipe after exposure to local combustion mixture ratios of 10, 18, 30, and 45 for a duration of 15 seconds. The cross plot of surface temperature versus local MR shows that the simple unlined design can withstand a local MR of 25 or higher without exceeding 1256°K (1800°F).

The results of a similar transient heating analysis for other materials are shown in Figure IV-58.

A 0.76-cm (0.3-in.) thick nickel liner could withstand a local MR of 22 if allowed to reach a maximum temperature of 1589°K (2400°F). The high thermal conductivity of copper was of little value in this case because of the low ignition temperature limits of this material in oxygen. The copper liner thickness was not sufficient to provide heat sink capacity for the 15-sec burn duration.

A ceramic liner formed from Al_2O_3 was considered because of its high melting temperature and oxidation resistance (see Figure IV-59). If the surface of the ceramic were limited to 1922°K (3000°F) ($T_{met} = 2256°K$ (3600°F)), local MR values as low as 18 could be accommodated. The interface of the ceramic liner and a stainless steel shell would reach about 1033°K (1400°F) due to the heat conduction through the liner. Although these temperatures were considered acceptable, there was concern about the ceramic withstanding the combined thermal shock and ignition pressure transient.

The use of a 0.025-cm (0.010-in.) coating of zirconia flame-sprayed over a 1.91-cm (0.75-in.) stainless steel liner was also evaluated. This was found to be approximately equivalent to the thicker alumina liner and was considered less likely to crack.

CHAMBER INSIDE SURFACE TEMPERATURE
VERSUS TIME

1.905-cm (0.75-in.) STAINLESS STEEL WALL

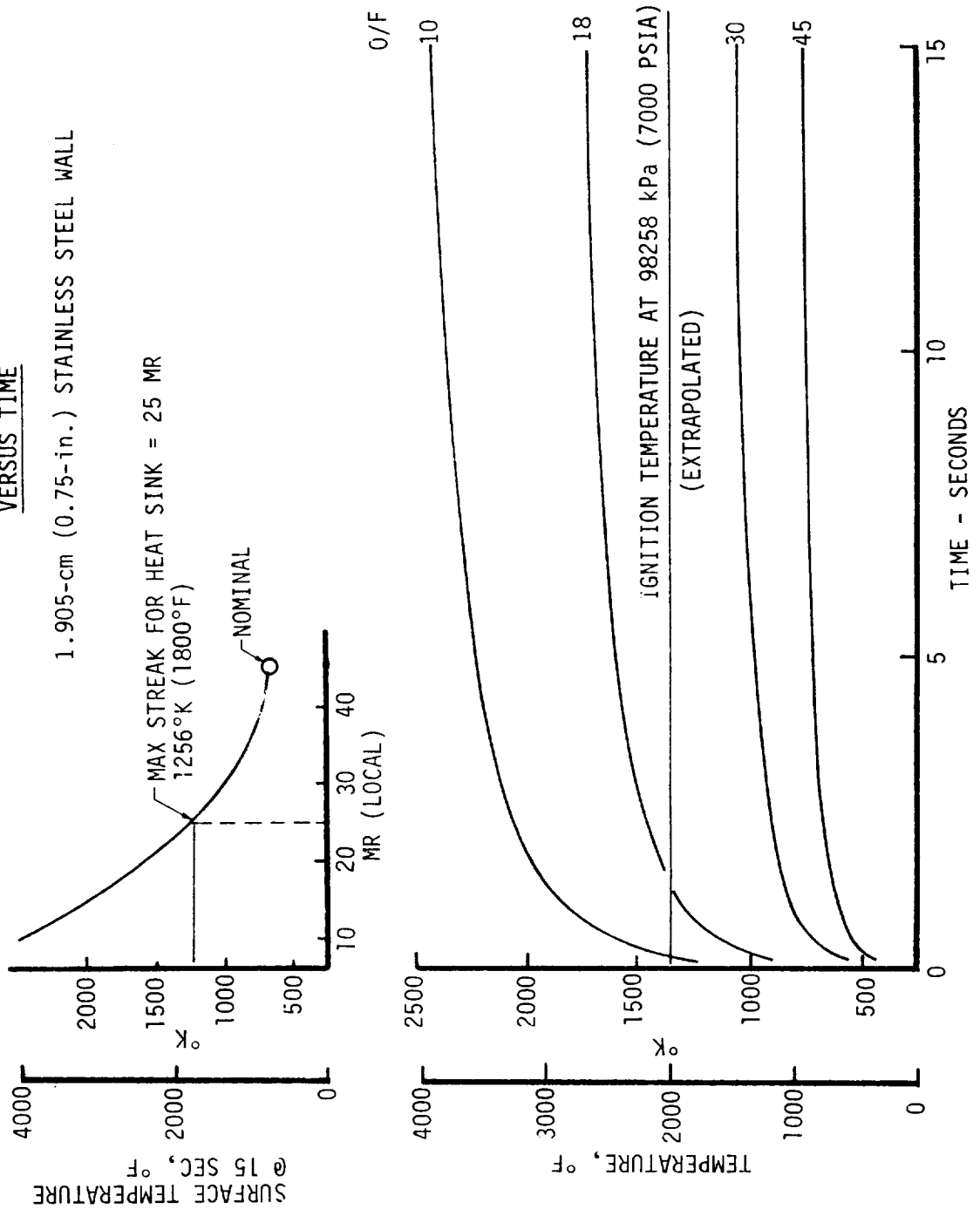


Figure IV-57. Chamber Wall Surface Heating Rate of 304 Stainless Steel Pipe

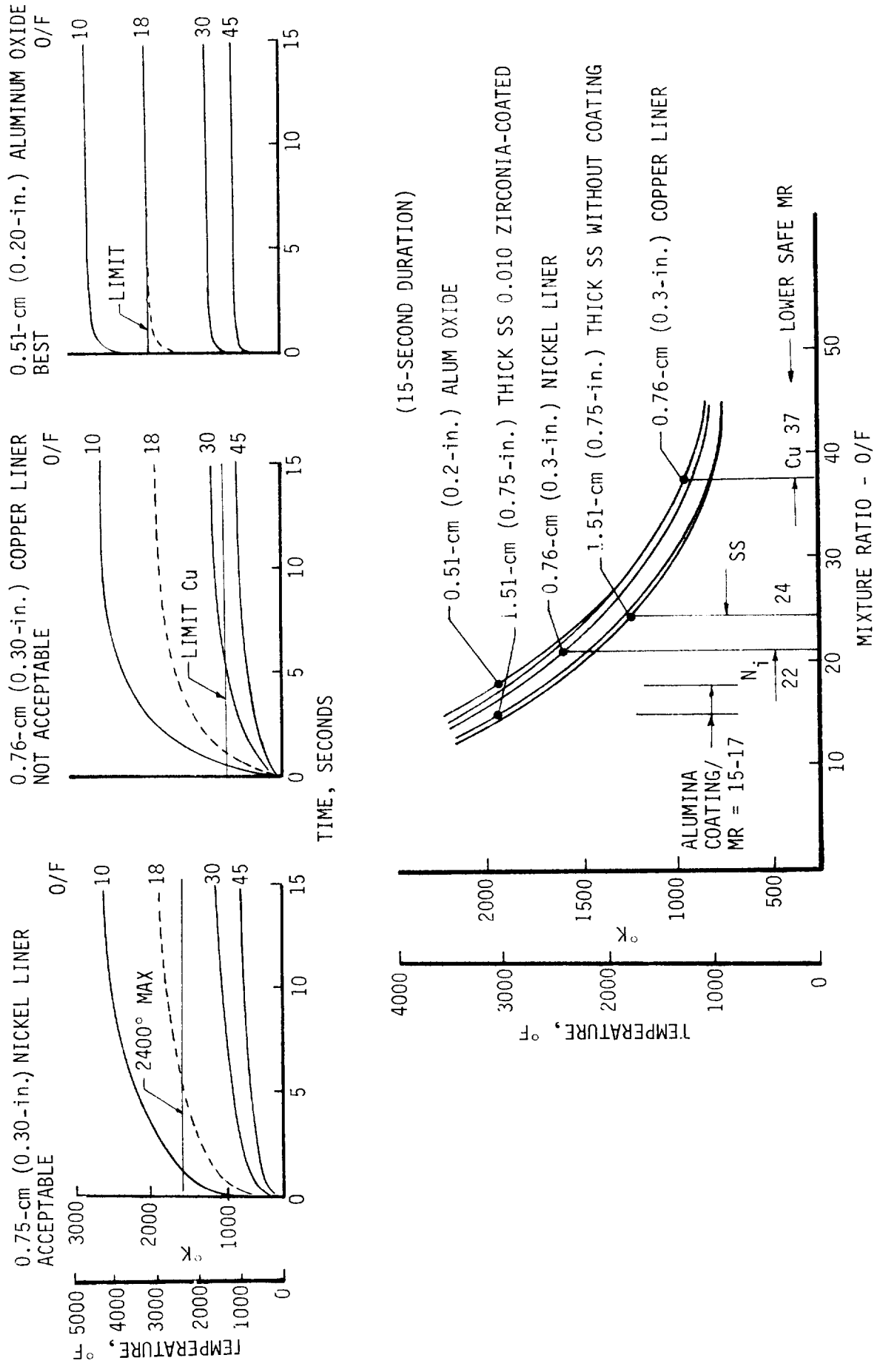


Figure IV-58. Transient Heating Analyses for Nickel, Copper, and Aluminum Oxide

CHAMBER WALL TEMPERATURE

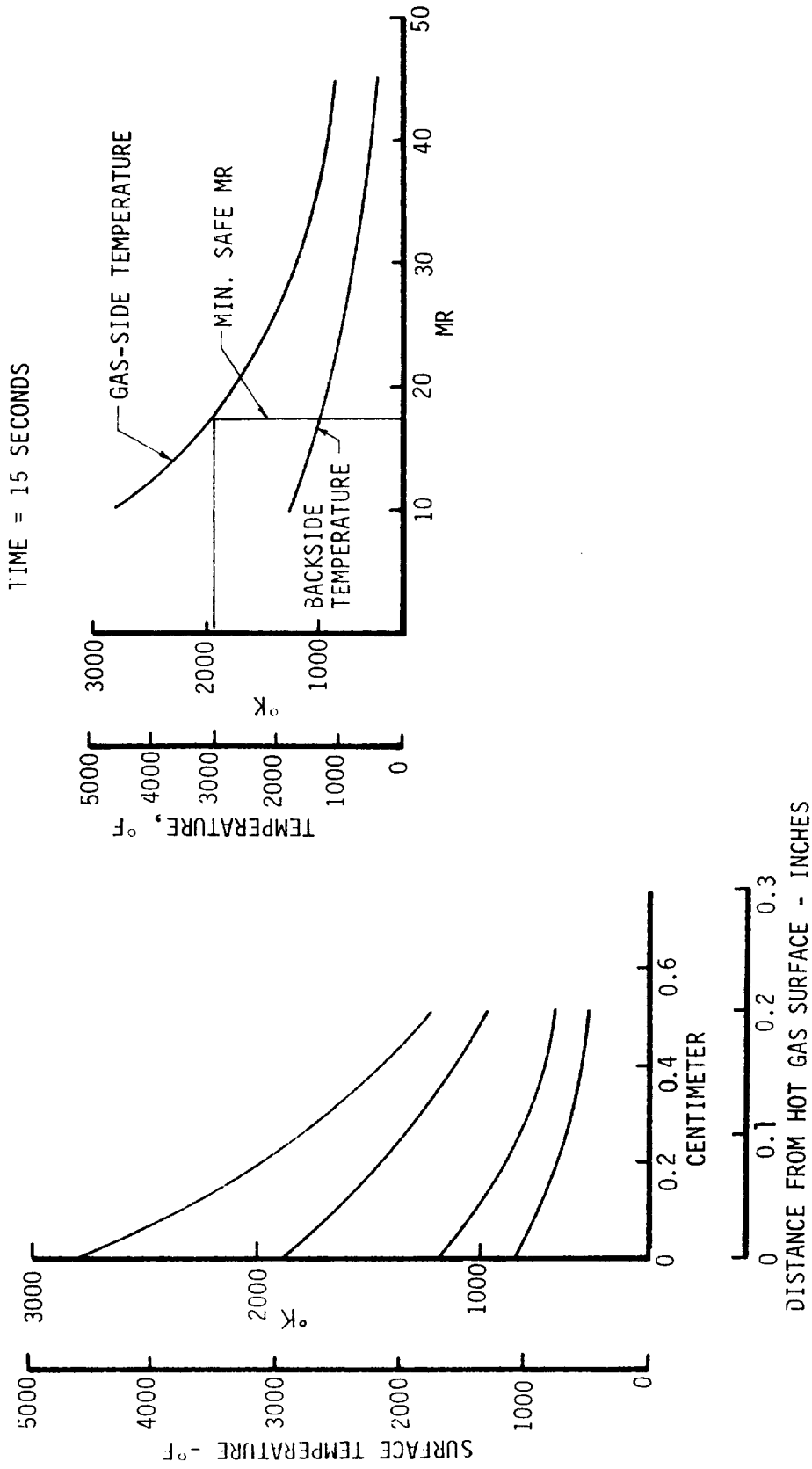


Figure IV-59. Wall Temperature Profiles for an Al_2O_3 -Lined Steel Chamber

IV, B, Oxidizer-Rich Preburner (cont.)

The replaceable liner concept was selected to protect the CRES 304 pressure vessel fabricated from 15.2-cm (6-in.) Schedule double-extra strong pipe. A Nickel 200 liner was recommended because it provided the best protection without dependency on a ceramic coating which might crack or spall. The higher conductivity of nickel over stainless steel (3:1) also provided better heat averaging capabilities to preclude local hot areas.

As an added protective measure, it was recommended that a 0.025-cm (0.01-in.) thick zirconia coating be deposited on the inside diameter of the nickel liner. ZrO_2 has an indicated maximum use temperature of 2756°K (4500°F) in an oxidizing atmosphere. A brief investigation revealed that Metco coating 202 NS (80% zirconia, 20% ytterbium oxide stabilized) was a good candidate material. This coating should also be applied to the turbulators, turbine simulator, and throat.

During the fabrication phase, it was determined that the availability of Nickel 200 pipe was limited to a wall thickness of about 0.5 cm (0.2 in.). This was not sufficient to fill the gap between the 15.2-cm (6-in.) pipe pressure vessel and 12.7-cm (5-in.) pipe liner. The gap was filled by flame spraying 0.5 cm (0.2 in.) of copper over the outside diameter of the nickel pipe. Figure III-22 shows the liner and chamber pressure vessel. The copper provides an additional advantage of preventing local hot zones from developing in the nickel.

7. Injector Pattern Selection

a. Objectives

The objectives of this activity were to evaluate candidate injector element types and element packaging for oxidizer-rich operation and to select the element type and quantity required to achieve the following technical goals:

- 1) Uniform gas temperature $\pm 28^\circ\text{K}$ ($\pm 50^\circ\text{F}$) at the turbine inlet
- 2) Stable combustion
- 3) Safe operation of the uncooled combustor (i.e., avoidance of metal ignition or melting at operating pressures up to 17235 kPa (2500 psia))

b. Design Requirements

The requirements which influence the element type selection for the oxidizer-rich injector are generally the same as those defined in Section IV.B.9 for the fuel-rich design, with the following exceptions:

IV, B, Oxidizer-Rich Preburner (cont.)

- 1) Coking and carbon deposition are not considered a problem
- 2) Protection of the chamber wall from fuel impingement is now more critical
- 3) Protection of the injector face from hot-gas recirculation is more critical than in the fuel-rich design

A comparison of the mixing efficiencies (E_{mf}) required of the fuel- and oxidizer-rich designs for a combustion gas temperature uniformity of $+28^{\circ}\text{K}$ ($+50^{\circ}\text{F}$) is shown in Figure IV-60 to be 93 and 97%, respectively. The allowable mixing inefficiency of the oxidizer-rich design is less than half that of the fuel design for the same allowable temperature variation in the gas stream.

As a mixing efficiency of 97% is in excess of the capabilities of known injector designs, the use of a mechanical mixing device to supplement the injector is considered to be an integral part of the injector design criteria.

c. Element Selection

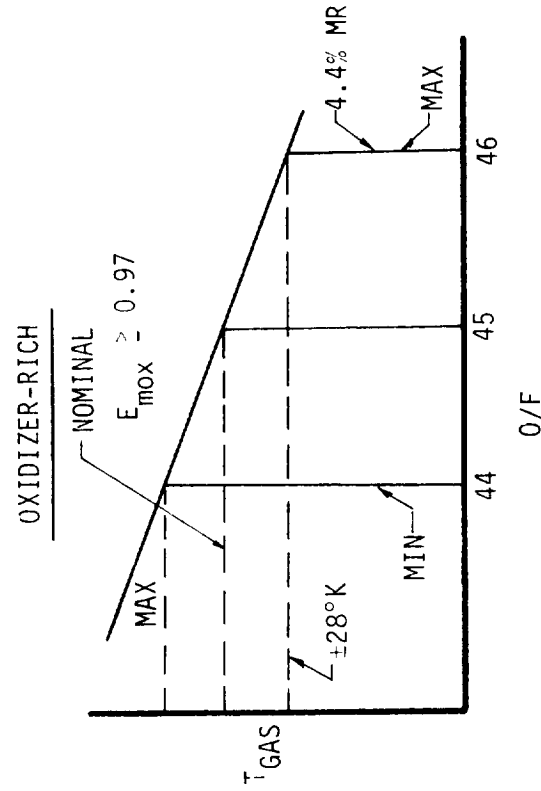
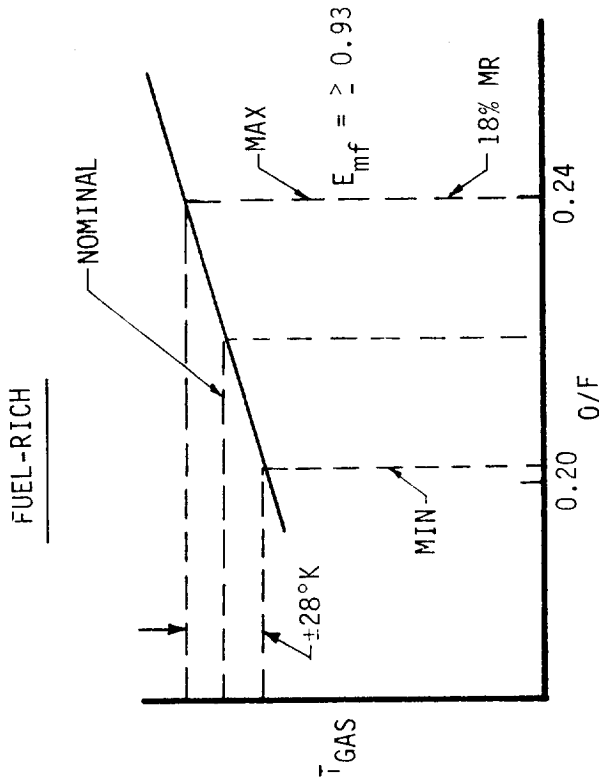
Candidate element types for propellant atomization fall into the following three categories:

- Like-on-Like (LOL) impingement configurations
- Unlike impingement configurations
- Self-atomizing elements (atomization is accomplished without stream impingement)

These are shown schematically in Figure IV-61.

The LOL elements are normally doublet-types where two jets of equal diameter impinge at a selected angle to produce a highly atomized spray fan. Doublet elements can be formed by drilling or electrical discharge machining (EDM) processes. The EDM process provides the advantage of eliminating burrs on the inlet of the orifices and thus provides more uniform jets and flow distribution.

Unlike impingement elements include doublets, triplets (2 on 1), reverse triplets, and pentads (4 on 1). Use of the unlike doublet was rejected because of the resultant large difference in propellant flow-rates. A small-stream diameter impinging on a large-stream diameter does not



PREBURNER DESIGN AND OPERATING REQUIREMENT:

	O/F	T _{NOMINAL}
FUEL-RICH	0.22	867°K (1100°F*)
OXIDIZER-RICH	45	922°K (1200°F*)
PERFORMANCE	98% ERE	
T _{GAS}	±28°K (±50°F)	

*ADVANCED HIGH-PRESSURE ENGINE STUDY FOR MIXED-MODE VEHICLE APPLICATIONS, CONTRACT NAS 3-19727, NASA CR-135141.

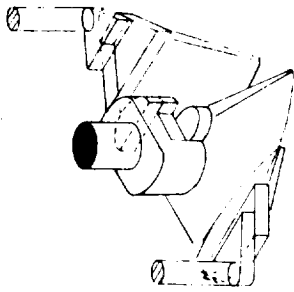
CONCLUSION: UNIFORM MANIFOLD INJECTION DISTRIBUTION IS MANDATORY. CHAMBER FILM-COOLING IS TOTALLY UNACCEPTABLE

Figure IV-60. Comparison of Required Mixing Efficiencies of Fuel-Rich and Oxidizer-Rich Injector

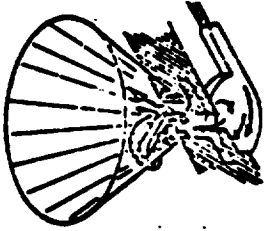
PROPELLANT INLET

 RICH

 LEAN



PRE-ATOMIZED TRIPLET

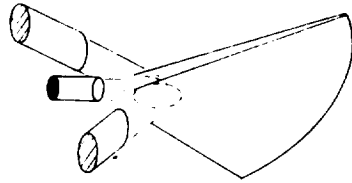


VORTEX

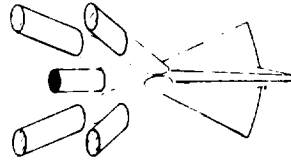
CANDIDATE ELEMENTS

● LIKE ON LIKE DOUBLET

● V-DOUBLET



TRIPLET



PENTAD

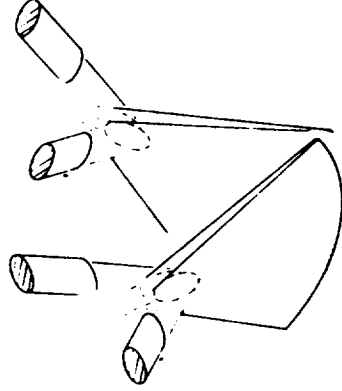


Figure IV-61. Conceptual Drawing of Element Candidates

IV, B, Oxidizer-Rich Preburner (cont.)

provide good atomization or mixing. The triplet and pentad patterns were also rejected because of the possibility that the large volume of liquid oxygen would freeze the small fuel flow volume before the small fuel stream could be atomized.

Self-atomizing elements include splash-plate and vortex types which allow fine sprays to be created without stream impingement of two liquid jets. Since a single stream can be employed to generate a spray, more sprays and better flow distribution can be provided for a given minimum orifice diameter. A showerhead element is a special type of self-atomizing design.

A self-atomizing concentric vortex element was selected as the primary design because it provides two very important advantages. First, it provides complete shielding of the injector face from the combustion products; secondly, it is predicted to have the most uniform mixture ratio (and thus temperature) distribution of all the candidate elements.

Since the concentric vortex element represents a relatively new design concept, the detail design and spray fan optimizations were accomplished through a combination of analysis and uni-element cold-flow verification. The details are discussed in Section VI.A.

A LOL element was selected as the alternate approach to meeting the program goals. Although the concentric vortex element is considered to be the best design, lack of a data base for its fabrication and performance characteristics dictated the decision to proceed with the optimization of the second-choice LOL pattern as well.

The LOL pattern was initially configured to surround the small fan produced by the minor propellant elements with two fans produced by the major propellant, as shown schematically in Figure IV-62. This was designed to reproduce an encapsulation of the fuel combustion source feature of the concentric vortex element with the oxygen. During this phase of the analysis, it was found that better MR distribution could be achieved if the minor element doublets were split into single showerhead elements and separated, as shown in the figure, thus providing twice as many sources of fuel injection without reducing the diameter. The use of a showerhead element also moved the flame front away from the injector face, thus improving face cooling. The following paragraph indicates that the loss of atomization capability with a showerhead element at high pressure is small.

The injection of fuel into high-density (high-pressure) combustion gases was modeled on the data of References 5 through 9. These data indicate that the atomization of a single high-velocity showerhead

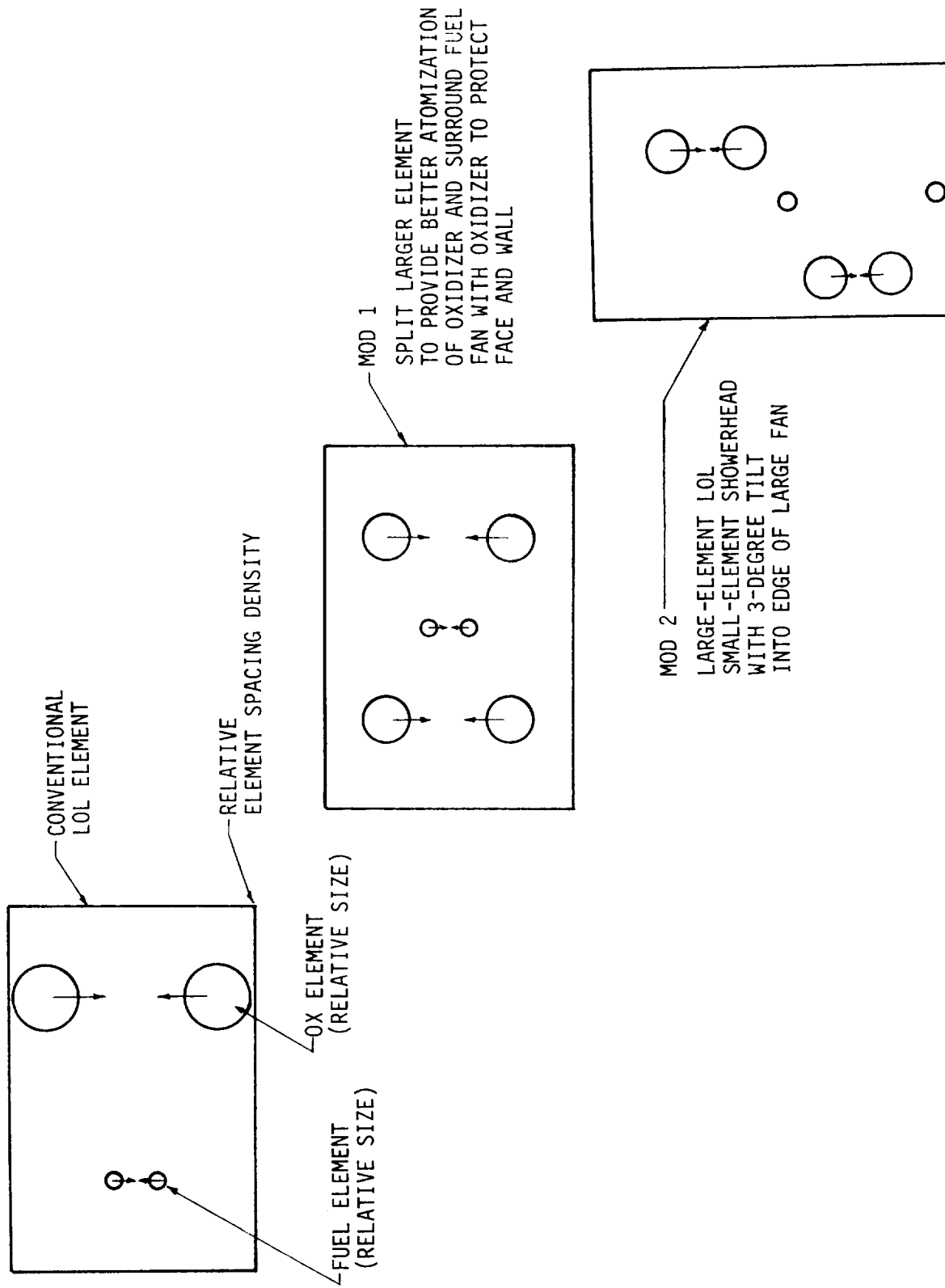


Figure IV-62. Evolution of Oxidizer-Rich LOL Element Pattern for High-Pressure Preburner Application

IV, B, Oxidizer-Rich Preburner (cont.)

element jet improves considerably when it is injected into a high-pressure gas. Thus the normally poor performance characteristics of a single showerhead element improve as the density of the downstream gas is increased. The density of the combustion products at 15365 kPa (2200 psia) and 922°K (1200°F) was sufficiently high to make the showerhead and like doublet-type element streams break up at nearly the same rate (see Figure IV-63).

The data developed in Figure IV-63 was analytically developed by combining the empirical works of Priem (Ref. 9) and Ingebo (Ref. 5). Ingebo provided a series of property exponents which infers that the mean showerhead droplet radius is proportional to the chamber gas density to the $-.3$ power. When Priem's showerhead drop-size correlation (Ref. 9) is normalized to a density ratio of unity ($\rho_{\text{gas ratio}} = 1$), and the Ingebo correlation is applied, it results in the curves shown in Figure IV-63. This combination of existing data has resulted in what is believed to be an improved showerhead element droplet-size prediction method for high-pressure engines, since it accounts for the density of the gas in the combustion chamber. This is especially critical for high-pressure preburners because the low combustion temperatures result in much higher than normal gas density. The combustion gas density of the preburners is approximately 40 times greater than the density for the normal pressure-fed engines and for the data used to develop the formulation of Reference 9.

Details of selected pattern designs, orifice diameters, and stream characteristics are defined in Tables IV-III, -IV, and -V.

Figures IV-64 and -65 define the element pattern layout and manifolding employed for the two selected designs.

EFFECT OF GAS DENSITY
ON DROP SIZE USING INGEBO
RELATIONSHIP: $r_m \approx \rho^{-.3}$

gas ratio

WHERE: $\rho_{\text{gas ratio}} = \rho_{\text{gas}} / \rho_{\text{Priem Ref. gas}}$

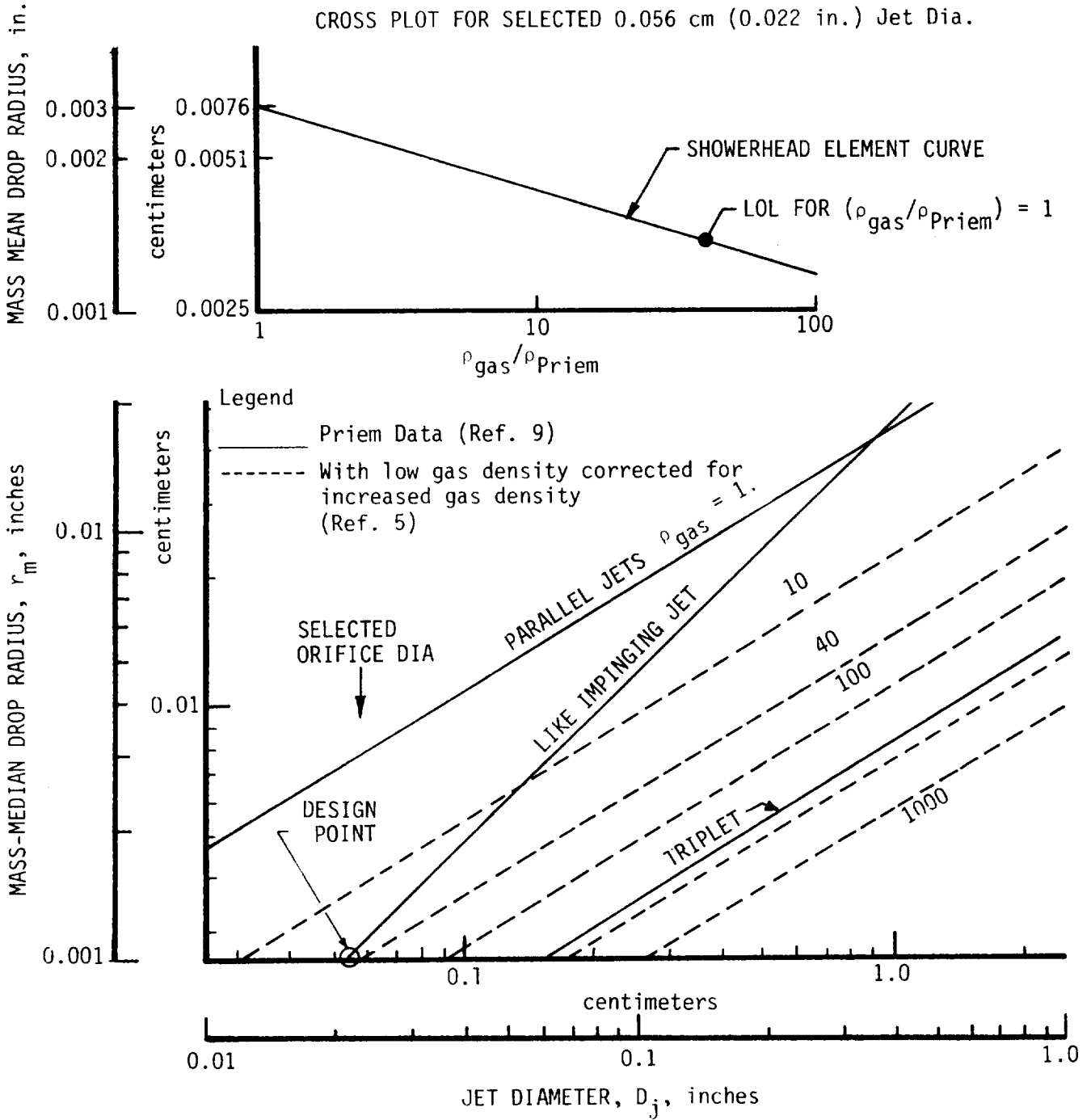


Figure IV-63. Effect of Gas Density on Drop Size

TABLE IV-III. - LOL INJECTOR ELEMENT PARAMETERS

	<u>OXIDIZER-RICH</u>
Chamber Diameter, cm (in.)	10.31 (4.06)
Throat Diameter, cm (in.)	5.029 (1.98) without turbine simulator; 6.375 (2.510) with turbine simulator
Geometric Contraction Ratio $\left(\frac{D_C}{D_T}\right)^2$	4.22 without turbine simulator; 2.6 with turbine simulator
Chamber Length, cm (in.)	61.0 (24.0)
Chamber Pressure Upstream of Turbine, kPa (psia)	15,167 (2200)
Mixture Ratio	40.9

	<u>FUEL ELEMENTS</u>	<u>OXIDIZER ELEMENTS</u>	
		<u>INNER ROW ONLY</u>	
Orifice Diameter, cm (in.)	0.056 (0.022)	0.040 (0.016)	0.229 (0.090)
Orifice L/D	4.2		5.5
Orifice Chamfer	None		45°
Orifice Cd	0.085		0.085
Orifice Type	Showerhead		LOL
Orifice Number	60	10	140
Pressure Drop, kPa (psid)	2758 (400)		2758 (400)
Flowrate, kg/sec (lb/sec)	0.94 (2.08)		38.56 (85.0)
Injection Velocity, m/sec (ft/sec)	88.4 (290)		72.2 (237)
Tilt Angle, degree	2°		-

TABLE IV-IV. - LOL PROPELLANT STREAM CHARACTERISTICS

PREBURNER		OXIDIZER-RICH		
ELEMENT	LOL	Showerhead		
PROPELLANT	LOX	RP-1		
Temperature, K° (°F)	100° (-280°)	294° (70°)	367° (200°)	422° (300°)
Fan Length, cm (in.)	7.85 3.09	3.73 1.47	4.19 1.65	4.45 1.75
Injection Velocity, m/sec (ft/sec)	73.2 (240)	78.3 (257)	83.5 (274)	88.3 (290)
Pressure Drop, kPa (psid)	2289 (419)	2247 (355)	2613 (379)	2758 (400)
ALRC Fan Model Drop Radius, cm (in.)	0.0147 (0.0042)	0.0099 (0.0039)	0.0089 (0.0035)	0.0084 (0.0033)
Combustion Time Lag, ms	1.24	0.57	0.42	0.36

CONCENTRIC VORTEX CHARACTERISTICS

PREBURNER		OXIDIZER-RICH	
PROPELLANT	LOX	RP-1	
Cone Angle, θ (degree)	60°	20° 12°*	
Orifice Diameter, cm (in.)	0.472 (0.186)	0.056 (0.022)	
Fan Length, cm (in.)	3.266 (1.286)	0.584 (0.230)	
Distance to 20% Vaporization, cm (in.)	0.015 (0.006)	0.419 (0.165)	
Drop Radius, cm (in.)	0.0056 (0.0022)	0.0023 (0.0009)	
Combustion Time Lag, ms	0.54	0.14	
Pressure Drop, kPa (psid)	2068 (300)	2068 (300)	
Velocity, m/sec (ft/sec)	61.0 (200)	71.6 (235)	
*Cold-flow Test Data			

TABLE IV-V. - PROPELLANT VAPORIZATION EFFICIENCIES VS FUEL TEMPERATURE

PREBURNER		OXIDIZER-RICH		
ELEMENT	LOL	Showerhead		
PROPELLANT	LOX	RP-1		
Temperature, °K (°F)	100° (-280°)	294° (70°)	367° (200°)	422° (300°)
Chamber Length, cm (in.)	30.5 (12)	30.5 (12)	30.5 (12)	30.5 (12)
η_{vap}	0.970	0.824	0.932	0.960
η_{tot}	N/A	0.966	0.969	0.970
$\eta_{c*} = \eta_{tot} * \eta_{lean}$	N/A	0.795	0.902	0.931
Chamber Length, cm (in.)	61 (24)	61 (24)	61 (24)	61 (24)
η_{vap}	0.991	0.934	0.986	0.990
η_{tot}	N/A	0.989	0.991	0.991
$\eta_{c*} = \eta_{tot} * \eta_{lean}$	N/A	0.924	0.977	0.981

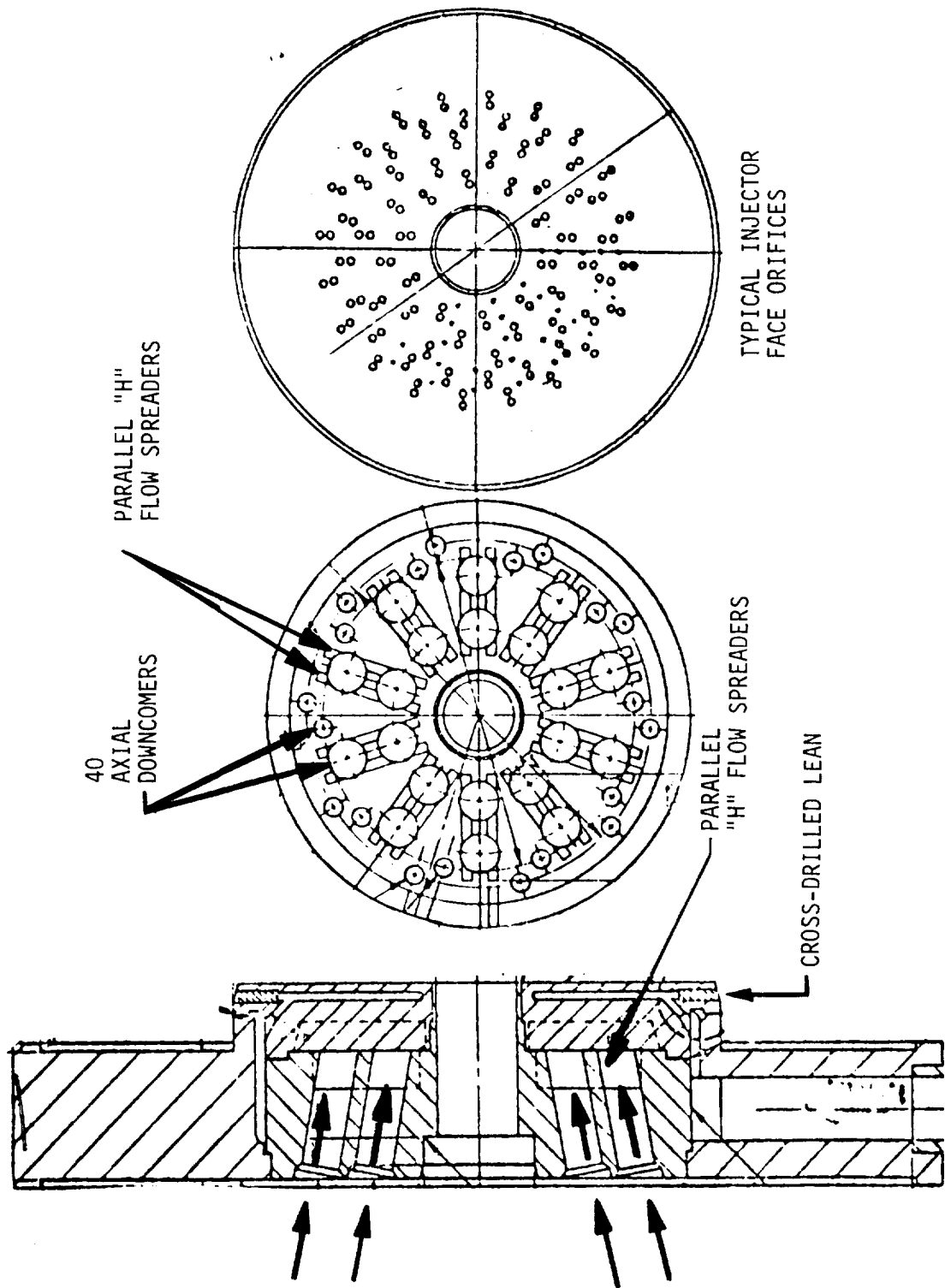


Figure IV-64. Manifold & Element Pattern Layout of Selected EDM'd Design

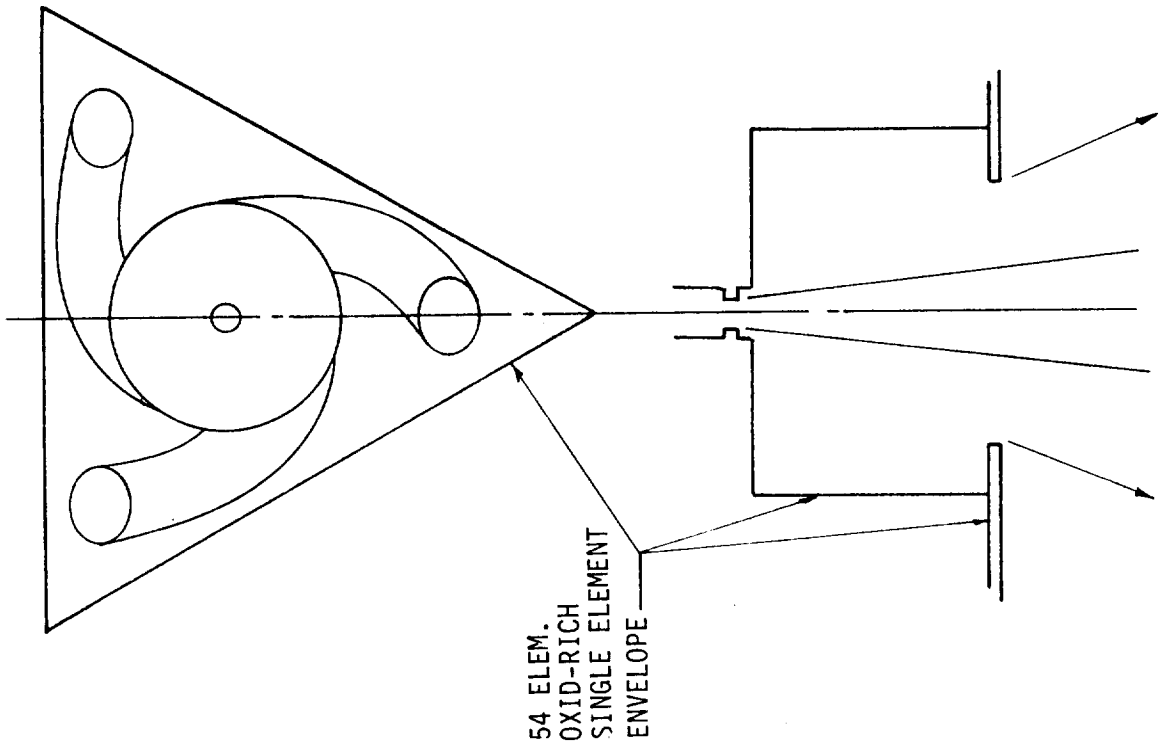
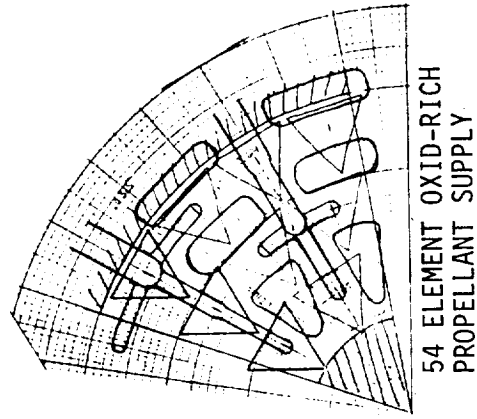
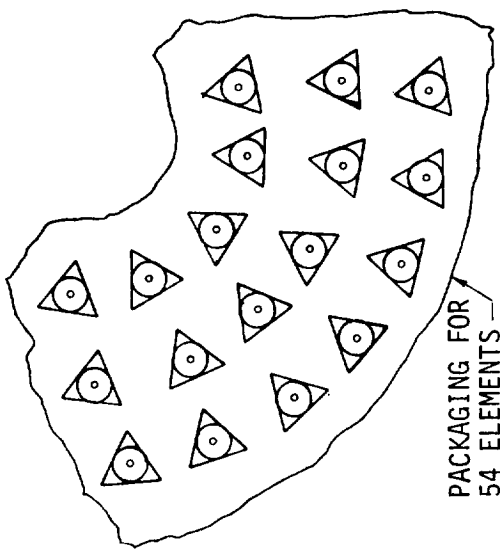


Figure IV-65. Coaxial Vortex Injector Element Configuration

V. HARDWARE FABRICATION

A. PROCEDURES

The fabrication of the designs shown in Section III of this report employed state-of-the-art manufacturing methods. Most of the parts fabricated were assembled from the standard forged slip-on and blind flanges shown in Figure V-1 and from commercial 12.7- and 15.2-cm (5- and 6-in.) diameter Schedule double extra strong pipe. CRES 304 was used for all parts except the turbine simulator blades and the injector faceplates to facilitate electron-beam welding.

The blind flanges were utilized in the fabrication of manifolds, resonators, throats, and the rake assembly. The slip-on flanges were utilized for the chamber spools and injector manifolds. These were match-machined to fit over the ends of the pipes for electron-beam welding. The end-surfaces and inside diameter were machined following the welding to provide the required diameter, alignment, and sealing surfaces.

As the majority of the manufacturing operations were completed without difficulty, further general discussion is not warranted. Table V-I and Figure III-4 define the items fabricated or purchased for this program. Detailed documentation of several nonconforming dimensions and the resulting dispositions is provided in Section V.C. (Product Assurance).

B. PROBLEMS

Problem areas did arise in the braze assembly of all four injectors. These problems, common to both the platelet and EDM'd designs, resulted during the hydrogen or vacuum brazing operations required for the final faceplate assemblies after all of the high-cost machining operations had been completed.

Although all brazing problems were associated with the joining of two thick flat plates, each of the four injectors had somewhat unique difficulties resulting from the differing combination of materials and nature of the joint design. There were no problems associated with the diffusion bonding of the platelet stack, only with the subsequent braze to join the bonded stack to the injector manifold body.

Fuel-Rich EDM'd Injector

As shown schematically in Figure V-2, the fuel-rich EDM'd injector developed two cracks during a hydrogen braze operation. These cracks were located directly over the thin wall area of the cross-drilled holes. The braze alloy employed was Nicoro (.35 Au, .62 Cu, .3 Ni) at $\approx 1303^{\circ}\text{K}$ (1885°F). One crack was fully repaired by EB-welding using filler wire, and the other was partially repaired by the same procedure. One of the welds can be observed in the photo of Figure V-2. An attempt to repair the remainder of the second crack by a hydrogen braze cycle utilizing Nioro (.82 Au, .18 Ni)

900 lb. BLIND FLANGES*

ASA B16.5-1953

ASTM A105—GRADE II

NOMINAL PIPE SIZE	OUTSIDE DIAM. OF FLANGE O	THICK. OF FLANGE Q*	DIAMETER OF RAISED FACE R	NUMBER OF HOLES	DIAM. OF BOLTS*	DRILLING TEMPLATE					APPROX. WEIGHT IN POUNDS	LIST PRICE
						DIAM. OF BOLT CIRCLE	1/4" RAISED FACE	LENGTH OF STUD BOLTS*		RING JOINT		
							MALE & FEMALE AND TONGUE & GROOVE					
3	9 1/2	1 1/2	5	8	7/8	7 1/2	5 3/4	5 1/2	6	32	PRICES ON APPLI-	
4	11 1/2	1 3/4	6 3/16	8	1 1/8	9 1/4	6 3/4	6 1/2	7	54		
5	13 3/4	2	7 5/16	8	1 1/4	11	7 1/2	7 1/4	7 3/4	87		
6	15	2 3/4	8 1/2	19	1 1/2	13 1/2	8 1/2	8 1/4	9	110		

900 lb. BLIND FLANGES

Part No. 94



All dimensions given in inches. Flanges are furnished faced, drilled, and spot faced or back faced. Standard Flange Facings—pages 160-161

- * The 1/4" raised face is not included in Thickness "Q."
- * Bolt holes are 1/8" larger than bolt diameters.
- * These lengths include thickness of two nuts but not height of crown.
- * These dimensions are the same as for 1500-lb. flanges.
- * When ordering specify nominal pipe size or "O" dimension in inches indicating which is being used, pressure rating of flange and part number, Ring Type Joint details—pages 162-164. Dimensional Tolerances—page 240. Pressure-Temperature Ratings—pages 263-268.

For information on stainless steel, alloy steel and non-ferrous metal flanges, refer to pages 225-236. Material Specifications—page 243.

900 lb. SLIP-ON FLANGES

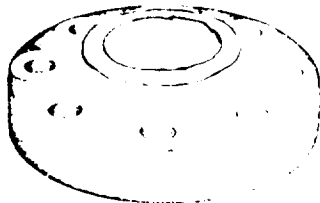
ASA B16.5-1953

ASTM A105—GRADE II

NOMINAL PIPE SIZE	OUTSIDE DIAM. OF FLANGE O	THICK. OF FLANGE Q*	DIAM. OF RAISED FACE R	DIAM. OF HUB AT BASE X	LENGTH THRU HUB Y*	DIAM. OF GROOVE W	DRILLING TEMPLATE					APPROX. WEIGHT IN POUNDS	LIST PRICE	
							NO. OF HOLES	DIAM. OF BOLTS*	DIAM. OF BOLT CIRCLE	1/4" RAISED FACE	LENGTH OF STUD BOLTS*			RING JOINT
							MALE & FEMALE AND TONGUE & GROOVE							
3	9 1/2	1 1/2	5	5	2 1/8	3.57	8	7/8	7 1/2	5 3/4	5 1/2	6	31	PRICES ON APPLI-
4	11 1/2	1 3/4	6 3/16	6 1/4	2 3/4	4.57	8	1 1/8	9 1/4	6 3/4	6 1/2	7	53	
5	13 3/4	2	7 5/16	7 1/2	3 1/8	5.66	8	1 1/4	11	7 1/2	7 1/4	7 3/4	83	

900 lb. SLIP-ON FLANGES

Part No. 91



All dimensions given in inches. Flanges are furnished bored, faced, drilled, and spot faced or back faced. Standard Flange Facings—pages 160-161.

- * The 1/4" raised face is not included in Thickness "Q" nor Length "Y."
- * Bolt holes are 1/8" larger than bolt diameters.
- * These lengths include thickness of two nuts but not height of crown.
- * These dimensions are the same as for 1500-lb. flanges.
- * Ring Type Joint details—pages 162-164. Dimensional Tolerances—page 240. Pressure-Temperature Ratings—pages 263-268.

For information on stainless steel, alloy steel and non-ferrous metal flanges, refer to pages 225-236. Material Specifications—page 243.

Figure V-1. Standard Flange Sizes

ORIGINAL PAGE IS OF POOR QUALITY

TABLE V-I. - PREBURNER AEROJET PARTS LIST AND MAJOR PURCHASED ITEMS

	Item No.	PN	Quantity
Spark Plug		115090	10
Housing			
Igniter	24	1191522	2
Injector Manifold	20	1191404	2
Injector Faceplate, Fuel-Rich Vortex	17	1191403-19 -39	1
Fuel-Rich EDM		1193105-19	1
Oxid-Rich Vortex	18	1191403-9 -29	1
Oxid-Rich EDM		1193105-9	1
Resonator Assembly	8	1191402	
Flange		1191402-3	2
Ring		1191402-4	4
Blocks		-12,-13,-14 -17 -5,-6,-7, -16	10 each 2 each
Lined Chamber, Long	4	1191401-29	1
Lined Chamber, Short	4	1191401-9	1
Unlined Chamber, Long	5	1191401-39	1
Unlined Chamber, Short	5	1191401-19	1
Injector Simulator Flange	14	1191402-8	1
Fuel-Rich Plate		1191402-10	1
Ox-Rich Plate		1191402-11	1
Blank Ring		1191402-15	1
Turbine Simulator Assy, Oxid-Rich	23	1191521-9	1 Body 2 Blade
Turbine Sim. Assy, Fuel-Rich	22	1191521-19	Sets
Throats, Fuel- and Oxid-Rich	6 7	1191402-1 1191402-2	1 each
Chamber Liners, Nickel		1191401-3	
Chamber Liners, Ceramic		1191401-6	
Chamber Turbulators		1191401-8	
Tooling, Proof Pressure End Plate		1191401-18	1
Cold Flow			
Platens and Pins			1
Nose Guide			1
Guide Pins Assembly			



Figure V-2. Fuel-Rich EDM'd Injector After Braze Repair with Reinforcing Ring

V, B, Problems (cont.)

at $\approx 1273^{\circ}\text{K}$ (1831°F) was successful; however, the second heat cycle resulted in additional crack indications over the remaining 18 cross-drilled holes. One of these was found to leak when pressurized with GN_2 ; the others did not.

A 0.05-cm (0.020-in.) thick stainless steel reinforcing ring was fabricated (as shown in Figure V-2) to provide a seal and eliminate the thin wall condition. A 0.0025 cm (0.001 in.) sheet of braze foil was also cut the same size as the reinforcing ring. This ring was brazed to the face, utilizing the same alloy and temperature as in the second braze cycle; however, the third cycle was conducted under vacuum conditions. This repair was found to provide a structurally sound leak-tight condition, and no further sign of crack development was noted afterwards.

Oxidizer-Rich EDM'd Injector

The braze assembly of the Ni face to the 304 manifold core did not provide the desired joint quality due to relative thermal growth of the nickel and stainless plates. This condition was corrected by modifying the subsequent electron-beam weld schedules. Section V.C. covers the problem and the repair in detail.

Fuel-Rich and Oxidizer-Rich Concentric Vortex Injectors

A braze problem was encountered in the joining of the pre-diffusion-bonded platelet stack to the machined body, as shown in Figure V-3. The hydrogen braze process employed 0.005-cm (0.002-in.) thick copper foil placed between the two subassemblies and heated to $\approx 1394^{\circ}\text{K}$ ($\approx 2050^{\circ}\text{F}$). The braze parameters employed resulted in six orifices in the fuel-rich and thirteen orifices in the oxidizer-rich assembly being plugged up. In both cases, the obstruction was confined to the minor propellant flow circuit where the orifice diameters were between 0.18 and 0.32 cm (0.070 and 0.125 in.). The plugged orifices were discovered during the first pattern check. The copper was successfully removed with a hot nitric acid bath; however, subsequent leak tests indicated that the acid had also removed a significant amount of the material at the braze interface. A small amount of interpropellant leakage indicated that the structural integrity of the bond was now questionable, thus a decision was made to remove the 2.057-cm (0.810-in.) thick platelet stack. This was accomplished with a band saw. The sawing operation required that four 0.051-cm (0.020-in.) thick platelets of the 43-piece stack be destroyed. A photograph of the two parts of the injector after separation and cleanup is provided in Figure V-4. Subsequent leak checks showed that the remaining diffusion-bonded stacks (fuel and oxidizer) and the machined body were gas-tight.

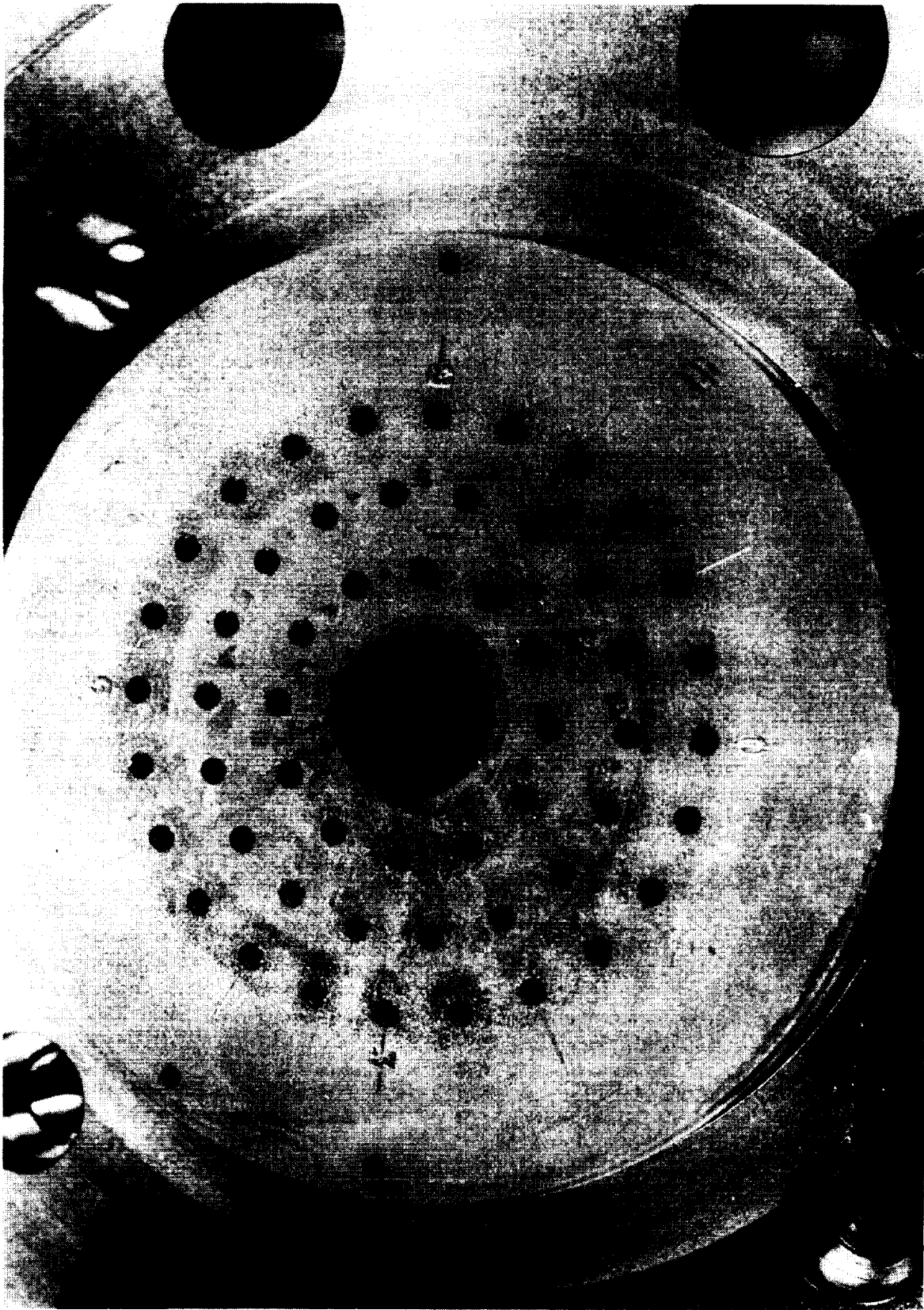
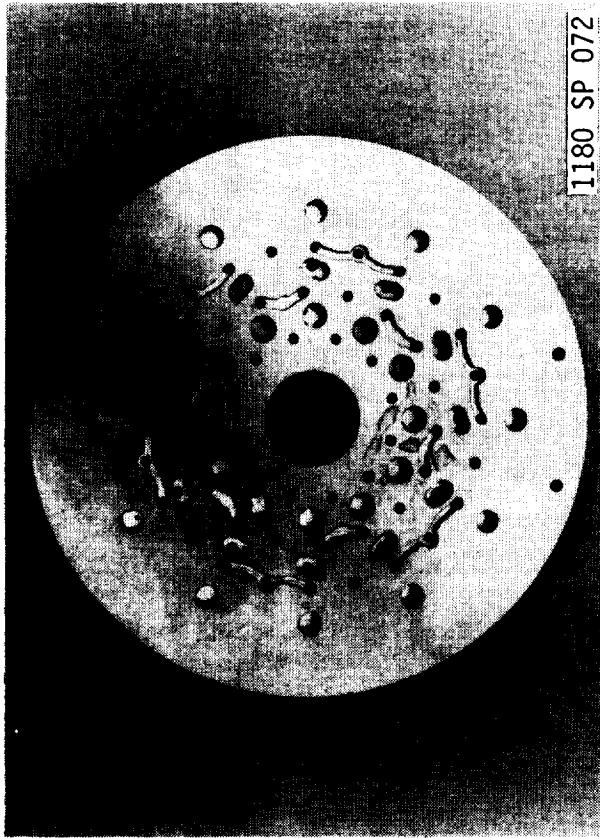
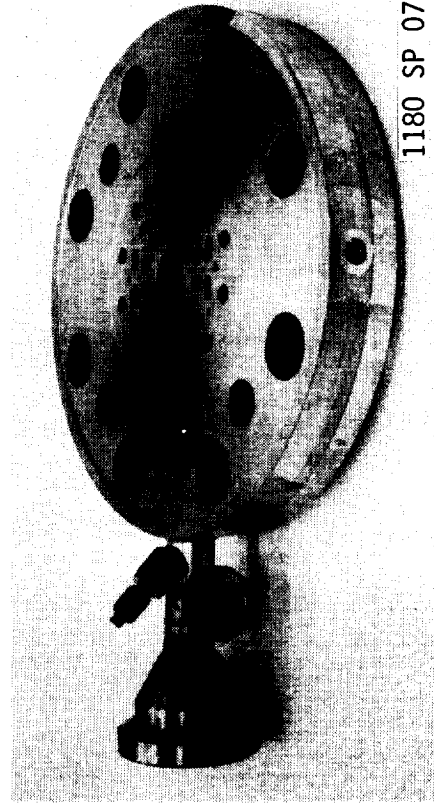


Figure V-3. Fuel-Rich Vortex Injector After Brazing of Faceplate

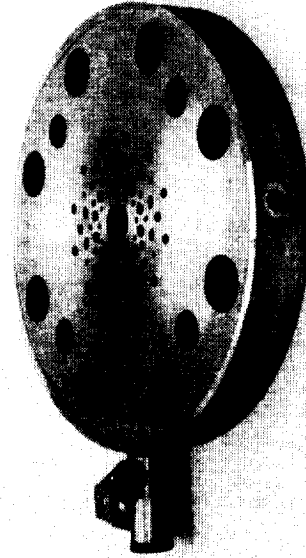


1180 SP 072

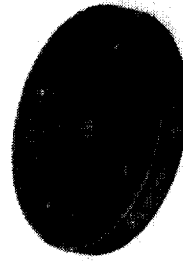


1180 SP 074

OXIDIZER-RICH



FUEL-RICH



1180 SP 073

Figure V-4. Platelet Injectors Following Removal of Faceplates

V, B, Problems (cont.)

Restoration of the fuel-rich platelet injector required the replacement of the four plates destroyed in the separating operation.

A series of vacuum braze process verification tests was conducted on plates containing orifices whose diameters were representative of the injector holes which had become plugged up in the earlier braze runs. Copper braze foil thicknesses of 0.005, 0.0025, and 0.0013 cm (0.002, 0.001, and 0.0005 in.) were employed in these tests. The 0.005-cm (0.002-in.) foil was found to plug up the holes, while the two lesser thicknesses produced gas-tight joints without any sign of plugging.

The machined body was joined to the bonded stack and to the four new plates in a single vacuum braze operation using 0.0013-cm (0.0005-in.) thick copper foil.

Subsequent leak checks with helium showed the fuel-rich assembly to be acceptable. The cold-flow tests showed that all elements were open and flowing properly.

The oxidizer-rich assembly, which has smaller holes at the manifold interface, however was once again plugged. The faceplate was machined off, and the interface holes were enlarged to the same size as those of the fuel-rich design. A new oxidizer-rich platelet stack was fabricated, bonded, leak-checked, and subsequently brazed to the modified body using 0.0012-cm (0.0005-in.) Cu foil. This assembly was leak-tight, and no passages were plugged.

Table V-II lists the cold-flow data obtained after the repair of these injectors. A comparison with the first assembly (after unplugging) shows no significant deviation in flow coefficient.

C. PRODUCT ASSURANCE

1. Weld Inspection

Activities in this task consisted of the dye-penetrant and ultrasonic inspection of twelve welds in the heat sink chambers and one weld in the oxidizer-rich EDM'd injector.

Four of the chamber (PN 1191401-9) welds inspected were 1.91-cm (0.75-in.) deep radial EB welds penetrating into a backing ring. After machining of the backing ring, dye-penetrant inspection (inside and out) showed only one surface flaw (external) at the end of the beam travel. This was repaired through TIG welding.

TABLE V-II. - COLD-FLOW DATA OF PLATELET INJECTORS AFTER REPAIR

Fuel-Rich

ΔP	Fuel Circuit		Oxidizer Circuit	
	w kg/sec (lb/sec)	Kw*	w kg/sec (lb/sec)	Kw*
kPa (psid)				
138 (20)	3.55 (7.83)	1.75	0.77 (1.7)	0.38
276 (40)	5.03 (11.09)	1.75	1.11 (2.44)	0.39
414 (60)	6.15 (13.56)	1.75	1.36 (3.06)	0.39
522 (80)	7.13 (15.72)	1.76	1.58 (3.48)	0.39
689 (100)	7.94 (17.50)	1.75	1.77 (3.90)	0.39
827 (120)	8.70 (19.17)	1.75	-	-
1,034 (150)			2.13 (4.7)	0.39
1,379 (200)			2.45 (5.4)	0.38
Previous Value Average		1.8		0.39

Oxidizer-Rich (Second Platelet Stack)

<u>Fuel Circuit</u>			<u>Oxidizer Circuit</u>		
ΔP	Flow	Kw	ΔP	Flow	Kw
kPa (psid)	kg/sec (lb/sec)		kPa (psid)	kg/sec (lb/sec)	
695 (100.8)	0.54 (1.20)	.119	75 (10.9)	5.53 (12.2)	3.71
1,379 (200.1)	0.76 (1.68)	.118	110 (15.9)	6.67 (14.7)	3.70
2,090 (303.1)	0.93 (2.05)	.118	144 (20.9)	7.66 (16.9)	3.69
2,689 (390.1)	1.03 (2.26)	.115	175 (25.4)	8.35 (18.4)	3.65
3,394 (492.3)	1.15 (2.54)	.115	201 (29.1)	8.94 (19.7)	3.65
3,467 (502.9)	1.20 (2.65)	.114			
Previous Value Average (First Assembly)		.117			3.73

$$*Kw = \frac{\dot{w} \text{ (kg/sec)}}{\sqrt{\Delta P \text{ (kPa)}} Sg} \quad \text{or} \quad \frac{\dot{w} \text{ (lb/sec)}}{\sqrt{\Delta P \text{ (psi)}} Sg}$$

Flow in Water Sg = 1

V, C, Product Assurance (cont.)

Four electron-beam welds of 5-cm (2-in.) minimum depth and four 0.635-cm (0.25-in.) fillet welds were inspected in the two unlined chambers (PN 1191401-19). Initial ultrasonic inspection of the deep welds showed 5.72-cm (2.25-in.) to 6.35-cm (2.50-in.) penetration and revealed the location of a number of small voids and one large void. Since weld depth is primarily designed to minimize flange rotation, the presence of the local internal voids was not considered significant. Dye-penetrant inspection showed an acceptable surface condition on all eight welds. A second ultrasonic scan of these same welds (documented in Figure V-5) revealed the weld depth to be less than the previously indicated values.

The weld penetration depths from Figure V-5 are as follows:

Short Unlined L* Section 4.06 cm (1.60 in.)
4.57 cm (1.80 in.) at the end with
SN stamp

Long Unlined L* Section 4.70 cm (1.85 in.)
3.61 cm (1.42 in.) at the end with
SN stamp

A structural review of the impact of the reduced weld penetration in conjunction with the fillet weld (not considered in the original stress analysis) suggested that the parts are acceptable provided the design margin (original design operating pressure 17,235 kPa (2500 psia) maximum) is reduced accordingly, as follows:

- ° Reduce the proof pressure based on 3.61-cm (1.42-in.) weld depth and yield stress at the fillet weld to 24,473 kPa (3550 psia) from the original proof pressure of 31,712 kPa (4600 psia) based on flange deflection
- ° Limit the maximum operating pressure for a 15-sec burn, based on heat soak and yield stress at maximum temperature to 17,924 kPa (2600 psia)

In order to validate the above stress analysis, it was recommended that the fillet welds and axial EB-welds be reinspected for potential cracks or changes following the 24,473 kPa (3550 psia) proof test. No changes were reported following these tests.

Dye-penetrant inspection of the injector manifold welds showed no other flaws of significance.

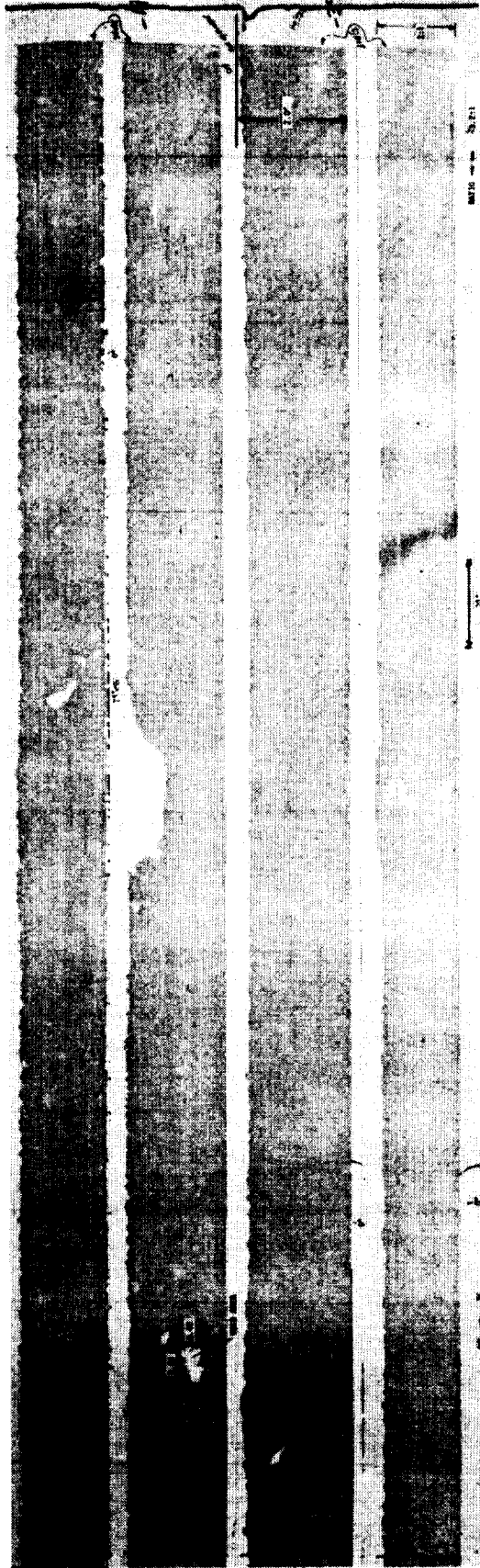


Figure V-5. Ultrasonic Inspection of Axial Welds on Unlined L* Sections (PN 1191401)

ORIGINAL PAGE IS
OF POOR QUALITY

V, C, Product Assurance (cont.)

A critical inspection of a nickel-to-stainless-steel butt weld on the oxidizer-rich LOL injector (PN 1193105-19) shown in Figure V-6 was undertaken following less than acceptable results of a vacuum furnace brazement of PN 1193102 and 1193103-2. These parts were assembled using a structural brazement and redundant EB seal welds (see Figure V-6). The vacuum furnace brazement of the nickel pattern plate to the 304 stainless steel down-comer plate resulted in only a partial bond joint due to the differential expansion rates of the two metals.

A subsequent structural reanalysis of the assembly indicated that the required strength could be realized without the brazement by increasing the penetration of the 4 electron-beam welds to the following dimensions:

- | | |
|---|-------------------------|
| 1) Internal Ni-to-304 butt weld | 0.76 cm (0.30 in.) min. |
| 2) Axial face weld around igniter port | 0.48 cm (0.19 in.) min. |
| 3) Backside flange-to-core weld (304-304 stainless) | 0.76 cm (0.30 in.) min. |
| 4) External Ni-to-304 butt weld | 0.51 cm (0.20 in.) min. |

The design allowable injector face pressure drop of 13,788 kPa (2000 psid) for that configuration compares with a predicted maximum pressure drop of 8700 kPa (1232 psid) during the most adverse start transient sequence. Weld No. 1 was the most highly stressed. Figure V-6 provides an ultrasonic inspection report showing that the required depth of Weld No. 1 was attained. Figure V-7 provides a photograph of this injector after the internal and prior to the final external weld assembly.

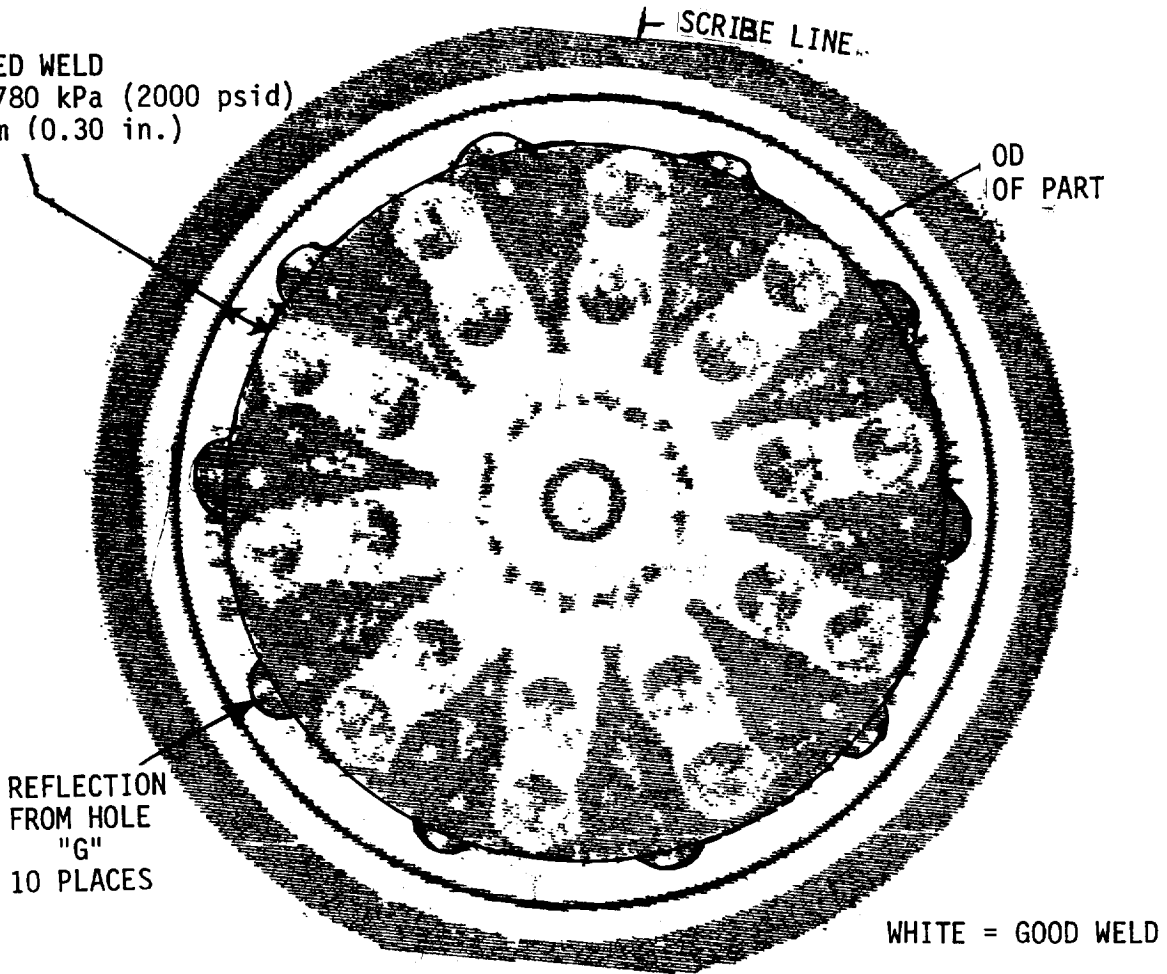
2. Dimensional Inspections

Dimensional inspection of the fuel-rich LOL injector (PN 1193105-19) indicated that the cross-drilled holes had been mislocated by 0.102 cm (0.04 in.) with respect to the injector face. The effect of this was to reduce the L/D of the oxidizer injection orifices. The dimensions involved are identified in Figure V-8.

A review of the hydraulics of these orifices indicated that 1) the flow would be detached in both the designed and as-fabricated condition and 2) no change in pressure drop or flow direction or stability would be expected. Figure V-8 documents the as-built part.

No other dimensional discrepancies of significance were recorded during the fabrication and inspection processes.

REQUIRED WELD
FOR 13780 kPa (2000 psid)
0.76 cm (0.30 in.)



SCAN DIRECTION

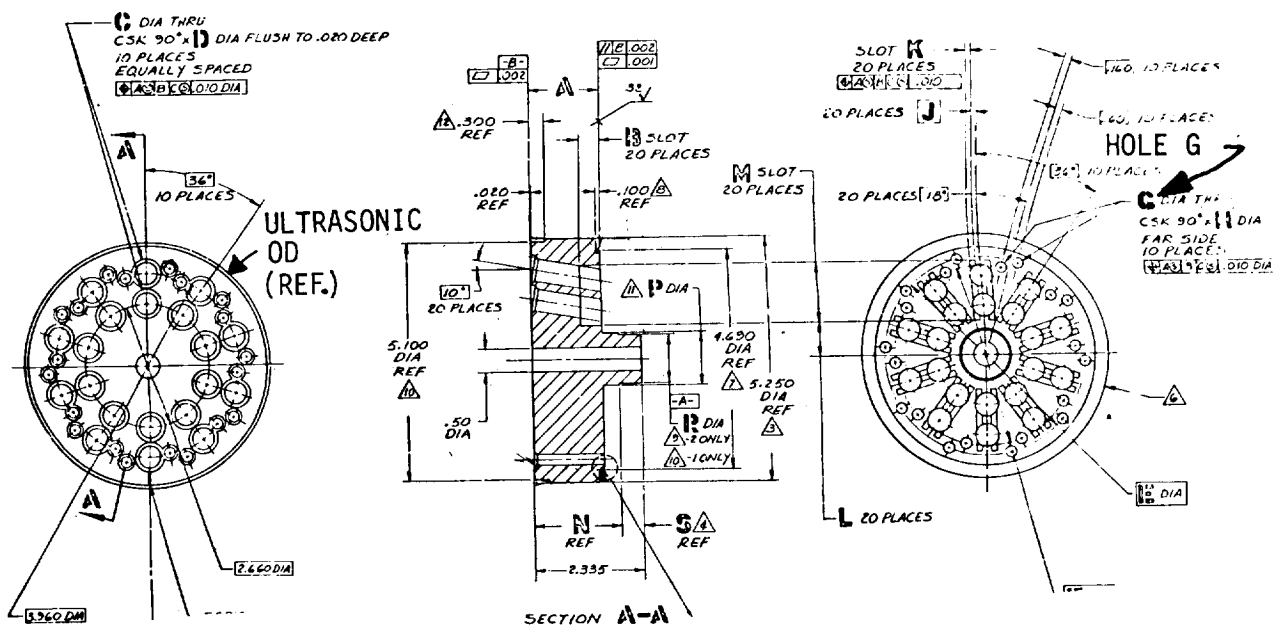
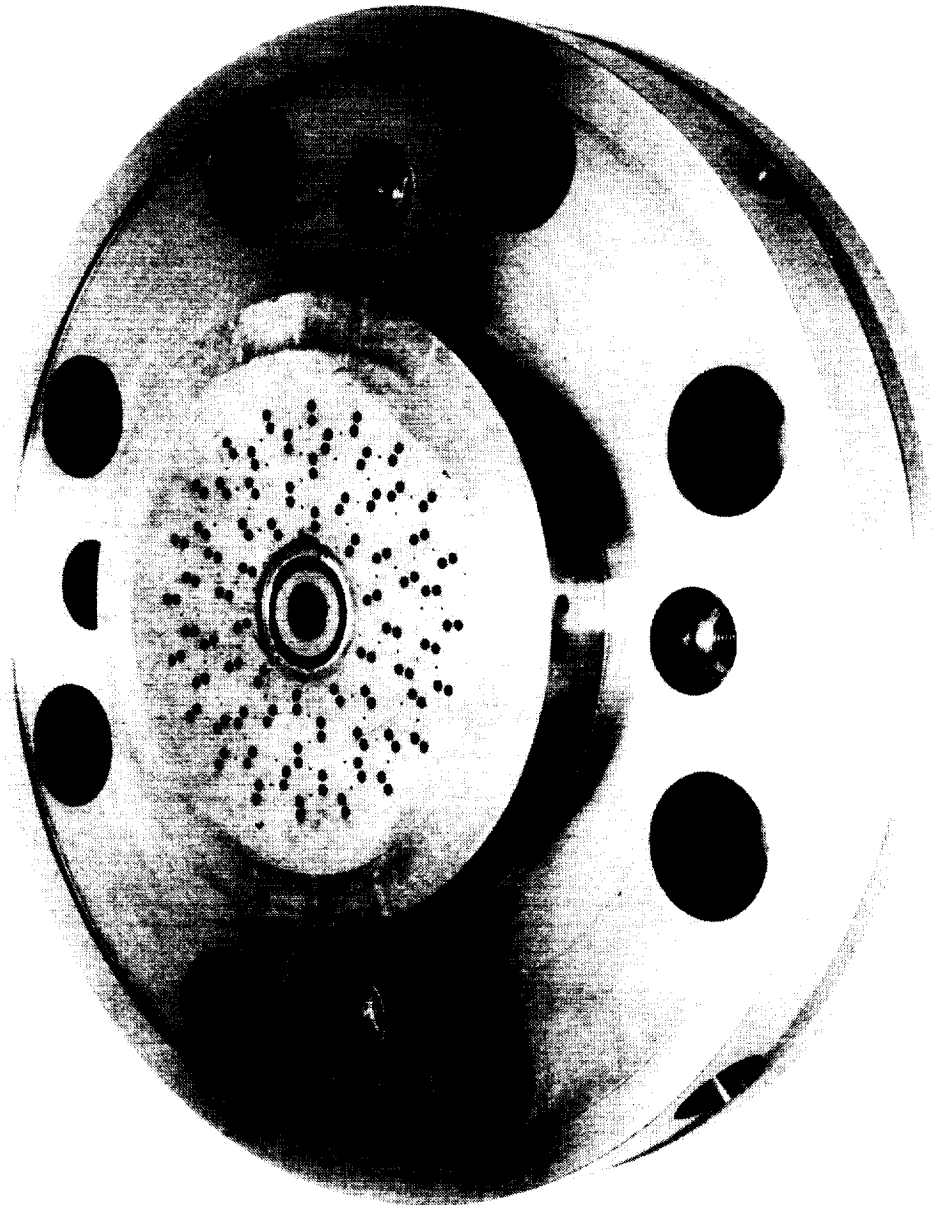


Figure V-6. Ultrasonic Inspection of Oxidizer-Rich EMD'd Injector PN 1193105-19

ORIGINAL PAGE IS
OF BEST QUALITY



0381 SP 024

Figure V-7. Oxidizer-Rich EDM'd Injector Before Final Weld Assembly

ORIGINAL PAGE IS
OF POOR QUALITY

VI. COLD-FLOW TESTING

Cold-flow testing consisted of the following activities:

- ° Water flow testing a single circuit (rich propellant) of a single element to optimize the swirler configuration.
- ° Water flowing a full-scale loose stack of concentric vortex injector platelets to verify the pressure drop and spray angles.
- ° Flowing the four final injector assemblies with water to verify the spray pattern, injection uniformity, and overall pressure drop.
- ° GN₂ flowing the complete preburner assembly to establish the correct spacing of the turbine simulator blades and define the main injector simulator flow vs pressure drop characteristics.
- ° GN₂ flowing the igniters to define the pressure drop vs flowrate characteristics.

A. SINGLE-ELEMENT COLD-FLOW TESTING

1. Background

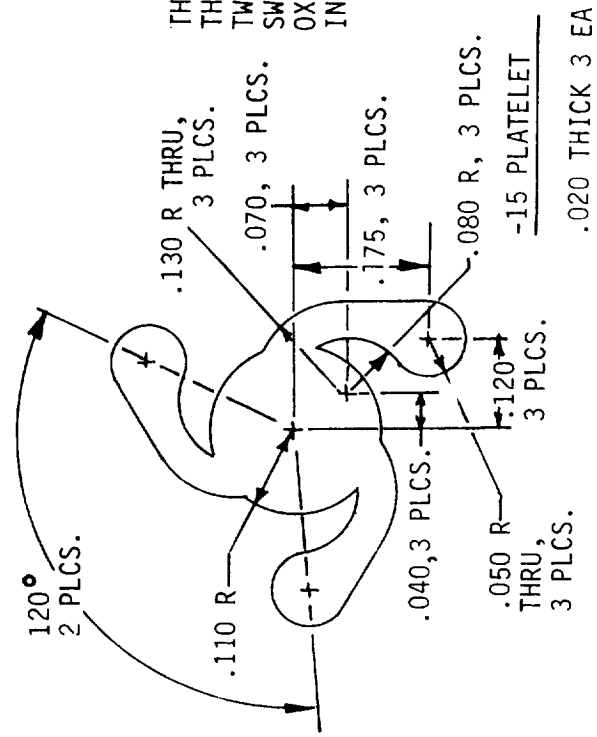
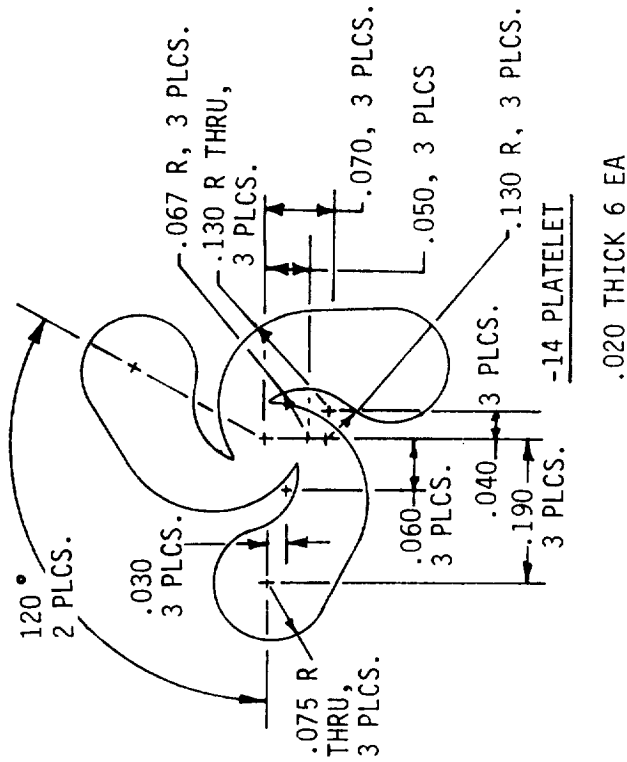
During the injector analytical design activity, the concentric vortex element was identified as having the greatest potential for providing the required uniform mixture ratio distribution. Because of limited experience with this element, it became difficult to identify which of several candidate approaches would provide the best hydraulic results. The major propellant circuit of the oxidizer-rich injector was identified as having the greatest packaging limitations and therefore was selected for cold-flow evaluation.

2. Objectives

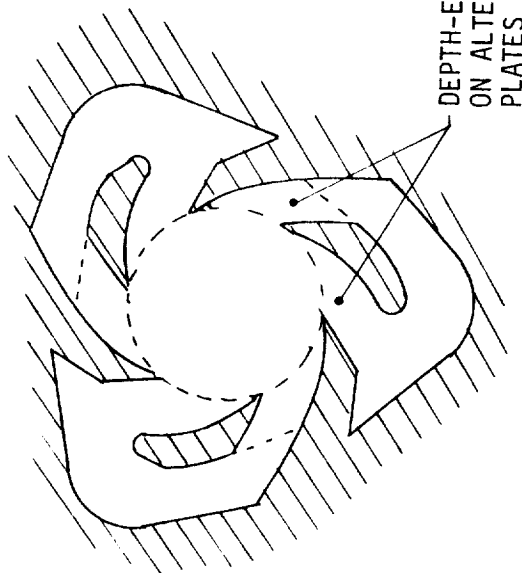
The objectives of the single element optimization activity were as follows:

- a) Determine if a two-stage 3-vane or a single-stage 6-vane configuration provided more uniform flow. The single-stage design is a structurally superior configuration.
- b) Verify the element pressure drop flow area relation.
- c) Verify the resulting spray cone angle predictions.

The designs selected for testing are shown in Figure VI-1.



THROUGH-ETCHED
THREE-VANE
TWO-STAGE
SWIRLER FOR
OXIDIZER-RICH
INJECTOR



DEPTH-ETCHED
SIX-VANE
SINGLE-STAGE
SWIRLER DESIGN

Figure VI-1. Swirler Element Designs Selected for Testing

VI, A, Single-Element Cold-Flow Testing (cont.)

Results

Photographs of the spray fans of selected configurations are shown in Figures VI-2, -3, and -4. The results of this cold-flow verification experiment showed that the predicted spray cone angles were correct. The observations also showed that the single-stage, depth-etched 6-vane configuration produced a more uniform spray than the two-stage three-vane design. The flow area of the vanes was also varied by varying the number of vane and orifice plates in order to relate the pressure drop to flow uniformity. The flow vs pressure drop data are provided in Figures VI-5 and -6. A larger number of orifice plates, downstream of the vane plates, improved the spray uniformity. The selected spray pattern is shown in the photograph of Figure VI-7.

B. LOOSE PLATELET STACK COLD-FLOW TESTING

1. Objectives

The objectives of cold-flowing the loose platelet stacks were as follows:

- a) Verify the swirler cone spray angles of the minor and major flow streams.
- b) Verify the element pressure drop.
- c) Verify the element-to-element flow repeatability.

2. Procedure

The platelets used to form the 54 elements were clamped between two heavy aluminum plates, with the back providing a means of flowing one or both circuits of any single element in the outer row. The flowrates and inlet line pressures were recorded over a range of flowrates, and the spray angles were documented photographically.

When the desired spray angles and pressure drops were not attained, as in the case of the fuel-rich design, the quantity, sequence of stacking, and orifice size were adjusted until the desired results were achieved. The final injector assembly incorporated the results and design modifications obtained from the loose-stack cold-flow testing.

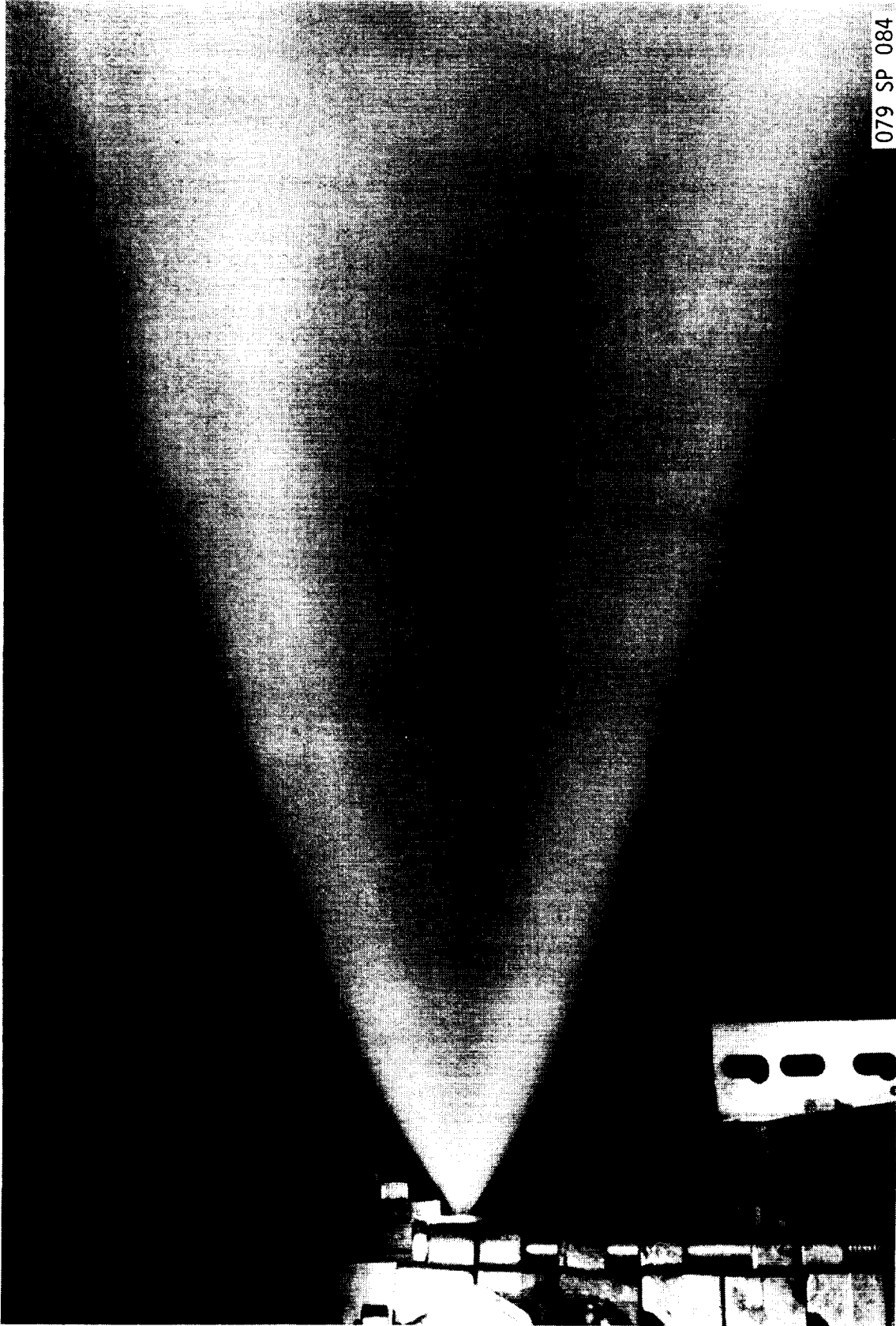


Figure VI-2. Six-Vane Swirler Spray, $\Delta P = 2.02\text{M N/m}^2$ (293 psia),
 $\dot{w} = 0.64 \text{ kg/sec}$ (1.40 lb/sec) H_2O (Configuration 1)

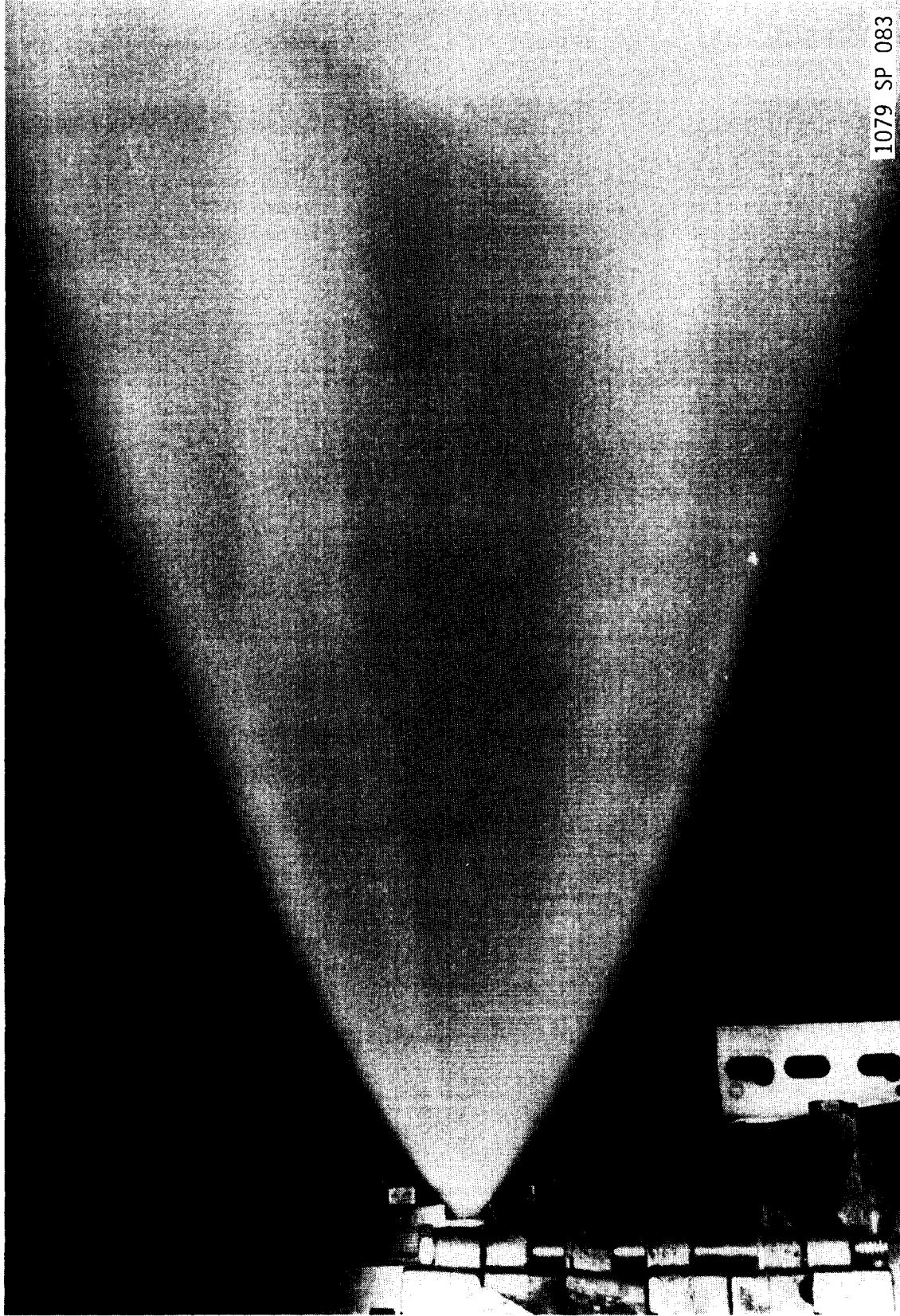
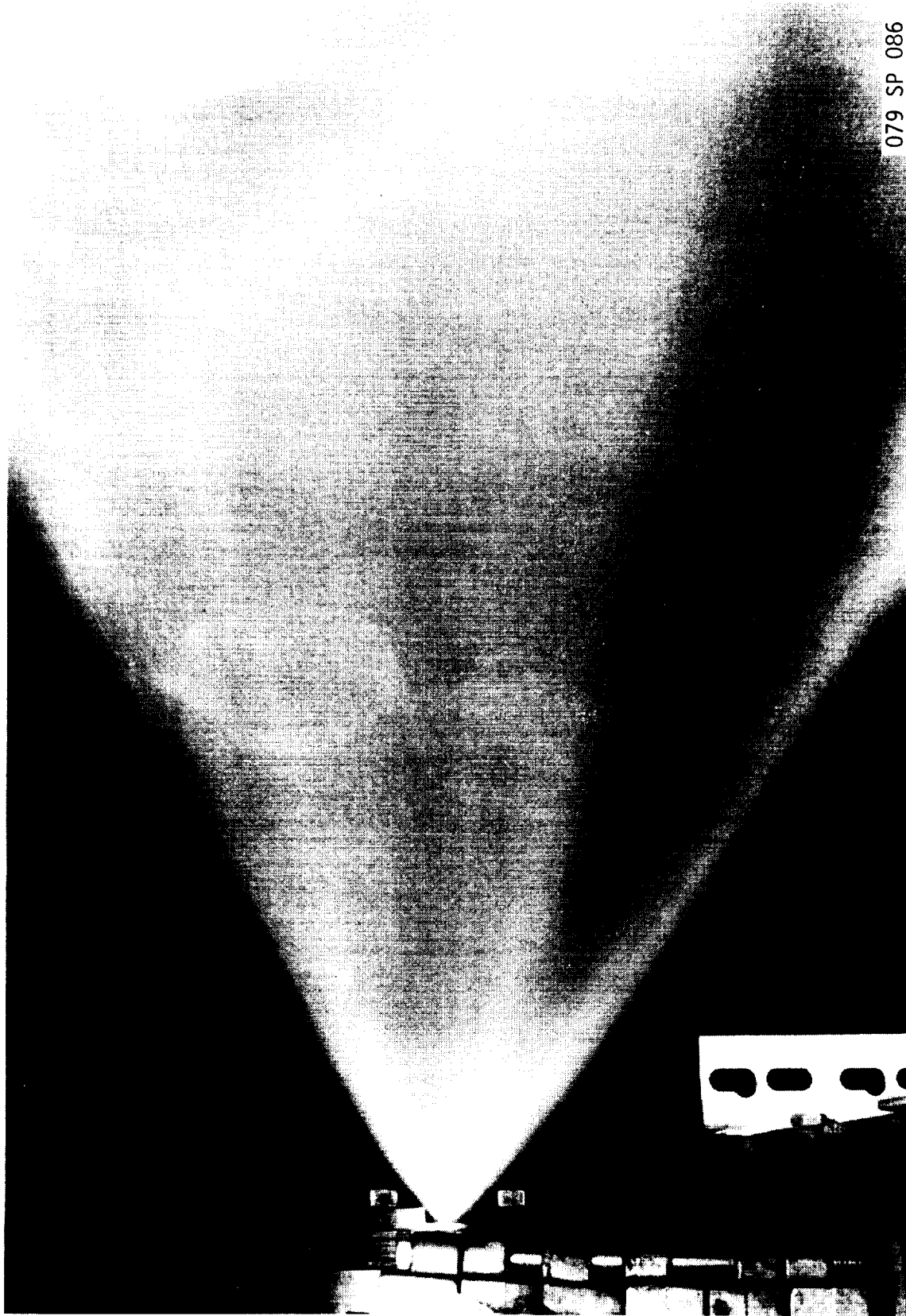


Figure VI-3. Six-Vane Swirler Spray, $\Delta P = 2.68\text{M N/m}^2$ (390 psid),
 $\dot{w} = 0.64 \text{ kg/sec}$ (1.40 lb/sec) H_2O (Configuration 3)



079 SP 086

Figure IV-4. Three-Vane Swirler Spray, $\Delta P = 2.19M \text{ N/m}^2$ (318 psid),
 $w = 0.64 \text{ kg/sec}$ (1.41 lb/sec) H_2O (Configuration 1)

CONFIG.	NUMBER OF ORIFICES AT 0.051 cm (0.02 in.) EACH	NUMBER OF SWIRLER PLATELETS AT 0.0752 cm (0.03 in.) EACH	Kw	T _{cm/in.}
1	1	6	0.0875	0.51 (0.20)
2	2	5	0.0832	0.48 (0.19)
3	4	4	0.0745	0.51 (0.20)

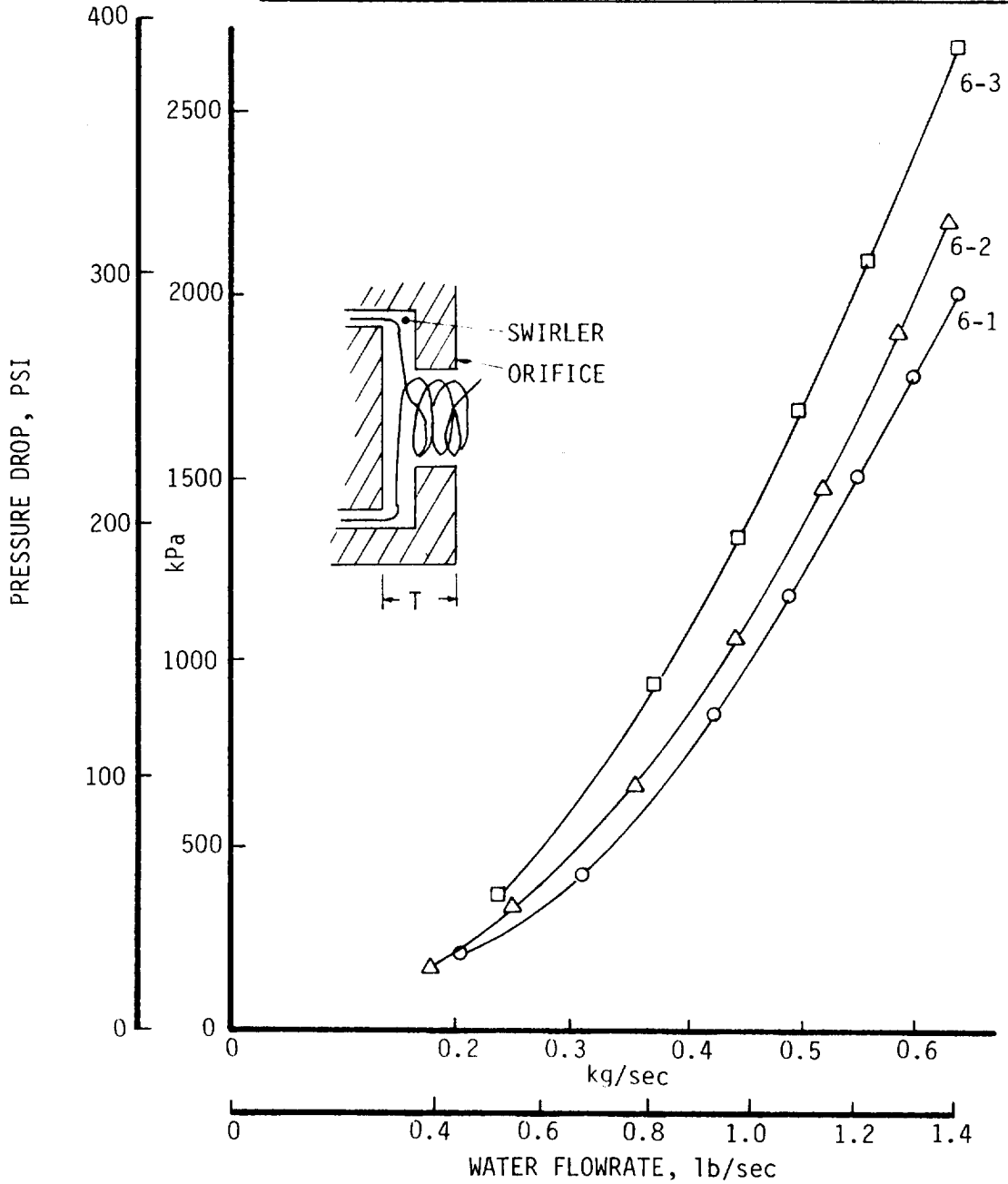


Figure VI-5. Six-Vane Swirler Pressure Drop Data

c-3

CONFIG.	NO. OF ORIFICE PLATELETS*	NO. OF PRE-SWIRL PLATELETS (STAGE 2)	NO. OF SWIRLER PLATELETS (STAGE 1)	K _w	THICK T _{cm/in.}
1	1	3	6	0.0841	0.51 (0.02)
2	1	4	5	0.0828	0.51 (0.02)
3	1	6	3	0.0778	0.51 (0.02)
4	4	6	3	0.075	0.66 (0.26)

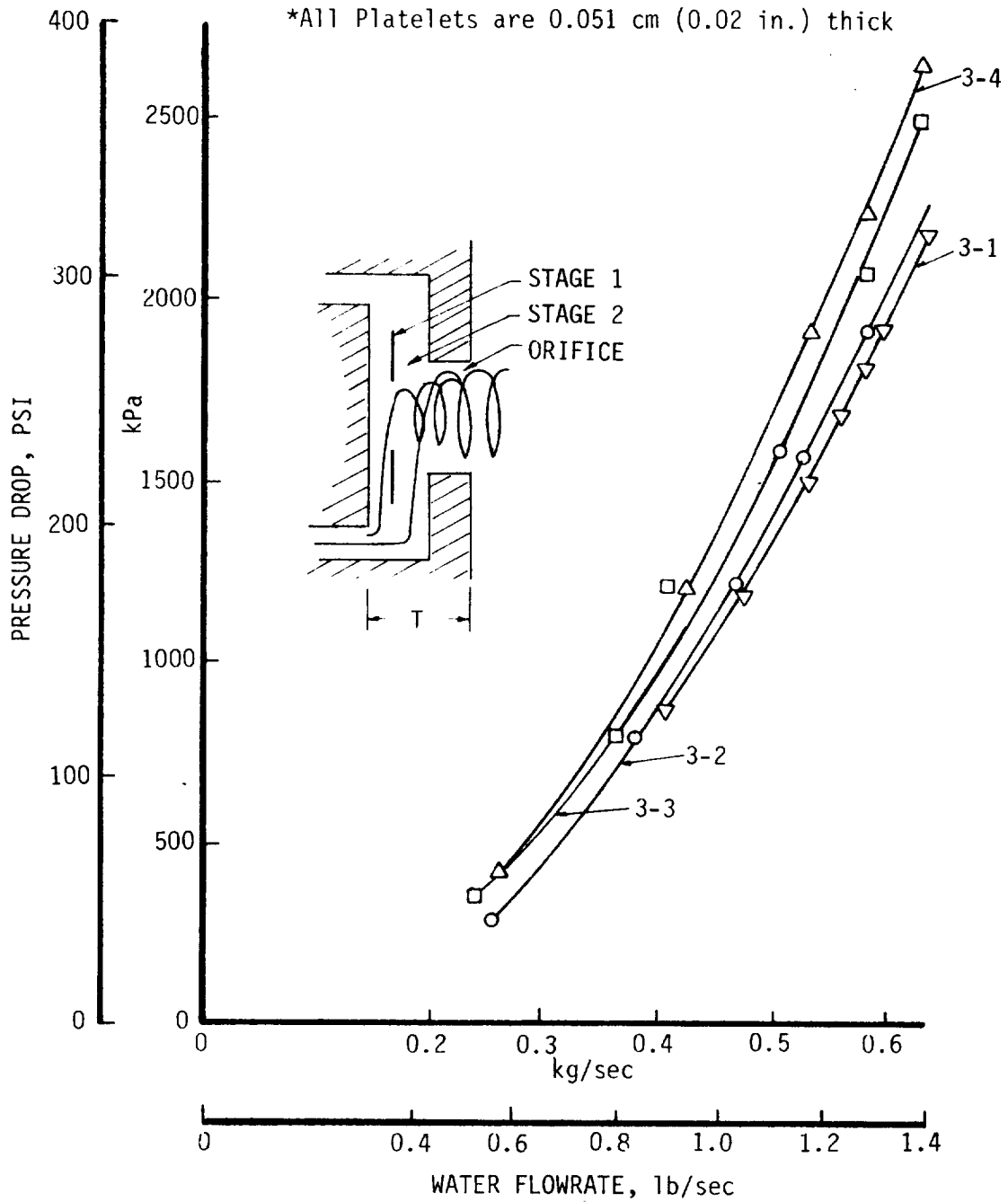
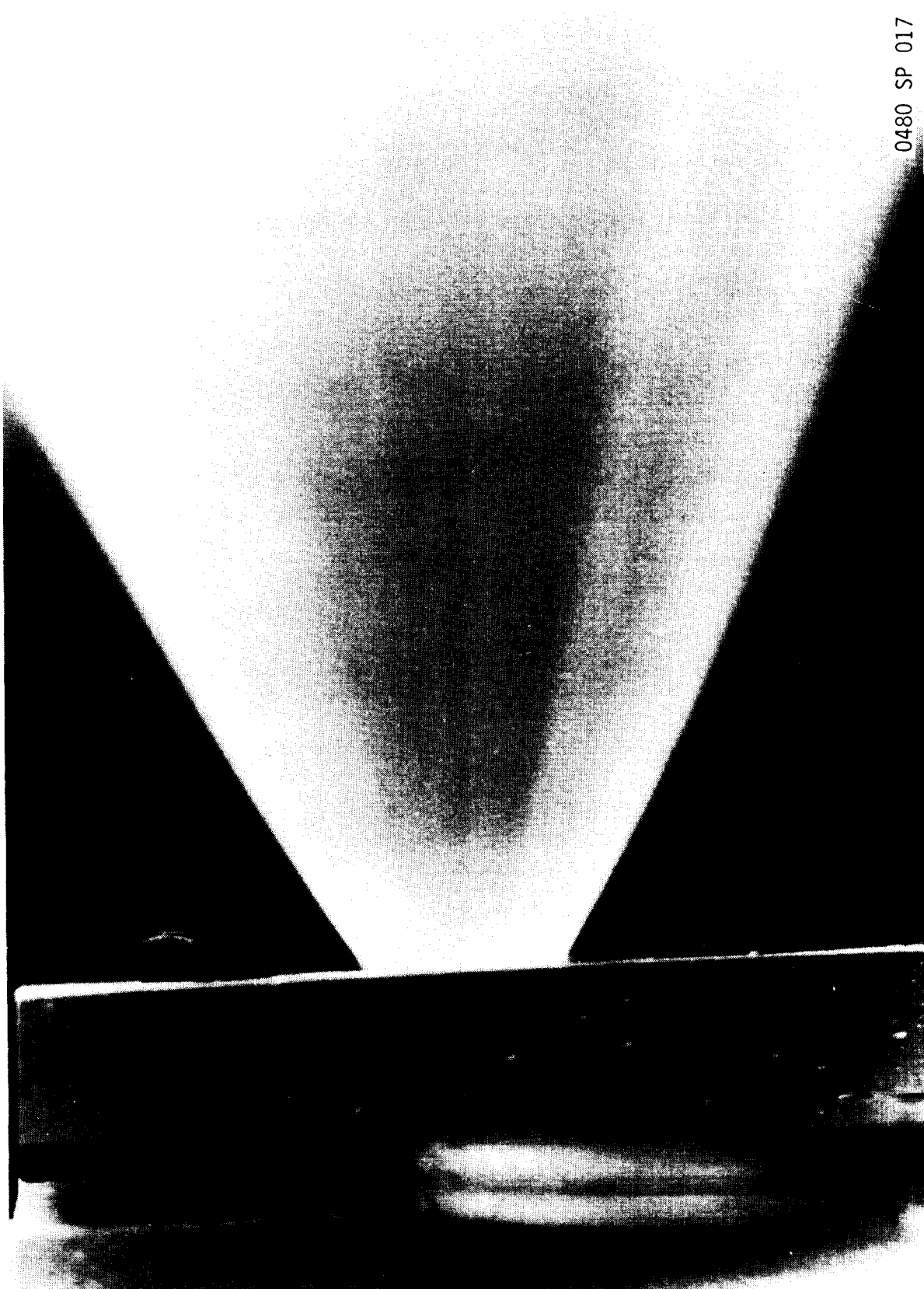


Figure VI-6. Three-Vane Swirler Pressure Drop Data



0480 SP 017

Figure VI-7. Major Circuit of Oxidizer-Rich Preburner, $\Delta P = 2.67M \text{ N/m}^2$
(400 psid)

ORIGINAL PAGE IS
OF POOR QUALITY

VI, B, Loose Platelet Stack Cold-Flow Testing (cont.)

3. Results

Oxidizer-Rich Pattern

The flow data obtained from the as-designed configuration are as follows:

Major Propellant Circuit (Oxidizer)

ΔP Water kPa (psid)	Flow kg/sec (lb/sec)		$K_w = \frac{\dot{w}}{\sqrt{\Delta P}} / \text{Element}$	$K_w (54 \text{ Elements})$
	Element #1	Element #2		
2758 (400)	0.644 (1.42)	0.649 (1.43)	0.071	
2068 (300)	0.562 (1.24)	0.567 (1.25)	0.072	
1379 (200)	0.463 (1.02)	0.458 (1.01)	0.072	3.895
689 (100)	0.327 (0.72)	0.327 (0.72)	0.072	

The flow coefficient ($K_w \sqrt{\Delta P}$ sg) for all 54 elements was 3.895 for the major circuit. The predicted element pressure drop for the required 39.0 kg/sec (86 lb/sec) LOX flow is 2799 kPa (406 psid). This is in good agreement with the single-element cold-flow data reported for the six-vane configuration (No. 3).

Minor Propellant Circuit

Inspection of the spray cone angles indicated that the minor spray cone should clear the major cone as predicted. The measured flow pressure relation is as follows:

P Water kPa (psid)	Flow kg/sec (lb/sec)		Single Element K_w Avg 10^{-5}
	Element #1	Element #2	
2758 (400)	0.0194 (0.0427)	0.0196 (0.0432)	215
2068 (300)	0.0167 (0.0368)	0.0171 (0.0377)	213
1379 (200)	0.0136 (0.0300)	0.0136 (0.0299)	212 X 54 Elem = 0.115
689 (100)	0.0095 (0.0209)	0.0093 (0.0206)	208

The calculated element pressure drop for 1.93 lb/sec of RP-1 is 2588 kPa (375 psid). Inspection and measurements subsequent to the cold flow indicated a fabrication flaw in one element of the minor circuit. A replacement orifice plate was substituted for the faulty plate. The orifice diameters of the replacement plate were 0.0673 to 0.0686 cm (0.0265 in. to

VI, B, Loose Platelet Stack Cold-Flow Testing (cont.)

0.0270 in.) as compared to a nominal 0.0635 cm (0.025 in.) for the plate which had been used in the cold flow. The replacement part dimension was closer to the nominal point value of 0.0686 cm (0.027 in.). The predicted element ΔP for the assembly containing the replacement part is ≈ 2068 kPa (≈ 300 psid) which was the original design value for this circuit.

4. Photographic Documentation

Photographs of the spray cone angles of the major and minor circuit are shown in Figures VI-7 through VI-10 at pressure drops of 1379 and 2758 kPa (200 and 400 psid). The supply pressure was found to have no measurable influence on the cone angles. The cone (1/2) angles obtained from the photographs are compared to the design values as follows:

<u>Major Circuit</u>	<u>Predicted Measured</u>	
$\Delta P = 1379$ kPa (200 psid) 2758 kPa (400 psid)	30°	31° 31°
<u>Minor Circuit</u>		
$\Delta P = 1379$ kPa (200 psid) 2758 kPa (400 psid)	10°	$\approx 11^\circ$ $\approx 9^\circ$

The measured values of the spray cone angles are noted to be in agreement with the expected values derived from the analysis and single element data from the previous section.

Fuel-Rich Pattern

Cold-flow testing of the full-scale fuel-rich loose stack provided the following data for each element:

Stacked As-Designed

ΔP kPa (psid)	<u>Minor Propellant Circuit</u>			<u>Major Propellant Circuit</u>		
	\dot{w} kg H ₂ O/sec (lb H ₂ O/sec)		Kw	\dot{w} kg H ₂ O/sec (lb H ₂ O/sec)		Kw
689 (100)	0.0337	(0.0742)	0.00742	0.163	(0.36)	0.036
1379 (200)	0.0494	(0.109)	0.11771	0.227	(0.50)	0.035
2068 (300)	0.0631	(0.139)	0.00802	0.281	(0.62)	0.036
2758 (400)	0.0730	(0.161)	0.00805	0.331	(0.73)	0.036
	54-element stack = 0.432			54-element stack = 1.94		

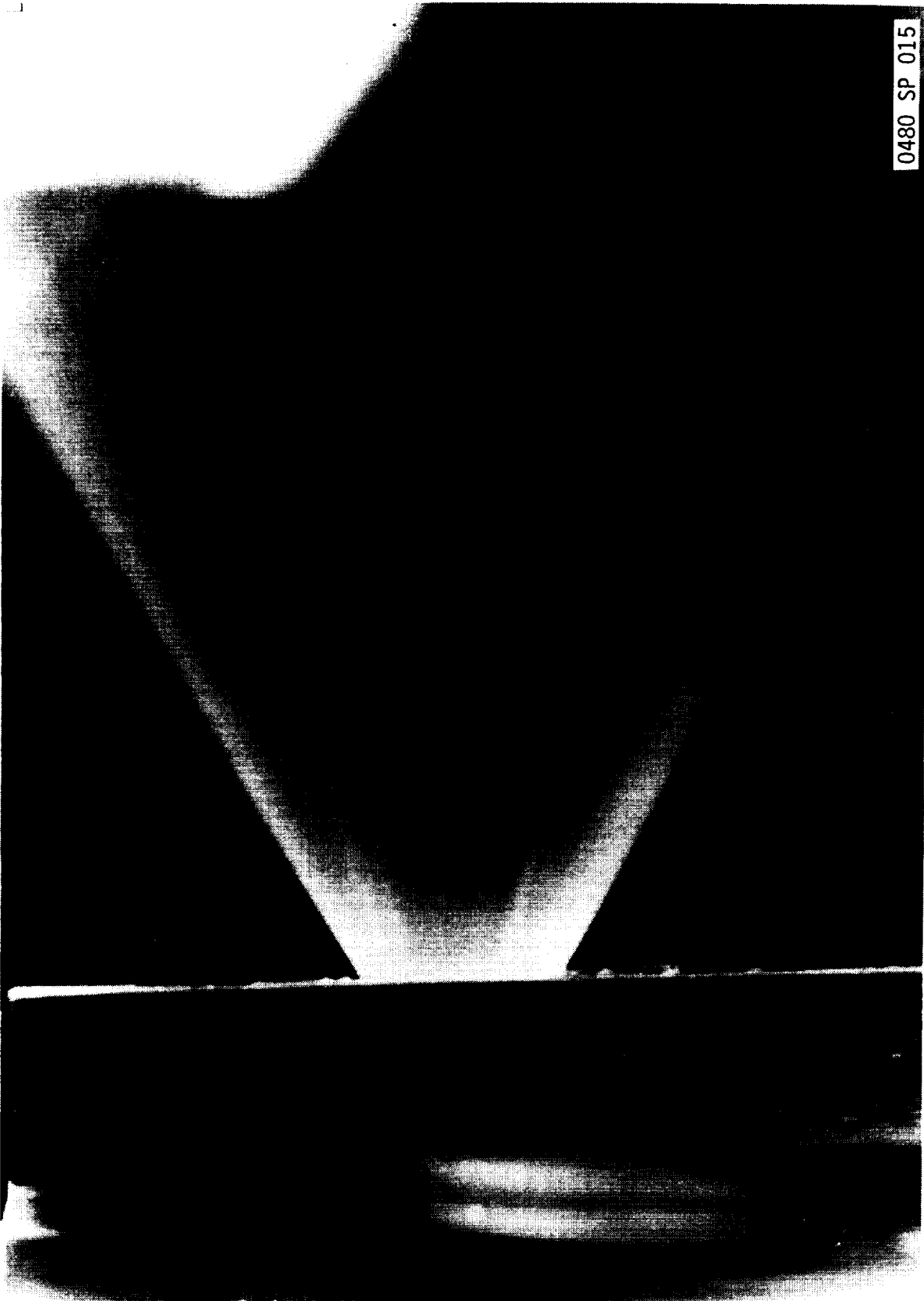


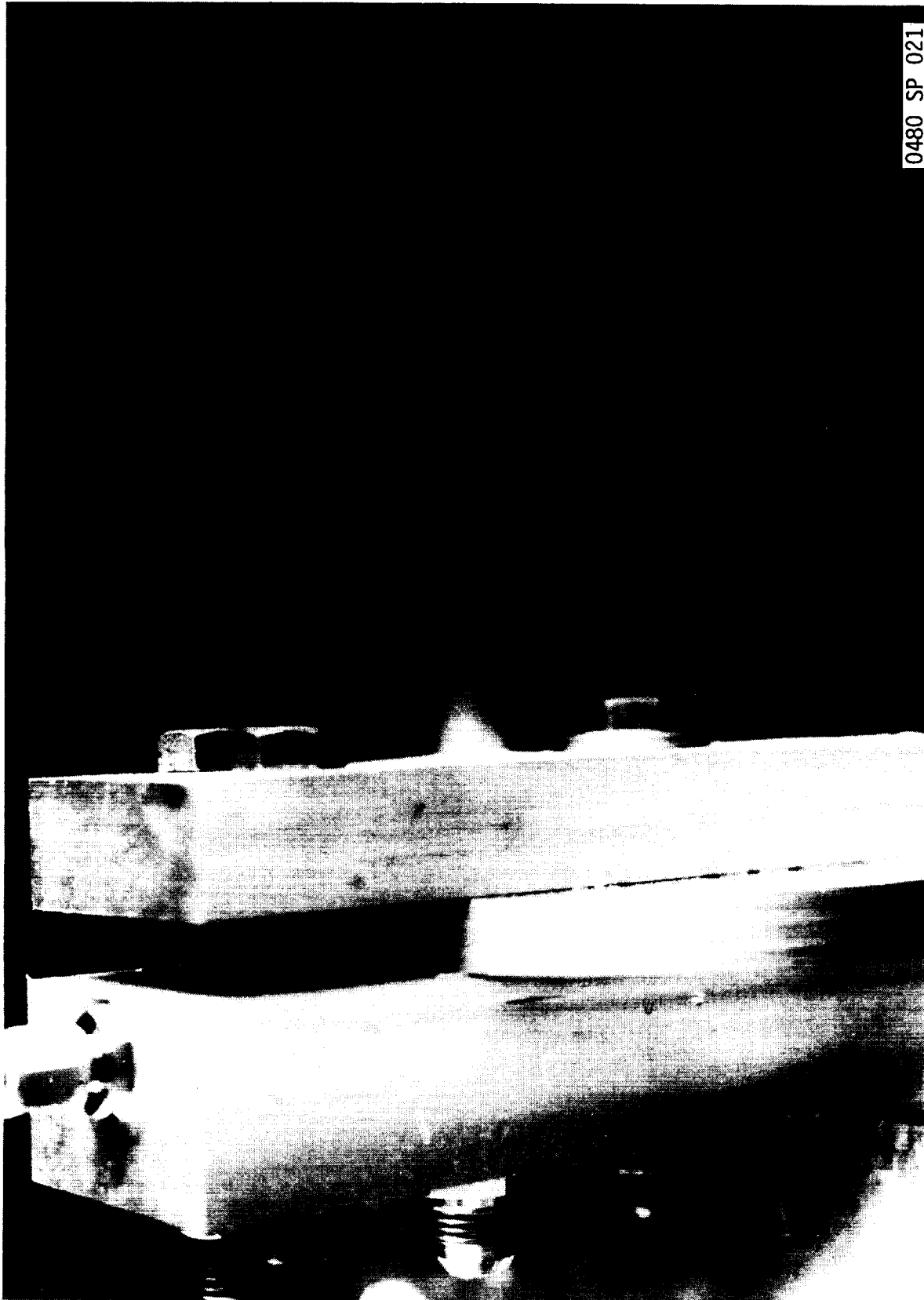
Figure VI-8. Major Circuit of Oxidizer-Rich Preburner, $\Delta P = 1.38M \text{ N/m}^2$
(200 psid)



0480 SP 020

Figure VI-9. Minor Circuit (Fuel) of Oxidizer-Rich Preburner,
 $\Delta P = 2.76M \text{ N/m}^2$ (400 psid)

ORIGINAL PAGE
OF POOR QUALITY



0480 SP 021

Figure VI-10. Minor Circuit (Fuel) of Oxidizer-Rich Preburner,
 $\Delta P = 1.38M \text{ N/m}^2$ (200 psid)

VI, B, Loose Platelet Stack Cold-Flow Testing (cont.)

The pressure drop of these circuits at rated propellant is calculated to be 2054 kPa (298 psid) for the major flow at 13.6 kg/sec (30 lb/sec) and 1965 kPa (285 psid) for the minor flow at 3.63 kg/sec (8 lb/sec). The design goal for these circuits was 2068 kPa (300 psid).

The measured spray angle of the minor flow was 34°. This was greater than predicted and resulted in minor spray impingement within the swirler cup. The degree of minor propellant swirl was reduced in stages by changing the number of swirler plates (-28) and adding available radial inflow plates (-26).

Table VI-I provides results of four successive design modifications that were evaluated to alleviate the impingement problem. These "on-the-stand" modifications resulted in reducing the spray included angle from the 34° baseline configuration to a 9° total angle in Modification No. 3. The Modification No. 3 spray pattern, shown in Figures VI-11 and 12 for the oxidizer and fuel circuits, respectively indicates a 9° divergence oxidizer angle. As this divergence was too close to that of a showerhead element, the spray angle was opened up to a 20° full angle (10° half angle) in Modification No. 4. The faceplate (-36) orifice diameter was also increased from the 0.330 cm (0.130 in.) design value to 0.414 cm (0.163 in.), which allowed the 20° spray cone to clear the face. The projected flow coefficients for the selected 54-element platelet assembly are 0.41 and 1.91 for the minor and major circuit, respectively, compared to design goal Kw's of 0.35 and 1.80. The addition of the remaining plates and manifolds is expected to reduce the projected values by approximately 5%, which is in reasonable agreement with the design goals.

The desired major circuit pressure drop was attained by removing one of the three major circuit swirler plates and enlarging the discharge orifice diameter in the -36 plate. Optimization of the -36 plate orifice diameter was achieved by obtaining data using two swirler plates (one each -33 and -34) with -36 plate orifice diameters of 0.368 cm (0.145 in.) and 0.414 cm (0.163 in.). These data are shown in Table VI-II. The 0.414-cm (0.163-in.) diameter orifice provides the same pressure drop with two swirler plates as the 0.330-cm (0.130-in.) diameter does with three.

A single-element spray pattern of the selected configuration, Modification No. 4, is shown in Figures VI-13, VI-14, and VI-15. Table VI-I documents the fabrication stacking sequences for the fuel-rich pattern and supersedes all previous drawing stacking data.

As a result of the problems encountered in the final braze operation which joins the prebonded stack to the machined body, a second set of loose platelets was assembled and cold-flowed. The visual appearance of the spray pattern from the second set was the same as the first. The experimentally determined flow coefficients from three elements in the outer row are

TABLE VI-I. - FUEL-RICH PATTERN SINGLE-ELEMENT LOOSE PLATELET COLD FLOW

Minor Propellant Circuit Flowrate kg/sec (lb/sec) H ₂ O		Kw			
Design Modifications: Baseline	1	2	3	4 (Sel. Mod.)	Selected Configuration
Number of Plates	8-28 Plates (2 extra)	10-28 (2 extra)	6-28 & -126	4-28 & 2-26	3-28, 1-26 3-28
ΔP kPa (psid)					
689 (100)	0.0337 (0.0742)	0.0340 (0.075)	0.0331 (0.073)	0.0345 (0.076)	0.0327 (0.072)
1,379 (200)	0.0494 (0.109)	0.0467 (0.103)	0.0490 (0.108)	0.0490 (0.108)	0.0485 (0.107)
2,068 (300)	0.0631 (0.139)	0.0599 (0.132)	0.0617 (0.136)	0.0599 (0.132)	0.0599 (0.132)
2,758 (400)	0.0730 (0.161)	--	--	0.0717 (0.158)	0.0680 (0.150)
Spray Angle Degree (full)	34°	28°	17°	9°	20°
All data with -36 plate removed and one extra -31 added between -30 and -32.					
Major Propellant Circuit Flowrate kg/sec (lb/sec) H ₂ O					
Number of Swirler Plates	3	2	2	2	2
Configuration	Baseline				Selected
-36 Orifice Diameter cm (in.)	0.330 cm (0.130 in.)	0.368 cm (0.145 in.)	0.414 cm (0.163 in.)		
ΔP kPa (psid)					
689 (100)	0.163 (0.36)	0.150 (0.330)	0.161 (0.355)		0.0355
1,379 (200)	0.227 (0.50)	0.199 (0.438)	0.227 (0.500)		0.0354
2,068 (300)	0.281 (0.62)	0.243 (0.535)	0.278 (0.613)		0.0354
2,758 (400)	0.331 (0.73)	0.281 (0.620)	--		--

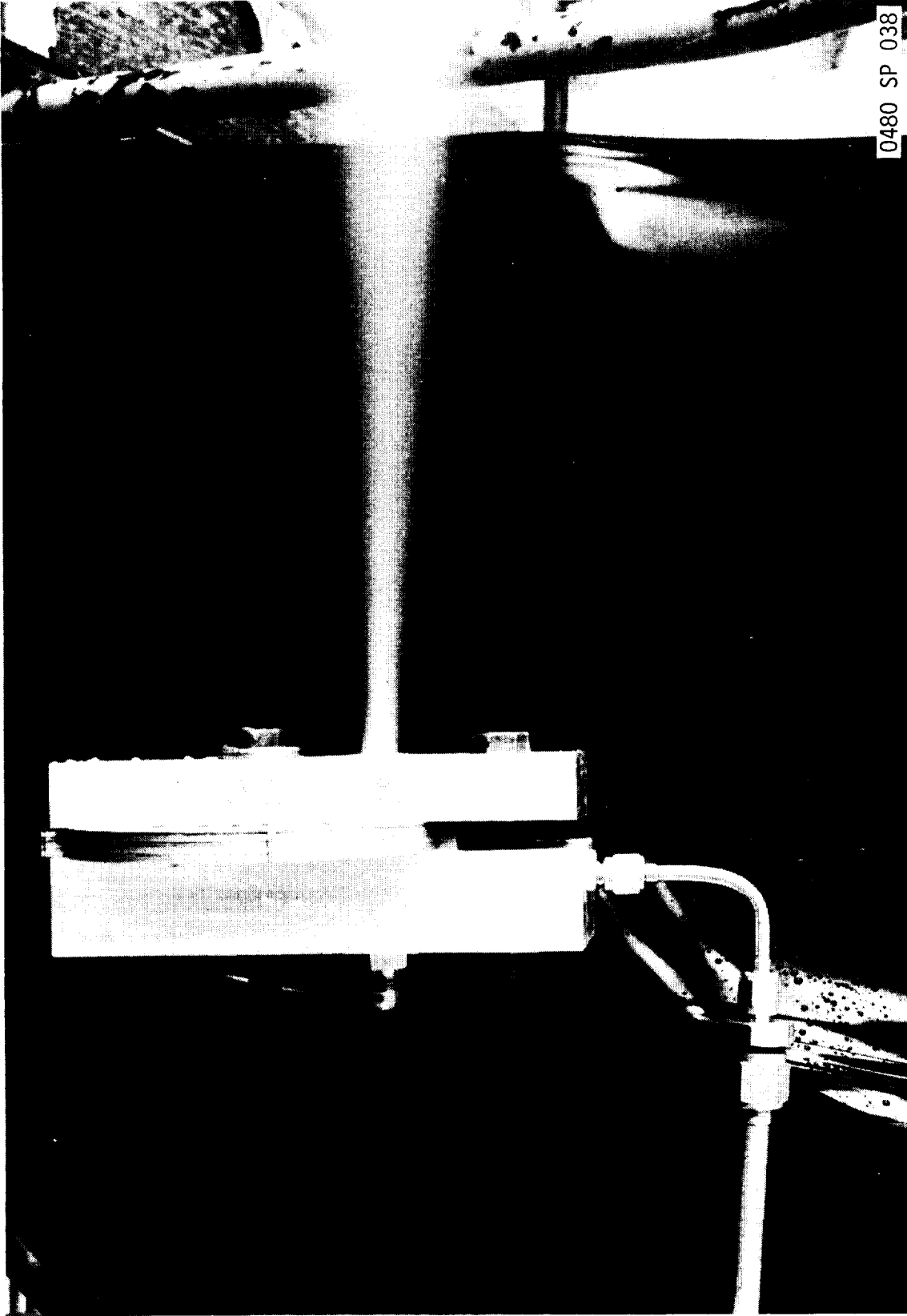
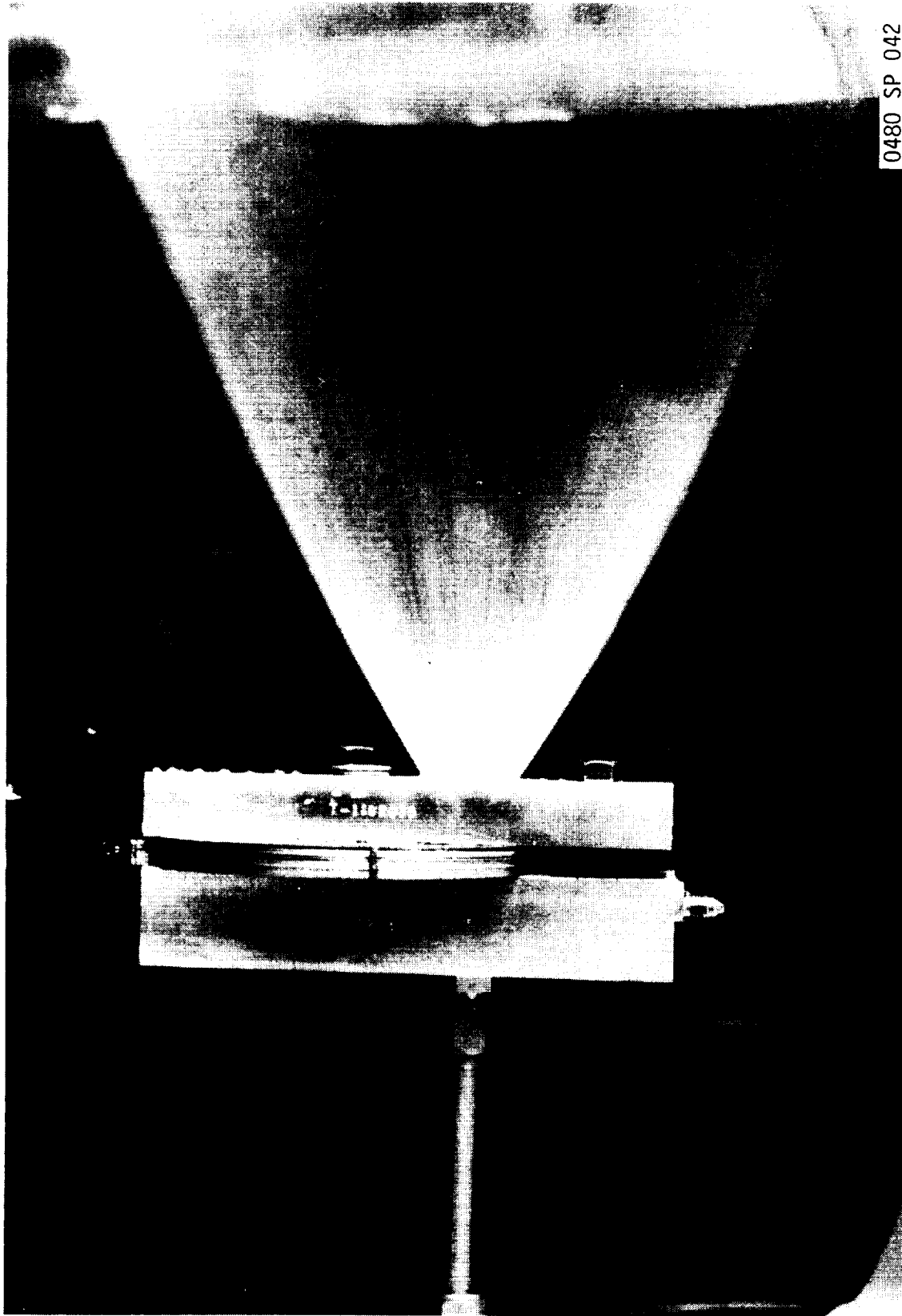


Figure VI-11. Fuel-Rich Vortex Injector Cold-Flow, Oxidizer Circuit,
 $\Delta P = 2.07M \text{ N/m}^2$ (300 psid), Design Mod. 3, Single-Element Flow

ORIGINAL PAGE IS
OF POOR QUALITY



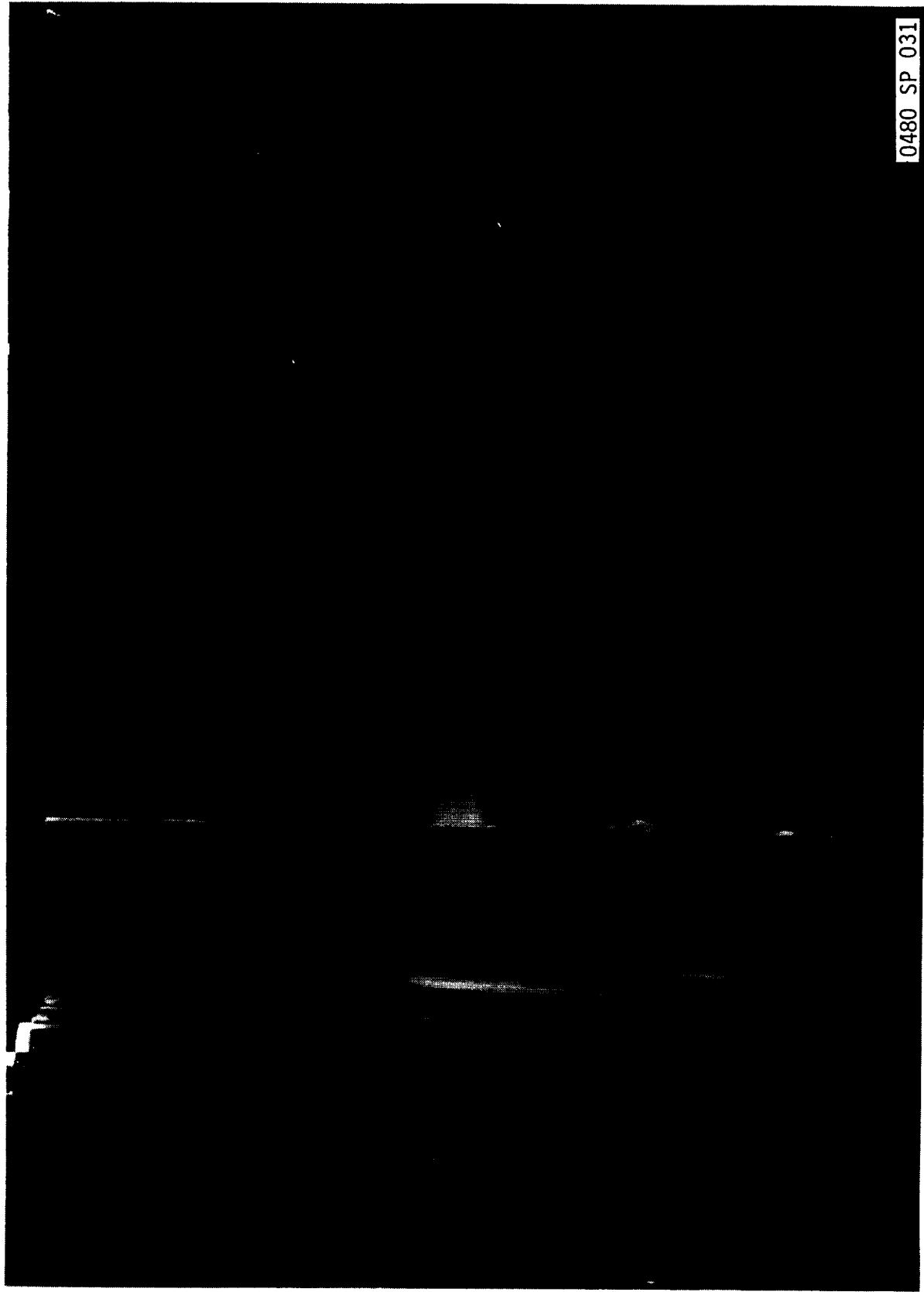
0480 SP 042

Figure VI-12. Fuel-Rich Vortex Injector Cold-Flow, Fuel Circuit,
 $\Delta P - 2.07M \text{ N/m}^2$ (300 psid), Design Mod. 3, Single-Element Flow

TABLE VI-II. - LOOSE STACK COLD-FLOW DATA FOR FUEL-RICH PLATELET INJECTOR SN-2

ΔP , kPa (psid)	<u>Fuel Circuit</u>			<u>Oxidizer Circuit</u>		
	1	2	3	1	2	3
689 (100)	0.0179 (0.0394)	0.0182 (0.0402)	0.0180 (0.0396)	0.00322 (0.00709)	0.00318 (0.0070)	0.00315 (0.00695)
1,378 (200)	0.0176 (0.0387)	0.0176 (0.0389)		0.00322 (0.00709)	0.00318 (0.0070)	
2,068 (300)	0.0176 (0.0387)	0.0177 (0.0391)	0.0179 (0.0394)	0.00318 (0.00700)	0.00318 (0.0070)	0.00319 (0.00703)
2,758 (400)	0.0168 (0.0371)	0.0176 (0.0387)		0.00323 (0.00713)	0.00318 (0.0070)	
Average		0.0177 (0.0390)			0.00319 (0.00703)	
Previous Unit Average		0.0161 (0.0354)			0.00340 (0.0075)	

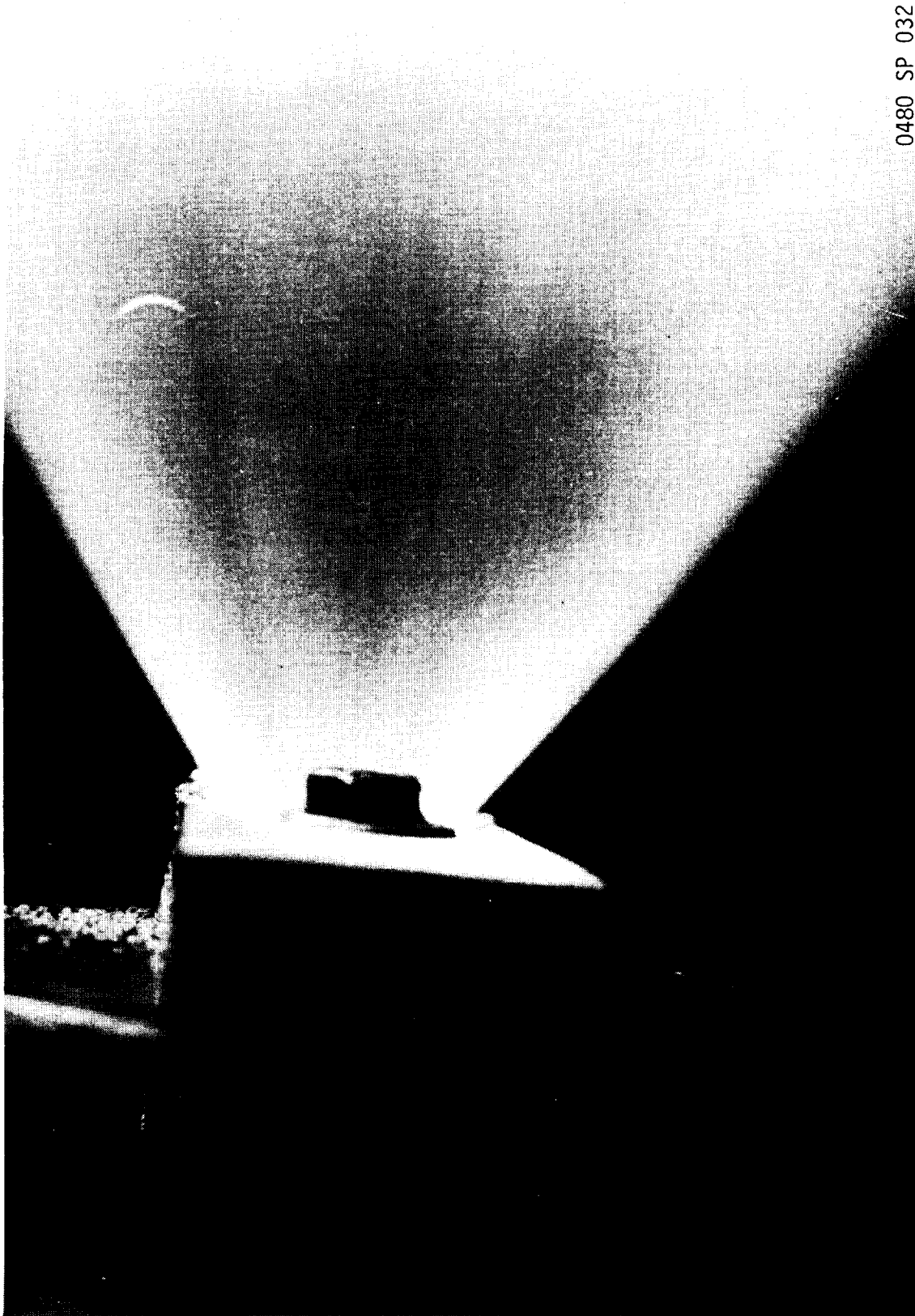
*Flow is measured in kg/sec (lb/sec)



0480 SP 031

Figure VI-13. Fuel-Rich Vortex Injector Cold-Flow, Oxidizer Circuit, $\Delta P = 2.07M \text{ N/m}^2$ (300 psid), Design Mod. 4, Single-Element Flow

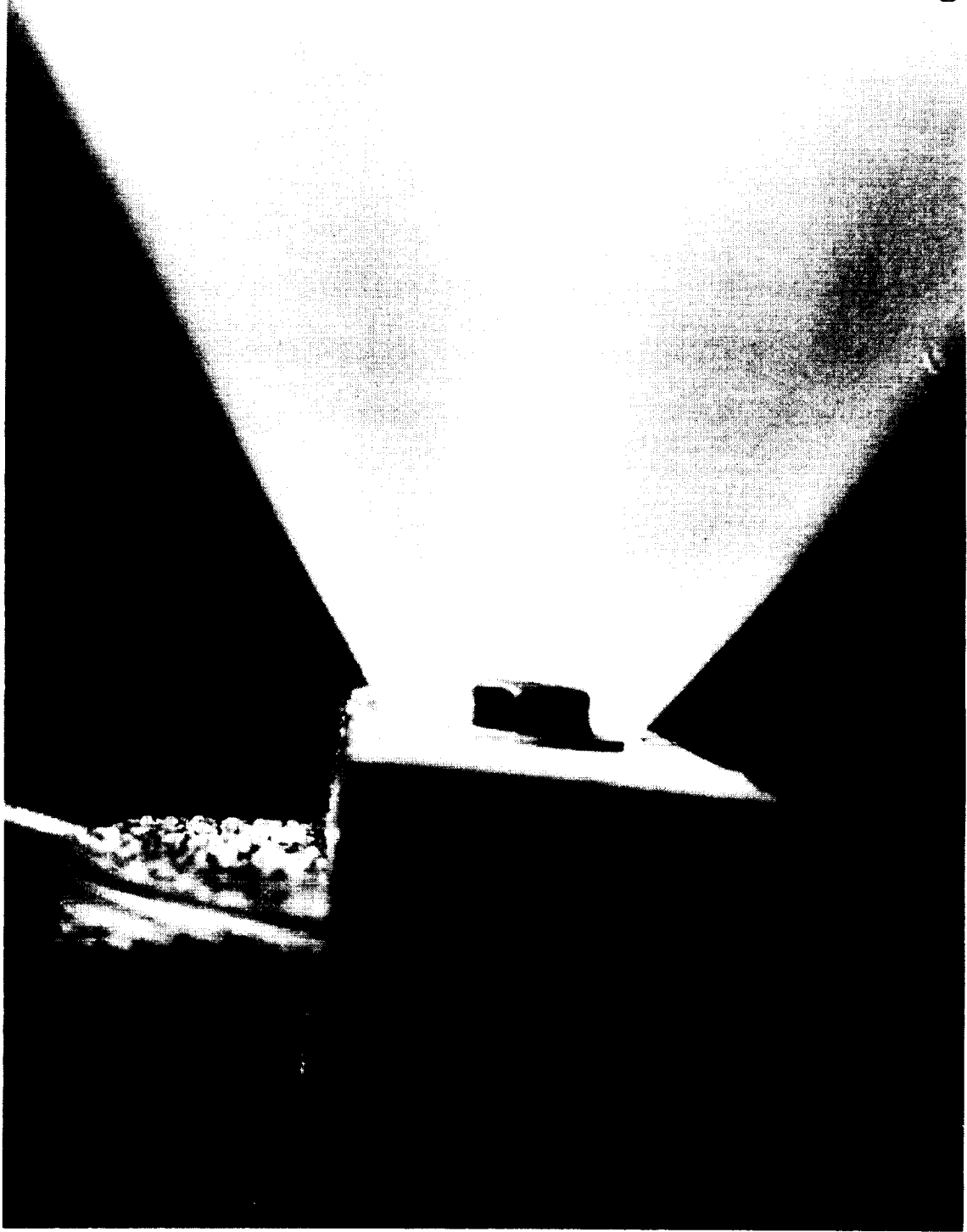
ORIGINAL PAGE IS
OF POOR QUALITY



0480 SP 032

Figure VI-14. Fuel-Rich Vortex Injector Cold-Flow, Fuel Circuit, ΔP - 2.07M
N/m² (300 psid), Design Mod. 4, Single-Element Flow

ORIGINAL PAGE IS
OF POOR QUALITY



0480 SP 033

Figure VI-15. Fuel-Rich Vortex Injector Cold-Flow, Both Circuits, $\Delta P = 2.07 \text{ N/m}^2$ (300 psid), Design Mod. 4, Single-Element Flow

VI, B, Loose Platelet Stack Cold-Flow Testing (cont.)

documented in Table VI-II. The element-to-element reproducibility is noted to be excellent. A comparative listing of the Kw's for the two sets is given below:

<u>Average Single Element Kw</u>					
	<u>First Set</u>		<u>Second Set</u>		
	kPa	(psid)	kPa	(psid)	
Oxidizer	0.0515	(0.00747)	0.0485	(0.00703)	- 6.2%
Fuel	0.2440	(0.0354)	0.2689	(0.0390)	+ 9.9%

C. FINAL INJECTOR ASSEMBLY COLD-FLOW TESTING

1. Objectives

The objectives of this task were as follows:

- a. Conduct pattern checks to determine that all orifices are open and flowing properly.
- b. Verify the spray angles or impingement accuracy in the case of the LOL doublets of the EDM'd patterns.
- c. Verify the pressure drop of the respective circuits.

2. Procedures

The procedures employed in these tests are identified in Figure VI-16. A photograph of a typical setup is shown in Figure VI-17.

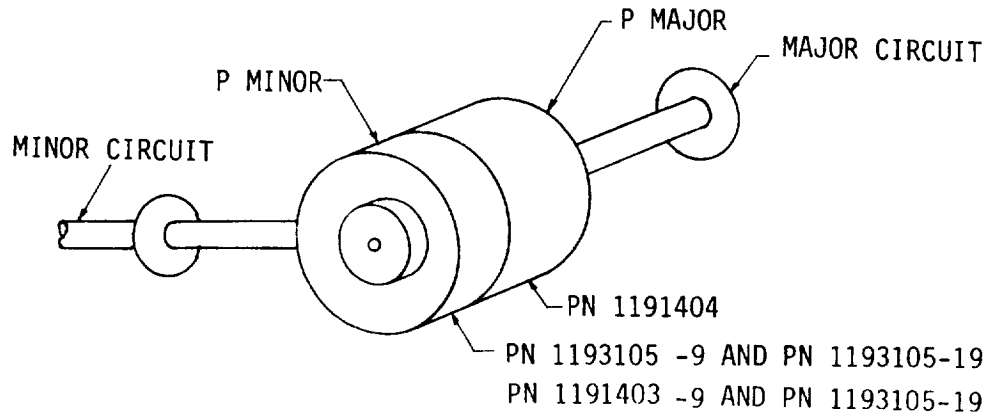
3. Results

- a. Fuel-rich EDM'd Injector (PN 1193105-9)

This injector was cold-flowed as per the procedures of Figure VI-16.

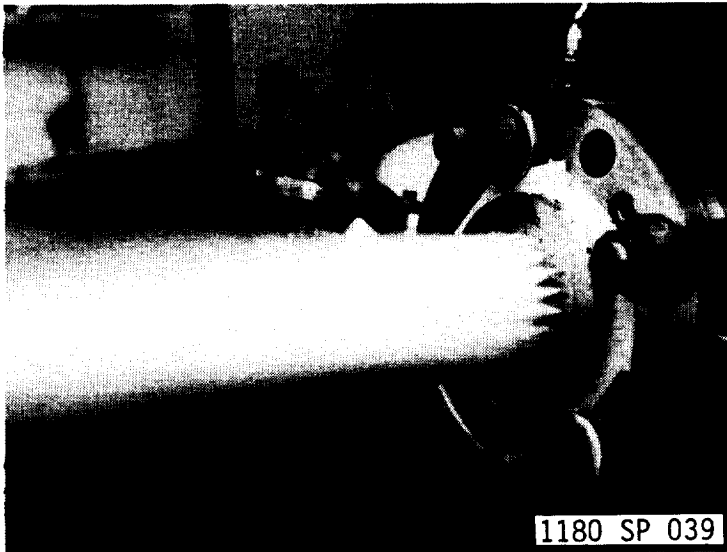
The pattern check showed that all elements were properly aligned and flowing as expected. Photographs of the spray patterns are shown in Figure VI-17.

The pressure drop/flow relation obtained for the fuel-rich EDM'd injector is recorded in the following table:



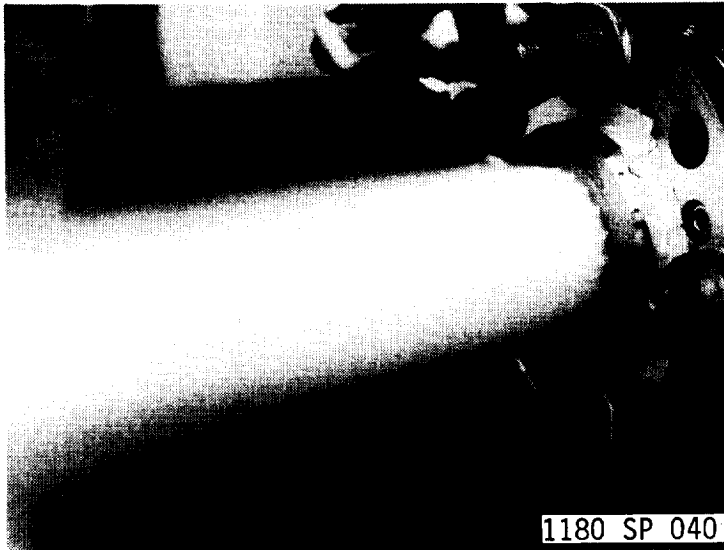
1. Back-flush all manifolds to remove dirt and chips.
2. Plug ports with proper fittings and caps.
3. Pressurize oxidizer circuit to 138 kPa (20 psia) and visually inspect each orifice for flow angle and uniformity.
 Note: Center holes are low flow for LOL design
 Document any holes which are not flowing properly.
4. Measure \dot{w} versus ΔP minor flow circuit
 ΔP values are to be between 689 and 2758 kPa (100 and 400 psia).
5. Photograph minor circuit at maximum practical pressure.
 Record negative # and flow pressure.
Look for leaks or misdirected streams.
6. Flow major circuit at = 68.9 kPa (10 psia) and inspect pattern for impingement uniformity and obstructions.
 All holes should flow the same.
 Document obvious problems, if any.
7. Flow at 3 pressures up to maximum facility capability (max. \dot{w} 9 kg/sec (20 lb/sec) expected).
8. Photograph fuel circuit spray at maximum practical pressure.
Look for leaks and misdirected streams.
9. Connect 2-cm (0.5-in.) flexure line between fuel and oxidizer lines and flow both circuits together.
 Photograph both sprays at maximum practical flowrate.
10. Review data with project engineer.

Figure VI-16. Cold-Flow Procedures for All Injector Assemblies

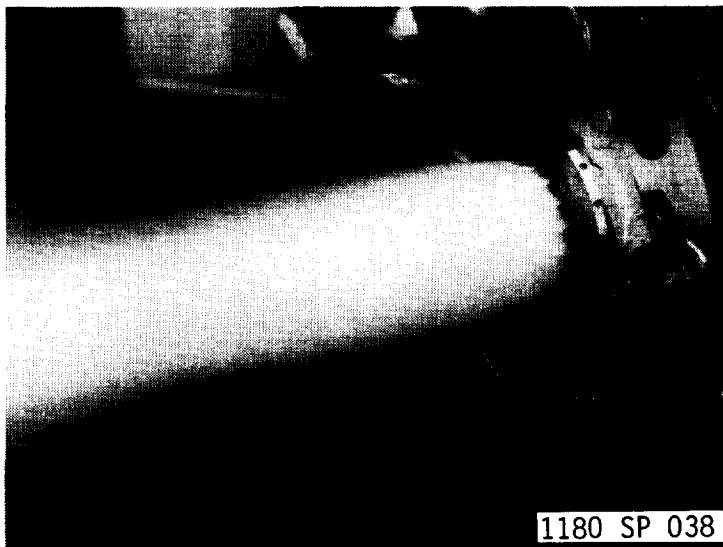


INJECTOR
(Oxidizer Circuit, Fuel
Circuit, Both Circuits)

Oxidizer Circuit Only
2758 kPa (400 psi)



Fuel Circuit Only
827 kPa (230 psi)



Both Circuits
689 kPa (100 psi)

ORIGINAL PAGE IS
OF POOR QUALITY

Figure VI-17. LOL - EDM'd Fuel-Rich Injector Cold-Flow (Oxidizer Circuit, Fuel Circuit, Both Circuits)

VI, C, Final Injector Assembly Cold-Flow Testing (cont.)

K_w is defined as $\frac{\dot{w}}{\sqrt{\Delta P} S_g}$

where ΔP is the pressure drop in kPa (psid)
 S_g is the specific gravity of the flow medium (1.0 water)

Fuel Side

ΔP Pfj kPa (psid)	\dot{w} kg/sec (lb/sec)	$K_w = \frac{\dot{w}}{\sqrt{\Delta P} S_g}$
172 (25)	4.13 (9.1)	1.820
300 (43.5)	5.49 (12.1)	1.835
410 (59.5)	6.35 (14)	1.815
855 (124)	8.94 (19.7)	1.769 (meter over scale)
558 (81)	7.48 (16.5)	1.833

Oxidizer Side

ΔP (Poj) kPa (psid)	\dot{w} kg/sec (lb/sec)	K_w
3130 (454)	2.91 (6.42)	0.301
665 (96.5)	1.36 (3.0)	0.305
114 (16.5)	0.54 (1.2)	0.295

The flow coefficient of the fuel circuit was found to be 1.82, which compares to a calculated value of 1.66. This translates to an effective orifice Cd of 0.93 for the chamfered inlet compared to the predicted value of 0.85.

The expected oxidizer circuit K_w for the combined cross-feed channel and the orifice was 0.33. The measured value was 0.30.

VI, C, Final Injector Assembly Cold-Flow Testing (cont.)

Inspection of the oxidizer EDM holes indicated that the actual orifice size was 0.1003 cm (0.0395 in.) compared to the nominal value of 0.0181 cm (0.040 in.). This would reduce the expected Kw value to approximately 0.32. The remaining difference can be accounted for by assuming a Cd of 0.64 for the short L/D orifice rather than the initial design value of 0.68.

The influence of the cross-flow velocity on the short L/D orifices was evaluated by collecting the flow from an individual 0.102 cm (0.040 in.) orifice in the outermost row of elements and an element which is of the same diameter and closest to the centerline. The individual orifice Kw's documented in the following table indicate that the cross velocity has no significant effect ($\approx 5\%$).

Data Point	1	2	3	4	Average
Outside	0.00432	0.00479	0.00458	0.00453	0.00456
Inside	0.00479	0.00482			0.00481

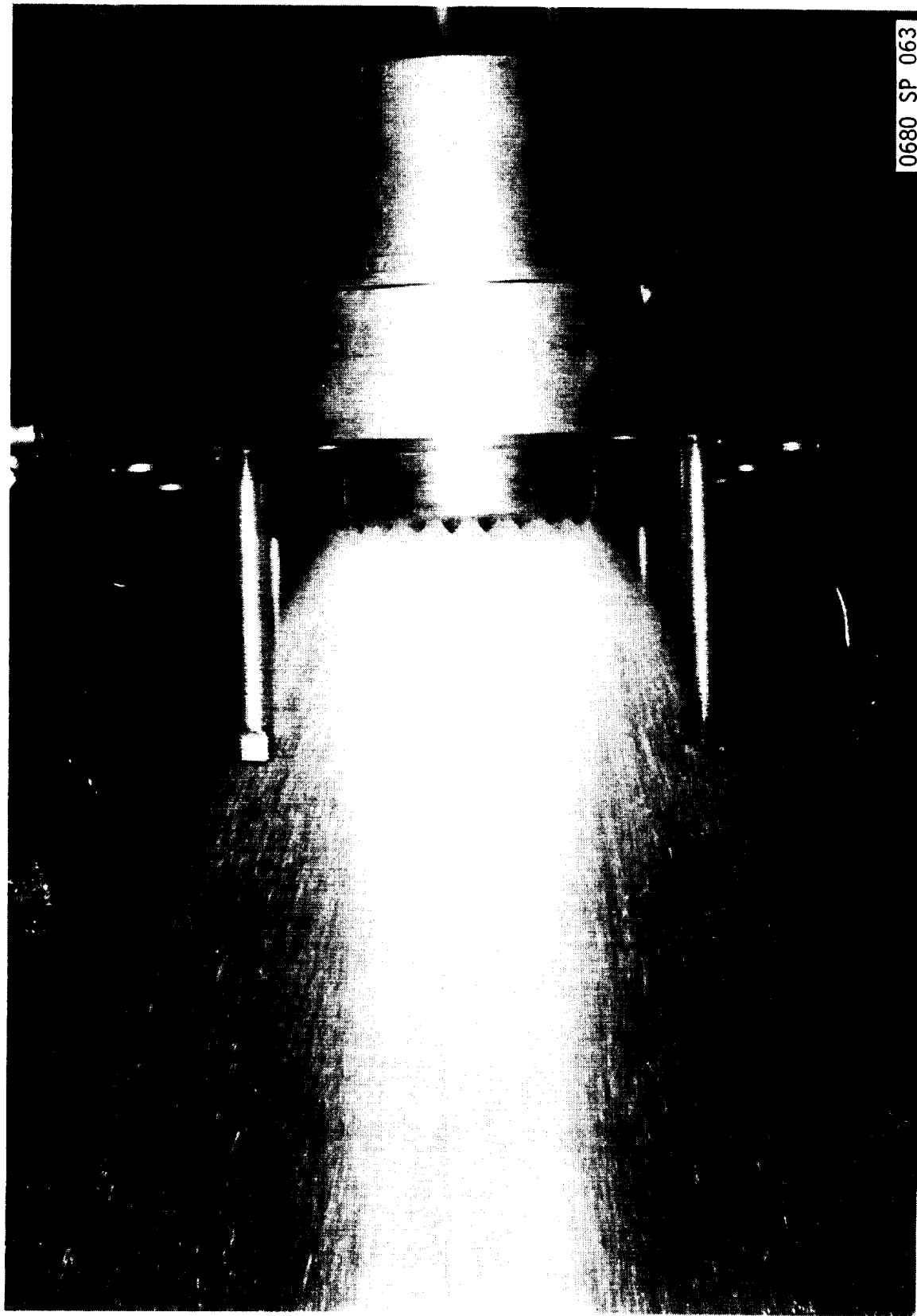
} = 5.3%

b. Fuel-Rich Platelet Injector (PN 1191403-39)

The flow procedures defined in Figure VI-16 were also employed for this injector.

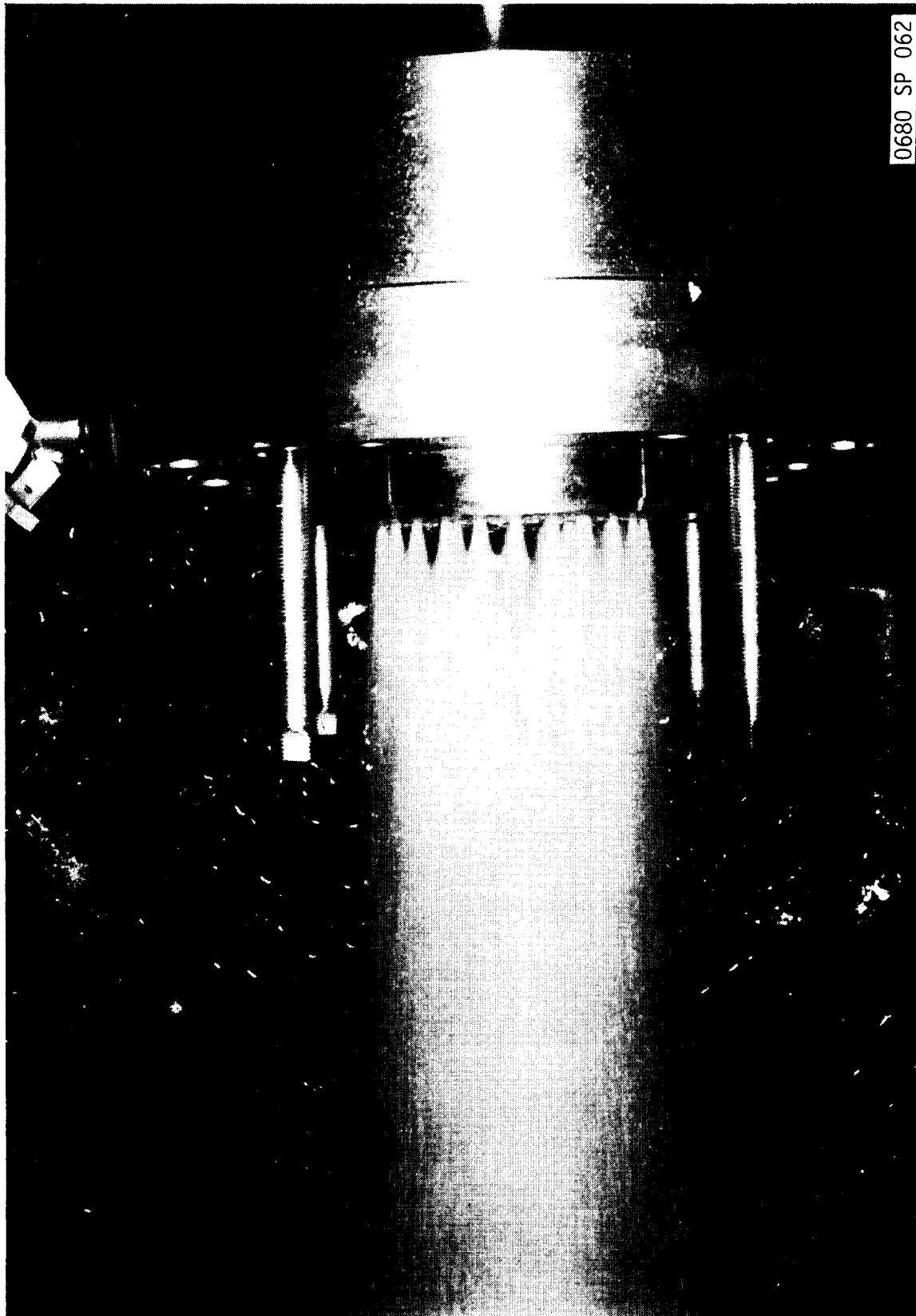
The initial pattern check indicated that six minor propellant flow circuit orifices in the intermediate row (every third hole) were not flowing. All other orifices of both the major and minor flow circuits were flowing properly. The photographs in Figures VI-18, -19, and -20 document the spray pattern of the major propellant flow, the minor propellant flow, and both circuits flowing together. The non-flowing orifices are not visible in these pictures. Table VI-III documents the pressure drop versus flowrate recorded in these tests. The Kw's for the major and minor propellant circuits were 1.79 and 0.347, respectively.

It was determined that the copper braze employed to join the platelet stack subassembly to the machined body was responsible for blockage of the six orifices. These holes were opened by chemically etching out the excess copper braze material. The minor propellant circuit was reflowed after the six holes were open, increasing the Kw by 14% as indicated in Table VI-III.



0680 SP 063

Figure VI-18. Fuel-Rich Injector Cold-Flow - Fuel Circuit



0680 SP 062

Figure VI-19. Fuel-Rich Injector Cold-Flow - Oxidizer Circuit

ORIGINAL PAGE IS
OF POOR QUALITY



Figure VI-20. Fuel-Rich Injector Cold-Flow - Both Circuits

TABLE VI-III. - FUEL-RICH INJECTOR COLD-FLOW DATA (PN 1191403-39)

Initial Cold Flow (6 holes not flowing)

<u>Oxidizer Circuit</u>	ΔP kPa	(psid)	\dot{w} kg/sec	(lb/sec)	Kw
	165.5	(24)	0.762	(1.68)	0.343
	344.7	(50)	1.089	(2.40)	0.339
	579.1	(84)	1.474	(3.25)	0.355
	696.3	(101)	1.619	(3.57)	0.355
	68.9	(10)	0.499	(1.1)	0.348
	34.5	(5)	0.037	(0.81)	0.362
	103.4	(15)	0.599	(1.32)	0.341
	137.9	(20)	0.680	(1.50)	0.355
Average					<u>0.347</u>
<u>Fuel Circuit</u>	344.7	(50)	5.81	(12.8)	1.81
	689.4	(100)	8.07	(17.8)	1.78
	896.2	(130)	9.25	(20.4)	1.79
	1,344.0	(195)	11.35	(25)	<u>1.79</u>
Average					1.79
Projected from loose-stack flow data					1.82
Reflow after opening 6 holes					
<u>Oxidizer Circuit</u>	68.9	(10)	0.567	(1.25)	0.395
	137.9	(20)	0.794	(1.75)	0.391
	344.7	(50)	1.234	(2.72)	0.385
	517.1	(75)	1.588	(3.50)	0.404
	689.4	(100)	1.814	(4.00)	<u>0.400</u>
Average					0.395
Projected from loose-stack flow data					0.39

VI, C, Final Injector Assembly Cold-Flow Testing (cont.)

A post-etching leak check revealed that the chemical etching had resulted in a small interpropellant leak at the braze joint.

The injector stack was parted at the bond line and reconstructed. The reconstruction procedures are defined in Section V of this report. Cold-flow data from the reconstructed assembly showed no measurable change in the pressure drop versus flow relation.

c. Oxidizer-Rich Platelet Injector (PN 1191403-39)

The cold-flow activities on this part paralleled those of the fuel-rich design. Thirteen of the minor propellant orifices were found to be plugged in this part, with the plugging appearing to be random. The smaller orifice size in the oxidizer-rich design was responsible for the more extensive plugging. These holes were chemically etched open prior to further flow testing.

Figures VI-20, -21, and -22 provide photographs of the spray cones for the oxidizer only, fuel only, and oxidizer and fuel flowing together. Visual inspection indicated that the spray cone angles were identical to those of the loose stack.

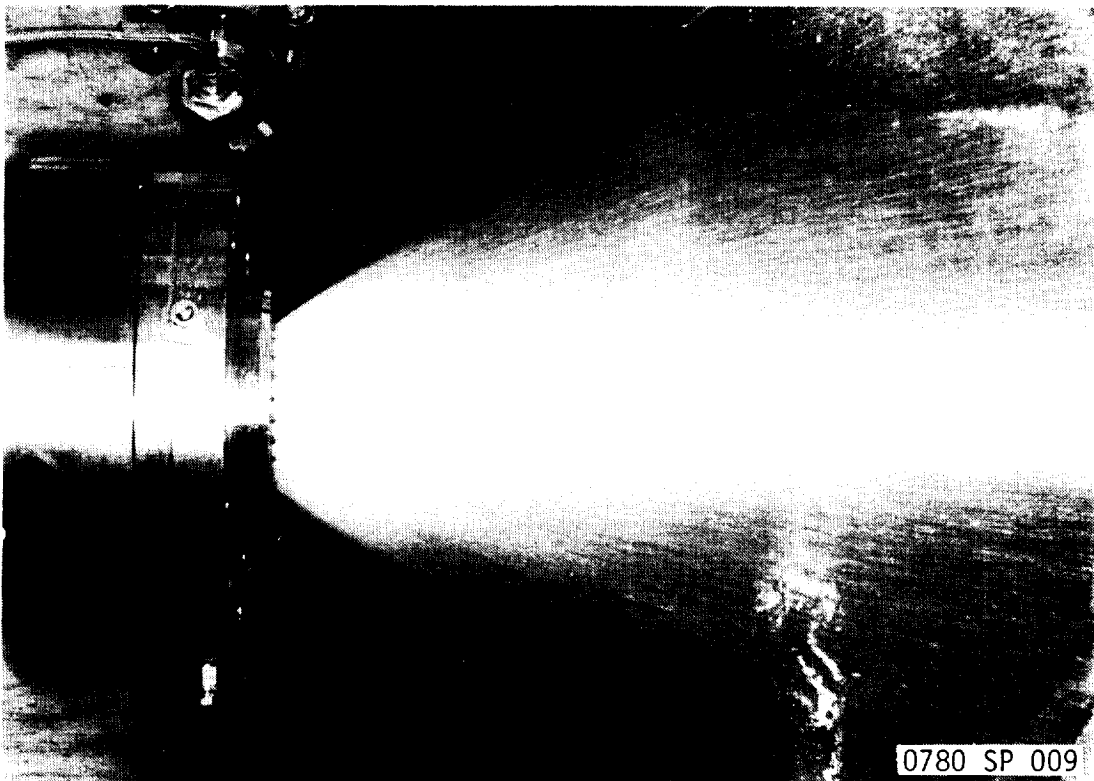
Table VI-IV documents the hydraulic characteristics of this design after the thirteen obstructed orifices were chemically cleaned. These data were further compared to the values calculated from the loose-stack data and found to be in good agreement. The pressure drops for this injector are predicted to be as follows:

Oxidizer Circuit	3109 kPa at 38.6 kg/sec (451 psid at 85 lb/sec)
Fuel Circuit	2723 kPa at 0.943 kg/sec (395 psid at 2.08 lb/sec)

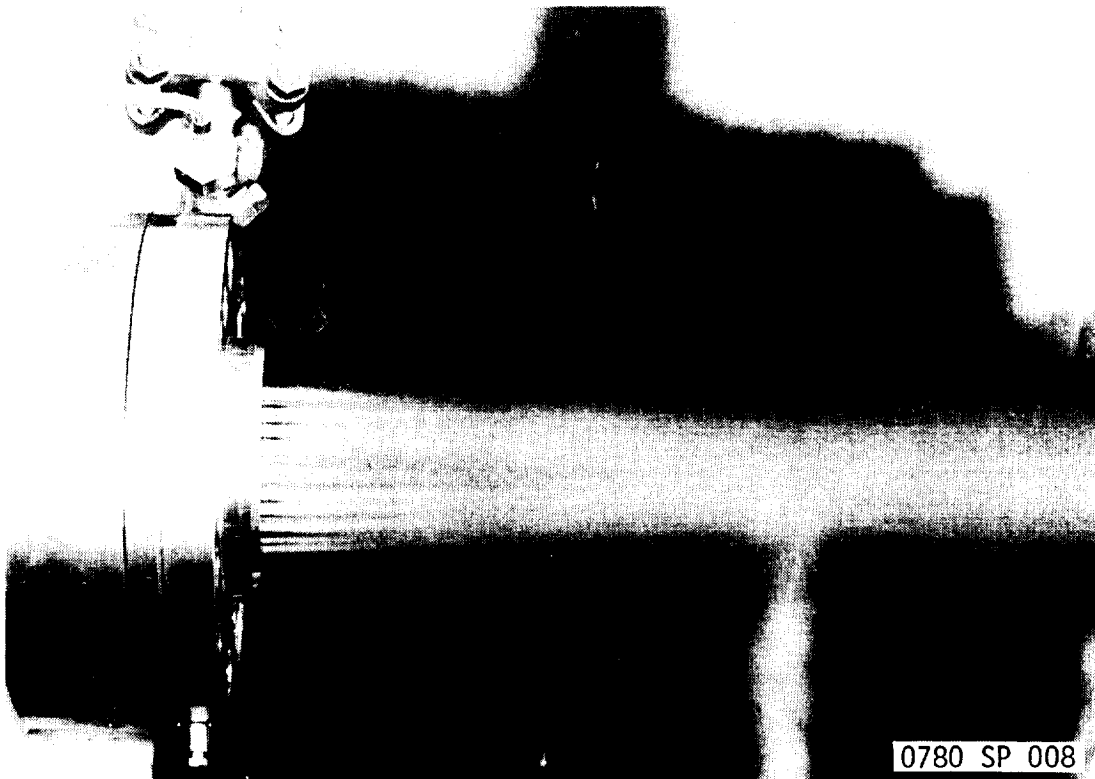
d. Oxidizer-Rich EDM'd Injector (PN 1193105-19)

The flow-check procedures for this injector were the same as before. Figures VI-23 and -24 provide photographs of the spray pattern. Table VI-V defines the measured flow versus pressure drop. The maximum facility flowrate was 8.2 kg/sec (18 lb/sec). The flow versus pressure drop and spray patterns were as predicted.

The variation in Kw of the fuel circuit is due to the onset of cavitation when the injector is flowed exhausting to atmosphere. The expected Kw under hot-fire operation will be 0.099 or slightly higher.



Ox Circuit Only (Major)



Fuel Circuit Only (Minor)

Figure VI-21. Oxidizer-Rich Vortex Injector - Oxidizer Circuit (Major);
Fuel Circuit (Minor)

ORIGINAL PAGE IS
OF POOR QUALITY



0681 SP 013

Figure VI-22. Oxidizer-Rich Vortex Injector - Both Circuits
Fuel $\Delta P = 689$ kPa (100 psi); Ox $\Delta P = 82.6$ kPa (12 psi)

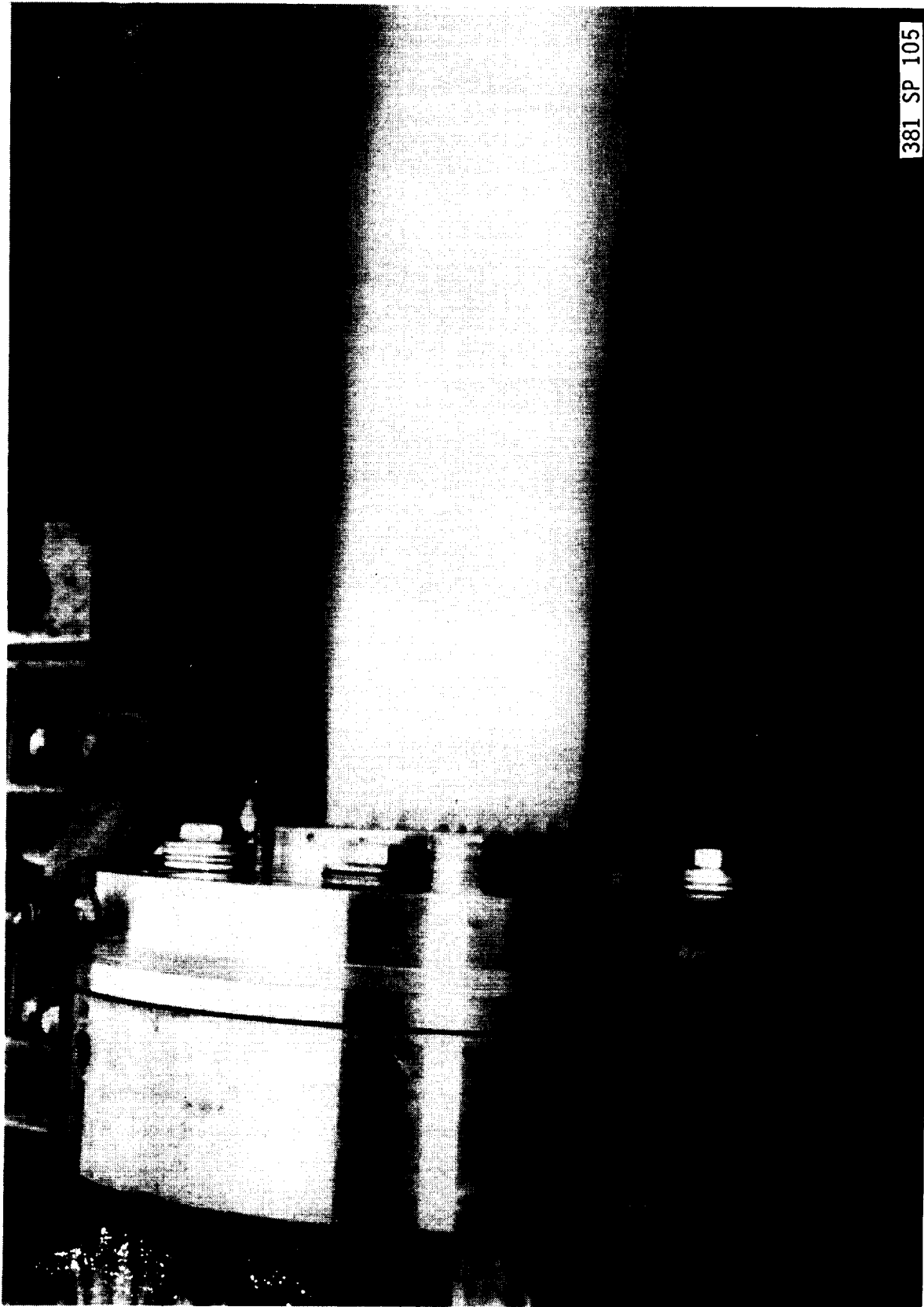
TABLE VI-IV. - OXIDIZER-RICH PLATELET INJECTOR COLD-FLOW DATA (PN 1191403-39)

Fuel Circuit after all holes were open:

ΔP kPa	(psid)	\dot{w} kg/sec	(lb/sec)	Kw
1,468	(213)	0.249	(0.55)	0.119
207	(30.0)	0.295	(0.65)	0.119
3,447	(500)	0.376	(0.83)	0.117
414	(60.0)	0.413	(0.91)	0.118
1,724	(250)	0.785	(1.73)	0.109
207	(30)	0.295	(0.65)	0.119
345	(50)	0.376	(0.83)	0.117
Average				0.117
Projected from single-element loose stack				0.115

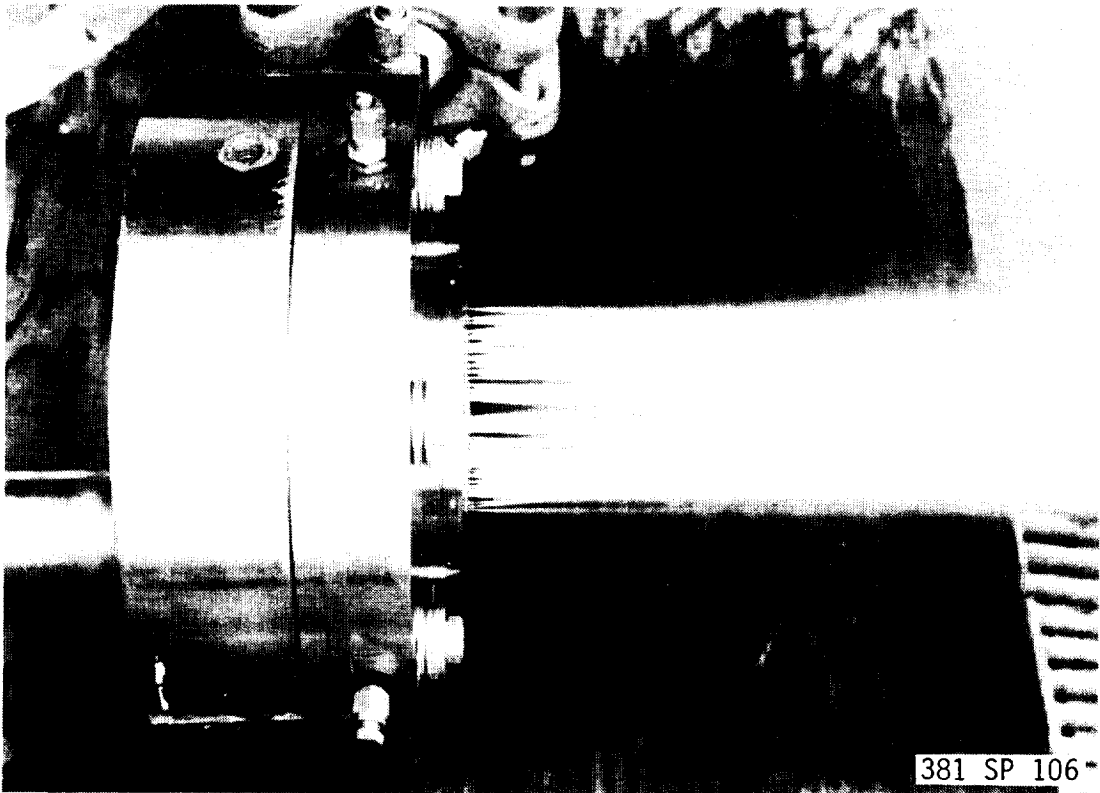
Oxidizer Circuit with all elements flowing:

ΔP kPa	(psid)	\dot{w} kg/sec	(lb/sec)	Kw
62	(9)	5.22	(11.5)	3.967
110	(16)	6.89	(15.2)	3.800
138	(20)	7.48	(16.5)	3.690
179	(26)	8.30	(18.3)	3.589
207	(30)	9.16	(20.2)	3.688
241	(35)	10.02	(22.1)	3.736
276	(40)	10.52	(23.2)	3.668
Average				3.734
Projected from single-element loose stack				3.89

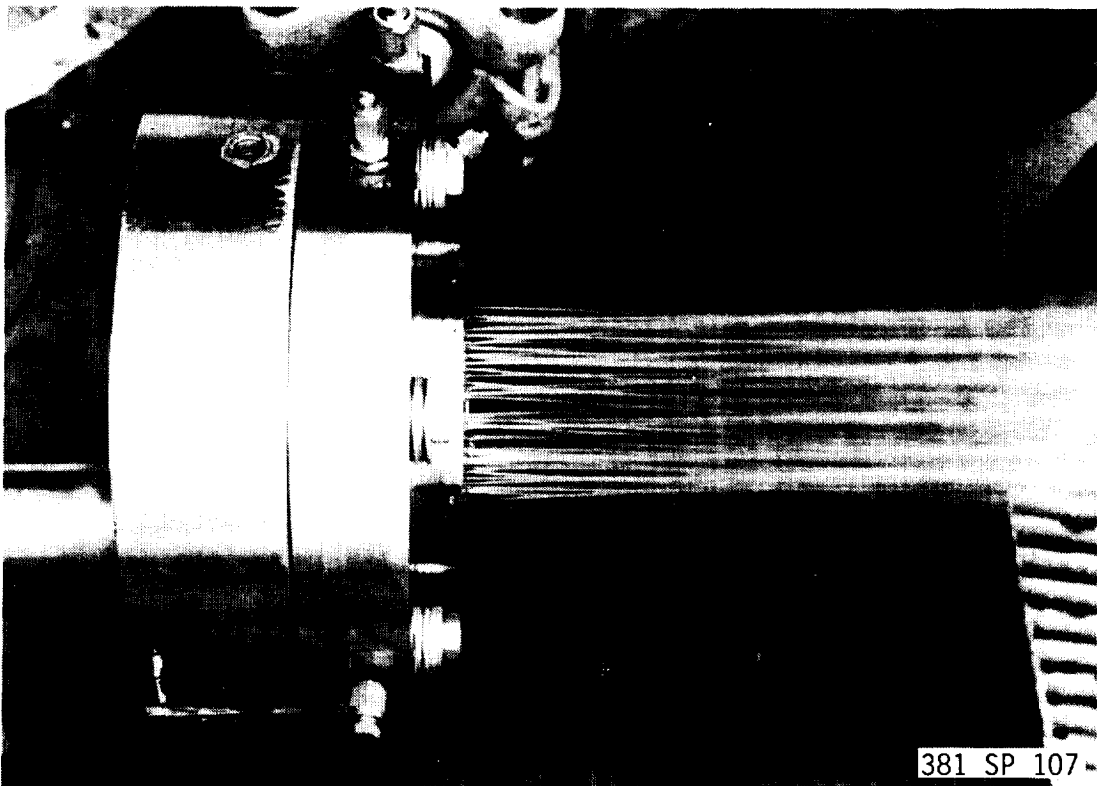


381 SP 105

Figure VI-23. LOL Oxidizer-Rjch Injector, Oxidizer Circuit,
 $\Delta P = 0.15M N/m^2$ (22 psid)



Fuel Circuit, $\Delta P = 689 \text{ kPa}$ (100 psid)



Fuel Circuit, $\Delta P = 345 \text{ kPa}$ (50 psid)

Figure VI-24. Oxidizer-Rich LOL Injector Cold-Flow (Fuel Circuits Only)

TABLE VI-V. - LOL OXIDIZER-RICH INJECTOR COLD-FLOW DATA

	ΔP		\dot{w}		Kw
	kPa	(psid)	kg/sec	(lb/sec)	
Oxidizer Circuit	148.9	(21.6)	8.30	(18.3)	3.94
	86.2	(12.5)	6.40	(14.1)	3.99
	42.7	(6.2)	4.54	(10)	4.02
Fuel Circuit	188	(27.2)	0.235	(0.518)	0.099
	378	(54.9)	0.303	(0.668)	0.090
	738	(107)	0.402	(0.887)	0.086
	1,124	(163)	0.490	(1.08)	0.085
	1,462	(212)	0.558	(1.23)	0.084
	2,854	(414)	0.771	(1.70)	0.085
	4,247	(616)	0.938	(2.07)	0.084

VI, Cold-Flow Testing (cont.)

D. TURBINE SIMULATOR COLD-FLOW TESTING

1. Objectives

The objectives of the cold-flow testing of these components were to a) establish the proper turbine simulator blade spacing to provide the desired pressure drop, b) measure the flow characteristics of the main injector simulator, c) establish sensitivity curves of ΔP versus area for the turbine simulator, and d) determine the influence of these components on the throat Cd.

2. Setup

The preburner assembly and the flow schematic are shown in Figures VI-25 and -26, respectively. Dry GN₂ was supplied from a cascade at pressures of 3447 to 10,341 kPa (500 to 1500 psia). The flowrates were measured by an NBS traceable critical flow nozzle. Upstream temperature and pressure measurements and critical flow nozzle flow calibration curves were employed to calculate the GN₂ flowrate.

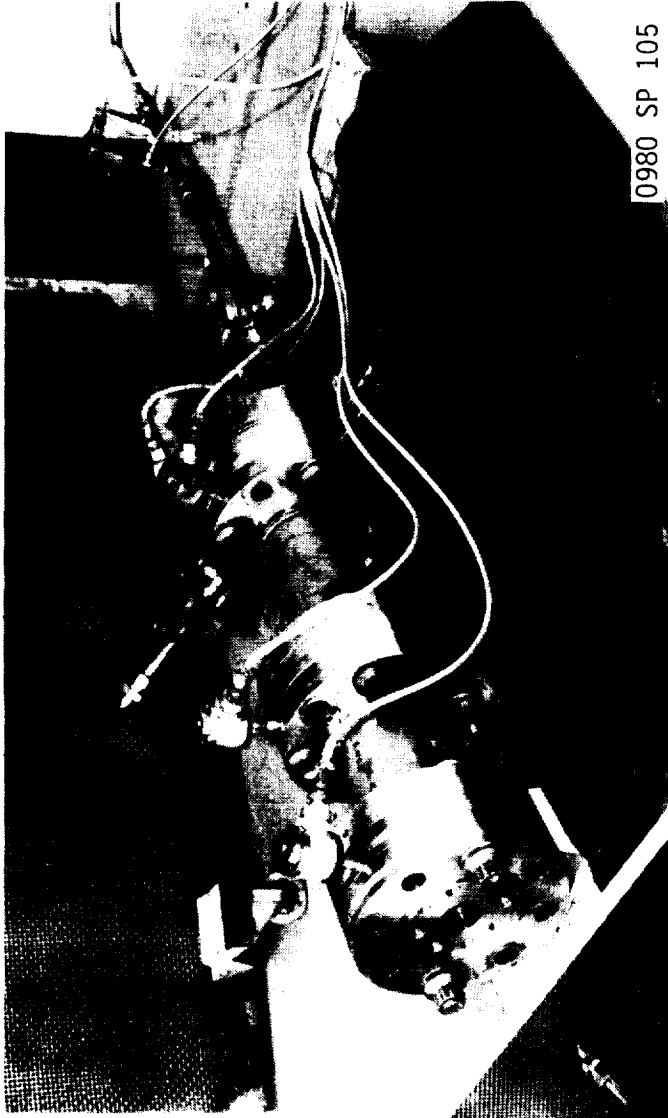
Additional pressure and temperature measurements were made using calibrated 172 and 345 kPa (25 and 50 psia) Class I pressure transducers at the locations shown in the flow schematic figures and photographs. Data were recorded on a digital recording system which provided an average of approximately 40 readings per instrument channel over a 2-sec period.

Each test consisted of four different flowrate conditions. The flowrate was adjusted by varying the GN₂ supply pressure.

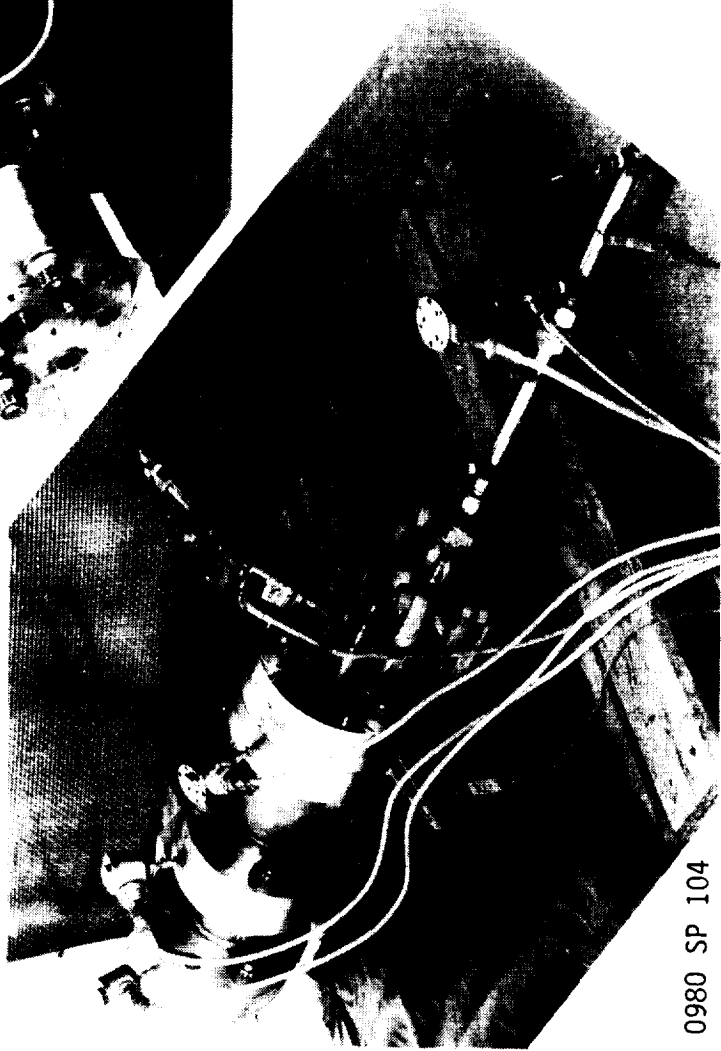
3. Test Procedures and Summary

The flow area in between the turbine blades was adjusted by shimming the blades. The area was reduced in successive tests until the desired pressure ratio was achieved. Table VI-VI identifies the thickness of the shims employed, plus the resulting gaps between blades. The gaps were determined by dropping 3.8-cm (1.5-in.) long gage pins between the blades. These gage pins were available in increments of 0.0025 cm (0.001 in.).

The flow area was calculated by using the maximum dimension pin which could be passed through each slot and the following nominal slot lengths:



0980 SP 105



0980 SP 104

Figure VI-25. Preburner Assembly Cold-Flow Test Setup

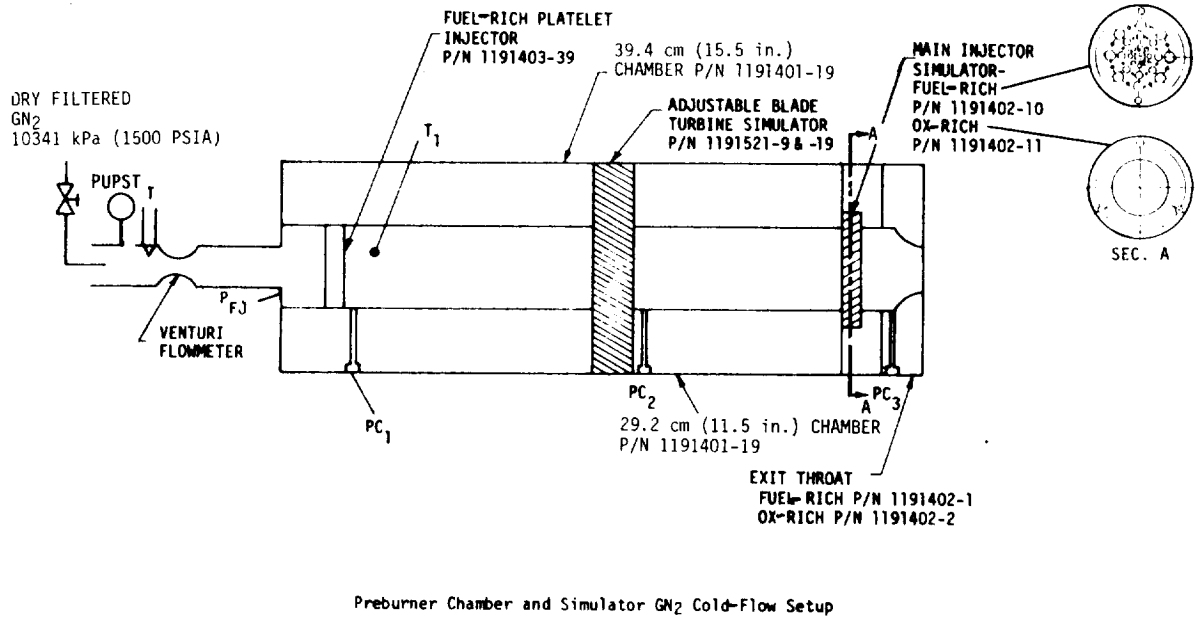
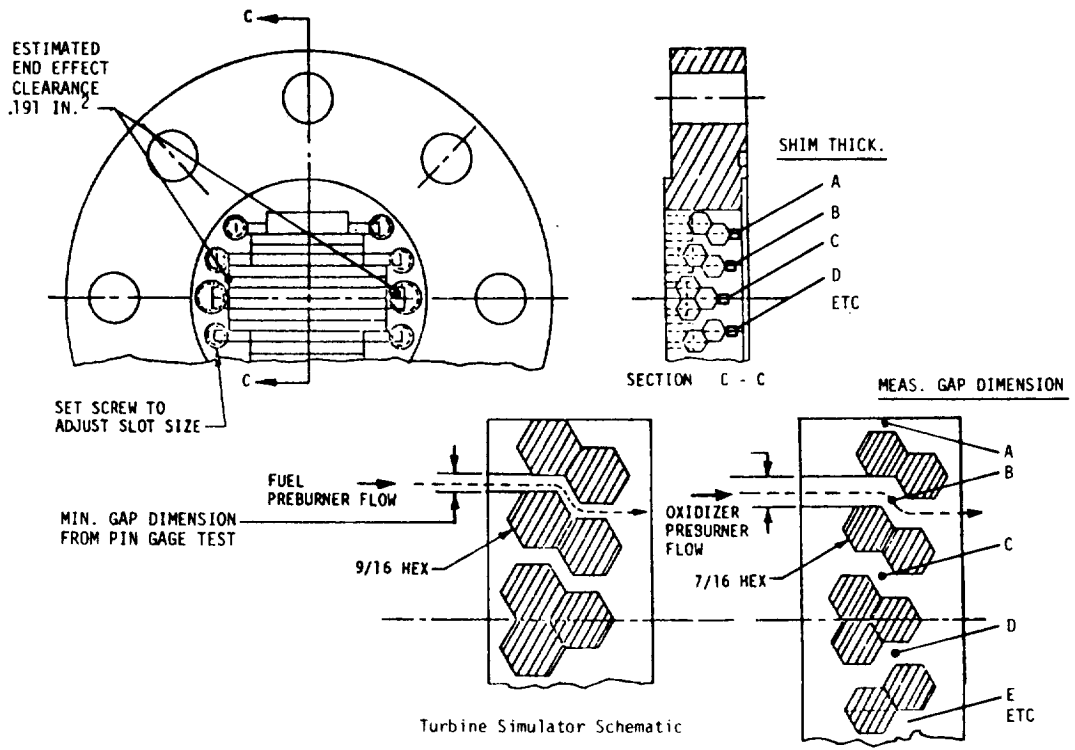


Figure VI-26. Preburner Assembly GN₂ Cold-Flow Setup Schematic

TABLE VI-VI(a) - TURBINE SIMULATOR COLD-FLOW TEST CONFIGURATIONS

Test No.	Configuration		Shim Thickness, (cm.)					Gap Width (cm.)					Total Area cm ² *	Open	
	Turb. Sim.	MIS** Throat	A	B	C	D	E	A	B	C	D	E			F
101	0-R	0-R	.191	.381	.419	.381	.485	.165	.800	.561	.538	.800	.211	24.84	29.7
102	0-R***	0-R	.191	.381	.419	.381	.485	.165	.800	.561	.538	.800	.211	24.81	29.7
102X	0-R	None	.191	.381	.419	.381	.485	.165	.800	.561	.538	.800	.211	24.81	29.7
103	0-R	0-R	.193	0	0	0	.465	.165	.584	.503	.488	.584	.211	20.74	24.8
104	F-R***	F-R	0	0	.168	0	0	.013	.488	.353	.356	.470	.076	15.12	15.1
105	F-R	F-R	.381	.051	0	.051	.381	.013	.257	.269	.269	.267	.076	10.37	12.4
106	F-R	None	.381	.051	0	.051	.381	.013	.257	.269	.269	.267	.076	10.37	12.4
107	F-R	F-R	.572	.132	0	.132	.572	.008	.163	.213	.208	.173	.076	7.93	9.48
108	F-R	F-R	.572	.183	0	.183	.572	.008	.203	.163	.175	.221	.076	7.75	9.26
109	F-R	None	.572	.183	0	.183	.572	.008	.203	.163	.175	.221	.076	7.75	9.26
Exh to atm															
110	Open	Open												1.201	9.26

*Includes 1.23 cm² (.19 in.²) gap on edges of blades

**MIS = Main Injector Simulator

***0-R/F-R = Oxidizer-Rich/Fuel-Rich

TABLE VI-VI(b) - TURBINE SIMULATOR COLD-FLOW TEST CONFIGURATIONS

Test No.	Configuration		Shim Thickness, (in.)					Gap Width (in.)					Total Area in. 2*	Open	
	Turb. Sim.	MIS Throat	A	B	C	D	E	A	B	C	D	E			F
101	O-R	O-R	.075	.150	.165	.150	.075	.065	.315	.221	.212	.315	.083	3.85	29.7
102	O-R	O-R	.075	.150	.165	.150	.075	.065	.315	.221	.212	.315	.083	3.85	29.7
102X	O-R	None	.075	.150	.165	.150	.075	.065	.315	.221	.212	.315	.083	3.845	29.7
103	O-R	O-R	.076	0	0	0	.075	.065	.230	.198	.192	.230	.083	3.215	24.6
104	F-R	F-R	0	0	.066	0	0	.005	.192	.139	.140	.185	.030	2.344	18.1
105	F-R	F-R	.150	.020	0.00	.020	.150	.005	.101	.106	.106	.105	.023	1.608	12.4
106	F-R	None	.150	.020	0.00	.020	.150	.005	.101	.106	.106	.105	.023	1.608	12.4
107	F-R	F-R	.225	.052	0.00	.052	.225	.003	.064	.084	.082	.068	.023	1.229	9.48
108	F-R	F-R	.225	.072	0.00	.072	.225	.003	.080	.064	.069	.087	.023	1.201	9.25
109	F-R	None	.225	.072	0.00	.072	.225	.003	.080	.064	.069	.087	.023	1.201	9.26
110	Open	Open	.225	.072	0.00	.072	.225	.003	.080	.064	.069	.087	.023	1.201	9.26

*Includes .191 in. 2 gap on edges of blades

VI, D, Turbine Simulator Cold-Flow Testing (cont.)

Slot A & F	5.08 cm (2.0 in.)
B & E	6.99 cm (2.75 in.)
C & D	9.53 cm (3.75 in.)

The clearance allowed for thermal expansion at the ends of the blades was estimated to be 1.23 cm^2 (0.19 in.^2).

The oxidizer-rich assembly was flowed first. Tests 101 through 103 of Table VI-VI identify the configuration of each buildup with respect to the components employed in each test.

The flowrates of Test 101 were too low to result in choked flow at the throat. Test 102 was a repeat test at higher flows. Test 102X was a repeat of 102, with the oxidizer main injector simulator (OMIS) removed from the flow stream.

Test 103 provided the required pressure drop with the indicated gap size.

Tests 104 through 110 were conducted using the fuel-rich assembly components. Test 106 was conducted with the fuel main injector simulator (FMIS) removed. Test 109 was conducted with the turbine simulator exhausting to atmosphere. Removal of the sections downstream of the turbine simulator (TS) had no effect on the upstream pressure. These results confirmed the hypothesis developed on Tests 104 through 108 that the turbine was flowing choked and that a high recovery shock existed on the downstream side of the turbine simulator. Test 110 was conducted with the TS and FMIS removed and only the throat section in place. Removal of the TS and FMIS was found to have a measurable influence on the throat Cd.

Table VI-VII documents the measured pressures, temperatures, and flowrates and the calculated pressure ratios based on measured static and corrected stagnation pressures. The static-to-stagnation pressure correction is defined in Figure VI-27, along with the nomenclature used in the cold flow.

4. Test Results

a. Throat Flow Data Analysis

The validity and consistency of the flowrate measurement technique was checked by computing the Cd of the throat section using the static Pc-1 measurement and the following actual measured diameters:

TABLE VI-VII(a) - COLD-FLOW TEST DATA SUMMARY*

Date	Run	PopST kPa	PFJ kPa	Pc-1 kPa	Pc-2 kPa	Pc-3 kPa	Tc-5 °K	Tc-1 °K	Mg kg/sec	(Pc-2) kPa	PFJ/PopST	Pc-1/PopST	(Pc-1/Pc-2)	(Pc-2/Pc-3)	Pc-2/Pc-3	Pc-1/Pc-2	Throat Cd	Choked Flow Cd A	Turn Flow Cd A		
9-25	0	98.11	100.96	101.25	101.46	101.23	304.3	289.2	0.465	122.2	.210	.218	1.151	.0745	.0804	1.385	.708*	1.385	1.385		
	-101A	2889	606.7	132.6	107.3	113.1	291.0	281.1	0.918	167.9	.211	.215	1.338	1.002	1.114	1.250	1.07	1.250	1.250		
	101B	5684	1197	209.9	156.2	151.1	293.4	277.4	1.252	223.8	.211	.213	1.352	1.035	1.155	1.263	1.07	1.263	1.263		
	101C	7741	1632	282.7	209.1	200.6	295.4	275.4	0.711	143.1	.209	.214	1.273	.9365	1.019	1.590	1.07	1.590	1.590		
	101D	4428	926.6	170.3	133.7	129.9	293.7	278.6													
	9-26	102A	9569	2025	350.9	258.5	248.2	284.0	260.0	1.577	276.4	.212	.213	1.357	1.022	1.139	1.269	1.05	1.269	1.269	
		102B	8749	1850	319.9	236.5	226.8	280.8	258.5	1.450	253.0	.211	.213	1.332	1.033	1.159	1.264	1.02	1.264	1.264	
		102C	8048	1699	293.7	217.1	208.2	278.8	257.3	1.339	232.3	.211	.211	1.315	1.006	1.139	1.267	1.02	1.267	1.267	
		102X	5271	1747	298.9	217.1	208.2	278.8	257.3	1.364	232.3	.211	.211	1.315	0.9006	1.000	1.287	1.04	1.287	1.287	
		103A	9583	2054	382.0	283.7	283.2	283.9	262.9	1.440	241.5	.211	.211	1.305	0.9834	0.910	1.407	1.04	1.407	1.407	
103B		9702	1837	346.8	255.9	240.0	286.6	276.9	1.440	241.5	.211	.211	1.305	0.9834	0.910	1.407	1.05	1.407	1.407		
103C		9600	1828	346.8	255.9	240.0	286.6	276.9	1.388	226.5	.211	.211	1.282	0.9339	0.816	1.407	1.06	1.407	1.407		
103D		9600	1828	346.8	255.9	240.0	286.6	276.9	1.217	210.9	.210	.210	1.217	0.8825	0.893	1.401	1.06	1.401	1.401		
103E		7431	1589	305.6	221.2	203.1	289.0	269.2													
103F		4888	1063	371.6	311.3	295.4	290.8	277.9	0.796	313.0	.218	.218	1.230	0.9595	0.9595	1.386	.988	1.386	1.386		
9-29	104A	4888	1063	371.6	311.3	295.4	290.8	277.9	0.905	346.1	.217	.217	1.242	0.9398	0.9398	1.217	.997	1.217	1.217		
	104B	5573	1209	421.2	333.7	332.8	292.6	275.4	0.852	332.3	.217	.217	1.232	0.9593	0.9593	1.188	.966	1.188	1.188		
	104C	5233	1133	395.0	320.5	313.7	291.0	274.2	0.725	286.8	.217	.217	1.232	0.9593	0.9593	1.157	.966	1.157	1.157		
	104D	4437	958.3	334.8	276.5	266.5	288.6	273.3													
	9-30	105A	3562	731.5	268.9	211.1	211.1	291.5	280.4	0.540	216.3	.215	.215	1.211	0.9720	0.9720	1.243	.980	1.243	1.243	
		105B	3655	797.0	292.4	259.1	259.1	291.5	278.7	0.596	234.9	.217	.217	1.241	0.9697	0.9697	1.242	.995	1.242	1.242	
		105C	4297	891.4	326.1	266.3	266.3	291.1	276.9	0.667	262.2	.216	.216	1.241	0.9674	0.9674	1.241	.996	1.241	1.241	
		105D	4314	939.7	343.8	269.4	269.4	290.6	275.7	0.704	276.0	.217	.217	1.241	0.9665	0.9665	1.241	.996	1.241	1.241	
		10-1	106A	3437	748.7	269.6	225.2	225.2	273.4	263.5	0.570	210.8	.215	.215	1.232	0	0	1.273	.967	1.273	1.273
			106B	3794	825.2	296.2	226.1	226.1	272.1	255.9	0.639	231.9	.217	.217	1.232	0	0	1.273	.967	1.273	1.273
106C			4061	882.4	315.9	242.1	242.1	272.7	258.6	0.683	247.4	.217	.217	1.232	0	0	1.273	.967	1.273	1.273	
106D			4362	947.2	338.6	259.4	259.4	273.4	257.9	0.733	265.2	.217	.217	1.232	0	0	1.273	.967	1.273	1.273	
10-2			107A	3229	716.3	289.5	224.9	224.9	284.1	274.8	0.526	208.2	.212	.212	1.241	0.645	0.645	1.290	.986	1.290	1.290
			107B	3592	794.9	320.2	226.4	226.4	286.4	274.2	0.590	230.3	.211	.211	1.241	0.647	0.647	1.290	.986	1.290	1.290
	107C		3937	870.7	349.9	247.4	247.4	288.9	278.2	0.633	251.8	.211	.211	1.241	0.648	0.648	1.290	.986	1.290	1.290	
	107D		4321	956.2	384.3	271.2	271.2	289.7	275.0	0.705	275.8	.221	.221	1.241	0.638	0.638	1.293	.996	1.293	1.293	
	108A		3222	713.5	290.9	202.7	202.7	290.0	278.9	0.519	206.1	.222	.222	1.435	0.0418	0.0418	1.412	.981	1.412	1.412	
	108B		3637	805.2	327.5	228.2	228.2	291.3	278.2	0.592	231.8	.222	.222	1.436	0.0418	0.0418	1.412	.981	1.412	1.412	
	108C	3938	863.1	353.7	246.5	246.5	292.4	275.2	0.639	250.5	.222	.222	1.436	0.0418	0.0418	1.412	.981	1.412	1.412		
	108D	4256	943.1	382.6	266.5	266.5	293.3	278.4	0.690	270.9	.221	.221	1.436	0.0418	0.0418	1.412	.981	1.412	1.412		
	10-2	109A	3229	716.3	289.5	224.9	224.9	284.1	274.8	0.526	208.2	.212	.212	1.241	0.645	0.645	1.290	.986	1.290	1.290	
		109B	3592	794.9	320.2	226.4	226.4	286.4	274.2	0.590	230.3	.211	.211	1.241	0.647	0.647	1.290	.986	1.290	1.290	
109C		3938	863.1	353.7	246.5	246.5	292.4	275.2	0.639	250.5	.222	.222	1.436	0.0418	0.0418	1.412	.981	1.412	1.412		
109D		4293	940.3	367.5	266.5	266.5	293.3	278.4	0.699	270.9	.221	.221	1.436	0.0418	0.0418	1.412	.981	1.412	1.412		
110A		3264	688.7	194.9	197.9	198.2	277.6	271.6	0.526	198.2	.211	.211	1.211	5.99	5.99	1.211	.972	1.211	1.211		
110B		3555	748.7	211.7	215.0	215.3	275.2	270.2	0.579	214.4	.211	.211	1.211	7.76	7.76	1.211	.971	1.211	1.211		
110C		3249	629.3	234.1	237.7	238.1	275.2	270.2	0.640	238.1	.210	.210	1.211	8.53	8.53	1.211	.971	1.211	1.211		
110D		4291	904.5	254.9	224.1	224.1	274.6	274.6	0.699	259.2	.211	.211	1.211	9.39	9.39	1.211	.971	1.211	1.211		

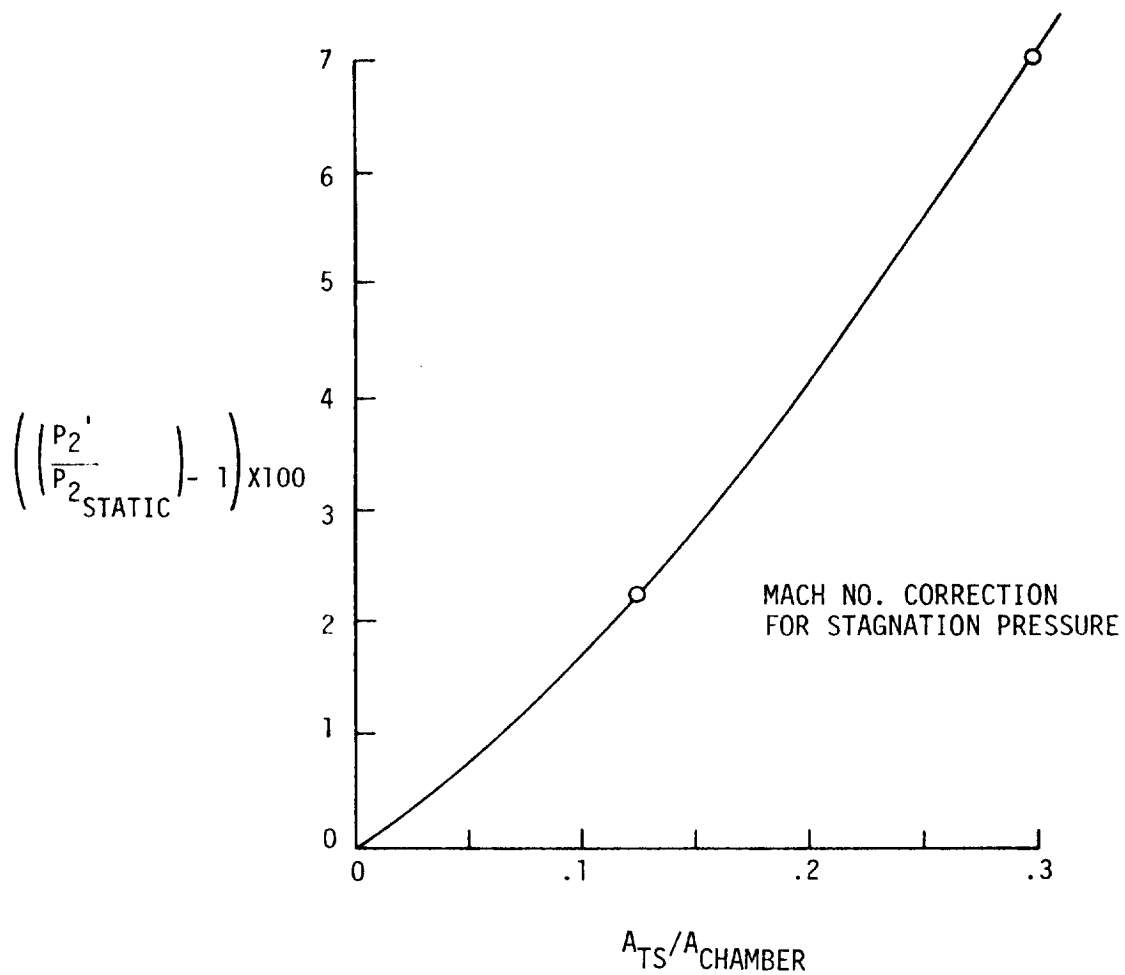
*Subsonic Flow

*See P. 225 for nomenclature

TABLE VI-VII(b) - COLD-FLOW TEST DATA SUMMARY*

Date	Run	PUPST psia	PFJ psia	PC-1 psia	PC-2 psia	PC-3 psia	TC-5 °F	TC-1 °F	Wg Lbm/sec	(PC-2) %	PFJ/PUPST	PC-1/PEJ	(PC-1/PC-2)	$\frac{(PC-2)-(PC-3)}{PC-2}$	$\frac{PC-2-PC-3}{PC-3}$	$\frac{PC-1}{PC-2}$	Throat Cd	Choked Flow Cd	Turb. Sim. Cd
9-25	0	14.2315	14.6444	14.6865	14.7171	14.6836	87.7	78.5											
	-101A	419.0	88.0	19.23	16.57	16.41	63.8	46.0	1.026	17.73	.210	.218	1.101	.0804	1.085	.706*			
	-101B	824.5	173.6	30.45	22.75	21.91	68.2	39.4	2.023	24.35	.211	.175	1.338	.1114	1.250	1.04			
	-101C	1122.8	236.7	41.0	30.33	29.1	71.7	35.7	2.760	32.46	.211	.173	1.352	.1155	1.035	1.07			
	-101D	642.3	134.4	24.7	19.4	18.84	68.7	41.2	1.567	20.76	.209	.184	1.273	.1019	1.190	.94*			
9-26	-102A	1388.1	293.8	50.9	37.5	36.0	51.2	9.0	3.477	40.1	.212	.173	1.357	.1139	1.269	1.05	2.673	.732	
	-102B	1269.1	268.3	46.4	34.3	32.9	45.5	5.3	3.197	36.7	.211	.173	1.353	.1035	1.264	1.02	2.832	.738	
	-102C	1167.4	246.5	42.6	31.5	30.2	41.9	3.1	2.951	33.7	.211	.173	1.352	.1039	1.264	1.02	2.853	.742	
	-102E	1199.8	253.4	43.35	31.47	33.68	51.1	13.3	3.006	33.68	.211	.171	1.378	0.0000	1.297	1.04	2.354	.742	
	-103A	1390.2	293.6	55.4	36.8	36.1	77.4	39.4	3.396	39.4	.211	.189	1.505	.0834	1.407	1.04	2.592	.806	
	-103B	1262.2	266.4	50.3	33.5	32.8	68.7	31.3	3.109	35.85	.211	.189	1.511	.0951	1.403	1.05	2.654	.813	
	-103C	1154.6	243.4	45.9	30.6	30.0	61.1	26.1	2.862	32.75	.211	.189	1.500	.0839	1.402	1.06	2.634	.820	
	-103D	1065.1	227.6	42.9	28.6	28.1	60.2	24.4	2.684	30.6	.210	.188	1.500	.0820	1.401	1.06	2.644	.823	
9-29	104A	709.0	154.2	53.9	43.7	42.85	63.5	40.3	1.755	45.4	.218	.349	1.232	.0595	1.188	.988	1.334	.59	
	104B	808.4	175.3	61.1	48.4	46.28	66.7	35.8	1.995	50.2	.217	.348	1.262	.0398	1.217	.997	1.355	.59	
	104C	759.0	164.4	57.3	46.5	45.5	63.8	33.6	1.878	48.2	.217	.348	1.232	.0593	1.198	.996	1.321	.59	
	104D	643.6	139.0	48.56	40.11	38.65	59.5	31.9	1.599	41.6	.216	.349	1.211	.0763	1.167	.998	1.321	.59	
9-30	105A	467.7	106.1	39.0	30.62	29.32	64.7	44.3	1.31	31.37	.218	.367	1.275	.0700	1.242	.980	1.271	.657	
	105B	531.6	115.6	42.41	33.29	31.89	64.5	41.6	1.315	34.08	.217	.367	1.274	.0687	1.242	.995	1.271	.657	
	105C	594.3	129.3	47.3	37.17	35.63	63.9	38.3	1.471	38.03	.218	.365	1.273	.0674	1.242	.996	1.271	.657	
	105D	626.8	136.3	49.8	39.16	37.54	63	36.3	1.552	40.04	.217	.365	1.272	.0666	1.241	.997	1.271	.657	
10-1	106A	498.5	108.6	39.1	29.86	30.57	32.1	14.2	1.257	30.57	.218	.360	1.309	0	1.279	.960	1.279	.657	
	106B	550.4	119.7	42.96	32.88	33.64	30.3	7.9	1.408	33.64	.217	.359	1.306	0	1.274	.997	1.274	.657	
	106C	589.	126.0	45.82	35.11	35.89	30.8	5.4	1.506	35.89	.217	.358	1.305	0	1.275	.998	1.275	.657	
	106D	632.7	137.4	49.11	37.65	38.47	32.1	4.3	1.616	38.47	.217	.358	1.305	0	1.275	.999	1.275	.657	
10-2	107A	468.4	103.9	42.0	29.72	28.37	51.4	34.7	1.159	30.2	.222	.404	1.413	.0645	1.390	.986	1.390	.976	
	107B	521.0	115.3	46.44	32.84	31.37	55.6	33.6	1.300	33.4	.221	.402	1.414	.0647	1.390	1.000	1.391	.991	
	107C	571.	126.3	50.75	35.88	34.28	60	35.4	1.418	36.5	.221	.401	1.414	.0648	1.389	.998	1.389	.988	
	107D	626.8	138.7	55.7	39.34	37.59	61.4	35	1.555	40.0	.221	.402	1.415	.0638	1.393	.998	1.393	.988	
	108A	467.3	103.5	42.2	29.40	28.14	62	42	1.144	29.9	.222	.408	1.435	.0418	1.412	.981	1.412	.964	
	108B	527.5	116.8	47.5	33.10	31.68	64.4	40.8	1.305	33.63	.221	.407	1.435	.0616	1.412	.994	1.412	.977	
	108C	570.7	126.5	51.3	35.75	34.21	66.4	41.2	1.409	36.33	.222	.406	1.436	.0620	1.411	.994	1.411	.977	
	108D	617.3	136.8	55.5	38.65	36.97	67.9	41.2	1.522	39.3	.221	.406	1.436	.0630	1.411	.993	1.411	.976	
10-2	109A	468.4	102.1	40.4			40.6	1.151			.219	.393	6.99					1.211	1.008
	109B	520.0	114.	44.7			38.7	1.292			.219	.392	7.76					1.225	1.023
	109C	571.2	125.2	48.9			38.6	1.414			.219	.390	8.53					1.229	1.023
	109D	622.7	136.4	53.3			37.6	1.540			.219	.391	9.29					1.228	1.022
	110A	473.4	99.9	28.27	28.71	28.75	39.6	1.159		28.75	.211							.972	
	110B	515.7	108.6	30.71	31.19	31.24	35.5	1.277		31.24	.211							.971	
	110C	471.3	120.3	33.95	34.48	34.54	35.4	1.511		34.54	.210							.971	
	110D	622.4	131.2	36.97	32.50	37.60	34.2	1.540		37.60	.211							.976	

*Subsonic Flow



NOMENCLATURE FOR COLD-FLOW TEST

- A = AREA IN.²
- P = STATIC PRESSURE
- p1 = STAGNATION PRESSURE
- T = TEMPERATURE, STATIC; T SUBSCRIPT = THROAT
- TS = TURBINE SIMULATOR
- OMIS = OX MAIN INJECTOR SIMULATOR
- FMIS = FUEL MAIN INJECTOR SIMULATOR
- M = MACH NO.
- J = INJECTOR
- Cd = FLOW COEFFICIENT
- Pupst = PRESSURE UPSTREAM OF VENTURI

Figure VI-27. Mach Number Corrections and Nomenclature for Cold-Flow Testing

VI, D, Turbine Simulator Cold-Flow Testing (cont.)

	Print		Actual	
	cm	(in.)	cm	(in.)
Ox-Rich	5.59	(2.200)	5.58	(2.195)
Fuel-Rich	3.81	(1.500)	3.81	(1.500)

The Cd values itemized in Table VI-VII are in good agreement with the theoretical values for the test configurations. The Cd value for the selected oxidizer-rich configuration of Test 102 is 1.05. This compares to a min/max value of 1.02 to 1.10 for a 5.58 cm (2.195 in.) diameter throat at the end of a 10.16-cm (4-in.) diameter pipe with a 7.62-cm (3.0-in.) diameter orifice located a short distance upstream of the throat, as shown in Figure VI-26.

The experimental Cd values for the 3.81-cm (1.500-in.) diameter fuel-rich throat were 0.99 as a result of the flow-straightening effects of the fuel main injector simulator. The theoretical Cd of the smaller throat diameter in a 10.16-cm (4-in.) diameter long pipe is 0.99. This value dropped to 0.97 when the turbine simulator and main injector simulator were removed from the flow stream in Test 110.

The relation between pressure drop, expressed as P_{c-1}/P_{c-2} (static), versus percent open area across the turbine simulators is presented in Figure VI-28. Reducing the percent of open area between the blades results in a higher pressure drop. The design pressure ratio for this device was 1.5. The initial estimates of the gaps between blades of 0.38 cm (0.15 in.) for the fuel-rich assembly and ≈ 0.64 cm (0.25 in.) for the oxidizer-rich assembly did not result in a high enough pressure loss. The data appear to indicate that the flow in the blade gaps is choked and that a high recovery is obtained. This results in an apparent increase in Cd from 0.6 to 1.0 (Table VI-VII) as the fuel blade gaps are closed. The consistency of Cd (calculated by assuming choked flow) for a fixed geometry even as flowrates are varied is proof that the choked flow assumption is correct.

Figure VI-28 shows the relationship between the experimental P_{c-1}/P_{c-2} value and the calculated flow area expressed as a percentage of the 10.32 cm (4.06 in.) pipe diameter. The recommended operating point for the fuel- and oxidizer-rich test configurations is shown. Testing in the steep part of the fuel-rich curve is highly desirable in that small changes in the open area will result in easily measurable large changes in the P_{c-1}/P_{c-2} ratio. This allows the effect of carbon deposition to be easily recognized.

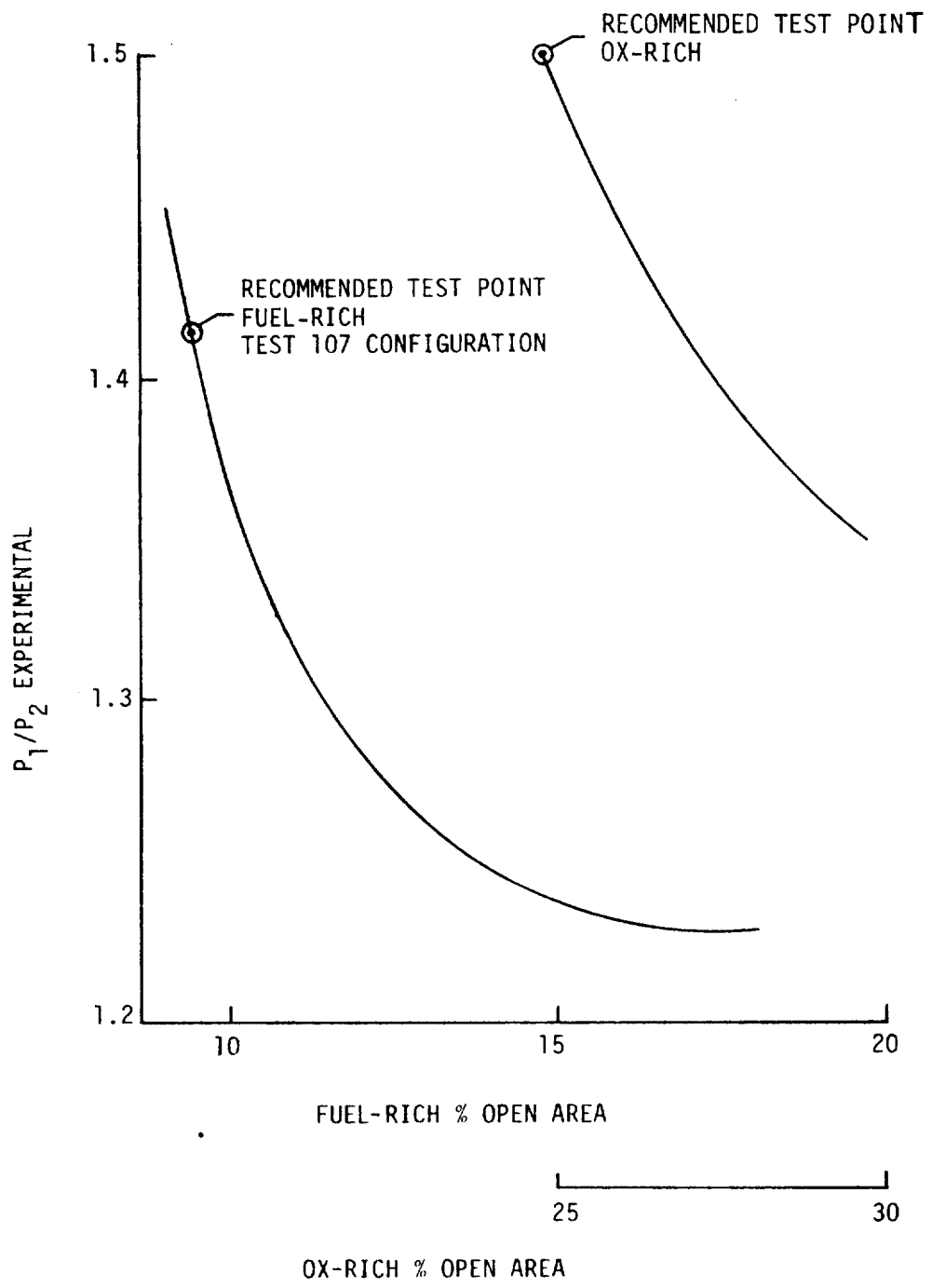


Figure VI-28. Pressure Ratio Versus Percent Open Area for Oxidizer- and Fuel-Rich Turbine Simulators

VI, Cold-Flow Testing (cont.)

E. IGNITER COLD-FLOW TESTING

1. Objectives

The objectives of the igniter cold-flow tests were to verify that all passages were open and flowing properly and to define the flowrate versus pressure relationship for both circuits of both igniters.

2. Procedures

Two igniters of the design shown in Figures III-26 and -27 were cold-flowed with GN₂. The flowrate was calculated from an NBS traceable critical flow venturi, using the pressure and temperature measured at the inlet.

Additional measurements were as follows:

P_{out} = Venturi discharge pressure is the same as igniter supply pressure

PCI = Chamber pressure measured in fuel injection manifold. (See Figure III-26.)

T_{out} = Temperature at venturi discharge assumed to be the same at igniter inlet.

Each circuit of each igniter was flowed separately at varying supply pressures. The data recorded in these tests are documented in Table VI-VIII.

3. Results

The test data of Table VI-VIII were employed to calculate the overall flow coefficient (CdA) for each circuit. The overall igniter flow resistance in cold flow is controlled by the 0.38-cm (0.150-in.) diameter drilled hole at the end of the brazed end of the 0.64-cm (0.25-in.) oxidizer and fuel feed tubes.

The data provided the following values for overall igniter CdA:

	Oxidizer cm ²	in. ²	Fuel cm ²	in. ²
SN-1	0.0877	(0.0136)	0.0877	(0.0136)
SN-2	0.0884	(0.0137)	0.0877	(0.0136)

TABLE VI-VIII(a) - IGNITER COLD-FLOW DATA

NBS Orifice Identification (Colorado #CB)

Igniter SN-1

		Venturi				Igniter				CdA Inlet/PFJ
	Point	P _{in} kPa	P _{out} kPa	T _{in} °K	T _{out} °K	PCI kPa	\dot{w} GN ₂ kg/sec	P _{out} / \dot{w} sec/cm ²	PCI/ \dot{w} sec/cm ²	
Fuel	1	101.3	101.3	296	295	101.3	0	0	0	
	2	2861	979	287	288	427.4	0.0193	21,013	9194	} <u>0.0138</u> 0.0318
	3	4274	1448	288	286	627.4	0.0298	20,652	8948	
	4	5688	1930	291	286	834.2	0.0399	20,548	8877	
	5	7066	2406	294	287	1041.	0.0499	20,452	8845	
Oxidizer	1	101.3	101.3	294	293	101.3	0	0	0	
	2	2861	979	288	289	197.9	0.0197	21,013	4252	} <u>0.0136</u> 0.0673
	3	4274	1461	289	287	294.4	0.0298	20,845	4200	
	4	5619	1917	292	287	390.9	0.0394	20,639	4206	
	5	6997	2392	294	287	487.4	0.0497	20,419	4161	
Igniter SN-2										
Fuel	1	2861	993	288	288	579	0.0197	21,355	12,458	} <u>0.0136</u> 0.0233
	2	3964	1365	291	288	807	0.0275	21,045	12,439	
	3	4240	1448	291	288	841	0.0296	20,781	12,071	
	4	4240	1461	292	288	848	0.0296	20,980	12,168	
	5	5619	1930	295	289	1131	0.0394	20,787	12,174	
	6	6997	2413	298	290	1413	0.0497	20,600	12,064	
Oxidizer	1	2861	979	289	286	193.0	0.0197	21,058	4103	} <u>0.0137</u> 0.0702
	2	4240	1455	288	286	282.7	0.0295	20,910	4058	
	3	5688	1937	291	286	372.3	0.0399	20,626	3961	
	4	7032	2406	294	287	461.9	0.0497	20,535	3942	
	5	8411	2882	296	288	489.5	0.0601	20.329	3452	

TABLE VI-VIII(b) - IGNITER COLD-FLOW DATA

NBS Orifice Identification (Colorado #C8)

Igniter SN-1

	Point	Venturi				Igniter				CdA Inlet/Pfj
		P _{in}	P _{out}	T _{in}	T _{out}	PCI	\dot{w} GN ₂ lb/sec	P _{out} / \dot{w} sec/in. ²	PCI/ \dot{w} sec/in. ²	
Fuel	1	14.7	14.7	72	71	14.7	0		0	} <u>0.0138</u> 0.0318
	2	415	142	56	58	62	0.0425	3257	1425	
	3	620	210	58	55	91	0.0656	3201	1387	
	4	825	280	63	55	121	0.0879	3185	1376	
	5	1025	349	70	57	151	0.1101	3170	1371	
Oxidizer	1	14.7	14.7	70	67	14.7	0	0	0	} <u>0.0136</u> 0.0673
	2	415	142	59	60	28.7	0.0435	3257	659	
	3	620	212	61	57	42.7	0.0656	3231	651	
	4	815	278	65	57	56.7	0.0869	3199	652	
	5	1015	347	70	57	70.7	0.1096	3165	645	

Igniter SN-2

Fuel	1	415	144	58	58	84	0.0435	3310	1931	} <u>0.0136</u> 0.0233
	2	575	198	63	58	117	0.0607	3262	1928	
	3	615	210	63	58	122	0.0652	3221	1871	
	4	615	212	65	58	123	0.0652	3252	1886	
	5	815	280	71	60	164	0.0869	3222	1887	
	6	1015	350	77	62	205	0.1096	3193	1870	
Oxidizer	1	415	142	60	55	28	0.0435	3264	636	} <u>0.0137</u> 0.0702
	2	615	211	58	55	41	0.0651	3241	629	
	3	825	281	63	55	54	0.0879	3197	614	
	4	1020	349	69	56	67	0.1096	3183	611	
	5	1220	418	73	58	71	0.1326	3151	535	

All pressures in psia

VI, E, Igniter Cold-Flow Testing (cont.)

These values translate to a Cd of 0.78 for the 0.38-cm (0.150-in.) flow-restricting orifice which is the expected Cd value for this geometry.

The cold-flow supply pressure versus flowrate for H₂ and O₂ was calculated by using the experimental CdA values (shown in Figure VI-29). The expected igniter inlet pressure, when cold-flowed with propellants at the rated flow of 0.0091 kg/sec (0.02 lb/sec) GH₂ and 0.0318 kg/sec (0.07 lb/sec) GO₂, is 1655 kPa (240 psia) for the fuel and 1434 kPa (208 psia) for the oxygen. These values will be useful in future testing if it becomes necessary to verify that the circuits are flowing properly.

A second CdA was calculated for each circuit utilizing the measured PCI value which is the pressure in the fuel injection plenum located upstream of the 0.038/0.051-cm (0.015/0.020-in.) annular gap defined in Figure III-26. The calculated CdA values for these data are as follows:

	Oxidizer		Fuel	
	cm ²	in. ²	cm ²	in. ²
SN-1	0.434	0.0673	0.205	0.0318
SN-2	0.453	0.0702	0.150	0.0233

These values represent the system flow resistances downstream of the 0.381-cm (0.150-in.) diameter hole in the feed line. The value of CdA based only on the 0.64-cm (0.25-in.) throat diameter is 0.316 cm² (0.049 in.²).

The following conclusions are drawn when the calculated CdA values are compared to each other and to the throat value:

- ° The flow resistance within the annular fuel gap is significant.
- ° The annular fuel gap of the SN-1 igniter is larger than that of the SN-2.
- ° The oxidizer flow across the annular gap formed by the spark plug and the igniter tube is sonic, and the static pressure in the fuel plenum is less than the static pressure further downstream.
- ° The position of the spark plug relative to the hydrogen injection annulus influences the measured value of PCI.

The above results, derived from the flowrate and PCI measurement, are of interest in understanding the operation of the igniter in cold-

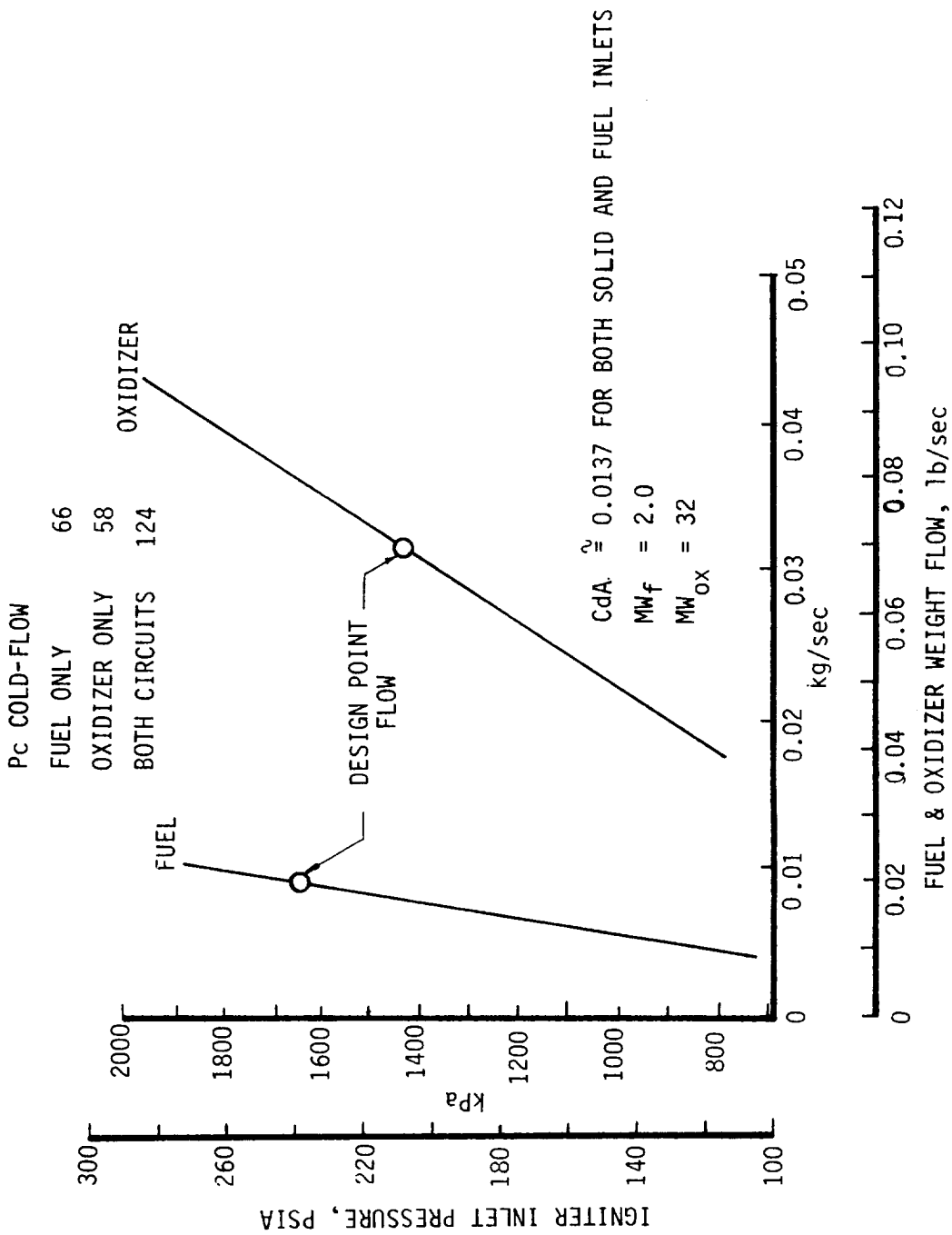


Figure VI-29. Cold-Flow Supply Pressure Versus Flowrate for H₂ and O₂

VI, E, Igniter Cold-Flow Testing (cont.)

flow and also in positioning of the spark plug. However, these are predicted to become items of secondary importance in a hot-fire test. When the igniter lights, the chamber pressure increases from the actual cold-flow value (400 and 455 kPa (58 and 66 psia), respectively) for the individual oxidizer and fuel flow conditions to approximately 2758 kPa (400 psia). This rise in back pressure causes the flow to become unchoked at all locations except at the throat.

4. Recommendations for Hot-Fire Testing

Proper control of the igniter flow and the prevention of back flow of preburner combustion products at preburner ignition require the addition of flow control orifices. These are to be located between the high-pressure supply and the igniter and as close as possible to the igniter inlet fittings. The supply pressure should be equal to or exceed the chamber pressure (i.e., 15167 kPa [2200 psia]). The fuel and oxidizer sharp-edged orifice diameters should be 0.130 and 0.117 cm (0.051 and 0.046 in.), respectively.

VII. CONCLUSIONS AND RECOMMENDATIONS

1. A uniform mixture ratio combustor provides the best design approach for high-pressure fuel-rich and oxidizer-rich preburners.
2. A secondary in-chamber mixing ring will be required to attain the gas temperature uniformity goals. The mixer will also provide a method of eliminating longitudinal modes of combustion instability.
3. A set of gas temperature measurement and gas sample rakes should be fabricated to verify the predicted gas temperature uniformity and the effectiveness of the in-chamber mixing ring.
4. The experimental data obtained from the fuel-rich testing should be employed to validate and update the fuel-rich combustion model developed in Task I.
5. The effectiveness of ceramic coatings in preventing metal ignition should be evaluated in the oxidizer-rich testing.
6. The use of an oxidizer-rich torch igniter in lieu of the fuel-rich should be considered for the oxidizer-rich testing.

PRECEDING PAGE BLANK NOT FILMED

REFERENCES

1. "Liquid Propellant Gas Generators - NASA Space Vehicle Design Criteria," NASA SP 8081.
2. Croy, S.E., "Analysis of Fuel/Oxidizer-Rich High-Pressure Preburner Bolted Flange," ALRC Report 9753:1203, 1 August 1979.
3. Henson, F.M., "Titan III Stage II Injector/Chamber RACO Seal Evaluation," ALRC Report CS-52; also Memo 9733:227, dated 2 August 1973.
4. Brown, P.E., "Fuel/Oxidizer-Rich Injector Manifold Analysis," ALRC Report 9753:1313, 21 March 1980, Rev. 1 Jellison, 7 Jan. 1981, CdN File 6006.
5. Ingebo, R.D., "Maximum Drop Diameters for the Atomization of Liquid Jets Injected Concurrently Into Accelerating or Decelerating Gas Streams," NASA TN D-4640, July 1968.
6. Lee, D.W., "Measurement of Fuel Distribution Within Sprays for Fuel Injection Engine," NACA Report 565, 1936.
7. Lee, D.W., "A Comparison of Fuel Sprays from Several Types of Injection Nozzles," NACA Report 520, 1935.
8. Hewitt, R.A., "LOX/RP-1 Fuel/Oxidizer-Rich High-Pressure Preburner LOL Injector Design Analysis," ALRC Report 9751-0436, 31 March 1980.
9. Priem, R.J. and Hiedmann, M.F., "Propellant Vaporization as a Design Criterion for Rocket Engine Combustion Chambers," NASA TR-R-67, 1960, p. 127.

PRECEDING PAGE BLANK NOT FILMED

APPENDIX
FUEL-RICH COMBUSTION MODEL BIBLIOGRAPHY

PRECEDING PAGE BLANK NOT FILMED

BIBLIOGRAPHY

- Barnett, H.C. and Hibbard, R.R.(19??) "Properties of Aircraft Fuels," NACA Technical Note 3276.
- Blazowski, W.S., Edelman, R.B., and Harsha, P.T. (1978). "Fundamental Characterization of Alternate Fuel Effects in Continuous Systems," EXXON Research and Engineering Company Report No. C00/1543-12 prepared for DOE Contract EC-77-C-03-1543.
- D'Alessio, A., Di Lorenzo, A., Sarofim, A.F., Beretta, F., Masi, S., and Venitozzi, C. (1974). "Soot Formation in Methane-Oxygen Flames," Fifteenth Symposium (International) on Combustion, The Combustion Institute, Pittsburgh, pp. 1427-1438. (Abbreviated 15th SIOC)
- Eberius, K.H., Hoyermann, K., and Wagner, H. Gg. (1973). "Structure of Lean Acetylene-Oxygen Flames," 14th SIOC, pp. 147-156.
- Engleman, V.S. (1976). "Survey and Evaluation of Kinetic Data on Reactions in Methane/Air Combustion," EPA Report No. EPA-600/2-76-003, Final Report, Contract No. 68-02-0224.
- Gardiner, W.C. Jr., Own, J.H., Clark, T.C., Dove, J.E., Bauer, S.W., Miller, J.A., and McLean, W.J. (1974). "Rate and Mechanism of Methane Pyrolysis From 2000° to 2700°K," 115th SIOC, pp. 857-868.
- Gosling, A.J., Lampard, D., and Fussey, D.E. (1973). "A Shock Tube Study of the Formation of Carbon Particles During the Pyrolysis of Hydrocarbons," Combustion Institute/European Symposium, pp. 388-393.
- Graham, S.C., Homer, J.B., Rosenfeld, J.L.J. (1975). "The Formation and Coagulation of Soot Aerosols Generated by the Pyrolysis of Aromatic Hydrocarbons," Proc. R. Soc. Lond. A, 344, pp. 259-285.
- Hein, K. (1972). "Recent Results on The Formation and Combustion of Soot in Turbulent Fuel Oil and Gas Flames," Comb. Sci. Tech. 5, pp. 195-206.
- Homann, K.H. (1967). "Carbon Formation in Premixed Flames," Comb. Flame 11, pp. 165-287.
- Howard, J.B. (1969). "On the Mechanism of Carbon Formation in Flames," 12th SIOC, pp. 877-887.
- Jensen, D.E. (1973). "Soot Formation in Liquid Propellant Rocket Motors: A Basic Modeling Approach," Combustion Institute/European Symposium, pp. 382-387.

BIBLIOGRAPHY (cont.)

- Jensen, D.E. (1974). "Prediction of Soot Formation Rates: A New Approach," Proc. R. Soc. Lond. A, 338, pp. 375-396.
- Lester, T.W. and Wittig, S.L.K. (1976). "Soot Nucleation Kinetics in Pre-Mixed Methane Combustion," 16thSIOC, pp. 671-680.
- Macfarlane, J.J., Holderness, F.H., and Witcher, S.E. (1964). "Soot Formation Rates in Premixed C5 and C6 Hydrocarbon-Air Flames at Pressures up to 20 Atmospheres," Comb. Flame 8, pp. 215-229.
- Maraval, L. (1972). "Characteristics of Soot Collected in Industrial Diffusion Flames," Comb. Sci. Tech. 5, pp. 207-212.
- McArragher, J.S. and Tan, K.J. (1972). "Soot Formation at High Pressures: A Literature Review," Comb. Sci. Tech. 5, pp. 257-261.
- Meier Zu Kocker, H. (1972). "Kinetics of Soot Formation: Investigations into the Mechanism of Soot Formation in Hydrocarbon Diffusion Flames," Comb. Sci. Tech. 5, pp. 219-224.
- Prado, G.P., Lee, M.L., Hites, R.A., Hoult, D.P., and Howard, J.B. (1976). "Soot and Hydrocarbon Formation in Turbulent Diffusion Flames," 16thSIOC, pp. 649-661.
- Tabayashi, K. and Bauer, S.H. (1979). "The Early Stages of Pyrolysis and Oxidation of Methane," Comb. Flame 34, pp. 63-83.
- Waldman, C.H., Wilson, R.P. Jr., Maloney, K.L. (1974). "Kinetic Mechanism of Methane/Air Combustion with Pollutant Formation," EPA Report No. EPA-650/2-74-045, Final Report, Contract No. 68-02-0270.
- Wersborg, B.L., Howard, J.B., and Williams, G.C. (1973). "Physical Mechanisms in Carbon Formation in Flames," 14thSIOC, pp. 929-940.
- Wersborg, B.L., Yeung, A.C., and Howard, J.B. (1974). "Concentration and Mass Distribution of Charged species in Sooting Flames," 15thSIOC, pp. 1439-1448.
- Zaghini, N. et al (1972). "Formation of Polycyclic Aromatic Hydrocarbons in a Vertical Flow Reactor," Comb. Sci. Tech. 5, pp. 225-236.
- Prepared by Cye H. Waldman, Ph.D. and SEA, Inc. for Aerojet Liquid Rocket Company.

DISTRIBUTION LIST FOR FINAL REPORT - CR-165404
NAS 3-21753

<u>Name</u>	<u>No. of Copies</u>	<u>Name</u>	<u>No. of Copies</u>
National Aeronautics & Space Administration Lewis Research Center 21000 Brookpark Road Cleveland, Ohio 44135 Attn:		National Aeronautics & Space Administration Langley Research Center Langley Station Hampton, VA 23365 Attn:	
Contracting Officer - MS 500-306	1	Library	1
Technical Utilization Office - MS 7-3	1	J. A. Martin, MS 365	1
Technical Report Control Office - MS 5-5	1		
AFSC Liaison Office - MS 501-3	2	NASA Scientific & Technical Information Facility	
Library - MS 60-3	2	P.O. Box 8785	
Office of Reliability & Quality Assurance - MS 500-211	1	Baltimore-Washington Intn'l. Airport Baltimore MD 21240	
N. T. Musial - MS 500-318	1	Attn: Accessioning Department	10
H. G. Price, Project Manager - MS 501-6	10	Office of the Director of Defense Research & Engineering	
E. A. Bourke - MS 501-5	5	Washington, DC 20301	
T. Brabbs - MS 86-5	1	Attn: Office of Ass't Director (Chemical Technology)	1
National Aeronautics & Space Administration Headquarters Washington, D.C. 20546 Attn:		Jet Propulsion Laboratory 4800 Oak Grove Drive Pasadena, CA 91103 Attn: Library	1
Office of Aeronautics & Space Technology	1		
RS/Director, Manned Space Technology	1	Defense Documentation Center Cameron Station Building 5 5010 Duke Street Alexandria, VA 22314 Attn: TISIA	1
RP/Director, Space Propulsion & Power	1		
RW/Director, Materials & Structures	1		
RP1/F. W. Stephenson	1		
Attn: Office of Manned Space Flight MT/Director, Advanced Manned Mission	1		
Attn: Office of Space Science SG/Director, Physics & Astronomy Programs	1		
SL/Director, Planetary Programs	1		
SV/Director, Launch Vehicles & Propulsion	1	Advanced Research Projects Agency Washington, DC 20525 Attn: Library	1
Attn: Office of Technology Utilization Division KT/Director, Technology Utilization	1		
National Aeronautics & Space Administration Ames Research Center Moffett Field, California 94035 Attn: Library	1	Aeronautical Systems Division Air Force Systems Command Wright-Patterson Air Force Base Dayton, Ohio Attn: Library	1
National Aeronautics & Space Administration Flight Research Center P.O. Box 273 Edwards, CA 93523	1	Air Force Rocket Propulsion Laboratory (RPM) Edwards, CA 93523 Attn: Library	1
National Aeronautics & Space Administration George C. Marshall Space Flight Center Huntsville, AL 35912 Attn:		Air Force FTC (FTAT-2) Edwards Air Force Base, CA 93523 Attn: Library	1
Library	1	Air Force Office of Scientific Research 1400 Wilson Blvd. Arlington, VA 22209 Attn: Library	1
J. L. Sanders/PD13	1		
R. Richmond/EP24	1		
J. A. Lombardo/EP21	1	U.S. Air Force, Office of Information Washington, DC 20333 Attn: Library	1
C. R. Bailey/EP23	1		
National Aeronautics & Space Administration Goddard Space Flight Center Greenbelt, MD 20771 Attn: Library	1	Air Force Aero Propulsion Laboratory Research & Technology Division Air Force Systems Command U.S. Air Force Wright Patterson AFB, OH 45433 Attn: Library (APRP)	1
National Aeronautics & Space Administration John F. Kennedy Space Center Cocoa Beach, FL 32931 Attn: Library	1	Arnold Engineering Development Center Air Force Systems Command Tullahoma, TN Attn: Library	1
National Aeronautics & Space Administration Lyndon B. Johnson Space Center Houston, TX 77001 Attn:			
Library	1	Bureau of Naval Weapons Department of the Navy Washington, DC Attn: Library	1
EP2/M. F. Lausten	1		

DISTRIBUTION LIST FOR FINAL REPORT - CR-165404 (cont.)

<u>Name</u>	<u>No. of Copies</u>	<u>Name</u>	<u>No. of Copies</u>
U.S. Naval Research Laboratory Washington, DC 20390 Attn: Library	1	Lockheed Missiles & Space Company P.O. Box 504 Sunnyvale, CA 94087 Attn: Library	1
U.S. Army Research Office (Durham) Box CM, Duke Station Durham, NC 27706 Attn: Library	1	Marquardt Corporation 16555 Saticoy Street Box 2013 South Annex Van Nuys, CA 91409 Attn: Library	1
U.S. Army Missile Command Redstone Scientific Information Center Redstone Arsenal, AL 35808 Attn: Document Section	1	Martin-Marietta Corporation P.O. Box 179 Denver, CO 83201 Attn: Library	1
U.S. Naval Missile Center Point Mugu, CA 93041 Attn: Technical Library	1	McDonnell Douglas Astronautics 5301 Bolsa Avenue Huntington Beach, CA 92647 Attn: Library	1
U.S. Naval Weapons Center China Lake, CA 93557 Attn: Library	1	Philco-Ford Corporation Aeronautics Div. Ford Rd. Newport Beach, CA 92663 Attn: Library	1
Aro Incorporated Arnold Engineering Development Center Arnold AF Station, TN 37389 Attn: Library	1	Purdue University Lafayette, IN 47907 Attn: Library	1
Battelle Memorial Institute 505 King Avenue Columbus, OH 43201 Attn: Library	1	Rocketdyne A Div. of Rockwell International 6633 Canoga Avenue Canoga Park, CA 91304 Attn:	1
Bell Aerosystems Inc Box 1 Buffalo, NY 14240 Attn: Library	1	Library F. M. Kirby G. Bremer	1 1 1
Boeing Company Space Division P.O. Box 868 Seattle, WA 98124 Attn: Library	1	Rocket Research Corporation Willow Road at 116th Street Redmond, WA 98052 Attn: Library	1
Chemical Propulsion Information Agency Applied Physics Laboratory 8621 Georgia Avenue Silver Spring, MD 20910	1	Thiokol Chemical Corporation P.O. Box 1000 Newton, PA 18940	1
Chrysler Corporation Space Division P.O. Box 25200 New Orleans, LA 70129 Attn: Library	1	TRW Systems, Inc. 1 Space Park Redondo Beach, CA 90278 Attn: Library	1
General Dynamics/Convair P.O. Box 1128 San Diego, CA 92112 Attn: Library	1	United Aircraft Corporation Pratt & Whitney Division Florida Research & Development Center P.O. Box 2691 West Palm Beach, FL 33402 Attn: Library	1
General Electric Company Missiles & Space Systems Center Valley Forge Space Tech. Center P.O. Box 8555 Philadelphia, PA 19101 Attn: Library	1	United Technologies Research Center East Hartford, CT 06108 Attn: Library	1
Grumman Aircraft Engineering Corporation Bethpage, L.I., NY Attn: Library	1		
Ling-Temco-Vought Corporation P.O. Box 5907 Dallas, TX 75222 Attn: Library	1		